Faculty of Computing, Engineer and the Built Environment

Ulster University at Jordanstown

Belfast School of the Built Environment

Development of innovative semi-flexible composite materials for pavement applications

By:

An Thao Huynh

BSc (Hons), M.Eng.

Thesis submitted for the degree of

Doctor of Philosophy

November 2020

Table of contents

List of Figures

List of Tables

Acknowledgements

The PhD thesis was carried out at the Faculty of Computing, Engineering and the Built Environment at Ulster University, under the supervision of Dr Bryan Magee and Dr David Woodward. The author would like to express her appreciation to Dr Bryan Magee for his consistent support, valuable feedback, attention to details, patience and encouragement during her PhD course. Her gratitude is also due to Dr David Woodward for his support, assistance, valuable discussions and contribution to the research works.

She also wishes to express thanks to the technicians at School of the Belfast School of Architecture and the Built Environment and School of Engineering: Mr Cormac Walls, Mr Ian Martin, Mr Graeme Craig and Dr John McGrath and other technicians in Nanotechnology and Integrated Bioengineering Centre for their assistance, guidance and recommendations throughout the research works. The author also extends her gratitude to the School of Built Environment for providing funding to complete this research and to Mrs Irene Moreland for her support during the research.

The author also offers her appreciation to Dr Khoa Tan Nguyen and Dr Hoang Nguyen for their support in terms of upcoming research topics and career aspects. Special thanks are extended to her fellow researchers, Dr Geoffrey Neale, Dr Mengmeng Dou and Monali Dahale, for their encouragement and friendship. Finally, the author would like to express her thanks to her parents and Alan for their support and encouragement during these very intense academic years.

This thesis is dedicated to the memory of her younger brother.

Abstract

Significant quantities of greenhouse gases have been emitted into the atmosphere from the processes of aggregate extraction and asphalt and Portland cement production in relation to the pavement construction industry. This issue can be tackled through the introduction of more sustainable construction materials made from industrial and construction wastes with low embodied carbon into infrastructure construction sector. As such, this research proposes innovative semi-flexible composite pavement materials (SFC) comprising reclaimed asphalt planing aggregate skeletons infused with geopolymer cement-based grouts. Both surface wearing and base courses were considered as potential applications for the proposed materials.

Geopolymer grout was formulated at ambient temperature using industrial by-products such as fly ash, ground-granulated blast-furnace slag, metakaolin and silica fume to offer potential economic and environmental savings relative to ordinary Portland cement. By considering diverse binders with different physical properties and chemical compositions, a wide range of grout performance in terms of compressive strength and workability (i.e. flowability, initial and final setting time) was achieved to facilitate the manufacture of SFC suitable for a broad range of practical pavement applications. Mixture proportions and types of geopolymer powder were found to play critical roles in fresh and hardened properties of geopolymer grout. As grout properties are fundamental to grouting processes and resultant SFC properties, four geopolymer grout types with contrasting performance classifications were investigated in detail to infuse open-graded RAP skeletons for subsequent assessment of SFC properties.

A diverse suite of SFC mixtures was produced based on the four selected grout mixes and open-graded RAP skeleton with various levels of solid contents, resulting in corresponding wide ranges of SFC properties such as permeable porosity, compressive strength and ultrasonic pulse velocity. Pronounced influences of grout properties and RAP content on SFC performance were found with increasing performance levels generally corresponded to highly flowable/high strength grout combined with decreasing RAP content. SFC materials with the ability to gain early strength with up to 84% of their 28-day strength value after three days also offer promising benefits for pavements where early exposure to traffic is mandatory. Comparable positive relationships enabling estimation of SFC elastic modulus based on rapidly attainable laboratory test methods such as ultrasonic pulse velocity and/or compressive strength are proposed to enable preliminary pavement designs incorporating layers made from SFC materials. The potential suitability of SFC materials for

base layers has been successfully proven, with strength levels conforming to the mechanical performance levels required by DMRB, volume 7, section 2, part 3 (Highways England, 2006a) for HBM base layers. The viability of SFCs as a replacement for traditional base layer materials were confirmed via preliminary pavement design examples. For instance, for heavy duty industrial hardstandings comprising 80 mm concrete block paving laid on a sand bed layer and subgrade CBR of 8%, base layer thickness requirements for SFC materials were lower than for conventional CBGM material.

In addition to mechanical and physical characterisation, costs of raw materials and greenhouse gas emissions to produce SFC base layers as an alternative to traditional CBGM base course in heavy duty pavements were carried out to evaluate its economic viability and environmental performance. SFC material costs and greenhouse gas emissions were lower than for traditional CBGM, highlighting their positive economic and environmental potential. By confirming a balance of technical, environmental and economic benefits associated with SFC, this reflects an excellent step towards a more sustainable future for pavement materials.

In addition to base course application, trafficking-related properties associated with pavement wearing courses, such as specimen weight loss, skid resistance, mean texture depth and surface texture changes of surface courses, were also assessed for SFC materials using standard experimental and close-range photogrammetry methods. Results from work to identifying suitable surface finishing methods for SFC showed that surface dressing is the most effective finishing method due to its high skid resistance values in dry and wet conditions. Based on this observation, further testing was carried out to determine its suitability for use in surface courses in pavements. SFC pavements with a surface dressing finish comprising RAP and four geopolymer grout types were exposed to simulated trafficking conditions using Ulster University's road test machine. Most of the investigated SFC specimens comprising average to high strength grout exhibited adequate endurance under traffic wear with low weight loss rate. As anticipated, SFC specimens comprising low strength grout showed significant weight loss associated with edge defects and cracks after a short length of time under polishing actions. Tested SFC specimens exceeded mean texture depth and skid resistance requirements for pavements made from conventional materials such as concrete or hot rolled asphalt with traffic of less than 2000 vehicle per day (Department for Transport, 2010; Highways England, 2006b) but fell short of requirements for high friction surface.

Close-range photogrammetry methods were found to provide valuable information on surface texture changes of SFC pavements during wearing process. Significant influences of simulated trafficking on SFC textures were highlighted based on notable changes in roughness, skewness and kurtosis parameters.

In general, the proposed SFC materials comprising geopolymer grout and recycled RAP as aggregates showed promising performance in terms of engineering properties as well as economic and environmental aspects to be used in pavement applications.

List of abbreviations

SFC	Semi-Flexible Composite
RAP	Reclaimed Asphalt Planing
CO_2	Carbon Dioxide
PC	Portland Cement
CO_2e	Carbon Dioxide Equivalent
FA	Fly Ash
GGBS	Ground-Granulated Blast-Furnace Slag
MK	Metakaolin
SF	Silica Fume
HDP	Heavy Duty Pavement
BS	British Standards
LA coefficient	Los Angeles coefficient
AIV	Aggregate Impact Value
WA	Water Absorption
RCA	Recycled Concrete Aggregate
UCS	Unconfined Compressive Strength
MCHW	Manual of Contract Documents for Highway Works
FHWA	Federal Highways Association
TRL	Transport Research Laboratory
NaOH	Sodium Hydroxide
Na_2SiO_3	Sodium Silicate
KOH	Potassium Hydroxide
K_2SiO_3	Potassium Silicate
Na_2SO_4	Sodium Sulfates
CaO	Calcium oxide
MOH	Alkali-Metal Hydroxide
C-S-H	Calcium Silicate Hydrate
Si	Silica
Al_2O_3	Alumina
Si-O-Al-O	Alumina-Silicate gel
–Si-O-Al-O	Poly(sialate)
–Si-O-Al-O-Si-O	Poly(sialate-siloxo)
–Si-O-Al-O-Si-O-Si-O-	Poly(sialate-disiloxo)
AAM	Alkaline-Activated Material

LS	Liquid-to-solid
HFS	High Friction Surfacing
DMRB	Design Manual for Roads and Bridges
LOI	Loss on Ignition
ASTM	American Society for Testing and Materials
HBM	Hydraulically Bound Material
CBR	Californian Bearing Ratio
ITSM	Indirect Tensile Stiffness Modulus
CBGM	Cement Bound Granular Mixtures
PSV	Polished Stone Value
AAV	Aggregate Abrasion Value
cv/lane/day	commercial vehicle per lane per day
BCB	Buff Calcined Bauxite
f_{cu}	Cube compressive strength
UPV	Ultrasonic Pulse Velocity
W_{ST}	Saturated mass
W_W	Apparent mass in water
ρ	Permeable porosity
SEM	Scanning electron microscope
RTM	Road Test Machine
SRV	Skid Resistance Value
MTD	Mean Texture Depth
AOI	Area of Interest
AVC	Air Void Content
E_s	Elastic Modulus
CBP	Concrete Block Paving
GHG	Greenhouse gas
Sa	Average roughness
Ssk	Skewness
Sku	Kurtosis
DNN	Deep Neural Network
R^2	R-squared
RMSE	Root Mean Square Error
MAPE	Mean absolute percentage error
SPSS	Statistical Package for the Social Sciences

Note on access to content

CHAPTER 1

Introduction

1.1 Background

This study introduces innovative semi-flexible composite (SFC) pavement materials comprising reclaimed asphalt planings (RAP) and geopolymer cement-based grouts. Pavement applications considered for this SFC includes both structural base course and surface wearing courses.

A key target of the research is to contribute to a reduction in the carbon footprint and demand for natural resources associated with the infrastructure construction industry. Infrastructure and road construction sectors have been claimed to consume large quantities of natural aggregates in Europe, where approximately 30,000 tonnes of aggregates are reportedly required to construct 1 km of roadway (European aggregates association, 2018). Annual production of virgin aggregate and minerals in the UK for concrete and asphalt production is approximately 390 million tonnes (Mineral Products Association, 2018a). Based on emission rates of 3.6 and 3.1 kg CO_2/tonne for crushed rock and sand respectively (Mineral Products Association, 2018b), this equals to over 2.6 million tonnes of CO_2 generated from aggregate extraction for construction purposes alone.

As a result, high demand for natural aggregates leads to overexploitation of mineral resources. Those extraction activities can destroy the ecological balance, damage the environment and endanger communities by causing air, noise, and water pollution (Blades et al., 2006; Page, 2011). Moreover, the imbalance of natural resources and overexploitation was reported to result in regional shortages of virgin aggregates (Loannidou et al., 2017). As stated in a report issued by the British geological survey (Hicks, 2008), despite having large resources of aggregate materials, the South, East and parts of central England showed a lack of crushed rocks resulting from the uneven geological distribution of primary aggregate in the UK. Although rock quarries are densely distributed in Northern Ireland and Scotland, they are located in remote areas with less demand for aggregates (British Geological Survey, 2019). Since aggregates are not economical for long-distance transportation, this would increase the cost of pavement construction and emit significant quantities of additional carbon dioxide. Indeed, transportation of aggregate was claimed to account for over 32% of CO_2 in the mineral extraction industry (Page, 2011). Asphalt and Portland cement concrete are two types of materials commonly used in pavement applications. The production of hot mix asphalt contributes significant quantities of greenhouse gas emissions, including 10% of all CO_2 emissions in the UK (Gibson, 2011). In addition, Portland cement production has significant impacts on the environment, responsible for up to 8% of worldwide carbon dioxide emissions (Farfan et al., 2019).

As international pressures of reducing CO_2 emission and minimising the use of natural resources grow, the uses of construction and industrial wastes as alternatives to raw materials can help to resolve environmental issues caused by their extraction processes and reduce landfill wastes. Hence, recycling of aggregates, such as RAP, generated from road surface or full-depth removal has drawn significant attention from researchers and scientists for many years. RAP generated from existing pavements may be considered as a sustainable aggregate source for the construction industry that can reduce CO_2 emissions linked to quarrying, mineral extraction and asphalt production. In a case study of a section of the M25 in England between junctions 6 and 7, a surface layer with 40% by mass RAP as an alternative to virgin aggregate offered CO_2 and energy savings of 9 tonnes and 134 GJ respectively relative to a conventional asphalt mixture with 100% natural aggregates. This saving was equated to a car travelling about 52,500 km (Wayman and Carswell, 2010).

For the SFC materials developed in the current research project, geopolymer grout has been used as the second main component, serving as a binder for RAP skeletons without the need of heating energy. The main constituent materials of the geopolymer grouts considered were industrial by-products, including fly ash (FA), ground-granulated blast-furnace slag (GGBS), metakaolin (MK) and silica fume (SF). These materials were chosen based on their reported ability to offer potential economic and environmental savings relative to traditional cementitious grouts (Huynh et al., 2020a).

1.2 Research questions

Research questions addressed by this study are as follows:

1. What are the roles of geopolymer grout and RAP in conventional asphalt and concrete pavements?
2. How do fresh and mechanical properties of geopolymer grout mixes vary regarding the type and composition of their raw materials?
3. What is the most suitable application for SFC materials in pavement structures in terms of mechanical properties?
4. How effective are SFC pavements at improving environmental and economic benefits compared to traditional heavy-duty pavements?
5. How do SFC pavements perform when subjected to simulated trafficking?
6. What are the most effective RAP contents and geopolymer grout types to optimise SFC pavement performance?

1.3 Research aim and objectives

This study aims to develop innovative, predominantly waste based SFC materials for pavement applications that do not require natural aggregates and heating energy.

Six specific objectives of this study include:

- Conduct a throughout literature search on relevant subjects including RAP, geopolymer materials and semi-flexible composite pavements.
- Investigate the possible range of fresh and mechanical properties of geopolymer grouts and select suitable grouts for further investigation of SFC materials.
- Evaluate the potential use of SFC in pavement applications in terms of mechanical properties.
- Identify the benefits of using SFC materials in pavement applications in terms of costs of raw materials and greenhouse gas emissions.
- Investigate trafficking-related properties of SFC surface courses subjected to simulated traffic wear.
- Provide recommendations for possible improvement for further research on SFC materials.

1.4 Thesis outline

This thesis is divided into 10 chapters as follows:

- **Chapter 1 - Introduction**

  This chapter provides insight into the background relating to the topic with data extracted from previous studies and professional organisations. Research questions and the aim and objectives of the study were identified in this chapter.

- **Chapter 2 - Literature review**

  This chapter presents the current literature relating to the proposed material, semi-flexible composites and their constituent materials, including geopolymer grouts and RAP. Typical properties and practical applications of RAP and geopolymer materials obtained from previous studies were discussed along with their contribution to the construction industry in terms of environmental aspects. Additionally, existing barriers of using the aforementioned materials for road applications were also provided.

  Since there has been little discussion on combining geopolymers and RAP in SFC materials, literature relating to traditional SFC with cementitious grouts and open-

graded aggregate skeleton is presented. Its typical properties and practical applications were reviewed based on previous research and specification from commercial products. Currently, there is no widely agreed standard or guidelines for SFC materials. Therefore, general specifications and requirements for traditional rigid and flexible pavements were reviewed to establish a framework of specifications for pavement design incorporating SFC materials.

- **Chapter 3 - Research methods**

  Specimen preparation and testing procedures used to characterise performance of geopolymer grouts, RAP and SFC materials were presented in this chapter. Presented is an experimental programme consisting of physical and mechanical testing, microscopic examination and 3D modelling, designed to achieve the research aim and objectives and identify the responses for research questions. To investigate the changes in SFC surface texture under simulated trafficking, setup for 3D surface texture modelling and analysing processes using close-range photogrammetry method are discussed in detail.

- **Chapter 4 - Geopolymer cement-based grout characterisation**

  This chapter presents an assessment of workability and mechanical properties of fresh and hardened geopolymer grouts. In order to offer positive environmental impacts compared to conventional Portland cement grout, the geopolymer grouts were formulated at ambient temperature using industrial by-products such as FA, GGBS, MK and SF. Properties of fresh grout including flowability and initial/final setting time were determined using Marsh flow cone and Vicat needle penetration methods. After 28 days curing at ambient temperature, compressive strength of hardened grout was determined. Effects of mix design parameters such as geopolymer powders and liquid-to-solid ratio on fresh and mechanical properties of geopolymer grouts were discussed. The performances in terms of flowability, setting time and compressive strength were then classified into various groups and favourable grout mixes were selected for further investigation.

- **Chapter 5 - Investigation into reclaimed asphalt planing properties**

  Properties of RAP and basalt aggregates such as density, water absorption, moisture content and aggregate impact values were determined based on standard methods in this chapter. Effects of RAP particle sizes, number of gyrations and pre-

heating temperature on air void content of compacted RAP using gyratory compactor were also investigated. RAPs were also compacted manually at ambient temperature to investigate the feasibility of reducing external force for compaction but still achieving the desired level of void content.

- **Chapter 6 - Investigation into engineering properties of SFC materials incorporating geopolymer grouts and RAP aggregates**
  Based on the mix design formulated in Chapter 4 and open-graded RAP with various levels of solid contents in Chapter 5, the physical, mechanical and microstructural properties of SFC specimens were assessed in this chapter. Effects of geopolymer grout mixes and RAP contents on the performance of SFC materials were investigated based on experiments including permeable porosity, compressive strength and ultrasonic pulse velocity. Control specimens consisting of Portland cement and basalt aggregates were also prepared and tested for comparative purposes. A preliminary methodology to predict elastic modulus of SFC material was established based on its ultrasonic pulse velocity and compressive strength values. Examples of thickness design for SFC considered as base course were presented based on a simplified analytical pavement design approach presented by Williams (1986) and (British In-Situ Concrete Paving Association, 2007). Costs of raw materials and greenhouse gas assessments were then undertaken on SFC base courses to evaluate economic viability and environmental performance.

- **Chapter 7 - Characterisation of SFC surface course subjected to accelerated trafficking action**
  In this chapter, trafficking-related properties of SFC as an innovative surface course were evaluated using standard experimental and close-range photogrammetry methods. Different surface texturing methods including surface dressing, brushed surface and exposed-aggregate finishes were examined to assess the most suitable method for enhancing friction properties of SFC pavements. SFC pavements with the most promising surface finish type were then progressed to consider effects of geopolymer grout types on SFC performances under accelerated traffic using road test machine. Parameters including weight loss, mean texture depth, skidding resistance and surface texture were assessed for SFC specimens. Additionally,

virtual 3D models of SFC surface texture were built and the changes due to traffic wear were examined using close-range photogrammetry techniques.

- **Chapter 8 - Discussion**

  The key findings from previous chapters are summarised and discussed in this chapter. The connection between results obtained from this study and current literature is also presented.

- **Chapter 9 - Conclusions**

  A summary of the main findings related to research questions identified in Chapter 1 is presented in this chapter.

- **Chapter 10 - Further recommendations**

  Relevant further research on SFC materials for the delivery of environmentally responsible infrastructure and building systems are recommended in this chapter.

CHAPTER 2

LITERATURE REVIEW

2.1 Introduction

This chapter aims to offer an insight into literature relevant to semi-flexible composite material and its constituents, reclaimed asphalt planings and geopolymer grout. This is required for understanding and establishing the significance of this research in the field of infrastructure construction. Definition and critical evaluation of the aforementioned materials and their typical properties were obtained from a substantial number of studies and summarised to give a clear picture of their mechanical behaviour.

This chapter not only discusses competitive advantages associated with the use of RAP and geopolymer materials in terms of environmental and mechanical performance, but also accesses current barriers to their widespread re-use. Practical applications of geopolymer and SFC materials for motorway, airport runways, aprons, pedestrian and cycle paths in the UK and other countries were also investigated to assess the suitability of SFC as pavement materials. Currently, since there is no specified standard for SFC pavements, general requirements and specifications for traditional asphalt and concrete pavements according to British standards, design manuals, guidelines and codes were reviewed, with a purpose of developing a framework of performance-related specifications for SFC materials.

2.2 Reclaimed asphalt planing

2.2.1 What is RAP?

Reclaimed asphalt planings are generated from road surface removal from existing pavements (Copeland, 2011). Recycling processes include partial or full-depth removal of pavement surfaces, milling and screening to a required size, transporting and stockpiling. It is considered to be one of the most recycled construction materials in Europe, with 76% of RAP content reclaimable back into pavement applications such as hot, warm and cold mix asphalt. Various replacement contents are possible depending on design purposes (European Asphalt Pavement Association, 2018).

2.2.2 Typical properties of RAP

RAP particles contain mainly old natural aggregate covered by an aged bitumen layer and clusters of fine particles. As a result, RAP properties are reported to be significantly influenced by the characteristics of these constituent materials (Chesner et al., 2017; Singh et al., 2017) and can be characterised depending on the RAP origin (e.g. from base or surface courses) and its years of service. However, RAP from different locations may be stored in the same stockpile, leading to high variability in properties (Heneash, 2013). This high variability can be seen in Table 2.1 which presents properties of RAP and natural aggregates including granite, basalt and limestone collected from previous studies along

with requirements for aggregates used in bituminous mixtures obtained from BS EN 13043:2002 (British Standards, 2002).

Table 2.1. Typical properties of natural aggregates and RAP obtained from previous studies and requirements for aggregates used in bituminous mixtures.

Properties	Requirements for aggregates [1]	Natural aggregates from previous studies [2]	RAP from previous studies [3]
Specific gravity (g/cm^3)	-	2.52-2.79	2.29-2.7
Los Angeles coefficient (%)	Maximum of 15-50%	18.8-23.86	19.3-33.6
Aggregate crushing value (%)	Maximum of 18-32%	19.25-20.10	16-22.52
Aggregate impact value (%)	Maximum of 25%	10-22	4.3-15.8
Water absorption (%)	Maximum of 1-2%	0.38-1.64	0.21-2.08
Bitumen content (%)	-	-	3.7-5.8

[1] BS EN 13043:2002 (British Standards, 2002)

[2] (Afonso et al., 2016; Hossiney et al., 2008; Huang et al., 2005; Mishra, 2015; Omranian et al., 2018; Oner and Sengoz, 2015; Taha et al., 2002; Tahmoorian et al., 2017)

[3] (Afonso et al., 2016; Horpibulsuk et al., 2017; Hossiney et al., 2008; Mishra, 2015; Pradyumna et al., 2013; Shadmani et al., 2018; Singh et al., 2017; Taha et al., 2002; Tahmoorian et al., 2017)

As presented in Table 2.1, compared to natural aggregates, RAP generally exhibits lower abrasion resistance and strength, corresponding to higher Los Angeles coefficients and aggregate crushing values. Bitumen in asphalt mixtures contains mainly asphaltenes, aromatics and saturates, which determine its rheological, adhesive and age hardening properties (Heneash, 2013). Compared to newly mixed asphalt mixtures with 5-7% bitumen by mass (Heneash, 2013), the bitumen content of RAP particles is lower (3.7-5.8%) due to loss of bitumen from fractionation and recycling processes. The bitumen layer coating RAP particles has been found to be stiffer than new bitumen from asphalt mixtures because of a reduction of volatile substances from oxidation during years of service (Singh et al., 2017). After recovery by centrifuge methods in a study by Pradyumna et al. (2013), aged bitumen from RAP possessed reduced penetration of 39 (x 0.1 mm) and higher softening point of 62^{o}C compared to new bitumen (VG-30) control specimens with comparative values of 64 (x 0.1 mm) and 48^{o}C respectively.

Clusters of fine particles in RAP were reported to contain a large amount of mineral fillers with original sizes of 50-75 μm (Heneash, 2013). Singh et al. (2017) used attrition and abrasion methods involving rotating RAP aggregates with fifteen steel balls (4.5 mm diameter, 380 g each) for 20 minutes in a tilting drum mixer to remove these fine particle clusters. After treatment by attrition and abrasion methods, the RAP fine particle content reduced by about 77% by mass. Results showed that treated RAP possessed improved properties with lower Los Angeles abrasion value of 16.3% and water absorption rate of 0.45% compared to the original RAP with comparable values of 19.3 and 1.83% respectively.

2.2.3 The use of RAP in pavement applications

Recycling RAP has drawn significant attention from researchers and scientists because of its environmental and economic benefits. The use of RAP as an alternative to natural aggregate has been proven to reduce up to 30% overall construction cost and 50% of construction wastes sent to landfills (Alam et al., 2010; Mishra, 2015).

RAP is usually used in new blends with other materials such as crushed rocks and recycled concrete aggregate (RCA) for base and sub-base layers. Arulrajah et al. (2014) proposed the sustainable usage of 15-100% RAP blended with RCA as materials for sub-base layer of pavements. The blend 15% RAP/85% RCA exhibited a moisture content range of 59- 83%, which met requirements for local highways in Australia for sub-base layer materials. In contrast, California bearing ratio of the blend containing 35-66% RAP was lower than the minimum of 80% required for sub-base materials established by the local highway authority. Freire et al. (2013) investigated the use of RAP, RCA and limestone for unbound granular base in the South of Lisbon, Portugal. Results from falling weight deflectometer testing showed that blending 70% crushed limestone with 30% RAP (by volume) attained similar stiffness values compared to 100% crushed limestone. A similar finding was observed in Mishra's study (Mishra, 2015) where 30% RAP substituting for natural aggregates was successfully employed in a base course of flexible pavement in India. The author also stated that RAP could be fully utilised as natural aggregate replacement for sub-base layer.

Although blending of RAP and virgin aggregate has proved the possibility of using RAP as aggregate substitutions in pavements, the percentage of RAP replacement was limited to a maximum of 30% by mass. Therefore, in order to completely replace coarse aggregates by RAP and improve performance, other studies focused on the use of Portland cement or geopolymer materials to stabilise RAP mixtures for sub-base and base courses of

pavements. Puppala et al. (2011) added 2% to 4% by mass of Portland cement dosage (types I/II) in RAP to enhance its properties such as resilient modulus determined by repeated load triaxial test following Texas Department of Transportation specifications. Cement-stabilised RAP mixtures were proven to be effective in improving resilient modulus of base course to maximum 50% compared to that of mixtures without cement. In another paper written by the same authors (Hoyos et al., 2011), RAP was stabilised by higher dosage levels of cement (2- 6% by total mass of solid content) and alkali-resistant glass fibres. Results from leachate, permeability and unconfined compression tests confirmed the possibility of using cement-stabilised RAP with glass fibres for base and subbase layers.

Hoy et al. (2018) studied the feasibility of using RAP in slag-based geopolymer to stabilise the sub-base and base courses of pavements in Thailand. The geopolymer material consisted of ground granulated blast furnace slag and alkaline activator with a $NaOH/Na_2SiO_3$ ratio of 1.5. Results from 7-day unconfined compressive test indicated the strength of mixtures containing RAP and 20% slag-based geopolymer could be used as base materials since its strength of 2.6 MPa met the requirements for base layer of low and high volume roads (UCS > 1.7 and 2.4 MPa respectively). The same authors also studied the feasibility of using mixtures containing RAP and fly ash-based geopolymer as road materials. Unconfined compressive strength of RAP stabilised with fly ash based-geopolymer after 7-day curing at 40^{o}C ranged from 3.6 MPa to 5.4 MPa, which complied with the requirements for base course of high-volume roads in Thailand (minimum UCS of 2.4 MPa).

Besides its potential use as sub-base and base materials, RAP has been used to partially replace virgin coarse aggregate in hot mix asphalt mixtures in surface courses to reduce the demand for natural resources. It was found that up to 3% by mass of the required bitumen content could be reduced by substitution of 50% (by mass) of RAP, since a substantial amount of bitumen coating the RAP particles could be recovered during the asphalt heating stage (Lavin, 2003). Fattah et al. (2017) investigated the use of RAP along with crushed quartz and limestone dust for surface layers of asphalt pavements. Indirect tensile strength and elastic modulus of specimens containing up to 25% (by mass) of RAP as replacement of crushed quartz aggregates reached nearly 1.2 MPa and 29 GPa respectively, which complied with the requirements for surface course in Iraq. Ogundipe (2020) conducted Marshall stability tests to investigate the incorporation of 20-100% (by mass) of RAP as alternatives to natural aggregates into asphalt mixture with 6.6% bitumen for pavement surface layers. Asphalt mixtures containing RAP achieved Marshall stability of 7.5-12.3 kN,

which satisfied specifications for surface layers in Nigeria (stability > 3.5 kN). The optimum percentage of RAP in asphalt concrete for surface layers of trunk road types A, B and C in Nigeria was 60% by total mass of aggregates. Trunk road type A is defined for federal roads such as dual carriages or major highways while local or town roads are considered as trunk road types B and C (O. Olubomehin, 2016).

In the UK, RAP can be used as a constituent material for asphalt mixtures after being tested to examine its compliance with the particular requirements for pavements (British Standards, 2016). According to MCHW Series 900, Clause 902 (MCHW Series 900, 2019), RAP with a maximum amount of 10% by mass is allowed for surface layers of motorways, while maximum allowable RAP contents for binder and base courses is 25%. Additional tests such as penetration of recovered binder from the RAP and indirect tensile stiffness modulus tests are required if mixtures contain higher amounts of RAP.

In 2019, a section of the M25 located between Junctions 25 and 26 was resurfaced with high RAP content (50% by total mass of aggregates) by FM Conway. Approximately 260 tonnes of asphalt mixture containing RAP, virgin aggregates and a specialised polymer modified binder were laid to a 45 mm thick surface layer. Testing results of 24 core specimens proved that the material satisfied all requirements for conventional surfacing materials, while reducing negative environmental impacts. RAP with the same content also had been used previously in the surface courses of trunk roads A40 and A1 in London by the same company. According to published project report number PPR468 by TRL Ltd (Wayman and Carswell, 2010), a section of the M25 was previously resurfaced with an asphalt mixture containing 23% RAP in 2007. Higher content of RAP (40% by total mass of aggregates) was employed for surfacing materials in a section of the M25 between Junctions 6 and 7 in 2009 by Tarmac. Compared to asphalt mixture with 100% virgin aggregate, the use of 40% RAP in the surface layer of the M25 was reported to reduce approximately 21.5% of carbon dioxide emission and save 134 GJ of energy (Wayman and Carswell, 2010).

2.2.4 Challenges of the use of RAP in pavement applications

Despite efforts to increase recycling contents in pavement applications, RAP has only been used as a partial replacement for natural coarse aggregates due to uncertainty of long-term performance levels (Al-Mufti and Fried, 2018; Hossiney et al., 2008; Lavin, 2003; Sultan and Guo, 2016). In addition, the composition and quality of RAP varies substantially depending on sources, making its widespread use challenging. According to Copeland (2011), if RAP is obtained from known sources with construction records in a project, some of the

properties (i.e. bulk specific gravity) can be considered the same as the original aggregate used in that project. Otherwise, it is referred to as unclassified RAP requiring further processing and testing to be re-used in pavements. Additionally, the surface of RAP particles might include an external thin-film of aged bitumen, which is reported to impact its performance (Chesner et al., 2017). Also, recycling processes including milling, crushing, screening, transporting and packing were reported to affect the physical and mechanical properties of RAP. As such, a limitation of 0 to 25% by mass is applied as the permissible level of substituting for natural aggregate in asphalt pavement layers in the UK (MCHW Series 900, 2019). Based on published industry data (European Asphalt Pavement Association, 2018), the UK had 6.1 million tonnes of RAP production in 2018, from which only 30% was re-used in hot and warm mix asphalt production. The remaining percentage of RAP was either recycled in other construction applications or sent to landfill.

Some studies attempted to use higher RAP contents (> 25%) for rigid pavements, which led to declining performance levels. Hossiney et al. (2008) introduced the use of up to 40% of RAP by mass of total aggregates in concrete mixtures for rigid pavements. RAP mixed with porous limestone was considered as coarse aggregate in concrete mixtures with a water-to-cement ratio of 0.53. Concrete properties such as elastic modulus, flexural strength, splitting tensile strength and compressive strength all reduced with increasing RAP content. Compared to conventional concrete, specimens containing 40% RAP exhibited 34% and 28% reductions in compressive and splitting tensile strength respectively. Similar trend of strength reduction occurred in other studies (Huang et al., 2005; Shadmani et al., 2018; Singh et al., 2017) where RAP fully replaced natural aggregates in concrete mixtures. In order to investigate the feasibility of applying high content RAP in asphalt mixtures, Lo Presti et al. (2014) proposed a mix design comprising 100% RAP and rejuvenators, without considering the origin of RAP. A blending model was built to predict the properties of the binders used for specified contents of RAP (0-100%). Two case studies were examined: short-term aged (minimum penetration of 30.4 dmm) RAP without rejuvenators and long-term aged (penetration < 10 mm) with rejuvenator. The study concluded that it was possible to use up to 90% long-term aged RAP with 7% rejuvenating agent for road surfacing material.

Recycling RAP in hot mix asphalt or concrete pavements is not the only challenge of using RAP in pavement applications. Several studies attempted to use high content RAP (> 60% by mass of total aggregates) for cold mix pavement, which in turn lowered its material properties such as stiffness or tensile strength (Afonso et al., 2016; Hugener et al., 2014;

Ojum and Thom, 2017). For this reason, according to the data provided by a report of the European Asphalt Pavement Association (2018), only 5% of a total of 49.5 million tonnes of RAP generated in Europe were used for cold mix asphalt in 2018.

2.3 Geopolymer materials

2.3.1 What is geopolymer?

The word 'geopolymer' usually refers to gels formed through alkaline liquids reacted with silica and alumina contained in aluminosilicate sources. Geopolymer grout can be described as a combination of alkaline activator mixed with high-silica sources such as fly ash, GGBS, silica fume, metakaolin, etc. and water. Incorporation of coarse and/or fine aggregate into this grout, or paste, creates geopolymer concrete.

One of the first geopolymer products patented in 1985 was PYRAMENT cement, which developed high strength soon after being mixed. It was claimed to have the ability to withstand the weight of a commercial plane after six hours of curing (Davidovits, 2018). Geopolymer products including grouts, mortars and concretes have been used in the construction industry as 'green' materials since their uses were reported to reduce a significant amount of the carbon dioxide footprint associated with conventional Portland cement products (Davidovits, 2018). Geopolymers are commonly used in the construction industry for highway repair applications, strengthening, pavement applications such as precast walkway panels, in-situ footpaths, bicycle lanes, as well as airport hard-standings.

2.3.2 Geopolymer components and geopolymerisation mechanism

Geopolymer components

The main components for producing geopolymer paste are solid aluminosilicate precursors and liquid alkaline activators. Depending upon local resources and availability, solid aluminosilicate precursors can be in natural forms such as zeolite, clays, shales and amphibole or in industrial by-products such as fly ash, GGBS, fayalite slag, metakaolin, silica fume, red mud, waste glass and wastes from agricultural activities such as rice hull and husk (Luukkonen et al., 2018). Alkali-metal hydroxide MOH, where M is alkaline metals such as potassium or sodium, and $R_2O(n)SiO_2$ silicate are used separately or in a blend to create alkaline activators (Ryu et al., 2013). Alkaline activators commonly used for geopolymer products can be either sodium hydroxide (NaOH), sodium silicate (Na_2SiO_3), potassium hydroxide (KOH), potassium silicate (K_2SiO_3) or sodium sulfates (Na_2SO_4).

Geopolymerisation mechanism

Geopolymerisation is a process that produces cementitious gel such as $Na_2O.2SiO_2.Al_2O_3.H_2O$ (N-A-S-H) or $K_2O.2SiO_2.Al_2O_3.H_2O$ (K-A-S-H). In comparison, conventional PC forms calcium silicate hydrate $CaO.SiO_2.H_2O$ (C-S-H) through hydration reactions between PC and water (Davidovits, 2016). According to Davidovits (2016), the geopolymerisation mechanism follows six stages: alkalination, depolymerisation of silicates, gel formation of oligo-sialates, polycondensation, reticulation/networking and geopolymer solidification. This mechanism was simplified in various studies (A.M. Mustafa Al Bakri et al., 2013; Wilkinson, 2017) to three primary phases: dissolution of silica and alumina, condensation of ions and polycondensation of monomers.

According to Görhan et al. (2016), geopolymerisation was described as follows: firstly, silica (SiO_2) and alumina (Al_2O_3) in aluminosilicate precursors are dissolved in alkaline activator in high pH conditions to create geopolymer precursor. Alkaline cations from alkaline solution facilitate the dissolution by increasing pH levels in the mixture (Luukkonen et al., 2018). The second phase involves alumina-silicate gel (Si-O-Al-O) and water formed from the precursor ions (Wilkinson, 2017). Figure 2.1 illustrates the formation schematic of geopolymers (Fitzpatrick-Schmidt et al., 2015). Three-dimensional polymer chains Si-O-Al-O react to Al-Si oxides to create three types of polysialate structures $nM_2O\text{-}Al_2O_3.xSiO_2.yH_2O$, known as 'zeolite precursor', corresponding to three atomic ratios of Si and Al (Figure 2.2) (Garcia-Lodeiro et al., 2015).

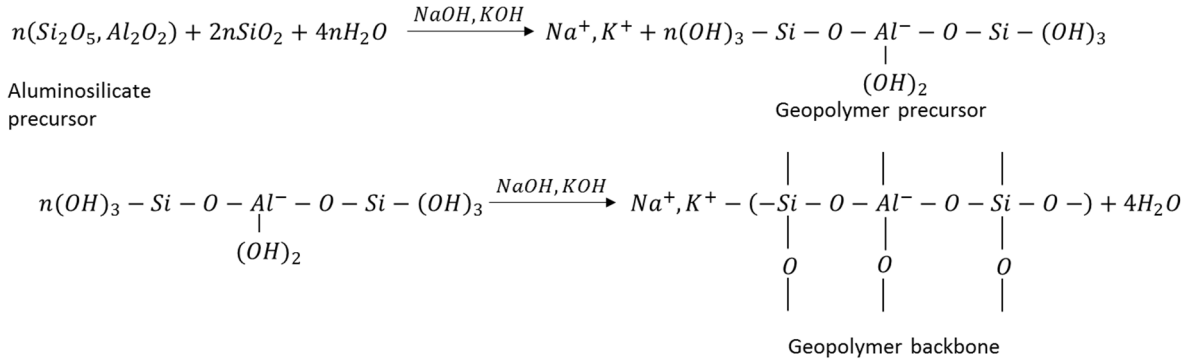

Figure 2.1. Formation schematic of geopolymers (Fitzpatrick-Schmidt et al., 2015).

According to a keynote speech delivered at Geopolymer camp 2018 by Davidovits (Davidovits, 2018), polymeric chains poly(sialate) –Si-O-Al-O, poly(sialate-siloxo) –Si-O-Al-O-Si-O and poly(sialate-disiloxo) –Si-O-Al-O-Si-O-Si-O- have different potential applications. For instance, poly(sialate) and poly(sialate-siloxo) can be used in brick, ceramic, cement

and concrete, while poly(sialate-disiloxo) can be used in foundry equipment and heat resistance composites. Geopolymer gel is hardened through polycondensation of hydrolysed silicate and aluminate species (Ryu et al., 2013). Geopolymerisation is completed with temperature, with requirements ranging from ambient to 90°C for a specified period of time (Görhan et al., 2016).

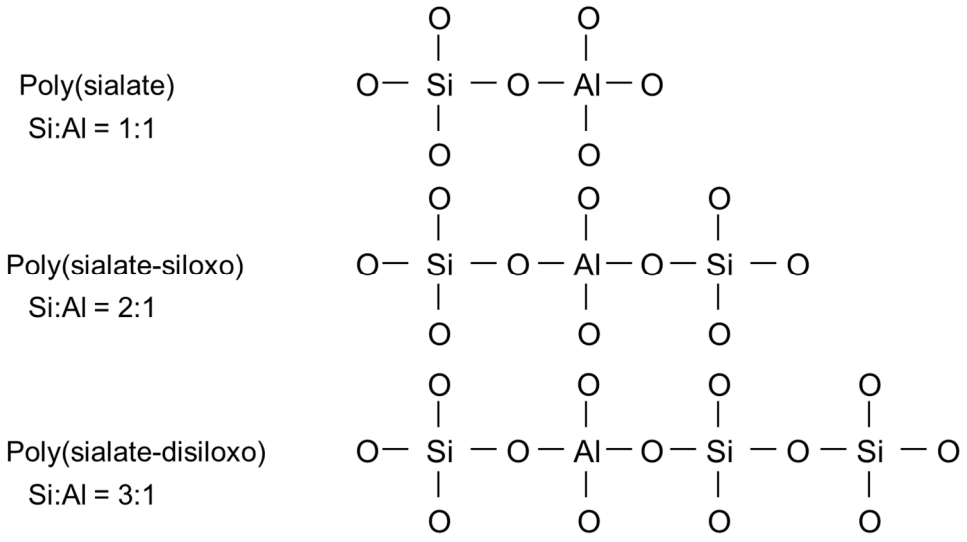

Figure 2.2. Structures of poly(sialate), poly(sialate-siloxo) and poly(sialate-disiloxo) corresponding to Si:Al ratios (Davidovits, 2016).

There is also ongoing debate in the literature around the use of the terminologies 'geopolymer' and 'alkaline-activated material' (AAM). In the current literature, geopolymer and AAM often have been used interchangeably (Luukkonen et al., 2018). AAM is a material sector which covers a broad range of any materials derived from the process of mixing solid silicate powders, such as aluminosilicate precursors or calcium silicate, and alkali metal sources in solid or dissolved states (Provis and Deventer, 2014). Its comprehensive historical review can be found in the study of Provis and Deventer (2014). Geopolymers were claimed as a subset of AAM by Provis and Deventer (2014), whereas Davidovit stated that the two concepts are dissimilar in terms of polymerisation process (Davidovits, 2018). The differences between both terminologies were discussed in detail in Wilkinson's thesis (Wilkinson, 2017). In short, AAM has lower coordination of Si atoms with two bridging oxygens (Q^2) and high calcium content, while geopolymer has higher coordination of Si atoms with four bridging oxygens (Q^4) and low levels of calcium (Luukkonen et al., 2018). In this thesis, the term 'geopolymer' refers to the binders formed

by mixing aluminosilicate precursor and alkaline activator since it is consistent with the determination for geopolymers stated in the study by Provis and Deventer (2014).

2.3.3 Typical properties of geopolymer materials

The properties of fresh and hardened geopolymer materials are equally important for pavement applications. Properties of geopolymer materials vary depending on proportions of the mixture, constituent materials and curing conditions. Table 2.2 shows the typical properties of geopolymer materials and PC obtained from previous studies.

Fresh properties of geopolymer grout such as normal consistency, flow time, yield stress, plastic viscosity and initial/final setting times are essential to the construction process, especially when geopolymers are considered as grouting materials (Güllü et al., 2019). In general, geopolymer grout exhibits a broad range of workability compared to PC grout (see Table 2.2). Normal consistency of geopolymer grout was found to vary by about 26 to 39% depending on mixture proportions and concentration of sodium hydroxide activator, which is similar to that of PC (Samantasinghar and Singh, 2019). According to Samantasinghar and Singh (2019), initial and final setting times of geopolymer grout containing various content percentages of GGBS and FA and sodium hydroxide concentration (2-16 M) varied from 25-300 minutes and 40-490 minutes respectively. Fluidity of geopolymer grout can be identified by Marsh cone and rheometer tests. Compared to conventional PC grout, geopolymer grout was typically found to exhibit lower flow times (16-462 s), yield stress (0.97-62.1 Pa) and plastic viscosity (0.0055-0.29 Pa.s).

Types of geopolymer powder play a vital role in the consistency, setting time and fluidity of geopolymer grout. Normal consistency of grout was reported to decrease with an increase in GGBS content, while its setting time was shortened since high calcium content in GGBS accelerated the pozzolanic reaction (Al-Majidi et al., 2016; Luukkonen et al., 2018; Samantasinghar and Singh, 2019). In contrast, the presence of FA was reported to prolong setting time. For example, geopolymer grout with a 100% FA binder cured at room temperature exhibited initial setting time of up to 12 hours (Samantasinghar and Singh, 2019). A similar effect of 100% FA in geopolymer grout was observed in the study of Cristelo et al. (2013), where FA was mixed with sodium activators and cured at room temperature. The grout set extremely slowly in the upper part of specimens that actually hardened. In comparison, lower specimen regions remained unset, thereby not enabling accurate setting time testing of the grout using the Vicat needle test. Moreover, the inclusion of FA was reported to enhance grout fluidity due to its spherical particle shape, which made the grout less viscous compared to other precursor powders (e.g. GGBS with

angular shape) (Samantasinghar and Singh, 2019). Güllü et al. (2019) studied the rheological behaviour of geopolymer grout for grouting applications, comprising FA class F (40-100% by total mass of solid precursors), SF and alkaline activator solution with an activator/precursor ratio of 0.4 by weight.

Table 2.2. Typical properties of geopolymer and PC grout/concrete from previous studies.

Properties		PC grout [(1)]	Geopolymer grout [(2)]
Fresh	Normal consistency (%)	26-36	26- 39
	Initial setting time (minutes)	150	25- 300
	Final setting time (minutes)	180-285	40-490
	Flow time (s)	11-144	16-462
	Yield stress (Pa)	0.07-10.8	0.97-62.1
	Plastic viscosity (Pa.s)	0.002-0.03	0.0055-0.29
Mechanical	28-day cylindrical compressive strength (MPa)	< 50	Up to 100
	Strength development	80% after 7 days	84% after 7 days
	28-day flexural strength (MPa)	6.3-8.4	3.1-8.9[(3)]
	Drying shrinkage (microstrain)	520-780	100-1300
	Freeze-thaw resistance	No	0.8-4.2% mass loss after 300 cycles
	Heat resistance	68-100% compressive strength loss after exposed to 500-800^{o}C	58-78% compressive strength loss after exposed to 500-800^{o}C

[(1)] (Afonso et al., 2016; Güllü et al., 2019; Ismail et al., 2011; Zhang et al., 2014)

[(2)] (Azarsa and Gupta, 2020; Cristelo et al., 2013; Davidovits, 1994; Güllü et al., 2019; Luukkonen et al., 2018; Samantasinghar and Singh, 2019; Zhang et al., 2014, 2019, 2018)

[(3)] 7-day flexural strength

Rheological properties such as yield stress and plastic viscosity were obtained within the range 0.97-62.1 Pa and 0.0055-0.29 Pa.s respectively, which were higher than for PC grout. The addition of FA decreased the yield stress and plastic viscosity of the geopolymer grout

where the grout with less than 30% (by mass) of FA was found to behave similarly to the conventional PC.

Liquid-to-solid ratio and the concentration of alkaline solution are reported to play an important role in the workability of grout. Increasing liquid-to-solid ratio, for instance, is reported to reduce the yield stress and plastic viscosity of grout (Güllü et al., 2019). The viscosity of geopolymer grout with highly concentrated sodium hydroxide of 4.0 M was higher than that with sodium hydroxide with 0.5 M as presented in the study by Zhang et al. (2019). This was because the higher the concentration of sodium hydroxide, the faster the leaching reaction; thereby prolonging the viscosity stage.

Geopolymer grout is consistently reported to achieve high strength and to resist freeze-thaw and high temperature conditions (Azarsa and Gupta, 2020; Davidovits, 1994; Luukkonen et al., 2018). Davidovits (1994) introduced a proprietary cement blend called Geopoly® containing kaolinitic clay, SF, alkali-disilicate and calcium disilicates cured at room temperature, which attained 28-day compressive strengths of 70-100 MPa. Compared to conventional cement grout, compressive strength of the geopolymer grout achieved about 80% of its 28-day strength after 7-days of curing. Moreover, 7-day flexural strength of geopolymer grout was observed to vary from 3.1-8.9 MPa, which was within the range of 6.3-8.4 MPa for PC grout aged for 28 days. However, drying shrinkage of geopolymer grout was found to vary from 100-1300 microstrain, which is higher than that of PC grout (Luukkonen et al., 2018). Content levels of powder precursors such as GGBS, FA or MK are known to greatly affect the mechanical properties of geopolymer grout. Fly ash-based geopolymer grout with 100% FA were observed to attain lower compressive strengths compared to grouts with inclusion of GGBS or MK. For example, at ambient temperature, geopolymer grout comprising 50% MK and 50% FA achieved strengths of 58 MPa. This compared to 100% FA grout with a strength of 15 MPa (Zhang et al., 2014). An increase in GGBS content can improve the compressive strength of geopolymer grout. This was proven by Samantasinghar and Singh (2019), where an increase of GGBS content from 0 to 100% led to enhancement in grout strength of up to 33 MPa. Meanwhile, grout containing high portions of GGBS were found to increase the rate of drying shrinkage; up to two times higher than fly-ash based grout. The same authors also discovered that high concentrated alkaline solution reduced the drying shrinkage and improve the compressive strength of geopolymer grout.

In cold climates, geopolymer materials have been confirmed to offer potential benefits in terms of freeze-thaw resistance compared to PC concrete. Azarsa and Gupta (2020)

compared freeze-thaw resistance of fly ash- and bottom ash-based geopolymer concretes. These were steam-cured at 80^{o}C for 24 hours and then subjected to 300 freeze and thaw cycles with temperature and humidity ranging from -17.8-44^{o}C and 10-95% respectively. In comparison to the bottom ash-based concrete (4.2% mass loss and 55% elastic modulus reduction), the fly ash-based geopolymer concrete exhibited higher freeze-thaw tolerance levels (0.8% mass loss and 20% elastic modulus reduction). The authors also concluded that bottom ash-based geopolymer concrete was able to adsorb heavy metals such as Hg, Si, Al, Cu, etc. Geopolymer grout is also reported to offer heat resistance advantages over PC grout. This was proven by Zhang et al. (2014), where the compressive strength of geopolymer grout comprising MK and GGBS dropped by 58% and 78% at 500^{o}C and 800^{o}C respectively, while PC grout lost its entire strength at 800^{o}C.

2.3.4 The use of geopolymer materials in pavement applications

Geopolymer materials comprising either FA or GGBS were considered as potential stabilising materials for the base course of asphalt pavements in several studies (Horpibulsuk et al., 2017; Hoy et al., 2018). Horpibulsuk et al. (2017) confirmed the feasibility of applying geopolymer material for pavement base course since it achieved unconfined compressive strength of approximately 6 MPa. This strength value satisfied the local requirements for base course in Thailand. The leaching of different types of heavy metals, such as copper, lead, zinc, mercury, cadmium and arsenic, into groundwater and soil from this material was found to be below the leaching limit values specified by the United States Environmental Protection Agency (2005).

For use in high-friction surfacing systems, there was an attempt by Wilkinson (2017) to replace calcined bauxite with artificial aggregate made from geopolymer mortar containing GGBS, FA, MK and SF. Even though it appeared that this artificial aggregate possessed lower skid resistance than calcined bauxite aggregates, the blending of 40% artificial geopolymer and 60% calcined bauxite aggregates, by mass, complied with the requirements for type 1 and 2 highways as stated in the HFS guidelines by the British Board of Agrement (2017). The same author also investigated performance of geopolymer mortar as road repair material after subjecting it to simulated trafficking using an accelerated road test machine. The geopolymer mortar showed sufficient durability and skid resistance to traffic wear, but shrinkage cracking occurred on the specimens leading to ultimate strength loss.

In 2015, geopolymer concrete was used for the construction of airport runways and aprons in Toowoomba Wellcamp airport in Sydney, Australia. According to Glasby et al. (2015), this

airport was claimed to be the largest project using geopolymer concrete in the world in terms of material quantity. About 100 thousand tonnes of geopolymer concrete were used as surfacing material for 435 mm thick heavy-duty pavements in the airport. Used below the unreinforced pavement layer was a 200 mm thick base course made from cement treated crushed rocks and a 150 mm thick capping layer. The geopolymer concrete used in this airport was introduced by Wagners company. It comprised GGBS and FA with water-to-binder ratio of 0.41, chemical activator, admixture and aggregate with maximum size of 40 mm. It was claimed to possess high flexural strength (4.8 MPa) and low shrinkage (450 microstrain) and its use was reported to reduce over 8500 tonnes of carbon dioxide compared to conventional concrete. Another example of a project that replaced PC concrete with geopolymer concrete was a path for cyclists and pedestrians in New Zealand (Concrete Institute of Australia, 2011). Each geopolymer slab, with length and width 12 and 1.5 m respectively, showed no visually detectable shrinkage cracks or damage compared to conventional PC slabs, which showed cracks at every 3 m.

2.3.5 Carbon dioxide emission of geopolymer materials

Emission of carbon dioxide, one of the primary greenhouse gases, has emerged as a serious problem that dramatically affects global climate change. In 2019, carbon dioxide emission was 351.5 million tonnes in the UK, which was 41% lower than that in 1990 thanks to renewable energy sources replacing coal and fossil fuels (National Statistics, 2019). Still, this number was substantially lower than the target for carbon dioxide reduction of 80% by 2050 specified by the Climate Change Act (UK Public General Acts, 2008), equating to approximately 158.8 million tonnes of carbon dioxide reduction. The carbon emission rate in the UK in 2019 also fell short of the target of 331.6 million tonnes CO_2 set by the Department of Energy and Climate Change (2015).

According to National Statistics (2019), CO_2 emission was caused by various sectors including transport (34%), energy supply (26%), residential (19%), businesses (18%), industrial processes and agriculture. Calcining limestone in the production of PC based on the reaction below is reported to be responsible for a large amount of CO_2 emission, with up to 8% of CO_2 emission globally (Farfan et al., 2019).

$$5CaCO_3 + 2SiO_2 \rightarrow (3CaO, SiO_2)(2CaO, SiO_2) + 5CO_2$$

One tonne of PC was claimed to produce up to one tonne of CO_2, which was a summation of 0.55 tonne of CO_2 derived directly from the aforementioned reaction and 0.4 tonne of CO_2 emitted from the combustion of fuel to maintain the kiln temperature of about 1480^{o}C

(Davidovits, 1994). The Mineral Products Association (2011) reported reducing the carbon footprint rate to 0.72 tonne of CO_2 generated from one tonne of PC. This was achieved by partial replacement of virgin fuel by wastes from other industries such as scrap tyres, sewage sludge, meat and bone wastes, etc. Manufacture of PC in the UK was reported to be about 9.4 million tonnes in 2017 by National Statistics (2018), corresponding to about 6.8 million tonnes of CO_2. This number was approximately 70% of the CO_2 emission from the industrial processes sector in the UK in 2019 (9.7 million tonnes) (National Statistics, 2019).

The manufacture of geopolymer material was reported to cut carbon footprint relative to the production of conventional PC by 90% (Davidovits, 1994). For every 100 g of CO_2 emitted from the manufacturing process, up to 358 g and 3365 g of PC and geopolymer cement were produced respectively. This means geopolymer manufacture was able to provide about 10 times more cement than PC with the same amount of CO_2 emission.

2.3.6 Challenges of the use of geopolymer materials

Despite its positive environmental implications and performance properties, practical employment of geopolymer materials for pavement applications is still limited since its introduction in 1984. This is due to several primary reasons. The first reason is the absence of applicable standards and specifications for geopolymer materials used in infrastructure construction. The Design Manual For Roads And Bridges (2016) - Volume 7: Section 5 specifies Portland cement, with or without the inclusion of FA and GGBS, as the material to be used for concrete surfacing. In addition, according to the standard for properties and manufacturing process of concrete, BS EN 206-2013 A1: 2016 (British Standards, 2013a), constituent materials for concrete must contain Portland cement. This standard defined the term ‘concrete’ as a combination of basic constituents such as PC, water and aggregates that develop its strength from cement hydration reactions. This definition was also applied in other standards for mechanical testing of concrete materials including compression, tensile and flexural tests (British Standards, 2019a, 2009, 2006, 2004). Even though this is not the definition for geopolymer concrete, the vast majority of researchers are still performing testing for geopolymer materials based on the standards for PC materials (Concrete Institute of Australia, 2011).

The inconsistent reactivity of alumina-silicate precursors was reported to account for the difficulty of standardising geopolymer materials (Davidovits, 2018). For example, physical and chemical properties of FA and GGBS were considered to be variable depending on its sources, collection techniques and storage conditions (Department of Energy and Climate

Change, 2017; Gunasekara, 2016). Gunasekara,(2016) investigated the behaviour of geopolymer concrete incorporating different types of FA collected from power plants across Australia. These types of FA possessed varying chemical components such as SiO_2 (49.9-73.1%), Al_2O_3 (21.5-31.4%) and loss of ignition (0.4-1.3%), which satisfied the requirements of AS 3582.1-1998 (Standards Australia, 1998). Results showed that the compressive strength of geopolymer concrete cured at 80^{o}C after 28 days widely ranged from 17.1-60.6 MPa due to the differences in chemical composition and particle sizes of FA.

Based on the findings yielded from a literature search, long-term performance of geopolymer materials in pavement applications appears to remain unknown. In contrast, long-term behaviour of traditional pavement materials, such as asphalt, has been widely studied. In a report by the Transport Research Laboratory (Nunn et al., 1997), the design life for heavily trafficked asphalt pavement is 40 years, determined based on long-term performance and construction costs of the pavement. Meanwhile, the longest period of time in which the long-term behaviour of geopolymer materials, such as compressive strength, stiffness, tensile strength and permeability, were investigated was 540 days (Wardhono et al., 2017).

Drying shrinkage concerns associated with geopolymer concrete were raised by several researchers (Collins and Sanjayan, 2000; Duran Atiş et al., 2009), given that it showed 3-6 times higher shrinkage rates than PC concrete. This matter was also addressed in the study by Wilkinson (2017), where geopolymer mortar was used as rapid road repair materials.

Another challenge for the widespread implementation of geopolymer materials is the long-term availability of aluminosilicate precursor materials (i.e. FA, GGBS). According to the Department of Energy and Climate Change (2017), the supply of FA was reported to be unpredictable during the year since it depended on the demand for electricity, while the availability of GGBS relied on the scale of pig iron production.

2.4 Semi-flexible composite pavement

Generally referred to as semi-flexible composite pavements (Bonicelli et al., 2019; Kowalski et al., 2016; Qingjun et al., 2015), semi-flexible concrete asphalt (Densit, 2018a), cementitious grouted macadam (Luo et al., 2018; Ricci, 2012), heavy duty macadam or resin-modified pavement (Anderton, 2000), this type of pavement was presented for the first time in the 1950s in France and used in the UK since the mid-1960s (Afonso et al., 2016; Road Surface Treatment Association, 2014). SFC pavements comprise cementitious grout filling open-graded aggregate skeletons with high air void contents.

2.4.1 Open-graded aggregate skeleton

Open-graded aggregate skeletons for SFC pavements comprise mainly coarse aggregates and binders, with the rigid skeletal structure having a high air void content ranging from 25-35% by volume (Oliveira, 2006). This void range is selected so that cementitious grouts can easily infiltrate into the aggregate skeleton (Oliveira, 2006). Since there is no specific technical standard developed for SFC pavement, physical and mechanical properties of aggregates were deemed to follow the specifications provided by researchers or the manufacturers (Oliveira, 2006).

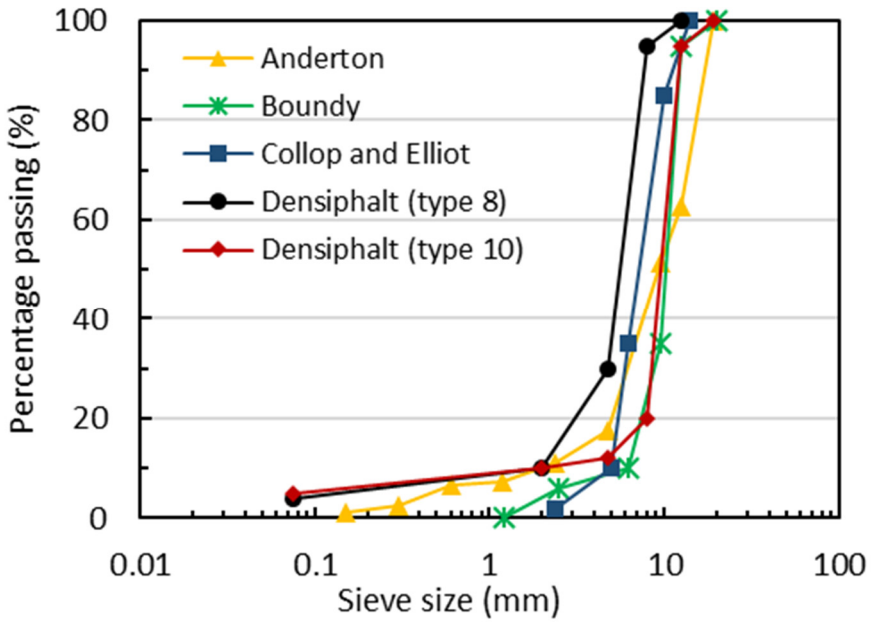

Figure 2.3. Gradation of aggregates used for SFC pavements obtained from previous studies (Collop and Elliott, 1999; Densit, 2018a).

Table 2.3 and Figure 2.3 present recommended properties and gradation for aggregates used in SFC pavements from previous studies. In general, aggregate size should be within the range 4.75-14 mm. Aggregates should be free of attached fine particles, low porosity with maximum water absorption of 2% by volume and strong enough for use as the main aggregates in pavement with LA coefficient less than 40% by volume (Anderton, 2000). A 10 mm nominal size crushed aggregate was used in some studies (Collop and Elliott, 1999; Ricci, 2012) to offer a uniform gradation.

Bitumen is normally used as a binder in aggregate skeletons, with suggested grades and contents presented in Table 2.4. Bitumen contents ranging from 3.4-4.6% by mass with penetration values varying from 40-200 pen were used for open-graded asphalt (Afonso et

al., 2016; Anderton, 2000; Collop and Elliott, 1999; Densit, 2018a). Anderton (2000) produced open-graded aggregate skeletons by heating limestone aggregates and 3.8% by mass bituminous asphalt cement to 135^{o}C to achieve 30% air void content. The bituminous asphalt cement grade AC-20 had penetration at 25^{o}C of 89 in units of 0.1 mm and viscosity of 2155 poises at 60^{o}C. Optional fillers such as hydrated lime, ground limestone or Portland cement can be added to increase adhesion of binder and aggregate in open graded asphalt mixtures (Australian Asphalt Pavement Association, 1997). Open-graded asphalt with void contents of 27% by volume and 3% by mass hydrated lime filler developed by Koting et al. (2007) was reported to achieve stiffness modulus of 2.7 GPa and compressive strength of 1.4 MPa.

Table 2.3. Recommendation for physical and mechanical properties of aggregates used in SFC pavements obtained from ASTM and previous studies.

Maximum permissible properties	Anderton (2000)	Densit (2018b)
Los Angeles coefficient (%)	40	25
Flat or elongated particles (%)	8	-
Flakiness index (%)	-	25
Apparent specific gravity (g/cm3)	-	2.6
Water absorption (%)	-	2
Sodium sulphate soundness (%)	9	10

Additionally, cold mixtures of open-graded aggregate skeleton were investigated in several studies (Afonso et al., 2016; Pratelli et al., 2018; Setyawan, 2013; Zoorob et al., 2002) where the aggregates were mixed with cationic bituminous emulsion or polymer modified emulsion with 4.6-6.8% content by mass at ambient temperature. Afonso et al. (2016) investigated the possibility of using cold asphalt mixtures for SFC materials. Results showed that the stiffness of SFC with hot mix porous asphalt and cementitious grout was 2.3 times higher than that with cold asphalt mixtures. The author also attempted to replace natural aggregates with RAP in SFC mixtures. The replacement of RAP for granite aggregates in cold SFC mixtures lowered the stiffness by approximately 3.5 times compared to SFC consisting of hot asphalt.

Table 2.4. Recommendation for bitumen grade and content obtained from previous studies.

Previous studies	Penetration grade at 25^{o}C	% by mass
Anderton (2000)	40-100	3.4-4.2
Oliveira (2006)	85-100	3.5-4.6
Collop and Elliott (1999)	200	-
Afonso et al. (2016)	100/150	4.2

2.4.2 Grouting materials

Cementitious grout for SFC is recommended to possess high workability and sufficient strength to easily permeate into the voids of aggregate skeleton as well as withstand trafficked load (Oliveira, 2006). Recommendations for grouting properties are shown in Table 2.5. Since there is no specific standard for SFC pavement grouting material, grout properties are often controlled by the manufacturer. Flowability of the grout after mixing was recommended to be within the range 8-10 s by Anderton (2000). However, this range was lower than commercial grout Densit, with flow times of 10-18 s reported (Oliveira, 2006).

Table 2.5. Recommendation for properties of grouting materials from previous studies.

Previous studies	Anderton (2000)	Densit® (Oliveira, 2006)
Flow time (s)	8-10	10-18
Compressive strength (MPa)	20-23	92-110
Drying shrinkage (microstrain)	-	3,341-5,431
Stiffness modulus (MPa)	-	18,925

As shown in Table 2.5, the compressive strength related to this flow time range was significantly higher than the grouts proposed by Anderton (2000) with higher flowability. Portland cement is considered as the basic constituent of grouting materials, with contents ranging from 34-40% by mass (Anderton, 2000). FA, sand, silica fume, resin grout modifier or superplasticiser could be added in the grout recipe to improve its workability. However, utilising these commercial products or Portland cement increases the cost and demand for cement production, resulting in significant amounts of carbon dioxide emission associated with the pavement construction sector. As such, geopolymer mortar containing waste mud

and sodium silicate activator was introduced as grouting materials for SFC materials to replace PC grout in the study by Afonso et al. (2016). However, this grout exhibited very low flowability (467 s) and high plastic viscosity (1.73 Nmm min), which was considered to be unsuitable for grouting materials.

2.4.3 Properties of semi-flexible pavements

SFC pavements are reported to combine different characteristics from their main constituent materials; namely the rigidity of cementitious grout or flexibility and durability of asphalt (Koting et al., 2007; Setyawan, 2013). More specifically, SFC pavement was considered to possess sufficient load-bearing capacity and resistance to high temperature, fatigue and oil spillage (Setyawan, 2013; Zhang et al., 2016). Table 2.6 presents properties of SFC pavements with hot and cold mixtures of open-graded aggregate skeletons obtained from commercial products Ready to Mix (RTM) and DensitD, as well as from previous studies.

In general, hot mixture SFC pavements with open-graded aggregate skeletons were reported to yield better performance in terms of strength, stiffness, stability and fatigue resistance than cold SFC mixtures. Afonso et al. (2016) investigated the mechanical properties of SFC pavements consisting of hot and cold asphalt mixtures with air void content ranging from 29-32% by volume and Portland cement grout. Results showed that hot mixtures yielded higher indirect tensile stiffness modulus (ITSM) (8.3-14 GPa), compressive strength (7-14.3 MPa) and Marshall stability (28.2-53.9 kN). In comparison, maximum cold mixture results were 5.9 GPa, 4.3 MPa and 29.9 kN respectively.

SFC pavement with hot asphalt mixtures also showed less deformation, with up to 0.2 mm rut depths after being subjected to 10,000 load cycles at 45^{o}C. The performance of SFC material combining porous RAP, milled glass and geopolymer grout as an alternative to PC grout was also investigated in this study. Results showed that SFC pavements with RAP and geopolymer grout exhibited the lowest compressive strength and stiffness (4.3 MPa and 2.1 GPa respectively) compared to conventional hot asphalt mixtures with PC grout.

Anderton (2000) introduced SFC pavements comprising open-graded asphalt concrete with 30% air void volume and resin-modified Portland cement grout. This material attained 2-7 times higher stiffness than typical asphalt concrete when subjected to haversine pulse loading by indirect tensile test at 40^{o}C. Thermal coefficients of this material were comparable to PC concrete and about 2-3 times lower than asphalt mixtures. A similar study (Setyawan, 2003) compared the fatigue behaviour of hot limestone porous asphalt, cold limestone porous asphalt and cold dolomitic limestone asphalt filled with cementitious

grouts containing silica fume using indirect tensile fatigue test at 20°C. Results showed that hot mix SFC pavement required a higher number of load cycles (90,000) to reach fatigue failure than its counterpart containing hot mix porous asphalt.

Table 2.6. Properties of SFC pavements obtained from commercial products (RTM, DensitD) and previous studies.

Properties	SFC pavements			
	Hot mixture of open-graded aggregate skeleton		Cold mixture of open-graded aggregate skeleton	
Indirect tensile strength (MPa)	0.99	Anderton (2000)	3.3	RTM (Pratelli et al., 2018)
Indirect tensile stiffness modulus (GPa)	8.3-14	Afonso et al. (2016)	2.1-5.9	Afonso et al. (2016)
			27.8	RTM (Pratelli et al., 2018)
Indirect tensile fatigue: strain ε (microstrain) and number of load cycles to failure N_f	ε = 69 N_f =90000	Setyawan (2003)	ε = 72- 87 N_f = 28389-88512	Setyawan (2003)
Dynamic elastic modulus (GPa)	8-12	Densit (2018a)	-	-
Compressive strength (MPa)	8-12	Densit (2018a)	22.1	RTM (Pratelli et al., 2018)
	7-14.3	Afonso et al. (2016)	2.6-4.3	Afonso et al. (2016)
Flexural strength (MPa)	1.5	Collop and Elliott (1999)	-	-
Marshall stability (kN)	28.2-53.9	Afonso et al. (2016)	9.9-29.9	Afonso et al. (2016)
Permanent deformation: rut depth in air (mm) after 10,000 cycles of wheel tracker at 45°C	0.1-0.2 mm	Afonso et al. (2016)	0.1-0.3	Afonso et al. (2016)
Wear resistance - $cm^3/50\ cm^2$	7-8	Densit (2018a)	-	-
Slip resistance	50-60	Densit (2018a)	-	-
Freeze-thaw resistance (tensile strength ratio)	0.89	Anderton (2000)	-	-

While it was recognised that SFC pavements with hot mixtures of open-graded aggregate achieved higher strength than cold mixtures, commercial products such as RTM and DensitD are reported to exhibit higher mechanical properties than hot mixtures of SFC developed by researchers. Pratelli et al. (2018) introduced a type of SFC material called Ready to mix, comprising cold mixtures of aggregate, bituminous emulsion (ECL 60-type C60B4) and patented cementitious grout (R2M Flowflex); the later containing cement binder, elastomeric polymers and micro-silica sand. Fatigue properties of the material were investigated using an accelerated pavement testing device comprising a fast-falling weight deflectometer on a trial section of an existing granular subgrade overlaid with a 120 mm thick RTM layer. Laboratory-scale results showed that the RTM exhibited a higher stiffness modulus of 27.8 GPa, which was higher than for hot mix SFC pavements developed by Afonso et al. (2016). On-site testing results confirmed its high load bearing capacity under repeated dynamic loading conditions, with no visible cracks or defects occurring after 60,000 load cycles.

Additionally, DensitD, a commercial product developed by Densiphalt® comprising hot mix porous asphalt with 8/11 mm granite aggregates and high strength cementitious mortar, was reported to possess wear resistance of up to 8 cm^3/50 cm^2 and slip resistance of up to 60 (Densit, 2018b).

2.4.4 Applications of SFC materials

SFC materials are considered to be highly suitable for the surface courses of heavy-duty areas such as bus stops, warehouses, cargo port, distribution centres, car parks and aircraft aprons (Oliveira, 2006). Some real-life practical applications of SFC pavement are 120,000 m^2 of pavement in London Gateway Container Terminal (the UK, 2013), 165,000 m^2 of airport apron in Copenhagen Airport (Denmark, 2000) and 170,000 m^2 of pavement in the port of Rotterdam (Netherland, 2000).

SFC construction processes consist of 30-100 mm thickness hot mix porous asphalt layer laid and lightly compacted over the base layer and impregnated with highly flowable cementitious grout (Afonso et al., 2016). Depending on whether a hot or cold mixture of open-graded asphalt is used, the construction time of SFC pavements can be up to two consecutive days (Pratelli et al., 2018). For hot mix SFC, construction times are usually longer due to a requirement to wait for the porous asphalt layer to cool down before grouting processes commence. In contrast, pavements with cold SFC mixtures could be opened to traffic sooner (Pratelli et al., 2018).

Commercial products such as Densit (Densit, 2018b) and Hardicrete (Boundy, 1979) incorporating single-size open texture aggregate with 25-30% voids by volume and specialised cement mortar were claimed to achieve high load-bearing capacities, rapid installation times and cost reductions compared to asphalt or concrete pavements. For example, considering the same number of labours (maximum of 6 workers) and one asphalt paving machine, the area applied per day of DensitD layer (approximately 1500 m^2) was reported to be similar to asphalt mixtures and higher than lean mix concrete. Plug et al. (2006) investigated the performances of SFC surface courses comprising porous asphalt with polymer modified bitumen and patented STEBO-FLEX grout in terms of indentation, indirect tensile and bending strength. Visual inspection from case studies applied in a transhipment port and container terminal in Rotterdam showed good performance with no visible rutting and cracking on the pavement surface after 2 years in service.

2.5 General requirements for pavements

Since there are currently no British standards for SFC pavements, various standards for asphalt and concrete pavements were adopted in this study to assess its properties and feasibility for pavement surface and base courses. The Manual of Contract Documents for Highway Works MCHW Series 800 (2016) and MCHW Series 900 (2019) are the two main guidance documents for the specification of pavement layers consisting of concrete and bituminous mixtures respectively. MCHW Series 800 (2016) provided general requirements such as aggregate properties, binder constituents, storage and handling, trafficking trials and testing methods for pavement consisting of unbound and cement bound granular mixtures. MCHW Series 900 (2019) contains guidance on the properties of bitumen, aggregates, bituminous mixture and surface finishes required for asphalt pavements. The Design Manual for Roads and Bridges (DMRB): Volume 7-Section 2 (Highways England, 2006a) provides details of mechanical properties of materials for new pavement or existing pavements.

The manual of structural design for heavy-duty pavements published by Interpave (Knapton, 2008) also provides a simplified thickness design method for pavement layers used in ports and other industrial areas. In this guide, finite element modeling integrated in GeoStudio software was employed to represent pavement structures and build the design charts for thickness analysis.

2.5.1 Requirements for base courses

According to DMRB: Volume 7-Section 2 (Highways England, 2006a), the recommended minimum compressive strength classification for SFC base layer is $C_{8/10}$, where the subscript

figures define values for cylinder specimens with a slenderness ratio of two and one and cube specimens. This strength class is relevant as SFC was considered in this study to behave similarly to hydraulically bound material (HBM) in accordance with BS 9227:2019 (British Standards, 2019b).

Table 2.7. General requirements for base layer in pavements.

Properties	Minimum value	Description	Guideline/Standard
Cylindrical compressive strength (MPa)	8	HBM base course	DMRB: Volume 7-Section 2 (Highways England, 2006a)
Cube compressive strength (MPa)	10	CBGM $C_{8/10}$ HDP base course	Knapton (2008)
Stiffness (GPa)	1.8	Asphalt base course containing over 25% RAP	MCHW Series 900 (2019)
Thickness (mm)	150	HBM base course	DMRB: Volume 7-Section 2 (Highways England, 2006a)
	200	Asphalt base course	
	200	CBGM $C_{8/10}$ HDP base course	Knapton (2008)

Constituent materials, production and testing of HBM was suggested to follow established requirements of Clauses 810 to 880 in MCHW Series 800 (MCHW Series 800, 2016). In order to ensure sufficient durability, it was stated in this design manual that HBM thicknesses must be a minimum of 150 mm in all regions in the UK, with the exception of Scotland with a limit of 175 mm. A minimum thickness of 200 mm is required for asphalt base course. This guideline also establishes four classes for foundation courses overlaid on subgrade with CBR of at least 5%, including classes 1, 2, 3 and 4 corresponding with minimum long-term stiffnesses of 0.5, 0.1, 0.2 and 0.4 GPa respectively. Nunn (2004) provided more details about these foundation classes. Minimum stiffness for asphalt base and binder courses containing over 25% RAP by volume with validation by ITSM testing at 20^{o}C in accordance with BS EN 12697-26:2018 (British Standards, 2018a) is required to be 1.8 GPa.

In the manual for HDP structural design (Knapton, 2008), materials used in HDP base layers include CBGM and slag/fly ash bound mixtures. Albeit $C_{8/10}$ CBGM was set to be the standard material for HDP base layers in this manual, if other materials were used for HDP base, material equivalent factors defined by the manual were employed to calculate pavement layer thicknesses. The minimum thickness and cube compressive strength required for HDP base were 200 mm and 10 MPa respectively (Knapton, 2008).

2.5.2 General requirements for surface courses

In terms of general requirements for surface courses made of bituminous and concrete mixtures, CD 236 (Highways England, 2020) and the design manual DMRB: Volume 7-Section 5: Part 1 (Highways England, 2006b) set out minimum values of surface interface related properties such as polished stone value (PSV) and aggregate abrasion value (AAV). Different surfacing finishes such as surface dressing, hot rolled asphalt, high friction surfacing system and thin surface course were considered in this design manual. Table 2.8 is a summary of the requirements for properties of pavement surfaces with or without chippings, high friction surfacing system and exposed aggregate concrete.

The required minimum PSV of 50 and maximum AAV of 14 were applied for pavement surface with or without chippings in various types of road with traffic at design life less than 250 commercial vehicle per lane per day (cv/lane/day). High friction surfacing systems with calcined bauxite aggregate require PSV of at least 70 for roads with high gradients (over 5%), crossing approaches surface and bends with radii less than 500 m. The manual also requires minimum texture depths of 1.5 and 1 mm for general roads with 6/10 mm coarse aggregates and low speed roads consisting of 4/8 mm coarse aggregates with velocity of less than 90 km/h respectively.

Additionally, a minimum skid resistance value (SRV) of 65 is suggested by the British Board of Agrement (2017). According to the guideline for pendulum skid resistance tester (Impact Test Equipment, 2020), minimum SRVs suggested for heavily trafficked roads with traffic less than 2000 vehicles per day and other non-critical locations are 55 and 45 respectively.

CD 236 (Highways England, 2020) (formerly DMRB, volume 7, section 5, Parts 2 (Highways England, 1999)) provides necessary details regarding the construction and testing techniques for different types of bituminous surface treatments (i.e. surface dressing, porous asphalt, thin wearing course, stone mastic, high friction surfacing). DMRB, Volume 7, Section 5, Part 3 (Highways England, 2016) introduces specifications for various types of concrete surfaces including low noise textured, transverse textured and exposed aggregate surfacing finishes. The Road Surface Treatments Association (2017) published a code of

practice for SFC pavements consisting of hot mix porous asphalt and cementitious grout, which considered the construction process of SFC including site layout planning, material preparation and logistics, construction implementation, quality assurance, health and safety procedures.

Table 2.8. Requirements for various types of surface course.

Property	Value	Application fields	Guideline/Standard
PSV	Minimum of 50	Surface course with or without chippings [(1)]	Highways England, (2020)
	Minimum of 70	High friction surfacing system	
SRV	Minimum of 65	High friction surfacing system	British Board of Agrement (2017)
	Minimum of 55	Heavily trafficked road [(2)]	Impact Test Equipment (2020)
	Minimum of 45	Other non-critical locations	
AAV	Maximum of 14	Surface course with chippings [(1)]	Highways England, (2020)
	Maximum of 16	Surface course with exposed aggregate concrete [(1)]	
Texture depth (mm)	Minimum of 1.5	General road with 6/10 mm sized aggregates	
	Minimum of 1	Low speed road (less than 90 km/h) with 4/8 mm sized aggregates	

[(1)] For road with traffic at design life of maximum 250 cv/lane/day

[(2)] For road with traffic less than 2000 vehicles per day

2.5.3 Critical review of literature

Important aspects of the proposed SFC material and its constituents including definitions, typical physical and mechanical properties, environmental performance and current

barriers were assessed in this chapter. Further comprehensive research needs to be conducted based on the critical review of literature below:

- RAP has been used as a partial alternative to conventional coarse aggregates in asphalt pavement layers, with up to 25% by mass in the UK (MCHW Series 900, 2019). Higher RAP contents used in rigid pavements were investigated by several studies (Huang et al., 2005; Shadmani et al., 2018; Singh et al., 2017) in which pavement performance levels were declined. There is a need to investigate the possibility of replacing 100% coarse aggregates by RAP in different pavement structural layers such as base and wearing courses to offer environmental and economic savings.
- Geopolymer material is considered a sustainable replacement of traditional Portland cement-based materials in pavement layers (e.g. base course, wearing course) due to its positive economic and environmental performance.
- The main constituent materials of SFC pavements are hot mixtures of open-graded aggregate skeletons with air void content of 25-35% by volume and high-workability cementitious grout. Cold mixtures of aggregate skeletons consisting of polymer modified or cationic bituminous emulsion were also investigated in the current literature. Hot mixture SFC pavements were found to possess more favourable performance in terms of strength, stability and stiffness than cold SFC mixtures.
- SFC materials are highly suitable for surface courses of heavy-duty areas (e.g. bus stops, distribution centres). Commercial products such as Densit (Densit, 2018b), comprising hot mix aggregate skeletons and specialised cement mortar, were claimed to yield high strength, rapid construction times and cost reduction compared to conventional pavement materials such as concrete and asphalt.
- There are limited studies on geopolymers used as sustainable grouting materials for SFC pavements. Therefore, more comprehensive research is required to better understand the impact of geopolymer grout with a wide range of properties (i.e. strength, flowability) on SFC behaviours.
- The mechanical behaviours and economic and environmental benefits of SFC using RAP and geopolymer grouts needs further investigation to address the possibility of utilising SFC in different pavement applications and develop a preliminary performance-related specifications for SFC materials.

CHAPTER 3

RESEARCH METHODS

3.1 Introduction

This chapter provides insight into the research methods used for the development and investigation of SFC materials consisting of various geopolymer grout mixes and open-graded RAP skeleton with varying levels of solid contents. Details of the experimental programme for investigation of SFC materials are presented in the schematic presented in Figure 3.1.

The experimental programme included two phases. In the first phase, geopolymer grouts were formulated with different mix designs at ambient temperatures while open-graded RAP was prepared by manual and gyratory compaction. Geopolymer grout was characterised in terms of flowability, setting time and compressive strength while open-graded RAP skeleton was characterised based on its void and solid content by volume. In the second phase, SFC material was then produced based on a selection of geopolymer grouts and RAP skeletons obtained from Phase 1. Its properties such as density, permeable porosity, ultrasonic pulse velocity and compressive strength were then evaluated through laboratory-scale testing. Machine learning-assisted numerical method, deep neural network, was employed to predict SFC compressive strength based on experimentally collected data including RAP content, geopolymer properties, SFC curing age and SFC compressive strength.

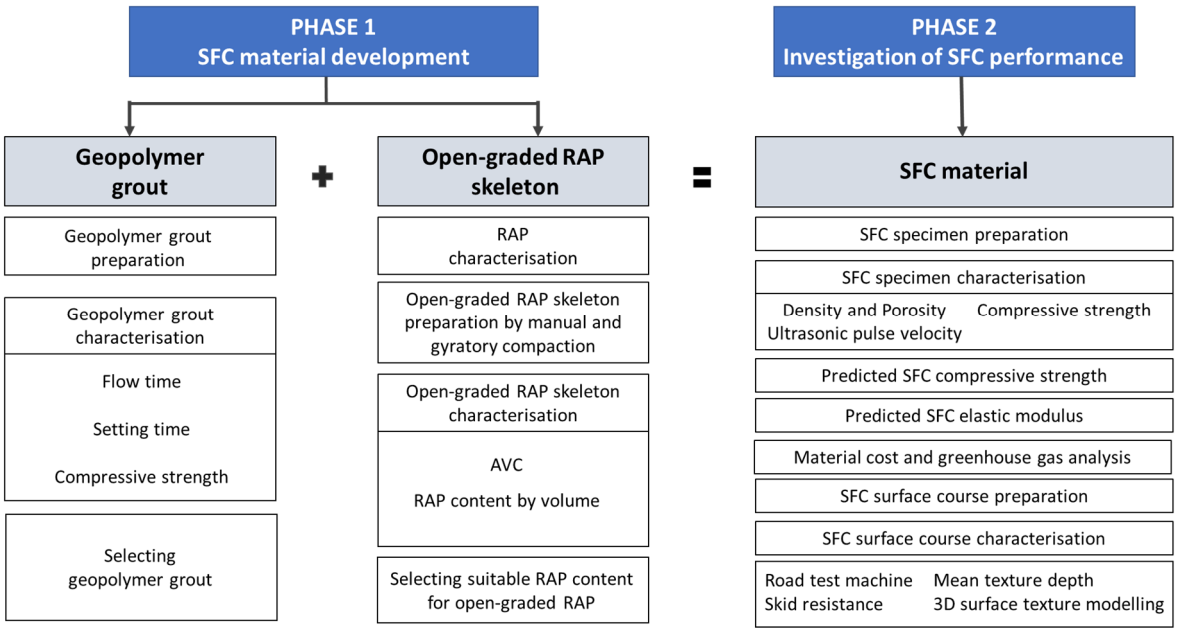

Figure 3.1. Schematic diagram of research methods.

Elastic modulus of SFC specimens was predicted based on theoretical equations extracted from previous studies. Material cost and greenhouse gas analysis were carried out to evaluate the practical implications and environmental performance of the work presented. British pendulum test and sand patch method were carried out to investigate the performances of surface courses made from SFC materials after subjected to simulated trafficking using road test machine. In addition to laboratory testing, the changes in surface textures due to traffic wear were also examined by close-range photogrammetry technique.

3.2 Preparation of geopolymer grouts

For mixtures containing FA and GGBS, potassium alkaline activator solution was added into FA powder and blended together for 10 minutes, including 1-minute to scrape any materials adhering to the sides of the mixing bowl. GGBS was then added and mixed for another 3 minutes at a fast rate of approximately 205 rpm (Hobart Equipment, 2009). The total mixing time was 14 minutes.

For mixtures containing FA, MK, SF and GGBS, all powders excluding GGBS were all dry blended together for 1 minute, then potassium activator liquid was added and mixed at slow speed for 10 minutes, followed by 1 minute of scraping materials from the sides of the mixing bowl. The mixture was mixed for another 5 minutes. GGBS was then added in the mixture and mixed for another 3 minutes at fast speed before casting. Total mixing time was 20 minutes. These mixtures required longer mixing time than mixtures containing GGBS and FA (13 minutes) stated in a previous study by Al-Majidi et al. (2016) because the mixtures investigated in this study had a tendency to form lumps when the mixing time was less than 10 minutes.

3.3 Geopolymer grout characterisation

3.3.1 Flow time test

Determined by measuring the time taken for 1200 ml of grout to flow through a Marsh flow cone apparatus with an internal orifice diameter of 12.7 mm (see Figure 3.2), geopolymer grout flowability was assessed according to ASTM C939-02 (2010).
This test has been commonly used by many researchers (Afonso et al., 2016; Anderton, 2000; Cai et al., 2019; Mohammed et al., 2014; Ricci, 2012; Zhang et al., 2016) because of its simplicity and effectiveness to obtain fluidity of cementitious grout or mortar.

Before testing with geopolymer grout, 1750 ml of water was drained through the flow cone with a recorded flow time of 8.1 s for calibration as prescribed in ASTM C939-02 (2010). For

the grout samples, a reduced volume of 1200 ml was poured into the flow cone while the orifice was blocked. The flow time was recorded from the time the orifice was released to the time the grout completely flowed through the testing cone. It should be noted that grout fluidity was reported as being 'ideal' for times in the range of 8-35 seconds, albeit that the standard considered grout volumes of 1750 ml. The testing amount of the grout was reduced in this study as some grout samples exhibited very slow flow rates and fast setting times. As such, should the standard volume of 1750 ml have been used, selective grout samples may have hardened inside the testing cone prior to complete discharge.

Figure 3.2. Flow cone (D is internal diameter).

3.3.2 Setting time test

Initial and final setting time of geopolymer grout was assessed by observing Vicat needle penetration according to BS EN 480-2:2006 (British Standards, 2006) (see Figure 3.3). Given geopolymer grout's tendency to set more quickly than conventional Portland cement grout, measurements in this study were recorded every 3-10 minutes instead of 10 minutes as stated in the standard to improve accuracy levels. Recorded values were the mean of three separate samples of fresh geopolymer grouts tested at room temperature (approximately 20^{o}C). Initial setting time was recorded from the time alkali activator liquid was added into the mix to the time the Vicat needle could not penetrate to a depth of approximately 4 mm

from the bottom of the truncated cone (Al-Majidi et al., 2016). Time recording then continued until the grout completely hardened to a point where it completely resisted needle penetration. This time was considered as final setting time.

Figure 3.3. Vicat needle apparatus.

3.3.3 Compressive strength testing

Compressive strength of geopolymer grouts at 28 days was measured using 50 mm cubes according to BS EN 1015:11:1999 (British standards, 1999). Fresh grout was poured into steel moulds with release agent coating inside surfaces to prevent the grout from sticking to the mould. Grout cubes were demoulded after 24 hours. Specimens were covered with polyethylene sheets and stored at room temperature for further test. Geopolymer grout cubes were tested using an ELE ADR Touch Control compression tester after 28 curing days (see Figure 3.4).

The platens of the compression machine were cleaned, and specimens placed into the centre of the lower platen. Maximum load at failure (F) for each cube was recorded to the nearest 0.1 kN. Compressive strength of testing cubes f_{cu} was calculated based on BS EN 12390-3:2019 (British Standards, 2019a) using the following equation:

$$f_{cu} = \frac{F}{A_c} \tag{3.1}$$

where: f_{cu} is the compressive strength of testing cubes (MPa); F is the maximum load at failure (kN); and A_c is the cross-sectional area of cubes (mm^2).

Figure 3.4. ELE ADR Touch Control compression tester.

3.3.4 Selecting geopolymer grout

Geopolymer grout properties including flowability, initial setting time and compressive strength were classified into different groups. Several grout mixes were then selected based on their contrasting performance for assessing their suitability as SFC grouting materials.

3.4 Preparation of open-graded RAP skeleton

3.4.1 Aggregate properties

A wide range of tests, including water absorption, moisture content and aggregate impact values were performed to assist in the determination of coarse aggregate properties for SFC materials. RAP and basalt aggregates were used as the aggregate constituent for SFC and control specimens respectively. RAP was crushed by a jaw crusher and graded into different sizes according to BS EN 933-1:2012 (British Standards, 2012a). All tests were performed at room temperature.

Aggregate density

Tests to determine bulk density were conducted according to BS EN 1097-3:1998 (British Standards, 1998), while apparent particle density and water absorption were determined based on BS 1097-6:2013 (British Standards, 2013b). RAPs with different particle sizes including 8/10 and 10/14 mm were immersed in water for 24 hours and surface-dried by a cloth to determine surface-dried mass. Next, mass underwater was recorded and RAP was dried in the oven at 110 ± 5^{o}C until constant mass was reached.

Moisture content

Moisture content of RAP and basalt aggregates was determined by oven-drying method following BS 812-109:1990 (British Standards, 1990a).

Aggregate impact values

Aggregate impact value (AIV) is the resistance of aggregate to sudden impact. AIV of RAP and basalt aggregates was determined in a dry condition based on BS 812-112:1990 (British Standards, 1990a). Aggregates with various particle sizes were dried in the oven for approximately 2 hours at 110 ± 5^{o}C and cooled down at room temperature. Loads in the form of 15 blows from a falling hammer at a height of approximately 380 mm were applied to dry aggregate particles by impact test machine. AIV of aggregates was determine by the following equation:

$$AIV = \frac{100M_2}{M_1} \tag{3.2}$$

where M_1 is the initial mass of oven-dried particles, M_2 is the mass of fine particles passing 2.36 mm sieve.

Soluble binder content of RAP

Soluble binder of RAP particles can be extracted by various methods such as ignition method (Copeland, 2011) or chemical solvents such as perchloroethylene (British Standards, 2012b), methylene chloride (Manolis, 2017) or turpentine with the aid of pressure (Tran, 2014). In this study, turpentine was used to dissolve aged bitumen layer covered RAP particles following the procedure described in Binh Tran's thesis without the aid of pressure (Tran, 2014) to simplify the process of identifying soluble binder content of RAP.

RAP particles with known weight (M_{BT}) were immersed in turpentine for at least 24 hours then drained through 75 µm sieve to discard the bitumen that dissolved in turpentine. The remaining particles on the sieve were then dried at room temperature and weighed to determine the change in weight (M_{AT}). Percentage of soluble binder content of RAP particles (SBC) was determined as bellows:

$$SBC\ (\%) = \frac{100(M_{BT} - M_{AT})}{M_{BT}} \tag{3.3}$$

3.4.2 Preparation of compacted RAP by gyratory compactor

Gyratory compaction method was achieved by applying simultaneously low-static compression and shear stress to specimens (Li et al., 2015). RAPs with different particle sizes were compacted either at room temperature or after being oven-heated at 100°C for 90 minutes by a gyratory compactor (as shown in Figure 3.5) with the number of gyrations ranging from 0-150 cycles based on BS EN 12697-31-2019 (British Standards, 2018b). RAPs were compacted in 100 mm diameter perforated cylindrical moulds under compaction pressure of 600 kPa at gyration angle of 1.25 degrees (Thapa, 2015). The height of specimens were recorded automatically after each gyration cycle during compaction process and they were used to calculate density and air void content of the compacted mixtures.

Figure 3.5. Gyratory compactor.

3.4.3 Preparation of compacted RAP by manual compaction

In order to define the feasibility of reducing compaction effort needed to achieve desired compaction levels mentioned in Chapter 5, RAPs were compacted by hand using a steel roller at room temperature following BS EN 12697-33 2013 (British Standards, 2013c) (see Figure 3.6). A thin layer of mould release oil was applied onto the inner surface of a mould before it was filled with RAPs with known weight in three layers. Each layer was tamped lightly with 25 strokes by a tamping rod to evenly spread the particles over the surface before the compaction process. RAPs were then compacted by a hand-driven steel roller with continuous forward-backwards motion until a required height was reached. This height was specified as the height of the mould used to compact the RAP according to requirements of the test (50 and 100 mm for slabs and cubes respectively).

Figure 3.6. Compacted RAPs by hand driven roller.

3.5 Preparation of SFC specimens

After suitable geopolymer grout mixes and RAP content were determined in chapters 4 and 5, SFC specimens were prepared for further tests in chapter 6. The grout was poured into a mould containing open-graded RAP skeleton from a height of approximately 30 cm. Geopolymer grout was expected to fully impregnate RAP skeletons by its own gravitation force without vibration works. The aim was not only minimising the energy used but also reducing construction-related noises due to vibration works. When the mould was

completely filled up, excess grout was scraped off by a trowel to produce an even surface for SFC specimens. All specimens were covered with polyethylene films and kept at room temperature for further tests.

3.6 Control specimen preparation

Control specimens made from Portland cement grout and 8/14 mm basalt aggregates were produced for comparative purposes. The mixing procedure for PC grout with liquid-to-solid ratio of 0.33 was based on BS 1881-125:2013 (British Standards, 2013d). Cement was mixed with about 70% water for two minutes. Then 2% Viscocrete 3000 superplasticiser mixed with the remaining water was added into the paste to enhance workability, followed by another two minutes of mixing. PC concrete specimens were prepared following similar procedures as for SFC materials.

3.7 SFC material characterisation

3.7.1 Ultrasonic pulse velocity test

Ultrasonic pulse velocity (UPV) is a non-destructive testing method that can be carried out on either laboratory-scale or on-site. It is commonly used to evaluate concrete quality or detect internal defects in concrete structures (Al-Mufti and Fried, 2018). For example, ultrasonic pulses travel through specimens from a transmitter by longer indirect routes should they meet air-filled voids or cracks in poor quality concrete before being picked up by the receiver transducer. This results in longer travelling times and lower UPV results.

In this study, 100 mm SFC cubes were assessed using a PUNDIT pulse velocity tester with 50 mm diameter transducers at 54 kHz based on BS EN 12504-4:2004 (British Standards, 2004). Petroleum jelly was applied to connect the surfaces of transducers and specimens. UPV measurements of at least 3 specimens per SFC mixture were performed in the centre of the specimen surface after 28 days curing at room temperature as shown in Figure 3.7. Before carrying out the test for SFC cubes, reference steel bars with known transit times of 26.3 μs and 25.9 μs were used to calibrate the pulse velocity tester.

UPV was determined by the path length divided by transit time (Equation (3.4)) which is the time taken to transmit from the transmitter to the receiver by direct transmission.

$$UPV = \frac{L}{T} \qquad (3.4)$$

where: UPV is the ultrasonic pulse velocity (m/s); L is path length of the shortest distance from two transducers (mm); and T is transit time, or the time spent by the ultrasonic pulse to transit through path length L (μs).

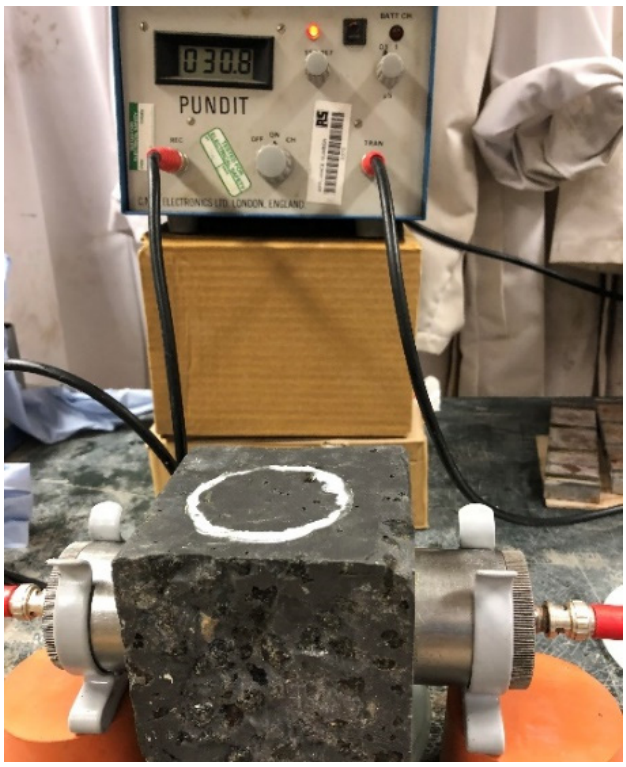

Figure 3.7. Setup for UPV test

3.7.2 Vacuum saturation method

Permeable porosity and apparent density of SFC specimens were determined by vacuum saturation method according to ASTM C1202 (ASTM, 2012). This method was considered more accurate than alternative ASTM techniques such as cold-water and boiling water saturation (Safiuddin and Hearn, 2005). Apparatus was built based on the study of Safiuddin and Hearn (2005) and is presented in Figure 3.8.

Testing involved splitting 100 mm SFC cube specimens into halves along the vertical plane with thin end layers removed to reduce edge effects. Specimen slices were then dried at 100 ± 10°C for over 24 hours, cooled at room temperature and weighed to determine oven-dry mass (W_D). For each test specimen, at least three SFC slices were placed in a sealed desiccator connected to a vacuum pump operating at a pressure of -90 kPa and exposed to air-drying for three hours followed by water saturation for a further one hour. The vacuum pump was turned off and the specimens were soaked underwater in the desiccator for a further 20 hours. After total 24 hours of vacuuming and soaking, surface moisture was removed using a towel and specimens were weighed to determine saturated mass (W_{ST}) and apparent mass in water (W_W). Permeable porosity ρ (%) and apparent density g_1 of SFC specimen were calculated using the equations below:

$$\rho(\%) = \frac{W_{ST} - W_D}{W_{ST} - W_W} \times 100 \quad (3.5)$$

$$g_1\ (\mathrm{g}/cm^3) = \frac{W_D}{W_D - W_W} \times \rho_w \quad (3.6)$$

where ρ_w is density of water, ρ_w= 1 g/cm^3.

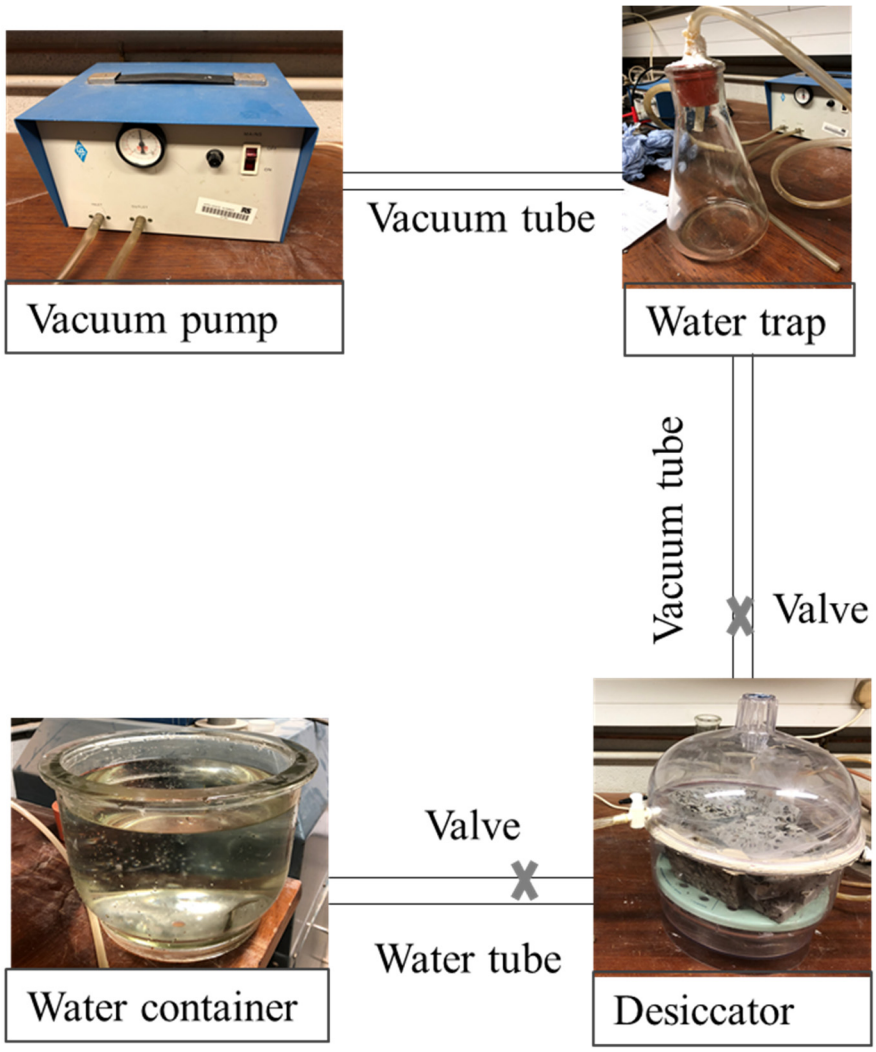

Figure 3.8. Apparatus setup of vacuum saturation method.

3.7.3 Compressive strength testing

For compressive strength measurement, 200 x 200 x 50 mm SFC slabs were initially cast, from which 50 mm cubes were cut using a diamond saw and discarding material from at least 15 mm from the slab edges. Testing was conducted using ELE compression machines with ADR Touch according to BS EN 1015:11 (British standards, 1999). An average value of

compressive strength was determined based on at least 3 specimens after 3, 7 and 28 days curing at room temperature.

3.7.4 Scanning electron microscope observation

Scanning electron microscope observation was used to examine the microstructure of interfacial transition zones between RAP - geopolymer grout matrices in SFC material and old aggregate - aged bitumen layer in RAP particle. Microstructural characteristic of SFC specimens and RAP particles with magnification of x200 was observed using SEM JEOL JSM apparatus as presented in Figure 3.9 (c). Except for RAP particles, all specimens with a dimension of approximately 15 x 15 x 12 mm were cut from SFC cubes using a diamond slicing wheel prior to sample preparation.

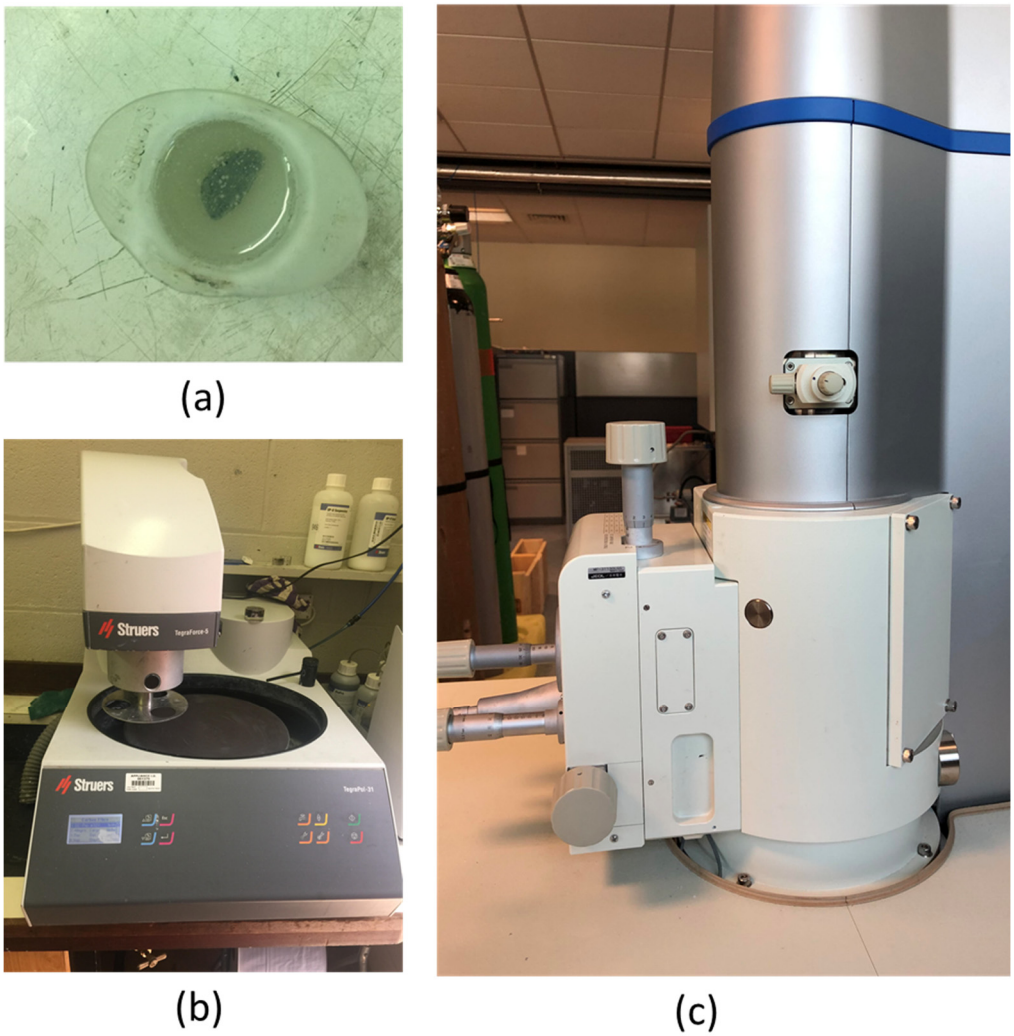

Figure 3.9. Sample preparation for SEM observation. (a) SFC specimen in a mould with epoxy. (b) Struers TegraPol 31 grinding/polishing machine. (c) SEM JEOL JSM apparatus.

All specimens were cleaned to remove dirt or dust particles before being immersed in EpoFix resin and hardener (see Figure 3.9 (a)). After 24 hours, they were unmoulded and polished using Struers TegraPol 31 (in Figure 3.9 (b)) grinding/polishing machine following manufacturer guidance (Struers, 2020). Different types of silicon carbide grinding papers including #320, #1200, #4000, MD-Dac and MD-Nap were used during the polishing process. The polished specimens were then applied with a gold coating using Emitech sputter coater before SEM observation following the procedure suggested by JEOL's manufacture (JEOL Ltd, 2017).

3.7.5 SFC compressive strength prediction using machine learning approach

SFC compressive strength was predicted using a machine learning-based Deep Neural Network (DNN) approach, integrated with sensitivity analysis. The DNN-based model was trained by datasets comprising inputs (i.e. geopolymer properties, RAP content and SFC curing age) and output (SFC compressive strength) obtained from compressive strength testing. Impacts of input factors on prediction performance was studied using sensitivity analysis. Three statistical measures including R^2, root mean square error (RMSE) and mean absolute percentage error (MAPE) were employed to evaluate the accuracy of the proposed DNN machine learning approach. R^2 is used to identify the relationship degree between actual and predicted data while RMSE and MAPE are commonly statistical validation techniques used in machine learning approaches (Dao et al., 2019). The three measures (R^2, RMSE and MAPE) were calculated using the following equations:

$$R^2 = \frac{(n\sum_i x_i\, x'_i - \sum_i x'_i \sum_i x_i)^2}{(n\sum_i {x'_i}^2 - \sum_i x'_i)^2 (n\sum_i x_i^2 - (\sum_i x_i)^2)} \tag{3.7}$$

$$RMSE = \sqrt{\frac{1}{n}\sum_{i=1}^{n}(x_i - x'_i)^2} \tag{3.8}$$

$$MAPE = \frac{1}{n}\sum \left|\frac{x_i - x'_i}{x_i}\right| \times 100 \tag{3.9}$$

where x_i and x'_i are the compressive strength obtained from experiments and DNN prediction respectively; n is the number of datasets.

DNN consists of more layers and neurons than typical machine learning techniques, such as artificial neural networks, leading to its ability to learn functions with a high degree of complexity (Huynh et al., 2020b). DNN possesses powerful representation ability of input

data and can reduce over-fitting issues in regression performance (Goodfellow et al., 2016). With powerful representational ability, DNN can achieve high accuracy in various tasks in advanced engineering fields. The structure of DNN-based models is presented in the schematic flowchart in Figure 3.10. SFC compressive strength was estimated by employing a DNN-based model comprising weight, normalisation and activation layers in regression tasks. The model was trained and validated using randomly shuffled datasets obtained from experimental works.

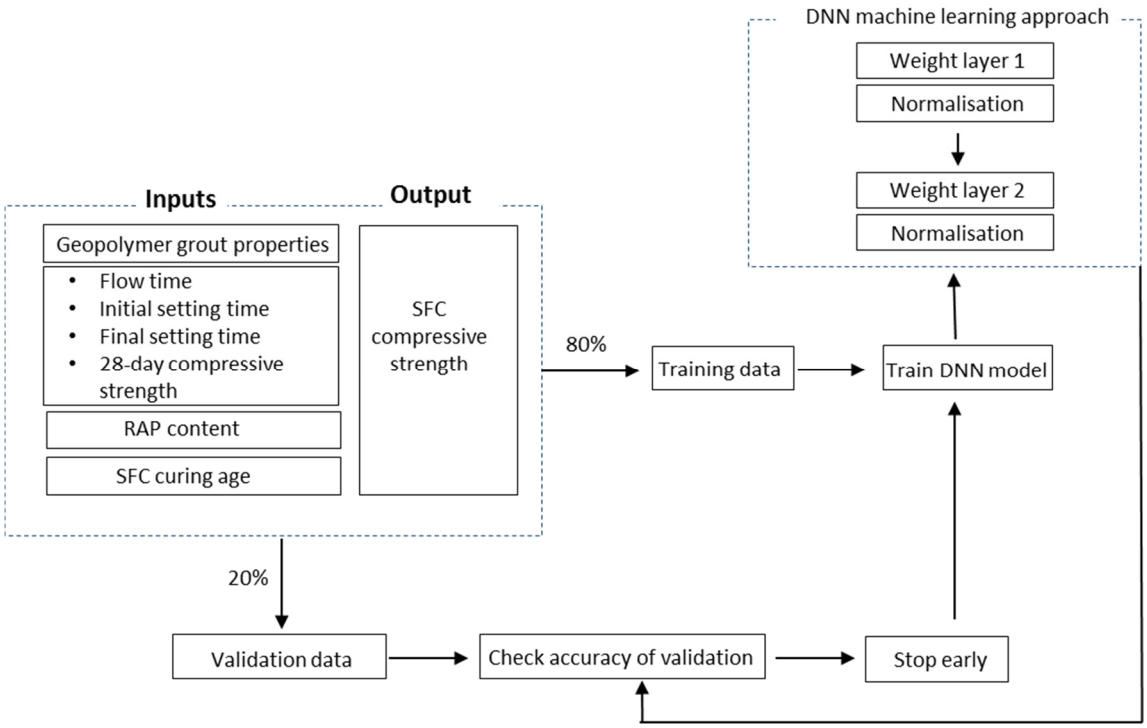

Figure 3.10. Schematic flowchart presenting DNN machine learning approach used to predict SFC compressive strength.

3.8 Characterisation of SFC materials as a surface course

3.8.1 SFC surface course preparation

SFC materials comprising 8/14 mm open-graded RAPs with solid content of 45% by volume and different grout mixes were employed as surface course of pavement in Chapter 7. SFC pavements with surface dressing and exposed-aggregate finishes were cast in 305 x 305 x 50 mm steel moulds. For surface dressing finish, 1.18/3.36 mm RAP chippings were spread on the surface of SFC specimens after grouting. For exposed-aggregate finish, surface textures of specimen were created by either brushing the surface by a stiff-bristled brush or leaving about one-third the size of RAP particles exposed on the specimen surface.

3.8.2 Road test machine testing

A road test machine (RTM), originally manufactured by TRL Limited, was used to simulate the impact of slow speed high stress trafficking conditions on the surface of pavements (McQuaid, 2015). Under the polishing action of traffic, the microtexture of aggregate particles are gradually changed leading to skid resistance reduction (Roe and Forest, 2005).

Figure 3.11. Specimen setup for road test machine.

The RTM is located in Ulster University's highways laboratory and allows researchers to investigate the characteristics of different types of road surfacing materials. In the RTM, up to ten 305 x 305 x 50 mm specimens can be tested at the same time on a 2.1 m diameter table which can rotate at a speed of 10 rpm (equivalent to 1.1 m/s). The trafficking condition was simulated by two Federal 195/70 R14 tyres attached vertically above the rotating table that applied a load of approximately 5 kN onto the pavement surface (McQuaid, 2015; Wilkinson, 2017). These tyres were able to move freely and laterally within the pavement's surface. Specimen setup for RTM is presented in Figure 3.11. The RTM test was conducted within a temperature of approximately 10^{o}C in dry conditions.

RTM was used in this study to assess the possibility of using SFC material as a surfacing material based on specimen weight loss, skid resistance value, mean texture depth and

surface texture change after traffic wear. Instead of 100,000 wheel passes corresponding to 5-8 years of road traffic in reality as recommended in (Nicholls, 1997), low numbers of wheel pass indicating a short period of traffic were carried out in this study until serious defects occurred on the surface of testing slabs. As such, equilibrium points of 20,000-40,000 wheel-passes previously reported in the literature (McQuaid, 2015) were not achieved in this study. The machine was stopped in between running-in process at intervals of 50-, 100-, 500-, 1000-, 2000- and 6350-wheel passes to examine the changes in surface textures of specimens.

3.8.3 Pendulum test method

The pendulum test method was used to determine skid resistance value in dry and wet conditions following BS EN 13036-4:2016 (British Standard, 2013). Pendulum testing is considered a common laboratory method to evaluate frictional performance of a surface when a rubber slider assembly of a pendulum tester (Figure 3.12) slides across a test surface (Uz and Gökalp, 2017).

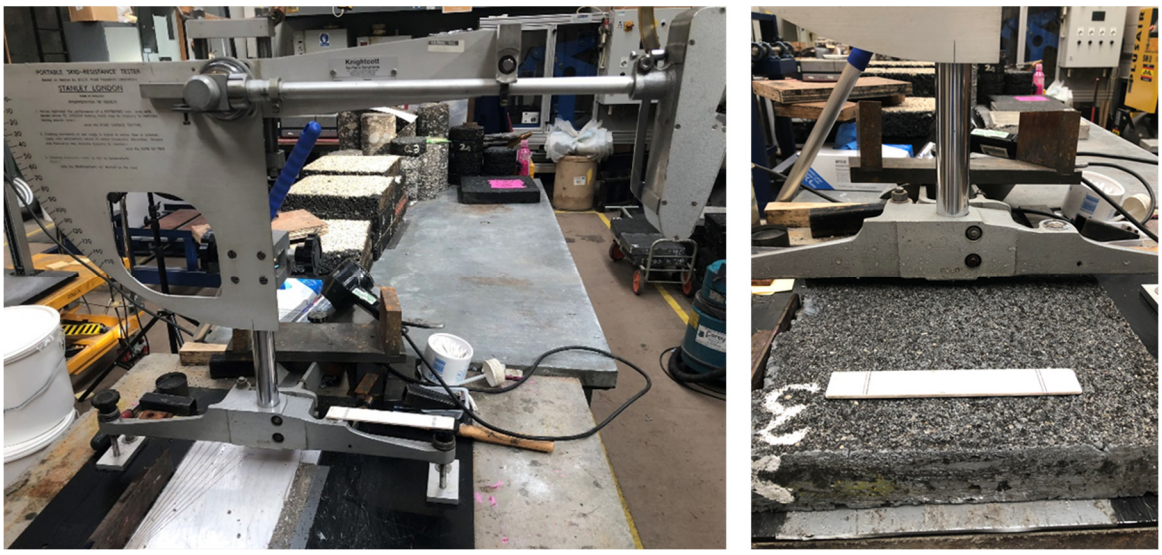

Figure 3.12. Pendulum testing to determine skid resistance.

The contact path length where the rubber pad contacts slab surface was defined as sliding length. According to BS EN 13036-4:2016 (British Standard, 2013), sliding length should be at least 125 mm when the pendulum tester is set properly. The slabs prepared for skid resistance test had dimension of 305 x 305 x 50 mm which complied with minimum dimension of at least 100 x 150 x 50 mm required by BS EN 13036-4:2016 (British Standard, 2013). Pendulum testing was conducted on each slab surface in both dry and wet

conditions. The latter was created by spraying water on testing specimen to generate a lubricant film on the contact area between the slider and test slab.

3.8.4 Sand patch method

Sand patch method is considered as one of the most common tests to determine mean texture depth of testing slabs according to BS EN 13036-1:2010 (British Standards, 2010). Firstly, loose aggregates were brushed off from testing pavement surface by a soft brush and fine dust inside the surface voids were removed using a vacuum cleaner. Sand with known volume was then poured on the centre of pavement surface. Next, the sand heap was smeared in a circular motion with a light pressure by a sand spreader until it was completely flattened, and surface voids fully filled to the peaks of surrounding aggregates. Four measurements of the circle diameter were then taken evenly at every 45^{o} of the circle. An average of four measurements was calculated and mean texture depth (MTD) was given by:

$$\mathrm{MTD} = \frac{4\mathrm{V}}{\pi \mathrm{D}^2} \qquad (3.10)$$

where V is volume of sand (mm^3) and D is mean value of sand patch circle (mm).

3.8.5 3D surface texture modelling using close-range photogrammetry

Close-range photogrammetry is an efficient and fast method to investigate surface texture during traffic wear (Kogbara et al., 2018). The technique involved establishing a virtual 3D model of the pavement surface texture from a set of multiples images of that surface. A digital camera was used for capturing photos at the central area of specimen surface before and after being tested by RTM. These photos were then used for 3D modelling of the surface using proprietary software such as 3DF Zephyr. The slab was rotated anticlockwise about 20 degrees to capture a sequence of at least 15 photos with overlapping fields of view. The size of area of interest (AOI) at the central area of pavement surfaces was 140 x 180 mm.

The setup for photographing testing slabs is presented in Figure 3.13. A 30 cm ruler was placed on the surface along the top side of a slab during photo-capturing process for setting a measurement scale for 3D modelling in 3DF Zephyr. The 3D modelling followed Mcquaid's study (McQuaid, 2015). A point cloud XYZ file created from Zephyr was then imported to a proprietary spatial information software named Digital Surf – MountainsMap to analyse the change in surface textures of testing slabs during traffic wear.

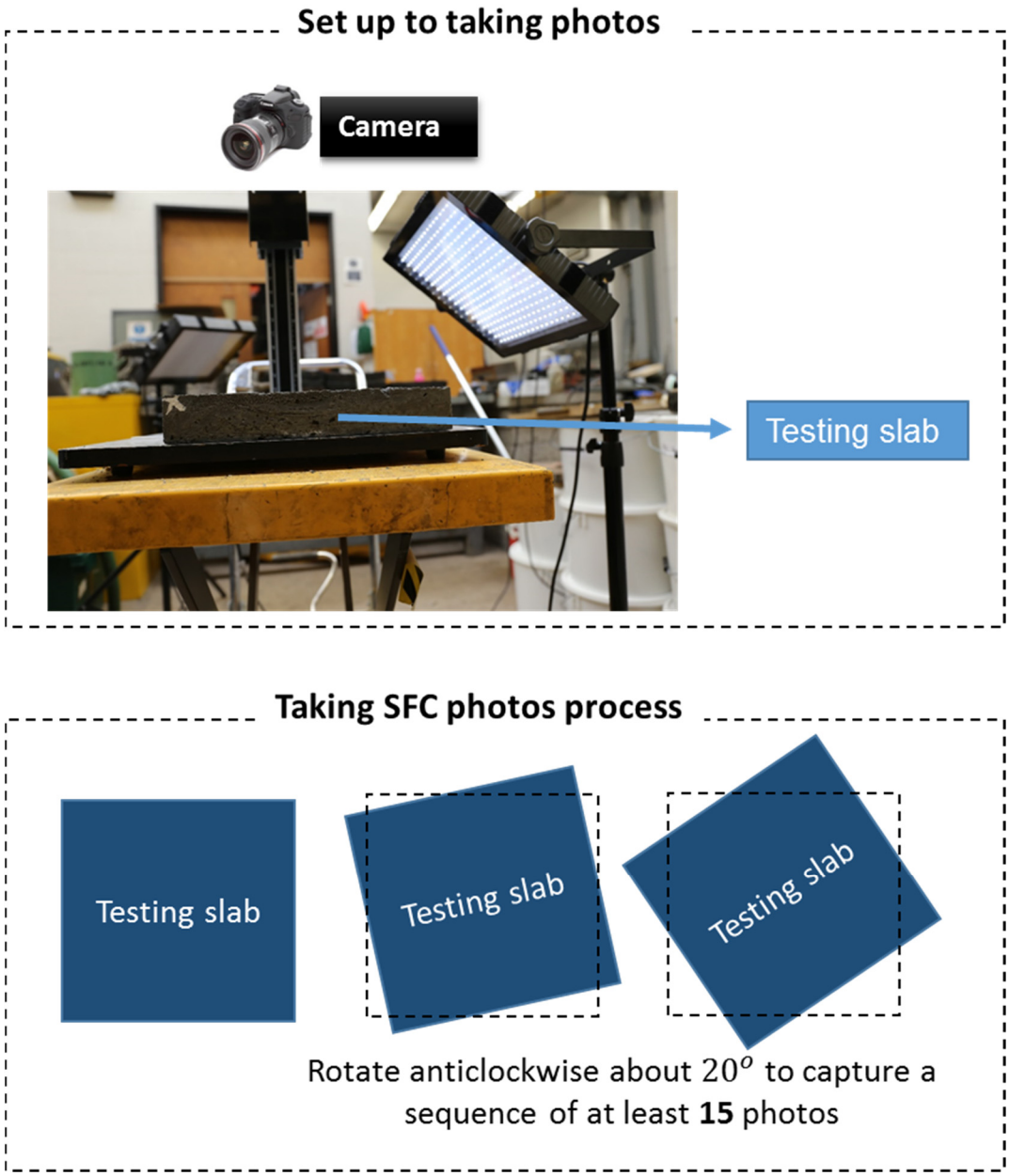

Figure 3.13. Set up to photograph surface of test slabs for 3D surface texture modelling.

CHAPTER 4

GEOPOLYMER CEMENT-BASED GROUT CHARACTERISATION

4.1 Introduction

In this chapter, geopolymer grouts with a range of fresh and mechanical properties are examined to develop grouting materials for SFC pavements, which will be discussed in more detail in the next chapter. In general, grouting materials require high flowability to easily infill the internal void structure of open-graded aggregate skeletons (Idrissi et al., 2018) and sufficient strength to resist damage under traffic loads (Ricci, 2012).

Portland cement grout has been widely researched as the main cementitious binder for SFC materials (Anderton, 2000; Collop and Elliott, 1999; Densit, 2018b; Husain et al., 2010). Commercial cement-based grouting products, such as Densit® mortar (Densit, 2018a), R2M Flowflex (Pratelli et al., 2018), Ulticrete (Ulticrete, 2018) and Hardicrete (Hardicrete, 2019), are claimed to possess high mechanical properties with 28-day compressive and flexural strengths of up to 110 and 15 MPa respectively (Densit, 2018b; Hardicrete, 2019; Pratelli et al., 2018; Ulticrete, 2018). However, cement has been considered as a costly and environmentally unfriendly material (Samantasinghar and Singh, 2019). Geopolymer grouts, therefore, have been considered as an alternative to Portland cement grout in several studies (Afonso et al., 2016; Ricci, 2012). Geopolymer products are formed through alkali liquid reacted with SiO_2 and Al_2O_3 contained in aluminosilicate sourced from by-product industrial wastes (Idrissi et al., 2018).

Ricci (2012) introduced the use of grouted macadam comprising hot porous asphalt with voids contents between 25-30% and geopolymer grout 'WMG1' containing recycled mining waste from Panasqueira, glass and metakaolin as geopolymer precursors and mixture of sodium silicate and sodium hydroxide as alkali activator. Even though the goal of this research was to lower energy consumption levels in the construction industry, the final grouted macadam product required heating curing at elevated temperature of 40^{o}C for 7 days.

Thus, to eliminate energy consumption from heating processes, in this chapter different types of geopolymer grout were formulated at ambient temperature to find suitable grouting materials for the target SFC pavement application. By eliminating the heat curing stage, the aim was to develop more convenient and efficient grouting materials suitable for practical construction applications. Industrial by-products such as fly ash, ground granulated blast furnace slag, silica fume and metakaolin were ultilised as binders to offer potential environmental savings relative to conventional Portland cement-based grouting systems (Afonso et al., 2016). According to McLellan et al. (2011), greenhouse gas emissions linked to the production of geopolymer concrete comprising fly ash, ground-

granulated blast-furnace slag and silica fume was reported to be 44-64% lower than for conventional concrete. The experimental programme initially assessed fresh grout flow (Marsh flow cone) and setting time (Vicat needle penetration), followed by compressive strength testing of hardened grout specimens after 28 days curing at ambient temperature. Finally, four grout types with contrasting performances were selected to facilitate the manufacture of SFC pavement suitable for a broad range of practical applications in the next chapter.

4.2 Materials

4.2.1 Geopolymer powders

Geopolymers – formed through reactions between an alkali liquid activator and Si and Al contained in alumina-silicate based binders – were developed in this study using binders principally sourced as industrial by-products. This included fly ash class F, GGBS, SF and MK. The chemical composition, particle sizes and specific gravity of the materials presented in Table 4.1 were obtained from the study of Wilkinson (2017). As presented in the table, the binders comprised contrasting proportions of mainly silica (SiO_2), alumina (Al_2O_3), and calcium oxide (CaO).

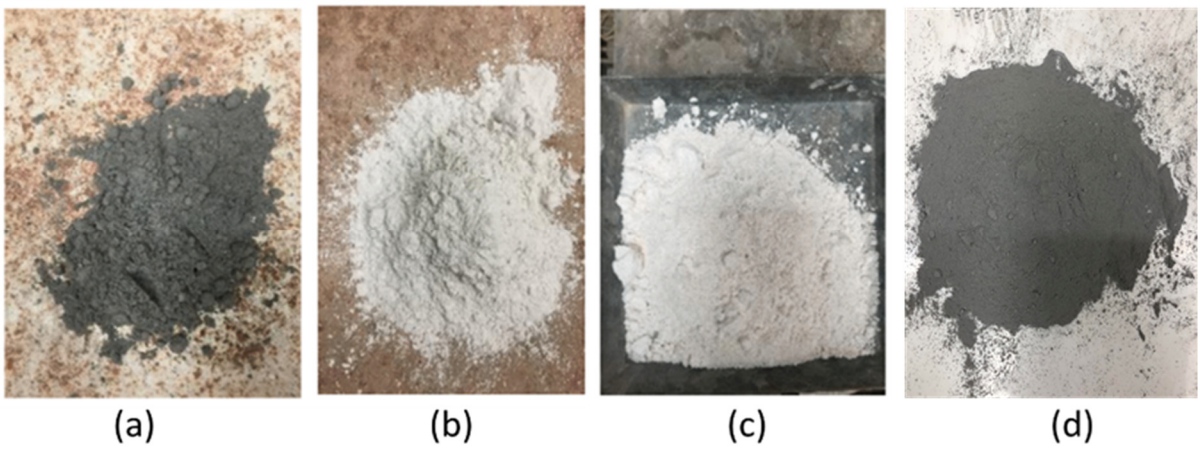

Figure 4.1. Geopolymer grout powders. (a) Fly ash. (b) GGBS. (c) Metakaolin. (d) Silica fume.

Fly ash (FA)

As shown in Figure 4.1, commercial fly ash, sourced from Kilroot power station in Northern Ireland, is a finely granular, dark-grey powder. FA is a by-product generated from coal burning in electricity power stations which is commonly used as one of the major components in geopolymer grout, mortar and concrete (Huseien et al., 2016; Kalaiyarrasi

and Partheeban, 2016; Wilkinson, 2017). As shown in Table 4.1, FA contains mainly SiO_2 and Al_2O_3 (up to 82% by total mass) which provides sources of silica (SiO_2) and alumina (Al_2O_3) for geopolymerisation processes. In addition, chemical components of FA were in compliance with category A defined in BS EN 450-1:2012 (British Standards, 2012c), with its total content of SiO_2, Al_2O_3 and Fe_2O_3 (87%) higher than the minimum value of 70% required.

Table 4.1. Chemical composition, particle size and specific gravity of geopolymer powders (Wilkinson, 2017).

Properties	Geopolymer powders			
	FA	GGBS	MK	SF
Chemical compositions (% by mass)				
SiO_2	57	36.5	55	96
Al_2O_3	24	10.4	40	0.8
CaO	3.9	42.4	0.3	0.5
Fe_2O_3	6	0	1.4	0.8
TiO_2	1.4	0.5	1.5	0.02
MgO	2	8.1	0.3	0.5
Na_2O	0.4	-	0.4	-
SO_3	1.6	-	-	-
K_2O	0.6	-	0.4	-
LOI(+)	3.1	1.4	0.7	1.35
Particle size (μm) (++)				
D(10)	2.9	1.1	0.9	0.1
D(50)	18.8	5.3	2.7	0.15
D(90)	124.6	22.5	8.2	0.4
Specific gravity (g/cm^3)	2.7	2.85	2.6	2.2

(+) LOI is loss on ignition

(++) D(10), (50) and(90) are the particle sizes below which 10, 50 and 90% of particles fall respectively.

Geopolymer grout containing FA tends to exhibit high fluidity and workability due to its spherical particle shape (Trimurtiningrum and Ekaputri, 2016). However, the presence of FA in geopolymer products may cause increased porosity and reduction of compressive strength. For example, 100% FA geopolymer paste was reported to exhibit higher porosity

and lower compressive strength (40% and 7 MPa respectively) compared to slag-based geopolymer paste (porosity of 10% and strength of 30 MPa) (Sasui et al., 2020). In addition, longer curing time (more than 200 days) was needed to reach full strength at room temperature in the case of grout with 100% FA compared to metakaolin and slag-based geopolymers (Idrissi et al., 2018).

Ground-granulated blast-furnace slag (GGBS)

GGBS contains a high amount of CaO (42.4% by mass), so it can react pozzolanically in aluminosilicate environments at ambient temperature in the presence of water to develop compounds having cementitious properties (Al-Majidi et al., 2016; Huseien et al., 2016). Off-white in colour (as shown in Figure 4.1), the GGBS used in this study was sourced from ECOCEM Ireland. In addition, as GGBS contains a significant amount of amorphous alumina (10.4%), silica (36.5%) and calcium oxide (42.2%), which plays an important role in strength development of the grout. For example, in the study of Samantasinghar and Singh (2019), mortar specimens containing 100% GGBS achieved 77% of their full strength after 7 days.

Metakaolin (MK)

MK is a product of the decomposition of kaolin material at high temperatures (minimum 650^{o}C) (Li and Ding, 2003). As shown in Table 4.1, MK contains a high amount of SiO_2 (55%) and Al_2O_3 (40%), and is considered as a primary source of aluminosilicate for geopolymer products (Huseien et al., 2016). In this study, MK with the commercial name 'Metastar 501' was sourced from IMERYS Minerals UK. MK possesses smaller particle sizes (0.1-0.4 μm) than FA and GGBS (2.9-124.6 μm and 1.1-22.5 μm respectively). MK was considered based on its small particle size associated with improved workability. For instance, mortar flow, defined by flow table method, of slag-based geopolymer increased from 14 to 19 cm with an addition of 15% MK as replacement of GGBS in slag-based geopolymer in the study by Huseien et al. (2016).

Silica fume (SF)

Silica fume is a by-product of silicon and ferrosilicon alloy manufacturing processes involving the carbothermic reduction of high-purity quartz in electric furnaces (Khater, 2013). In this study, SF with the commercial name 'Elkem Microsilica' was sourced from Elkem UK. SF was considered based on its reported significant contribution to good flow and high silicate content (96% by mass). In previous research, replacement of 20% fly ash

with MK in geopolymer mortar improved mortar flow by approximately 13% compared to mixtures without MK (Jithendra and Elavenil, 2020).

4.2.2 Alkali activator

Alkali solution was used in this study as liquid activator to react with aluminosilicate materials by breaking down Si-O-Si and Al-O-Al covalent bonds to form geopolymer (Ricci, 2012). Commercially available liquid activator, Geosil, with 45% solid potassium silicate (K_2SiO_3) content by mass, molar ratio of 1.6 and density of 1.51 g/cm^3, was sourced from Woellner and used throughout for all geopolymer grout mixes.

4.3 Geopolymer grout mix design

A wide range of geopolymer grout properties was aimed to achieve by combining various binder types with different liquid-to-solid (LS) ratios. Geopolymer grout with precursor-to-activator ratio of 5 (equivalent to LS = 0.20), introduced by Ricci (2012) for grouted macadam, exhibited very low flowability of 467 s which is not suitable for grouting. When 40% of water was added into this grout mix, meaning a LS increase to 0.68, the result was low strength grouted macadam after 7-day curing (less than 6 MPa). Hence, this study investigated grout with LS ranging from 0.27 to 0.52, which was within the range 0.20-0.68 reported in Ricci's study (Ricci, 2012). The aim was to achieve both proper workability and higher compressive strength.

Provided in Table 4.2 is a mix design summary of the various geopolymer grout types considered. Investigated were binder combinations GGBS+FA, GGBS+FA+MK and GGBS+FA+MK+SF with liquid-to-solid (LS) ratios ranging from 0.27 to 0.52. Based on previous related research (Oakes et al., 2019), these binder combinations were chosen to offer a range of grout performance levels in terms of flow, setting time and compressive strength, appropriate for a range of potential SFC pavement applications.

By considering diverse binders, the aim was to achieve a range of geopolymer grout properties. The diversity of the mix proportions considered centred on the differing binder powder sizes, shapes and properties. Geopolymer grout GGBS+FA was initially investigated with different percentages of GGBS and FA to establish a general understanding of the grout behaviours. GGBS was chosen based on its reported significant contribution to strength development without the need for heat curing (Hadi et al., 2017). However, high content of GGBS might have a negative effect on the workability and consistency of fresh grout (Samantasinghar and Singh, 2019). As mentioned in the literature review (Chapter 2), geopolymer grout should exhibit high flow rate as well as good mechanical properties.

Thus, as high levels of grout flowability were potential required, FA was considered based on its spherical shape and relatively smooth surface texture.

Table 4.2. Geopolymer grout compositions.

Binder combinations	Geopolymer powder contents (% by mass of total binder)				Liquid-to-solid ratios (LS)
	GGBS	FA	MK	SF	
GGBS+FA	80	20	0	0	0.27, 0.33, 0.38, 0.52
	60	40	0	0	
	50	50	0	0	
	20	80	0	0	
GGBS+FA+MK	40	40	20	0	
GGBS+FA+MK+SF	40	20	20	20	

Before beginning the experimental process, MK and SF were considered based on their reported contribution to good flow and high silicate and aluminium content (Hadi et al., 2017). This was undertaken in an attempt to improve the overall workability of GGBS+FA grout, which displayed a very dense mixture state when the LS = 0.27. Additionally, as shown in Table 4.1, SF contains mainly SiO_2 (96%) and has very small particle sizes (average approximately 0.2 μm), which contribute to porosity reduction and strength improvement of geopolymer products. For example, fly ash-based geopolymer mortar incorporating 5% SF investigated in the study by Dutta et al. (2010) showed 23.5% reduction in porosity and improved strength (38.4%) compared to mortar without SF. The main activator used in all geopolymer grout mixes was liquid activator Geosil containing 45% solid potassium silicate by mass.

4.4 Flowability of geopolymer grout

Figure 4.2 illustrates the relationships between liquid-to-solid (LS) ratio, binder materials and flow time of geopolymer grouts. As can be seen in this figure, flow times of geopolymer grout with various binder combinations and LS ratios ranged from 9 to 841 s. This flow time range was much broader than cementitious grouting materials (up to 144s) reported in previous studies (Afonso et al., 2016; Anderton, 2000; Oliveira, 2006). Alkali activator content was the clear dominant factor, with flow times generally decreasing with increasing LS ratio for all binder types considered. For instance, flow times of geopolymer

grouts significantly increased from 18 to 841 s between LS of 0.27 and 0.38, whereas very similar flow values (9-10 s) were noted for all binder types at LS ratios greater than 0.38. This was particularly true for mixtures with a LS ratio of 0.27. GGBS+FA+MK binder exhibited the lowest level of flowability at this LS ratio, with a flow time of over 800 s. At the lowest LS ratio considered (0.27), the GGBS+FA+MK+SF binder combination offered the lowest flow time of 80 s, or in other words, the highest flowability.

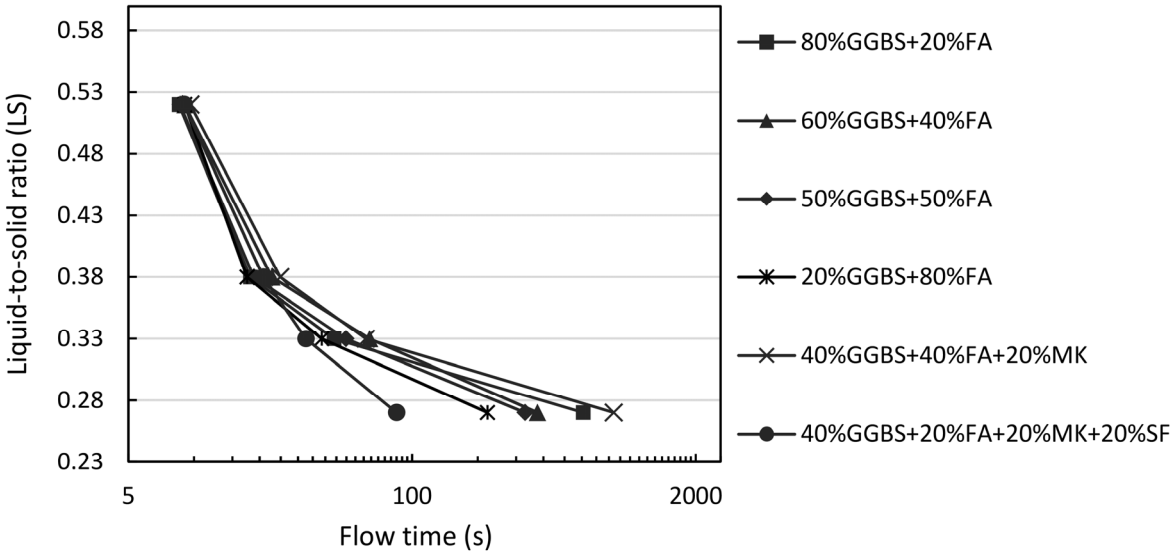

Figure 4.2. Effects of geopolymer binder content and liquid-to-solid (LS) ratio on flow time of geopolymer grouts.

Geopolymer powders and binder combinations were also considered as the dominant controlling factor of geopolymer flowability. For geopolymer group GGBS+FA, it can be seen from Figure 4.2 that the grout containing higher GGBS contents attained lower flowability. For example, at a constant LS ratio of 0.27, the grout with 80% GGBS content by mass recorded 609 seconds while the 20% GGBS grout achieved significantly higher flowability (flow time of 222 seconds). Longer flowing time presented by high GGBS content grout could be explained by the angular shapes of GGBS reducing its flowability. The reported negative effects of GGBS content to grout flowability were confirmed in studies by Al-Majidi et al., (2016), Huseien et al., (2016) and Xie et al., (2019).

MK addition was found to decrease geopolymer flowability, with the lowest flowability (flow time = 841 s) observed in grout type GGBS+FA+MK at LS ratio of 0.27. According to Li and Ding (2003), MK showed a great ability to absorb water, thus its addition in low water

content grout leading to poor flowability. This is also in good agreement with the study by Favier et al. (2014). On the contrary, the addition of 20% SF with small particle size (0.1-0.4 μm) and rich in silica (96%) in grout type GGBS+FA+MK+SF showed a significant gain in flowability. For example, grout type GGBS+FA+MK+SF showed up to 10 times quicker flow than others at the same LS ratio of 0.27. Previous studies (Jithendra and Elavenil, 2020) identified that up to 20% MK can be used in geopolymer mixtures to achieve improved workability, whereas mixtures containing over 20% MK exhibit reduced workability due to large surface areas of MK (approximately of 1950 m^2/kg) (Shadmani et al., 2018).

4.5 Setting time

Figure 4.3 illustrates the relationships between LS ratio, binder materials and initial and final setting time of geopolymer grout. Initial and final setting time of geopolymer grout with various binder combinations and LS ratios were within the ranges 13-450 and 30-840 mins respectively. In contrast to flow time, LS ratio had a much less significant influence on grout setting time, particularly for LS ratios greater than 0.38 where performance levels attained steady state. Such behaviour can be explained by high ratio LS (≥ 0.38) leading to thinner grout with high water content, hence delaying the setting time (Azadi et al., 2017).

Binder combination played an important role in grout setting time, with a wide disparity of results recorded across all LS ratios considered. For geopolymer mixtures GGBS+FA, results indicated that grout containing higher GGBS content showed faster initial/final setting time (13/30 mins) compared to other grouts. This can be explained by high content of calcium oxide in GGBS (42.4% by mass - see Table 4.1) leading to an acceleration of geopolymerisation processes and reduction in setting time (Jithendra and Elavenil, 2020; Zhang et al., 2019). Substituting 20% GGBS by 20% MK in geopolymer type 60%GGBS+40% FA delayed the initial setting time by a maximum of 28 minutes. This is in agreement with the findings from Huseien et al. (2016), where increasing MK content (0-15%) in geopolymer mortar led to extended initial and final setting times (3-10 and 6-19 mins respectively).

Furthermore, the addition of 20% SF in the grout type GGBS+FA+MK+SF prolonged initial setting time compared to most grouts except for the grout mix 20%GGBS+80%FA. Some specimens of grout mix 20% GGBS+80% FA with high liquid content (LS exceeding 0.38) did not set completely at ambient temperature, even after days of curing. The results from Figure 4.3 were collected from specimens that had hardened completely. Additionally, this grout exhibited a very slow final setting time (over 800 minutes). Therefore, this grout mixture was eliminated from further investigations.

Similar to flowability, grout setting time has practical significance when considering in situ applications. Whereas large area pours are likely to require prolonged setting times, smaller or emergency repair pours may require much shorter initial setting times.

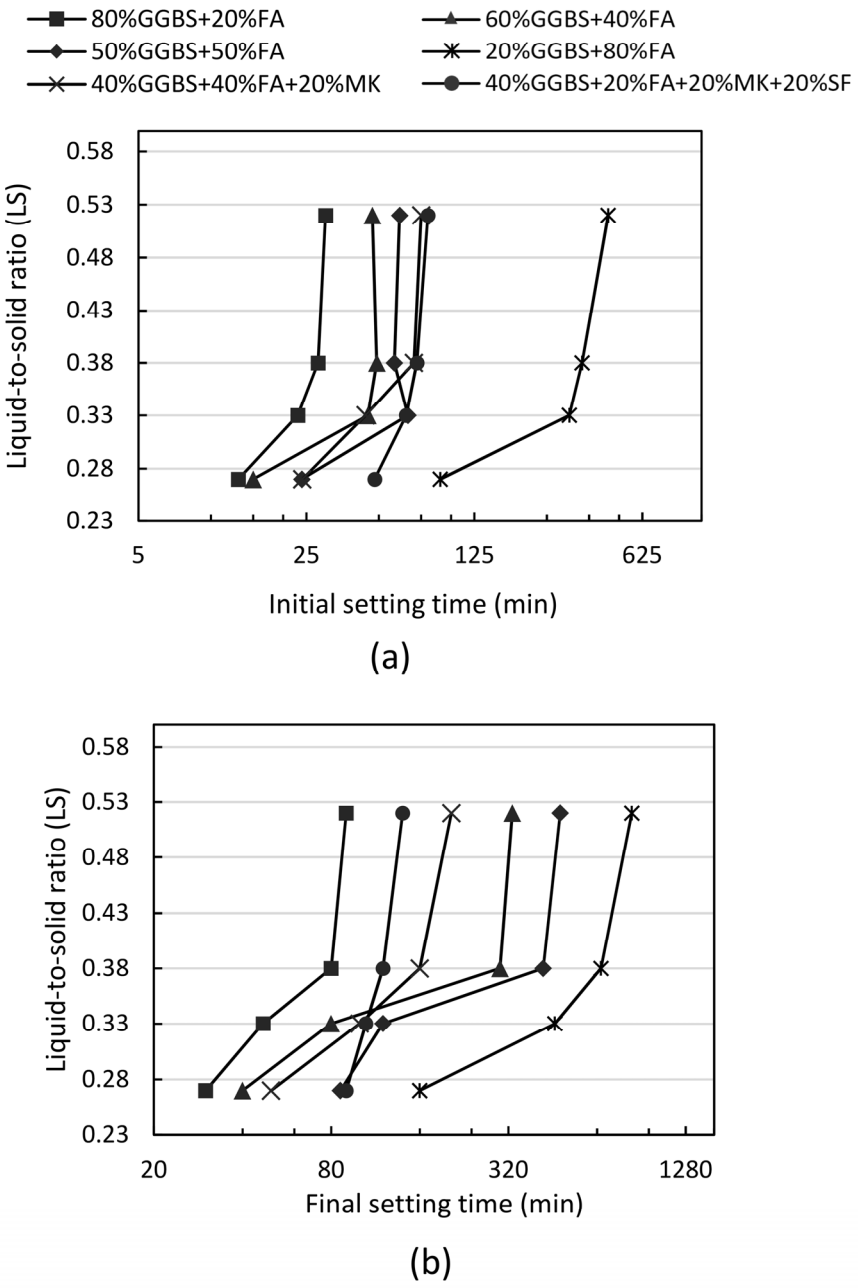

Figure 4.3. Effects of geopolymer binder content and liquid-to-solid (LS) ratio on setting time of geopolymer grout: a) Initial setting time; and b) Final setting time.

4.6 Compressive strength

Figure 4.4 illustrates the relationship between LS ratio, binder material and 28-day compressive strength for geopolymer grout. Recorded compressive strength of up to 108

MPa reflects the established ability of geopolymer grouts to attain similar strength to commercial cementitious grouting materials (92-110 MPa) such as Densit (Densit, 2018b). The general trend of all grout types was increasing strength corresponding to decreasing LS ratio. For instance, grout strength increased dramatically from 19-40 MPa to 44-108 MPa when LS dropped from 0.52 to 0.27.

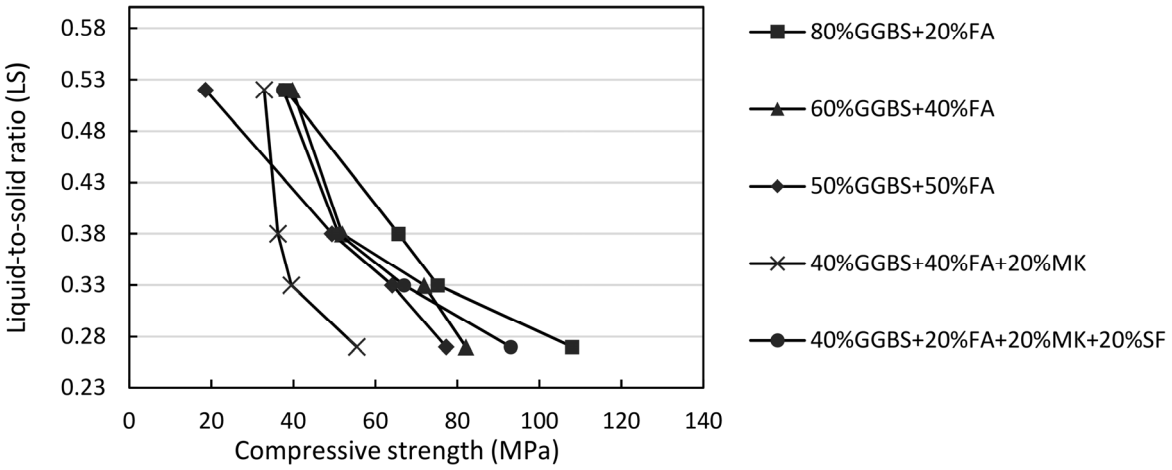

Figure 4.4. Effects of geopolymer binder content and LS ratio on compressive strength of geopolymer grout.

Binder types and combinations had a significant influence on geopolymer grouts. Figure 4.4 shows that there was an improvement in compressive strength for geopolymer grouts with high GGBS content. For instance, grout type 80%GGBS+20%FA (with highest GGBS content) reached the highest strength of 108 MPa, while grout type 50%GGBS+50%FA showed the lowest strength of 77 MPa at LS = 0.27. This observation can be explained by the fact that the high volume of calcium oxide contained in GGBS formed calcium silicate hydrate gel (C-S-H); thus increasing the strength of grout (Diaz et al., 2010; Saludung et al., 2018).

Geopolymer group GGBS+FA exhibited higher compressive strength than the grouts with an addition of 20% MK (GGBS+FA+MK). Moreover, an addition of 20% SF in geopolymer type GGBS+FA+MK+SF showed 1.8 times higher strength than grout mix GGBS+FA+MK. This can be explained by the highly effective pozzolanic activity and small size (about 0.15 µm) of SF leading to reducing porosity and enhancing compressive strength (Khater, 2013; Nmiri et al., 2019).

4.7 Selecting geopolymer grout for further investigation

As described in Section 4.3, geopolymer grouts should exhibit a high flow rate as well as good mechanical properties. However, these properties are inversely proportional. For example, grout type 80%GGBS+20%FA exhibited a low flow time of over 600 seconds, high compressive strength of 108 MPa and fast initial setting time of 13 minutes.

In this phase of the research, all 20 of the GGBS+FA, GGBS+FA+MK and GGBS+FA+MK+SF geopolymer grout mixes listed in Table 4.2 were characterised in terms of flow time, initial setting time and 28-day compressive strength. A combination of Figure 4.2, Figure 4.3 and Figure 4.4 with grout property classification is presented in Figure 4.5. Clearly from Figure 4.5, and perhaps not surprisingly given the diverse suite of mixes considered, a wide range of performance levels was achieved. It should be noted that mixture 20%GGBS+80%FA was removed since it was difficult to get the specimens set completely at room temperature. As shown in this figure, there is an element of performance contradiction. This was particularly the case for flow time and strength results, with mixes with the highest level of flowability (a characteristic likely to be deemed as favourable for large area pours) exhibiting the lowest values of strength, and vice versa.

To help categorise performance, flowability, initial setting time and compressive strength results were respectively classified as follows:

- *Flow time (s):* *'High' (<24); 'Average' (24-80); 'Low' (>80);*
- *Setting time (mins):* *'Fast' (<25); 'Average' (25-75); 'Slow' (>75);*
- *28-day strength (MPa):* *'Low' (<40); 'Average' (40-80); 'High' (>80).*

Within the ranges of performance levels of flow time, setting time and compressive strength recorded, opportunity exists for selecting mixes with contrasting performance characteristics. This is highlighted by the solid and dashed lines added to Figure 4.5, which demonstrate that for a starting design specification of 'high' flowability, for instance, mixes with 'average' setting time and either 'average' or 'low' strength can be chosen. Given the variation of pavement applications envisaged for this technology, this flexibility offers a significant benefit in terms of subsequent SFC implementation.

High flow grout was classified based on the flow time of cement grout in a study by Afonso et al. (2016) where a lower volume of cement grout (1000 ml) was defined as high fluidity with flow time of up to 20 s.

Albeit that setting time classifications were based on laboratory-based processing in this study, grout setting time clearly has practical significance when considering in-situ

applications. Whereas large area pours are likely to demand 'average' or 'slow' setting times, smaller or emergency repair pours may require much shorter initial setting times. Similar compressive strength classification can be found in Oliveira's study (Oliveira, 2006), where weak grout yielded strength of 35 MPa and high strength grout Densit® modified grout yielded strength of 92 MPa.

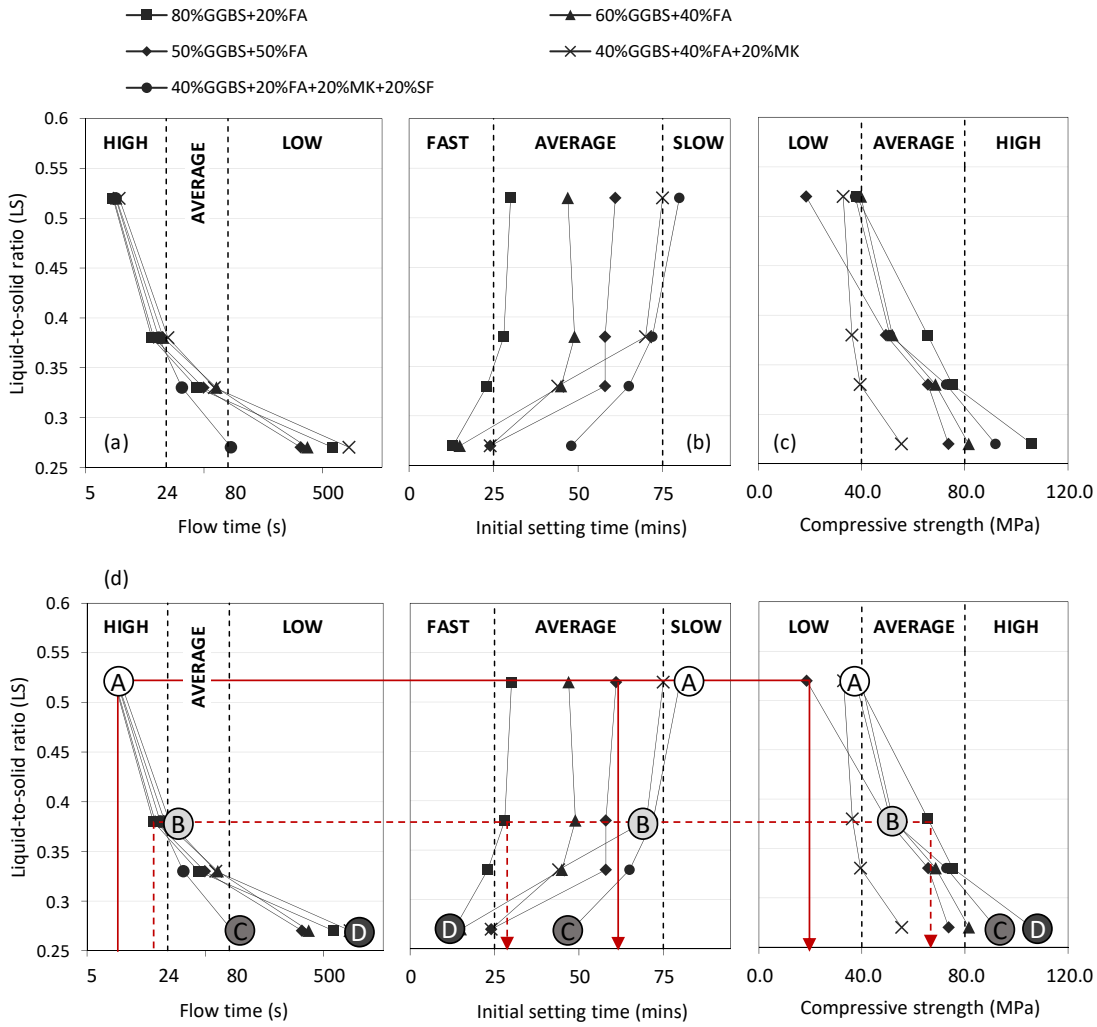

Figure 4.5. Performance of 20 geopolymer grout mixtures in terms of: (a) flow time, (b) initial setting time and (c) 28-day compressive strength; (d) summary of selected grout mixtures (Mix A, B, C and D) for subsequent SFC characterisation phase.

From the 20 grout mixes previously described, four (labelled mix A, B, C and D from this point forward) were chosen for future investigations as highlighted in Figure 4.5 (d) and summarised in further detail in Table 4.3. Mix A, B and C were selected from the 40%GGBS+20%FA+20%MK+20%SF binder category and mix D from the 80%GGBS+20%FA

category, based on the provision of contrasting performance classifications in terms of grout flowability, setting time and compressive strength as follows:

- Mix A (*'High' | 'Slow' | 'Low'*)
- Mix B (*'Average' | 'Average' | 'Average'*)
- Mix C (*'Low' | 'Average' | 'High'*)
- Mix D (*'Low' | 'Fast' | 'High'*)

4.8 Summary

The aim of this section was to investigate properties of geopolymer grouts such as flowability, setting time and compressive strength. Based on the results obtained, the concluding remarks in this chapter are following:

- To facilitate the manufacture of SFC suitable for a broad range of practical applications, a diverse suite of 24 geopolymer grouts was initially produced using binder combinations GGBS+FA, GGBS+FA+MK and GGBS+FA+MK+SF with liquid-to-solid (LS) ratios ranging from 0.27-0.52. The results were wide ranges of grout performance in terms of flow (9-841 s), initial setting time (13-450 mins), final setting time (30-840 mins) and 28-day compressive strength (19-108 MPa).
- LS ratio and binder contents played a significant role in geopolymer grout compressive strength and fresh properties. Pronounced influences of LS ratios on geopolymer flowability were noted in all binder types with LS ratio below 0.38, particularly at LS ratio of 0.27. Looking forward to in situ application of this technology, grout flowability is a key property to control, particularly for large area grout pours into potentially well-compacted RAP. Higher content of GGBS resulted in low flowability, quick setting and higher compressive strength. The addition of MK with high water-absorbing ability reduced the flowability, delaying setting time while addition of SF increased the flowability, prolonged the setting time and improved the strength of geopolymer grout.
- Grout properties such as flowability, setting time and compressive strength could be significant factors affecting grouting works and properties of open graded aggregate skeleton in the next chapter. Thus, four grout types including Mix A (*'High' | 'Slow' | 'Low'*), Mix B (*'Average' | 'Average' | 'Average'*), Mix C (*'Low' | 'Average' | 'High'*) and Mix D (*'Low' | 'Fast' | 'High'*) were chosen based on contrasting performance classification to impregnate RAP skeleton in the next chapter.

Table 4.3. Properties and composition of geopolymer grouts using for SFC pavement material.

MIX	GGBS/FA/MK/SF binder composition (%)	LS	Grout properties			*Grout performance summary:* Flowability | Setting time | Strength[+]
			Flow (s)	Setting time (mins)	Strength (MPa)	
A	40/20/20/20	0.52	9.0	80	36.0	*'High' | 'Slow' | 'Low'*
B	40/20/20/20	0.33	32.6	65	67.0	*'Average' | 'Average' | 'Average'*
C	40/20/20/20	0.27	84.8	48	93.0	*'Low' | 'Average' | 'High'*
D	80/20/0/0	0.27	608.6	13	108.0	*'Low' | 'Fast' | 'High'*

[+]*Grout performance summary classification:*

Flow time (s):	>80	24-80	<24
Flowability:	*'Low'*	*'Average'*	*'High'*
Initial setting time (mins):	>75	25-75	<25
Setting time:	*'Slow'*	*'Average'*	*'Fast'*
28-day compressive strength (MPa):	<40	40-80	>80
Strength:	*'Low'*	*'Average'*	*'High'*

CHAPTER 5

INVESTIGATION INTO RECLAIMED ASPHALT PLANING PROPERTIES

5.1 Introduction

This chapter presents the properties of reclaimed asphalt planings (RAP) to be used to replace natural aggregates in SFC materials. Generated from road surfacing maintenance works or full-depth pavement removal and reconstruction, RAP has been the most important source of recycled materials used in the pavement construction for many years (Copeland, 2011). It can be recycled into hot, warm and cold asphalt mixture with up to 100% aggregate replacement levels possible depending on different design purposes (Afonso et al., 2016; Lo Presti et al., 2014; Mallick and Bergendahl, 2009; Oner and Sengoz, 2015).

RAP was provided by an Irish road construction company that had been collected from different sources at various times. This reflects real-life situations, as RAP is typically collected from different locations and stock-piled prior to processing and re-use. As the utilisation of RAP was at laboratory-scale, results were only determined on the first sample of RAP received (Carswell et al., 2011). While it was recognised that the properties of RAP would vary slightly throughout the research, properties determined for the initial sample were deemed to be representative based on visual inspection. Properties such as particle density, water absorption, moisture content and aggregate impact value for different sizes ranging from 8/10 mm and 10/14 mm were determined in this chapter.

Despite the positive contribution to the environment in terms of recycling, the use of RAP in a cold mixture needs more compactive effort to achieve the designed air void content than traditional hot mix asphalt. This is due to old bitumen films with high viscosity covering RAP particles, causing higher internal frictional resistance (Heneash, 2013). The desired level of AVC was in the range of 25-35%, as recommended for SFC with open-graded asphalt mixtures by various studies (Afonso et al., 2016; Anderton, 2000; Oliveira, 2006). However, the suitability of this range for SFC with open-graded RAPs and geopolymer grout remains unknown due to insufficient studies relating to cold SFC mixtures. As such, this chapter investigates the suitable particle sizes, number of gyrations and temperature of compacted RAP to achieve the required AVC range using gyratory compaction. RAP was also compacted manually using a hand operated steel roller at ambient temperature to investigate the feasibility of reducing external force for compaction, whilst still achieving the desired level of AVC. An initial trial of SFC specimens with the maximum AVC suggested (35%) and dense geopolymer grout (Mix D) was undertaken to visually assess feasibility.

5.2 Properties of RAP aggregate

RAP aggregates were collected three times from a local construction company throughout the research process. Samples received weighed approximately 360 kg. RAP with different size ranges of 8/10 mm and 10/14 mm as presented in Figure 5.1 were assessed for properties including density, water absorption, moisture content and aggregate impact value according to (British Standards, 2013b, 1998, 1990b) respectively. Soluble RAP binder content was determined using chemical turpentine following the procedure in Tran's thesis (Tran, 2014) without applying pressure. Additionally, properties of 8/14 mm sized basalt rocks used in PC concrete specimens were examined for comparison.

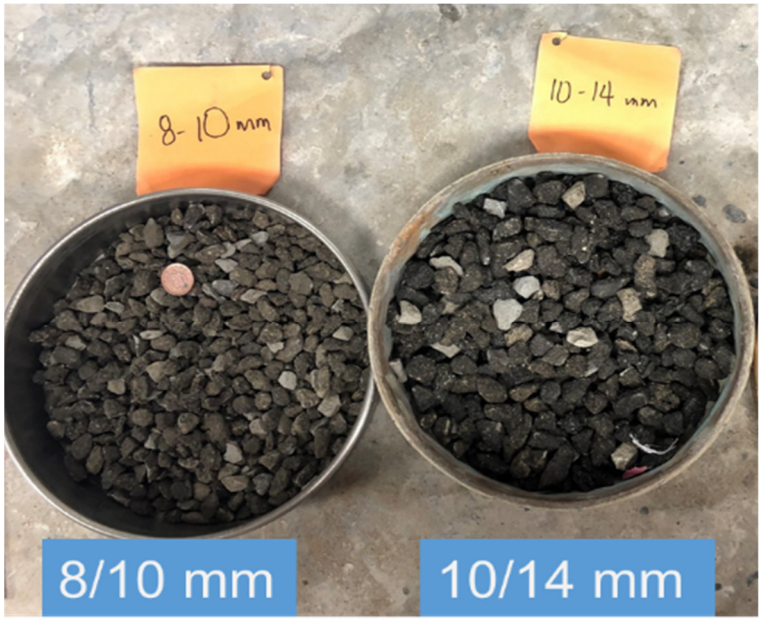

Figure 5.1. RAP with particle size fractions 8/10 and 10/14 mm.

5.2.1 Particle size distribution and formation of RAP particles

Aggregate fractionation was performed on two RAP samples, namely Samples A and B, according to BS EN 933-1:2012 (British Standards, 2012a). Each sample, of approximately 5 kg, was directly sampled from different RAP stockpiles. The overall particle size distributions recorded are presented in Figure 5.2, which shows that 100% of particles passed the 28 mm sieve. Particles retained on the 8-, 10- and 14-mm sieves (as shown in Figure 5.2) were then used for further experiments to characterise RAP properties.

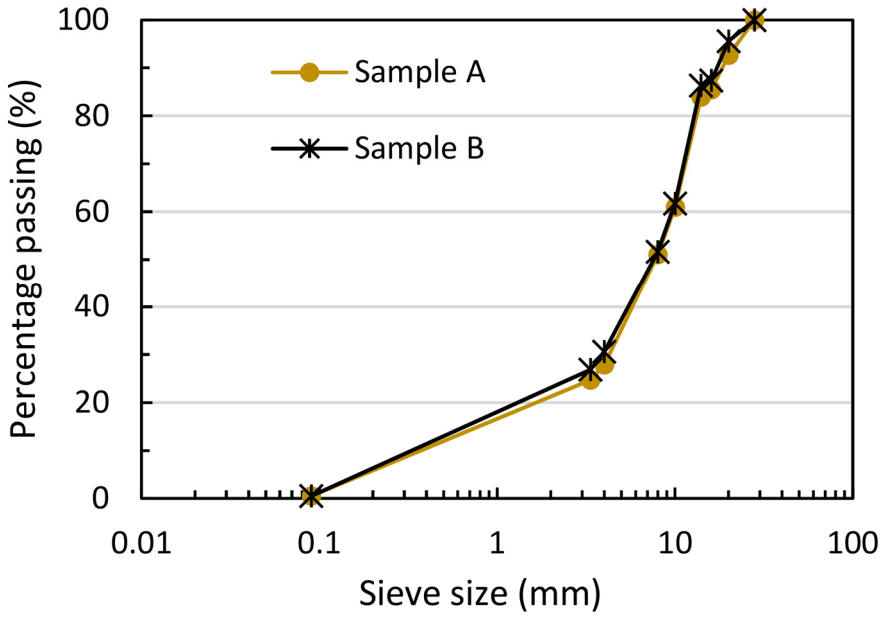

Figure 5.2. Particle size distribution of RAP.

Based on visual cross-sectional assessment, RAP samples comprised a range of aggregate/bitumen configurations as shown in Table 5.1. Images of RAP cross-section were taken from specimens comprising RAP and geopolymer grout. Since the purpose of this section was to develop an understanding of RAP formation, details of grout types and RAP content in the specimen were neglected.

As can be seen in Table 5.1, RAP samples comprised: coarse aggregates with no bitumen content (labelled Type 1); coarse aggregates fully or partially coated in adhered bitumen (Type 2); clusters of small aggregates embedded in bitumen (Type 3); and particles of aged bitumen only (Type 4). This observation was also stated in a study by Sunarjono and Hidayati (2019) where RAP particles were classified into six similar groups based on their formation. RAP formation Type 2 with old aggregate particle coated in aged bitumen was commonly studied in related available literature (Saliani et al., 2019; Singh et al., 2017).

Table 5.1 indicates that sorting RAP particles by sieve size in the dry condition only was not likely to create similar samples in terms of RAP composition type. This would certainly be an issue if the RAP was being re-used in hot-mix asphalt as the aged bitumen content would be liquefied during heating processes, causing degradation into finer particles (Sivilevičius et al., 2017). However, for the SFC materials in this study, RAP was used as a substitute for conventional aggregate in cold mix conditions. As such, all aged bitumen

remained in a stiff form attached to old aggregate, thereby minimising any effects of content variability.

Table 5.1. Type of formation of RAP particle derived from visual observations.

Type of formation	Cross-section of RAP particle	Diagram	Aggregate/bitumen configurations
Type 1	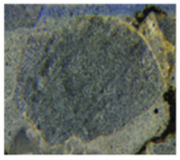	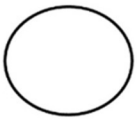	Only old coarse aggregate
Type 2	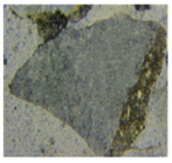		Old coarse aggregate + adhered old bitumen
	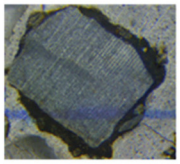		
	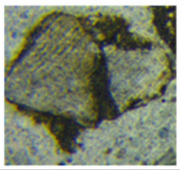		
Type 3	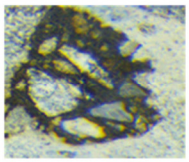	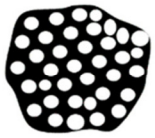	Old fine aggregate + adhered old bitumen
Type 4	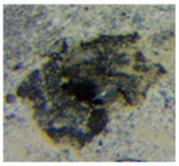		Only adhered old bitumen

5.2.2 Properties of RAP and basalt aggregate

Properties of RAP and basalt aggregates are presented in Table 5.2. All testing methods for assessing density, water absorption, moisture content, aggregate impact value and binder content were performed on at least three batches of RAP and basalt aggregates and mean values recorded. In general, RAP particles had lower densities, water absorption and moisture content than the basalt aggregate owing to the RAP comprising aged bitumen and fine aggregate particles attached to the old aggregate. Densities of RAP with different particle sizes were similar, with bulk and apparent particle densities within the ranges of

1.17-1.25 and 2.50-2.58 g/cm^3 respectively. Apparent density of RAP obtained from this study (2.50-2.58 g/cm^3) encompassed the density range of RAP extracted from previous studies (2.29-2.70 g/cm^3) (see Table 2.1). Apparent density of basalt aggregates (2.66 g/cm^3) was within the range of 2.6-3.0 g/cm^3 for basalt aggregate in the UK (Sims et al., 1998). RAP particles possessed water absorption of approximately 1% by mass, which was lower than the maximum required value of 2% stated in BS EN 13043:2002. This indicated that RAP can be assumed to be freeze-thaw resistant (British Standards, 2002). The AIV range for RAP was 4.17-5.10%, which was considerably lower than the required value of AIV of 25% stated in (British Standards, 1992) for concrete aggregate (Sims et al., 1998). The low AIV values obtained indicated that RAP particles were able to absorb more sudden impact load compared to natural aggregates owing to the existence of aged bitumen layers on the covered outside natural aggregate of RAP. This is in good agreement with findings from the study by (Reta et al., 2018), where AIVs of RAP (approximately 9.4%) were found to be significantly lower than natural aggregates (18.7%) due to the additional layers of aged bitumen.

Soluble binder content of RAP aggregates obtained from turpentine extraction method varied from 5.77-6.93% by mass. These results were slightly higher than bitumen content of RAP particles (3.7-5.8% by mass) from previous studies (Pradyumna et al., 2013; Shadmani et al., 2018), which was possibly attributed to the loss of fine particles in RAP aggregates (< 75 μm) during extraction process using turpentine. The fine particles were washed away along with bitumen in RAP particles using turpentine, resulting in decreased weight change M_{AT} associated with increased soluble binder content (SBC) in Equation (3.3) in Chapter 3.

Table 5.2. Summary of RAP and basalt aggregate properties.

Aggregate properties	Unit	Particle sizes (mm)		
		RAP		Basalt
		8/10	10/14	8/14
Bulk density	g/cm^3	1.25	1.17	1.29
Apparent particle density	g/cm^3	2.58	2.50	2.65
Water absorption	%	1.03	1.04	1.72
Moisture content	%	0.30	0.55	0.47
Aggregate impact value	%	5.10	4.17	4.80
Binder content	%	5.77	6.93	N/A

5.3 Air void measurement of compacted RAPs by gyratory compactor

Since there are no previous works investigating the air void content of compacted RAP mixture using a gyratory compactor, this work was undertaken to investigate the suitable particle sizes and temperatures of compacted RAP to achieve AVC of 25-35% as recommended from previous studies (Afonso et al., 2016; Anderton, 2000; Oliveira, 2006). The RAP size factions 8/10 and 10/14 mm were compacted using a gyratory compactor with the number of gyrations ranging from 1 to 150 cycles in order to achieve various levels of AVC. Increasing compactive effort typically results in higher density and lower AVC in pavement mixtures (Nicholls et al., 2010).

RAP was compacted either at ambient temperature or after being oven-heated at 100°C for 90 minutes. Sivilevičius et al. (2017) suggested the temperature of 100-120°C for pre-heating RAP to retain heat during compaction processes without significantly reducing properties of aged bitumen layers. Density and air void contents of the compacted test specimens were calculated using the following equations according to BS EN 12697-31:2019 (British Standards, 2018b):

$$Density_i = \frac{M_{RAP}}{Ah_i} \qquad (5.1)$$

$$AVC_i = 100\left(1 - \frac{M_{RAP}}{\delta_{RAP} A\, h_i}\right) \qquad (5.2)$$

where: i is the number of gyrations; $Density_i$ is the density of specimen after "i" gyrations (g/cm^3); AVC_i is the air void content after "i" gyrations (%); M_{RAP} is the weight of RAP particles (g); δ_{RAP} is the apparent density of RAP (g/cm^3); A is the cross-section area of the specimen (cm^2); h_i is the height of specimen after "i" gyrations (cm).

Figure 5.3 (a) and (b) illustrate the variation of density and air void content of compacted RAP in relation to the number of gyrations in the range 1 to 150 and temperature. AVC values for all samples tested decreased sharply in the first 40 gyrations. On the contrary, density values of all samples increased significantly in the first 20 gyrations. Clearly after 150 gyration cycles, RAP pre-heated at 100°C for 90 minutes had lower AVC (approximately 21%) than that of RAP at 26°C (24-26%), confirming that pre-heating lead to increased compaction levels.

The gyratory curves of density and air void content versus number of gyrations in Figure 5.3 show typical trends of aggregates compacted in a gyratory compactor, which is in agreement with findings from a study by Li et al. (2015). As shown in Figure 5.3 (a), relationship of density and gyration numbers of single-size RAP (12.5 mm) compacted at ambient temperature obtained from Li et al. (2015) were broadly similar to RAP with sizes of 8/10 mm and 10/14 mm investigated in this study.

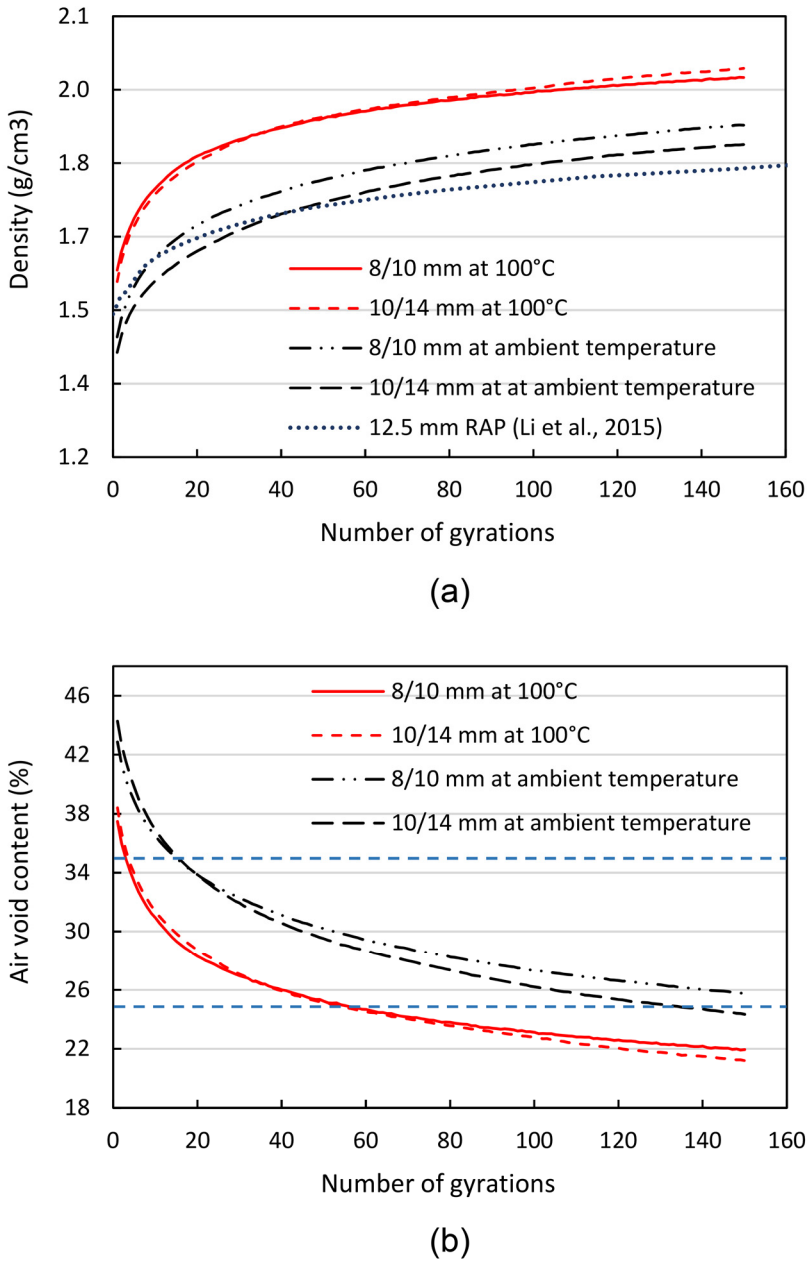

Figure 5.3. (a) Density and (b) Air void content of compacted RAP mixtures in relation to temperature and number of gyrations.

The impact of this is illustrated in Figure 5.4, which shows that 10/14 mm RAP samples at room temperature fell apart after being extruded from the mould, while RAP pre-heated at 100°C for 90 minutes maintained its compacted shape. Within the recommended AVC range 25-35% by Anderton (2000), the highest AVC of 35% for open-graded aggregate skeleton for SFC could be easily obtained with low compaction effort, with approximately 5 and 17 gyration cycles for pre-heated RAP and RAP at room temperature respectively.

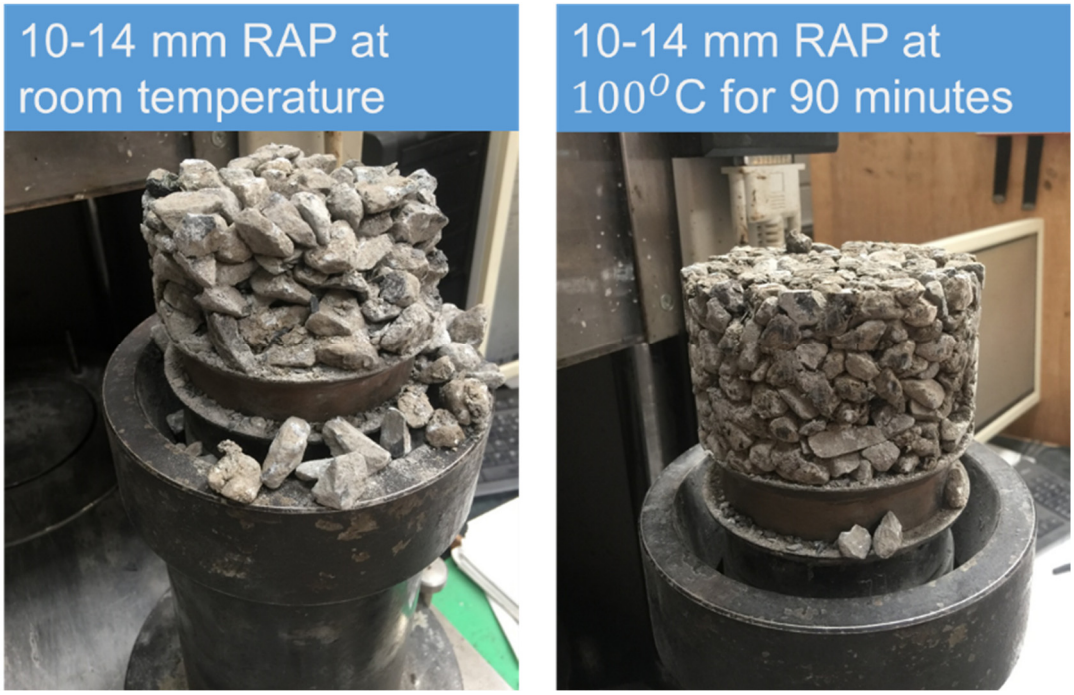

Figure 5.4. Compaction of 10/14 mm RAP at ambient temperature (left) and at 100°C for 90 minutes (right) extruded from perforated mould after 150 gyration cycles.

Figure 5.5 compares percentage AVC differences in relation to number of gyrations (1 versus 150), temperature (ambient versus 100°C) and particle sizes (8/10 versus 10/14 mm). Number of gyrations played the most important role in the percentage of air voids (40-45% differences), followed by RAP pre-heating temperature (10-17% differences). On the other hand, RAP particle size did not greatly affect AVC, with differences ranging from 1-6%.

5.4 Open-graded RAP test specimen production by manual compaction

The highest AVC of 35% within the recommended range 25-35% for open-graded aggregate skeletons for SFC were easily obtained with low gyration levels (within 17 cycles) at

ambient temperature. To explore the feasibility associated with less compaction effort while still achieving the desired compaction level, RAP test specimens were compacted manually by a hand operated steel roller (17.5 kg) in accordance with BS EN 12697-33:2013 (British Standards, 2013c).

Since the recommended AVC of open-graded RAP (25-35%) was higher than bituminous mixture (maximum 7% (MCHW Series 900, 2019)), a smaller steel roller was used than that suggested for bituminous mixture compaction (400-1100 mm diameter) stated in BS EN 12697-33:2013 (British Standards, 2013c). Since particle size did not play a significant role in density and AVC as shown in Figures 5.3 and 5.5, test specimens were compacted using 8/14 mm size particles to optimise the amount of recycled content.

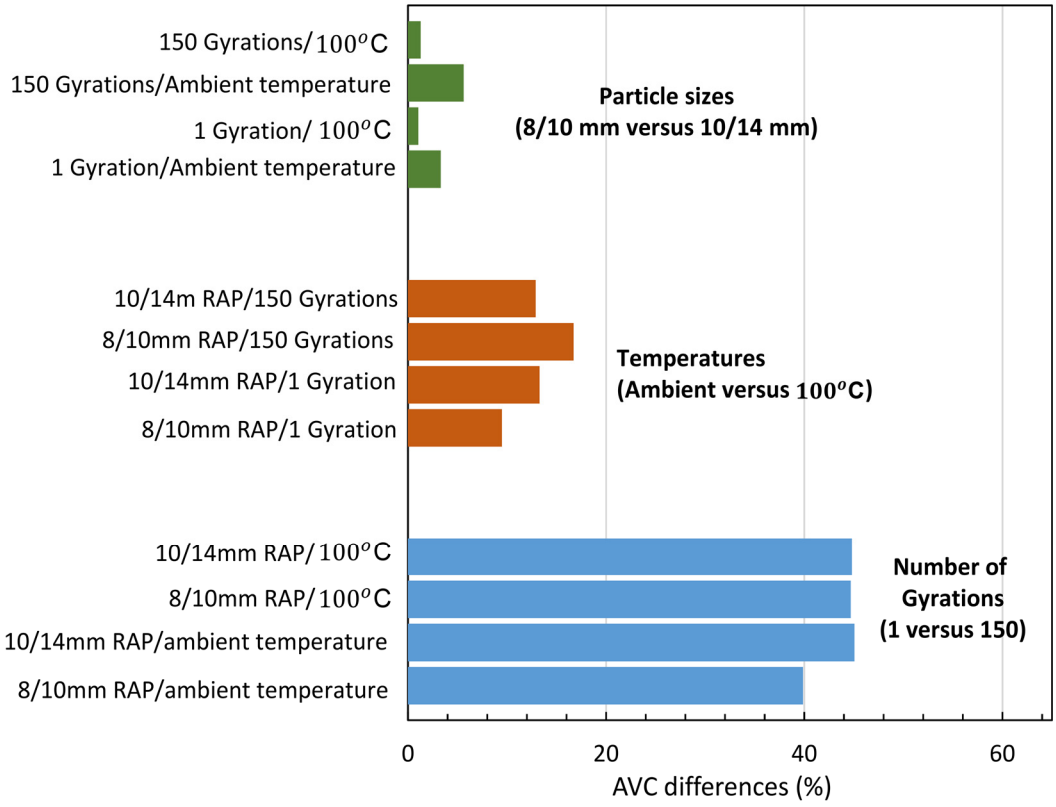

Figure 5.5. Percentage difference of AVC between gyration numbers (1-150), temperatures (ambient-100°C) and particle size (8/10-10/14 mm) of RAP mixtures.

5.4.1 Initial assessment of suitable air void content for open-graded RAP test specimen

The AVC range of 25-35% was recommended for open-graded asphalt skeleton filled with high-flowable cement grout (maximum flow time of 10 s) in Anderton's study (Anderton, 2000). However, the geopolymer grouts investigated in this study possessed a broad range of flowability (9-609 s). Many of the grouts were not suitable for open-graded RAP mixtures. As such, the feasibility of test specimens with high porosity of RAP (35% AVC) and geopolymer grout with low flowability (Mix D) was investigated. The purpose was to obtain a visual inspection of the feasibility of filling up the voids with grout. Mechanical properties, such as compressive strength, were not examined.

The 8/14 mm sized RAP was compacted manually to achieve AVC of 35% in a cylindrical mould of 100 mm diameter and height. RAP with weight M_{RAP} = 1.3 kg defined by equation (5.3) stated in BS EN 12697-33:2013 (British Standards, 2013c) was gradually placed into the mould and compacted until the height of 100 mm was obtained. Geopolymer grout Mix D was then poured into the surface of the compacted test specimen.

$$M_{RAP} = 10^{-9} \times V_{Total} \times \delta_{RAP} \times \left(\frac{100 - AVC}{100}\right) \qquad (5.3)$$

where: M_{RAP} is the weight of RAP particles (kg); V_{RAP} is the volume of the mould (mm^3); δ_{RAP} is the density of RAP (kg/m^3); AVC is the air void content of compacted RAP (%).

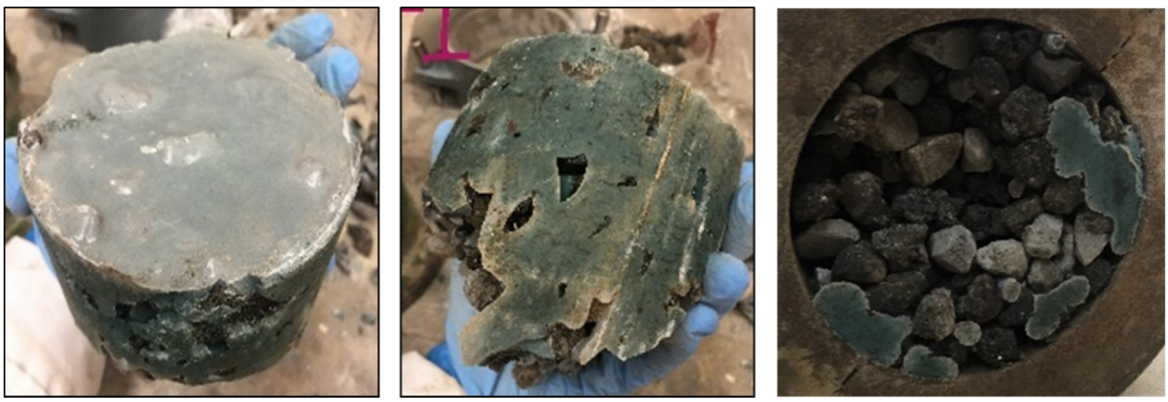

(a) (b) (c)

Figure 5.6. Specimen comprising open-graded RAP skeleton (AVC = 35%) and geopolymer grout Mix D (flow time = 609 s). (a) Top view. (b) Side view. (c) Bottom view.

As shown in Figure 5.6, geopolymer grout Mix D did not entirely fill all the interconnected voids of the RAP test specimen. The specimen fell apart when it was demoulded. This suggested that the AVC of open-graded RAP studied in this thesis needed to be higher than 35%.

5.4.2 Open-graded RAP skeleton preparation for further investigation of SFC

To prepare open-graded RAP with AVC greater than 35%, 8/14 mm RAP was placed into a 100x100x100 mm mould without compaction to achieve the highest AVC and the weight of un-compacted solid RAP was recorded as M_{RAP1}. In order to achieve various AVC levels, compaction was performed on gradually increasing RAP contents at intervals of 8, 16 and 32% of the weight M_{RAP1}. RAP content by volume was determined by Equation (5.4) while AVC of open-graded RAP skeleton structure was calculated by Equation (5.2), where h_i in this case is the mould's thickness (mm).

The production of open-graded RAPs was conducted at room temperature without the addition of virgin bitumen or heat energy.

$$RAPCONTENT(j) = \frac{100\ M_{RAP}(j)}{\delta_{RAP} \times V_{Total}} \qquad (5.4)$$

where: j is percentage of added weight ($j = 8\%, 16\%, 32\%$ of the weight M_{RAP1}); $RAPCONTENT(j)$ is the RAP content by volume at j% added weight (%); $M_{RAP}\ (j)$ is the weight of RAP particles at j% added weight (kg); δ_{RAP} is the density of RAP (kg/m^3); V_{Total} is the mould volume (m^3).

5.4.3 Characterisation of open-graded RAP test specimens

Figure 5.7 shows AVC and RAP contents (% by volume) of the open-graded RAP test specimens with different weights of compacted RAP as a percentage of un-compacted RAP weight (M_{RAP1}). The AVC of un-compacted RAP was 55% while the three levels of RAP test specimens compacted manually were 51, 46 and 38%. The reduction in AVC was associated with an increase in RAP content from 45% to 62%.

It can be seen that the range of AVC levels that manual compaction delivered was 38-55%, which was higher than that of the failed specimen (AVC = 35%). Rather than follow the suggested AVC of 25-35% from the current literature, for SFC with cold RAP mixtures and

geopolymer grouts, higher AVC of 38-55% (i.e. 45-62% solid RAP content by volume) was selected for further investigation in the next chapter.

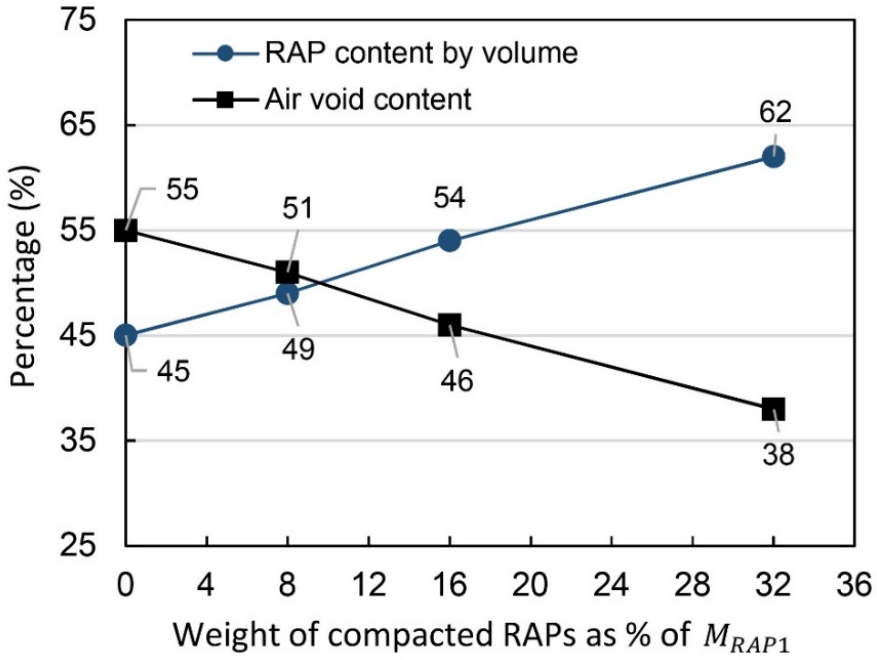

Figure 5.7. Percentages of air void content and RAP content of open-graded RAP skeletons.

5.5 Summary

Properties of RAP with different particle sizes 8/10 and 10/14 mm, to be used as a substitute for natural aggregates in SFC materials, were assessed in this chapter. Air void contents of RAP compacted by gyratory compactor and hand-roller were investigated. The following is a summary of the findings:

- Particle size had a minor role in RAP properties such as particle density, water absorption, moisture content and aggregate impact value.
- Compaction of RAP at ambient temperature achieved AVC of 24-26% and densities of 1.84-1.88 g/cm^3 after gyratory compaction.
- Compaction of pre-heated RAP at 100^{o}C decreased AVC to 21-22% and densities to 1.97-1.99 g/cm^3.
- The number of gyrations exhibited considerable influence on AVC of RAP compaction.
- RAP particle sizes had a slight influence on AVC of RAP compaction.

- Open-graded RAP test specimens were prepared at room temperature and compacted manually to minimise energy. As particle sizes did not play a significant role in AVC, 8/14 mm sized RAP was used to optimise the use of RAP and decrease the processing cost for RAP fractionation.
- Visual observation of compacted test specimens with AVC of 35% and geopolymer grout with low flowability showed that the recommended AVC of 25-35% from previous studies was not suitable for all geopolymer grout mixes within the scope of this study due to the incomplete RAP penetration.
- Open-graded RAP test specimens with RAP contents of 45-62%, associated with AVCs of 55-38%, by volume were identified as suitable for further investigation.

CHAPTER 6

INVESTIGATION INTO ENGINEERING PROPERTIES OF SFC MATERIALS INCORPORATING GEOPOLYMER GROUTS AND RAP AGGREGATES

6.1 Introduction

Semi-flexible composite (SFC) pavements, generally referred to as grouted macadam or resin-modified pavements, commonly consist of lightly compacted, open-graded hot mix asphalt with void contents of 25-35% by volume and Portland cement grout. This material combines the properties of flexible and rigid pavements such as high durability and strength, temperature and freeze-thaw resistance, as well as reduced permeability (Anderton, 2000; Qingjun et al., 2015). SFC materials have typically been used for heavy-loaded and slow-trafficked areas like fuelling areas, distribution centres, industrial area, bus terminals, hardstandings and airfields. Often the construction of typical SFC pavements takes at least two days, including the time for overlaying hot porous asphalt layer and allowing it to cool down, grout injection and hardening time of minimum 18 hours (Oliveira, 2006; Pratelli et al., 2018). This prolonged construction duration has the potential to increase cost and delay in reopening the road to traffic.

To facilitate more rapid construction processes, SFC pavements comprising cold mix asphalt have been considered by numerous studies (Afonso et al., 2016; Li et al., 2018; Oliveira, 2006; Pratelli et al., 2018; Setyawan, 2013). Ready to Mix (RTM), a proprietary product owned by CVR SpA, was reported to achieve higher stiffness modulus of 27.8 GPa and compressive strength of 22.1 MPa after 28 days (Pratelli et al., 2018). In this study, RTM consisted of coarse aggregates coated with cationic bituminous emulsion and commercial cementitious grout R2M Flowflex. The authors also affirmed a cost for RTM construction of about EUR 5.7/cm^2, which was 25% lower than traditional SFC pavement containing hot mix asphalt (EUR 9/cm^2). Although no further R2M Flowflex property information was given in this study, it is apparent that grout properties such as flowability and strength have considerable impacts on the behaviour of SFC materials (Afonso et al., 2016; Setyawan, 2013). In the study by Afonso et al. (2016), formulations of PC and geopolymer grouts were designed based on flowability to impregnate porous aggregate skeletons. SFC material with high flow PC grout (17 s flow time in accordance with Marsh flow cone test) exhibited low compressive strength of 7.0 MPa, while its counterpart with low flow (144 s) achieved higher strength of 11.4 MPa. On the contrary, SFC material containing geopolymer grout with the longest flow time (467 s) exhibited the lowest compressive strength of 2.6 MPa. While no detailed explanation was given in this paper, this low strength might be explained by the low fluidity grout failing to completely impregnate the aggregate skeleton. As this study only considered one type of geopolymer grout, the lack of diversity in the grout types

makes it difficult to find a wider range of properties for SFC materials, thereby losing a great potential of practical application.

Against this background, this chapter aims to develop an innovative suite of semi-flexible composite pavement materials comprising geopolymer grout with a wide range of performance in terms of fresh and mechanical properties (as presented in Chapter 4) and cold mix reclaimed asphalt planings with varying levels of porosity. SFC materials were produced at ambient temperatures using industrial by-products as binder and construction wastes (RAP) as the main aggregates to offer an economic and sustainable alternative to PC grouted systems.

The effect of grout type and RAP content on SFC material performance was evaluated via laboratory testing of permeable porosity, compressive strength and ultrasonic pulse velocity. Since the SFC pavements introduced in this study comprised cold mix open-graded RAP skeletons with no universally accepted standard to determine performance, it was considered to behave similarly to hydraulically bound material (HBM) in accordance with BS 9227:2019 (British Standards, 2019b). As such, control specimens made from PC grout, 8/14 mm sized basalt aggregates with solid content of 45% and 2% superplasticizer at ambient temperature were used for comparison. In addition to experimental techniques, SFC compressive strength was predicted based on either ultrasonic pulse velocity values, RAP content and geopolymer grout compressive strength or machine learning-based Deep Neural Network approaches integrated with sensitivity analysis. Outcomes from sensitivity analysis are expected to identify the critical input parameters in SFC strength prediction and control them carefully during SFC manufacturing process.

As confirmed in TRL Report 615 (Nunn, 2004), elastic modulus is normally used to design pavement thickness in the UK. As such, a key output from this chapter is a preliminary methodology to predict the elastic modulus of geopolymer-based SFC material based on rapidly attained laboratory or site-based test methods including compressive strength and ultrasonic pulse velocity. Application of these relationships was applied in a preliminary pavement design example utilising SFC as a base layer in heavy duty pavement (HDP) for industrial hardstanding, as heavily loaded areas are one of the most common applications of SFC (Densit, 2018a; Plug et al., 2006). Material cost analysis and greenhouse gas assessment were also conducted to investigate the performances of SFC materials in terms of economic and environmental aspects.

6.2 Preparation of SFC materials incorporating geopolymer grout and RAP

6.2.1 Geopolymer grout selection

As discussed in Chapter 4, ideal grout mixes for SFC materials should have adequate performance for the final product. Geopolymer grouts investigated in this study provided a wide range of performance in terms of flowabilty (flow time from 9-609 s), initial setting time (13-80 minutes) and compressive strength (19-108 MPa). Given the broad range of practical applications for pavement envisaged for this technology, this flexibility offers an important benefit in subsequent SFC implementation. However, there was performance contradiction among a diverse suite of 20 geopolymer grout mixes studied in the previous chapter. For instance, grout with the highest level of flowability exhibited the lowest values of strength and vice versa. Hence, to assess a more comprehensive understanding of SFC behaviour and explore the impact of grout performance on the properties of resulting SFC specimens, a suite of 16 SFC mixtures was prepared based on the four grout types: Mix A, Mix B, Mix C and Mix D selected from the 20 grout mixes previously described. As explained in Chapter 4, these mixes offered diverse performance classifications with respect to flowability, initial setting time and compressive strength as follows:

Mix A (‘High’ | ‘Slow’ | ‘Low’)

Mix B (‘Average’ | ‘Average’ | ‘Average’)

Mix C (‘Low’ | ‘Average’ | ‘High’)

Mix D (‘Low’ | ‘Fast’ | ‘High’)

The first three grout types (mixes A, B and C) with flow times of 9-85 s, setting times of 48-80 mins and compressive strengths of 35.8-92.7 MPa, were selected from the GGBS+FA+MK+SF binder category. Mix D, with the lowest flowability value of 609 s, fastest setting time of 13 mins and highest compressive strength of 108 MPa, was selected from the GGBS+FA binder group.

6.2.2 Open-graded aggregate skeleton

As described in Chapter 5, open-graded aggregate skeletons were prepared using 8/14 mm RAP aggregates with solid content levels ranging from 45-62% by volume. RAP aggregates were placed in moulds without compaction to achieve the 45% solid content level. Otherwise, RAP skeletons were compacted manually to achieve the required solids content level. Both the compacted and un-compacted aggregate skeletons used in this study were

prepared at ambient temperature and without the addition of any heating energy or virgin bitumen. The main properties of RAP aggregate are shown in Table 5.2.

6.2.3 SFC specimen preparation

An indication of the RAP skeleton preparation process is presented in Figure 6.1 (a-e). SFC samples were prepared by pouring geopolymer grout into moulds containing RAP skeletons from a height of around 30 cm to ensure full grout penetration (Figure 6.1 (c)). Overfilled grout was scraped off after no air bubble formation appeared on the surface of specimens. All SFC specimens were covered with polyethylene film and kept at room temperature until time of testing (Oakes et al., 2019).

Microstructural characteristics of RAP particles and SFC specimens were observed using SEM JEOL JSM-601PLUS apparatus. Except for RAP particles, all specimens with a dimension of approximately 15x15x12 mm were cut from SFC cubes using a diamond slicing wheel prior to sample preparation.

6.3 Preparation of control specimen

Since the SFC mixtures designed in this study comprised cold mix RAP skeletons (over 38% air void content) and different geopolymer grout mixes without an accepted standard to determine performance, it was assumed to behave similarly to hydraulically bound material (HBM) following BS 9227:2019 (British Standards, 2019). Manufacturing procedure without the need for heating energy proposed for SFC was also simpler than the traditional SFC with hot mix porous asphalt and cementitious grout. Therefore, control specimens with similar manufacturing processes comprising cold basalt mixtures grouted by cementitious grout were chosen as control specimens.

Control specimens (referred to as: PC Control) were manufactured at a laboratory-scale using Portland Cement grout and 8/14 mm basalt aggregates with solid content of 45% by volume for comparative purpose (see Figure 6.2). Specimen preparation followed a similar process as for SFC materials. The specimens for UPV and permeable porosity testing of conventional concrete were cast in 100 mm cubes while compressive strength testing was performed on 50 mm cubes sawn from concrete slabs. The properties of the basalt aggregate used are presented in Table 5.2. The grout, referred to as PCG Control, was prepared using general purpose cement provided from Lafarge, water-to-cement (w/c) ratio of 0.33 and 2% (by mass of PC content) Viscocrete 3000 superplasticizer.

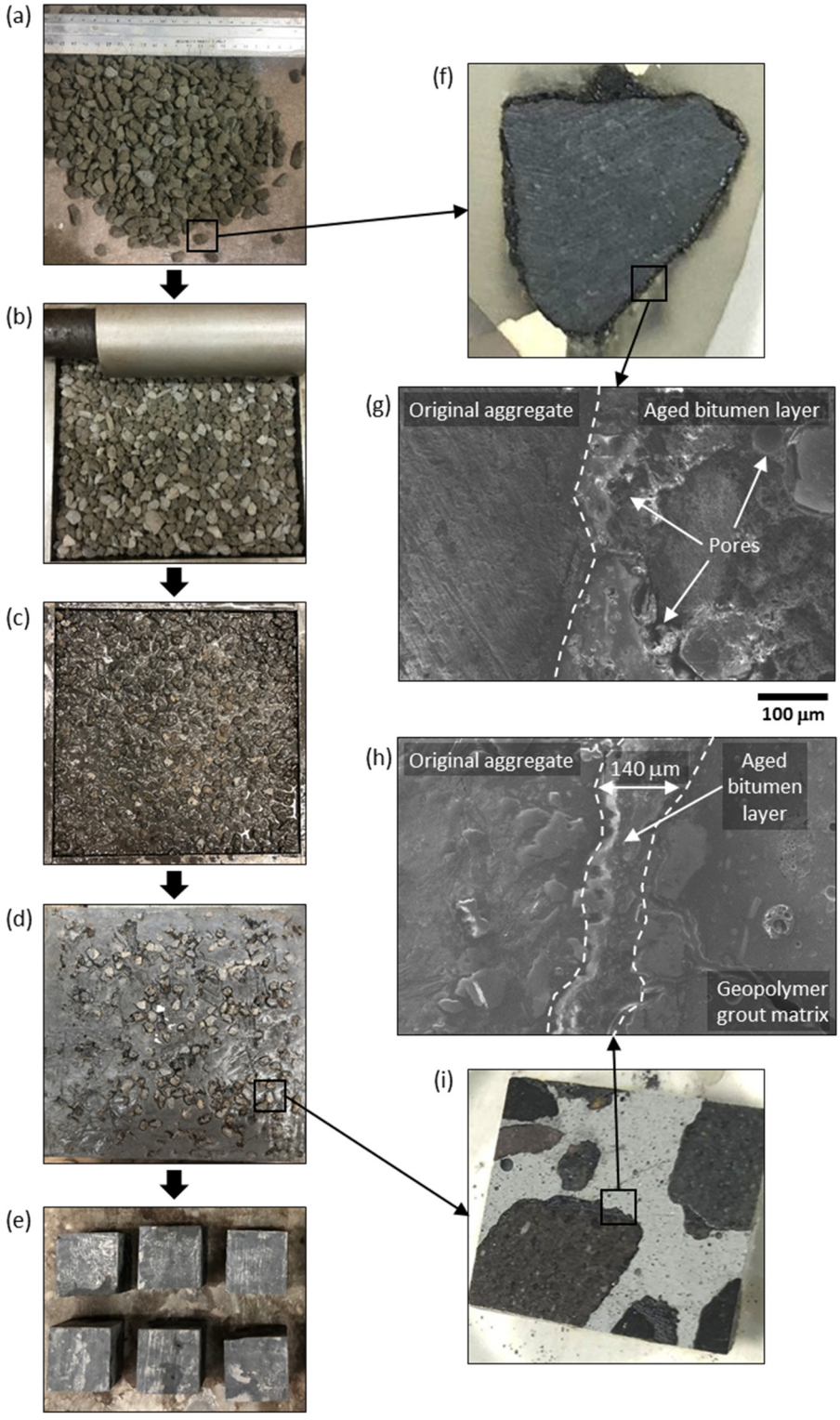

Figure 6.1. SFC manufacturing steps, including: (a) preparation of single-sized RAP particles; (b) hand compaction of RAP particles; (c) RAP particles infused with fresh geoplolymer grout; (d) hardened SFC slab (305x305x50 mm); (e) extraction of SFC specimens for testing (50 mm cubes for compressive strength testing shown). SEM characterisation of RAP particle (f,g) and SFC specimen (h,i).

The w/c of the control grout was chosen based on the suggested w/c ratio range of 0.30-0.35 for the SFC commercial product named Densit®; a super plasticised cement paste produced by CIP Densiphalt (Densit, 2018a). The 2% dosage of superplasticiser was chosen based on the manufacturer's recommendation. The measured flow time, initial setting time and 28-day compressive strength of PCG Control grout was 52 s, 250 mins and 84 MPa respectively. With respect to the classification of geopolymer grout defined in Table 4.3, PC grout PCG Control falls into the ('Average' | 'Slow' | 'High') category in terms of flowability, initial setting time and compressive strength.

Figure 6.2. Control specimens comprising PC grout and basalt aggregates with solid content of 45% by volume.

6.4 Characterisation of SFC materials

To develop a more comprehensive understanding of SFC behaviour, grout mixes A, B, C and D were then used to manufacture SFC test specimens comprising RAP skeletons with 45, 49, 54 and 62% solid contents by volume. Figure 6.3 shows the compressive strength of SFC and PC Control materials after 3, 7 and 28 days while Figure 6.5 shows the permeable porosity and UPV values of SFC materials after 28 days curing along with performance summary for grout mixes A, B, C and D.

6.4.1 Compressive strength of SFC materials

Figure 6.3 (a-d) presents the compressive strength development of SFC specimens incorporating geopolymer grout mixes and RAP with solid contents ranging from 45-62%,

while Figure 6.3 (e-h) shows the SFC strength relative to the compressive strength of the parent grout at the same age. Results of compressive strength for the 16 SFC mixtures show wide ranges of performance at all ages. At 28-day for instance, and reflecting the wide range of mixture proportions considered, strength values ranged from 9 MPa (grout Mix A, RAP content 62%) to 32 MPa (grout Mix D, RAP content 45%). The 28-day compressive strength of SFC materials is in compliance with the recommended minimum compressive strength of 8 MPa for base layer established by the Design Manual for Roads and Bridges (DMRB), volume 7, section 2 (Highways England, 2006a), considering SFC as behaving similarly to HBM in accordance with BS 9227:2019 (British Standards, 2019b).

Based on these findings, grout Mix B was identified as delivering the highest value of 28-day SFC compressive strength (18 MPa) at the maximum usage of RAP (62%). Comparable SFC strengths for grout mixes A and C were 9 and 16 MPa respectively, whilst SFC with grout mix D was not achievable. Even though Mix D 'Low flow/Fast set/High strength' grout achieved less porous structures than the others, a negative impact of increasing RAP content did emerge. The grout failed to penetrate into specimen depth due to its low flowability and fast setting time (see Figure 6.4) leading to insufficient grout penetration. As a result, these SFC specimen types were deemed to have failed at the manufacturing stage and further performance characterisation was not attempted.

In terms of strength development with time, Figure 6.3 (a-d) shows that, on average, SFC specimens gained 66-84% of their 28-day strength value after three days. This trend reflects the established ability of geopolymer grouts to gain early strength rapidly (Samantasinghar and Singh, 2019) and offers significant benefits for pavement applications where high early strength leading to early potential exposure to traffic is preferential.

Also clear from Figure 6.3 is a general negative influence of RAP addition on compressive strength. If considering geopolymer grout Mix B, for example, corresponding SFC strength at 28 days were 34, 32, 29 and 26% of the parent grout strength (67 MPa) as the RAP content increased from 45, 49, 54 to 62% respectively. Similar trends were noted for all SFC mixes, irrespective of the parent geopolymer grout type used (see Figure 6.3 (e-h)). This means that, unlike permeable porosity or pulse velocity, both RAP content and parent grout strength had significant influences on compressive strength of SFC materials, with increasing SFC strength corresponding to increasing grout strength and decreasing RAP contents respectively.

Mix A: 40%GGBS+20%FA+20%MK+20%SF; LS = 0.52

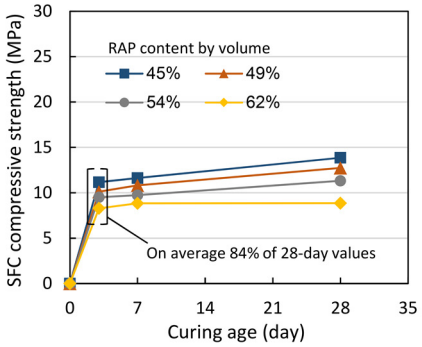

(a)

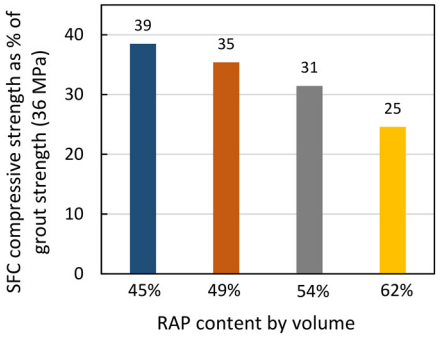

(e)

Mix B: 40%GGBS+20%FA+20%MK+20%SF; LS = 0.33

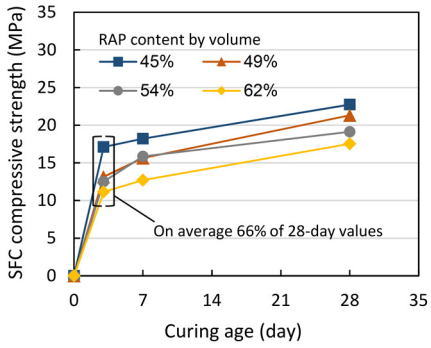

(b)

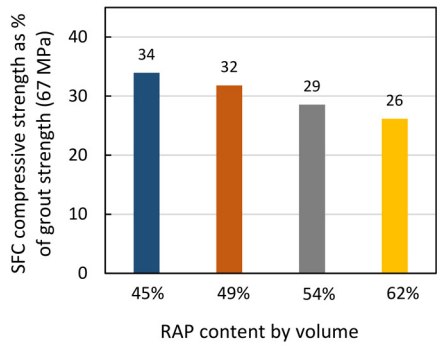

(f)

Mix C: 40%GGBS+20%FA+20%MK+20%SF; LS = 0.27

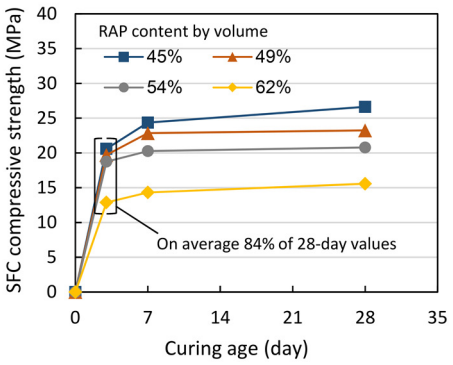

(c)

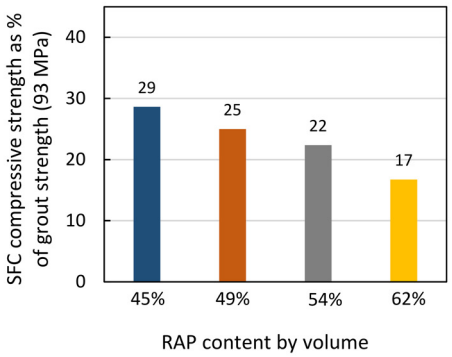

(g)

Mix D: 80%GGBS+20%FA; LS = 0.27

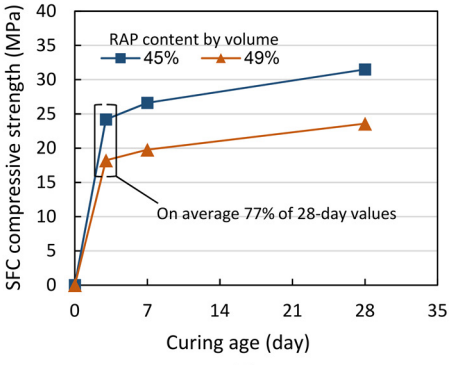

(d)

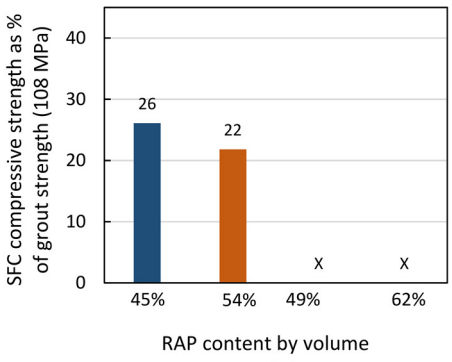

(h)

PC Control: Cement grout + 45% Basalt aggregates

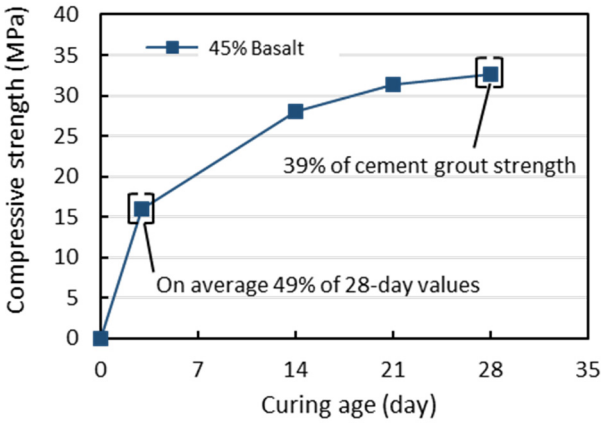

(j)

Figure 6.3. (a-d) SFC compressive strength development with time data; (e-h) 28-day SFC strength relative to the compressive strength of the parent grout at the same age; (j) PC Control compressive strength development with time data.

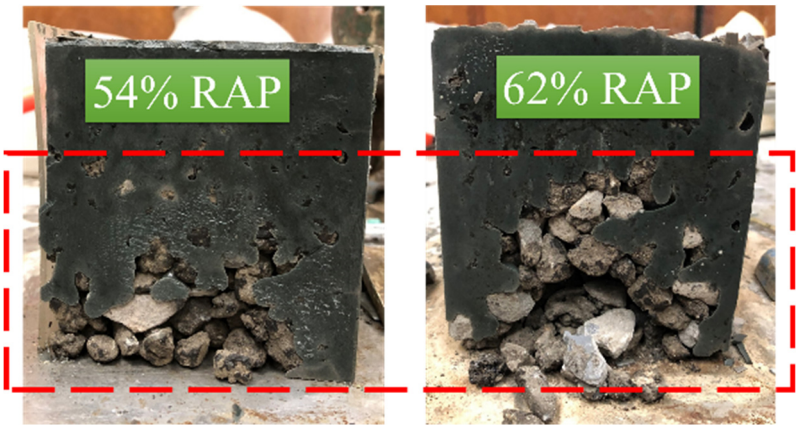

Figure 6.4. Failure of SFC specimens incorporating geopolymer grout Mix D and open-graded RAP with solid contents of 54% and 62% owing to insufficient grout penetration.

Figure 6.3 (j) shows the compressive strength development from 0-28 days of PC Control specimen containing 45% by volume of basalt aggregates. As shown in this figure, PC Control specimens gained 49% of their 28-day strength value after three days, which was lower than that of SFC specimens (66-84%). This indicates that SFC pavements offer the advantage of earlier opening to traffic over conventional concrete pavement. Compressive strength of PC Control specimens was broadly similar for the SFC specimens comprising 45% RAP and high strength geopolymer grout such as mixes C and D.

However, corresponding compressive strength of PC Control at 28 days was 39% of the parent grout strength (84 MPa) while its counterpart of geopolymer grouts with higher strength such as Mix C (93 MPa) was 29%. As expected, RAP had negative influences on compressive strength of SFC compared to natural basalt aggregates. This is in agreement with findings from previous studies where increasing RAP content associated with reduced compressive strength in concrete mixtures (Hossiney et al., 2008; Huang et al., 2005; Singh et al., 2017) and hot mix asphalt mixture (Fattah et al., 2017; Lavin, 2003).

6.4.2 Apparent density and permeable porosity

Permeable porosity and apparent density of SFC and PC Control specimens were determined by vacuum saturation method according to ASTM C1202 (ASTM, 2012) and ASTM 642-97 (ASTM, 1997) after 28 days curing at room temperature. Apparent density values of SFC and PC Control specimens are presented in Table 6.1. As presented in this table, apparent density of SFC specimens ranged from 2.34-2.45 g/cm^3 while PC Control specimen had the highest density of 2.68 g/cm^3. Apart from SFC specimen incorporating grout Mix D with the highest density, no significant correlation between other grout types and apparent density of SFC materials was obtained.

Table 6.1. Apparent density of SFC specimens

Specimens	RAP content (% by volume)	Apparent density (g/cm^3)			
		Mix A	Mix B	Mix C	Mix D
SFC	45	2.40	2.37	2.34	2.45
	49	2.35	2.35	2.37	2.44
	54	2.35	2.37	2.43	-
	62	2.39	2.40	2.38	-
PC Control	45$^{(*)}$	2.68			

$^{(*)}$ PC Control with basalt aggregates

Permeable porosity, known as open porosity, is one of the influencing factors on concrete properties such as strength or durability related to freeze-thaw cycles and alkaline-aggregate reaction (Safiuddin and Hearn, 2005). For instance, low porosity rate in geopolymer concrete with high content of GGBS could result in increased compressive strength by up to 162% (Al-Majidi et al., 2016). However, low permeable porosity could also be an issue for the frictional properties of SFC material as a wearing course since the

denser the SFC material, the more difficult it would be for the water film to absorb into its surface, causing a slippery condition.

Figure 6.5 (d) shows results of permeable porosity ρ (%) for SFC specimens with a selection of geopolymer grouts arranged in order of increasing RAP content. As shown in this figure, the main factor influencing permeable porosity was the type of the parent grout used, with porosity values ultimately ranging from 20% for SFC specimens comprising grout Mix A ('High' | 'Slow' | 'Low') to 11% for those comprising grout Mix D ('Low' | 'Fast' | 'High'). This trend corresponded well with the behaviour of conventional concrete, indicating that permeable porosity reduced with increasing compressive strength and reduced flowability and setting time (Safiuddin and Hearn, 2005). This can be explained by a significant amount of alkali aluminosilicate gel in high strength geopolymer grout and aged bitumen layers covering RAP particles and blocking the flow route of water ingress in SFC specimens. This led to decreasing saturated mass W_{ST} in Equation (3.5) in Chapter 3 and resulted in reducing permeable porosity of SFC specimens. An opposite trend was noticed in conventional concrete PC Control with high strength (84 MPa), where it exhibited high permeable porosity of 19.5%. Such behaviour could be explained by denser microstructure and lower permeability of geopolymer concrete compared to conventional concrete (Ma et al., 2018; Neupane, 2018; J. Wang et al., 2020). This trend is also in agreement with previous studies by (Aliabdo et al., 2018) where conventional concrete possessed 17% higher void content than geopolymer concrete at the same strength (27 MPa). The porosity of mixtures in the same grout type group showed a slight change with a gain in RAP content while the porosity of mixture with different grout types showed a significant change. Overall, the properties of grouts played a more important role in the permeable porosity of SFC pavement than the structure of RAP skeleton. For example, grout type Mix C ('Low' | 'Average' | 'High') with RAP content of 62% showed higher porosity than Mix B ('Average' | 'Average' | 'Average') with the same RAP content as it low flowability caused obstruction for grout to infill most pores in specimens.

6.4.3 Ultrasonic pulse velocity of SFC materials

Ultrasonic pulse velocity (UPV) is considered as a practical factor to evaluate quality of concrete such as strength, integrity or internal defects (e.g., voids, cracks) (Al-Mufti and Fried, 2018; Bondar, 2009). High value of UPV indicates good quality concrete while low UPV indicates discontinuity concrete with voids or internal defects (Singh, 2018). According to IS 13311 (Part 1):1992 (Indian Standards, 1996), UPV value can be used to classify

concrete quality. For example, concrete with UPV in the range 3000-4500 m/s corresponds to a 'Medium-Good' quality classification.

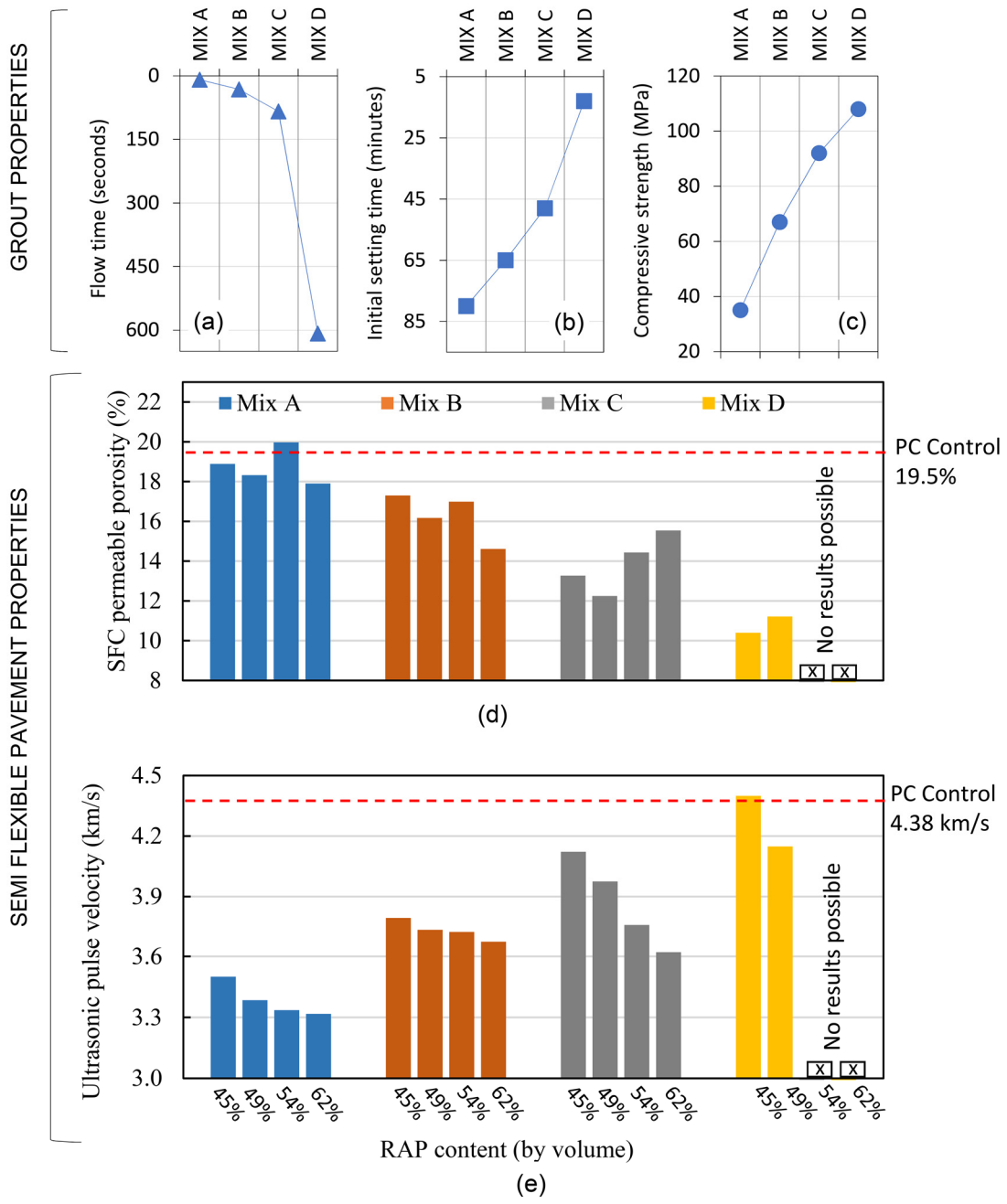

Figure 6.5. (a-c) Performance summary for grout Mix A, B, C and D; SFC performance in terms of: (d) permeable porosity and (e) ultrasonic pulse velocity.

In this study, ultrasonic pulse velocity measurement was used to estimate material properties such as compressive strength and elastic modulus (Panzera et al., 2011; Trtnik et

al., 2008; Turgut, 2004; Yildirim and Sengul, 2011). UPV values were determined by a PUNDIT pulse velocity tester based on BS EN 12504-4:2004 (British Standards, 2004). Effects of geopolymer grout types and RAP contents by volume (%) on the UPV of SFC specimens after 28 days curing are shown in Figure 6.5 (e). Reflecting improving paste microstructures, a general trend of increasing pulse velocity with increased strength and reduced workability of parent grouts is apparent in this figure. Like permeable porosity, the lowest (3.32 km/s) and the highest (4.40 km/s) values of UPV were achieved by grout mixes A ('High' | 'Slow' | 'Low') and D ('Low' | 'Fast' | 'High') respectively. It is worth noting that, for conventional concrete, this range corresponded to performance quality category 'Medium-Good quality' as defined in IS 13311 (Part 1):1992 (Indian Standards, 1996). In addition, conventional concrete specimen PC Control attained the highest UPV 4.38 km/s as a result of high strength cement grout (84 MPa) and natural basalt aggregates.

A similar general trend with permeable porosity was noted where a minor influence of increasing RAP content occurred for SFC specimens comprising grout mixes A and B with flow times ranging from 'High' to 'Average'. For grout mixes C and D with 'Low' flowability, however, a clear influence emerged, with decreasing UPV corresponding to increasing RAP content. For example, the UPV value for SFC with grout Mix C decreased from 4.12 to 3.62 km/s as the RAP content increased from 45 to 62% by volume. This was because the higher content of RAP, the more difficult geopolymer grouts to fill up voids between RAP particles by gravitational force resulting in high porosity specimen (see Figure 6.5 (d)), and the pulse travelled slower through specimens with high porosity.

6.4.4 Microstructural properties of SFC material

Figure 6.1 (h) and (i) show images of an SEM image of the aggregate-asphalt-geopolymer ITZ (grout Mix B) and typical SFC specimens embedded in epoxy resin respectively. It is noted that this SFC sample was taken from unloaded SFC cubes before subjected to compressive load. The visible aged bitumen layer in Figure 6.1 (h) is approximately 140 μm wide, with any non-visible localised pores and fine cracks filled/bounded by well-formed geopolymer grout, while the aggregate-asphalt ITZ in RAP particle shown in Figure 6.1 (g) presents a fairly porous structure. On further analysis of SEM images of this nature, networks of cracks with width of approximately 20 μm were evident in the ITZ between aged bitumen and geopolymer grout in the SFC specimens. This is a common mechanism reported in the literature (An et al., 2016) for materials incorporating cementitious and bitumen-based materials. While this phenomenon may help to impede crack propagation in SFC materials and improve its energy-absorbing capacity (An et al., 2016; Huang et al.,

2006; Li et al., 1998; Okafor, 2010; Topçu and Uygunoglu, 2016), their presence will contribute to reduced levels of compressive strength.

6.5 SFC compressive strength prediction

6.5.1 Compressive strength prediction based on UPV

Having undertaken the preliminary SFC characterisation steps described in Section 6.4, work progressed to review how the ultrasonic pulse velocity and compressive strength results might be utilised to provide meaningful rapid performance predictions.

In the first instance, this was achieved by analysing the relationship between UPV and compressive strength for SFC, a relationship defined from the study by (Panzera et al., 2011) by the exponential equation:

$$f_{cu} = a.e^{(b.UPV)} \quad (6.1)$$

where: f_{cu} is compressive strength (MPa); and a and b are empirical parameters determined by the least-squares method.

The relationship between UPV and compressive strength for the SFC results measured in this study are presented in Figure 6.6, compared to published relationships for Portland cement concrete (Nasht et al., 2005; Turgut, 2004).

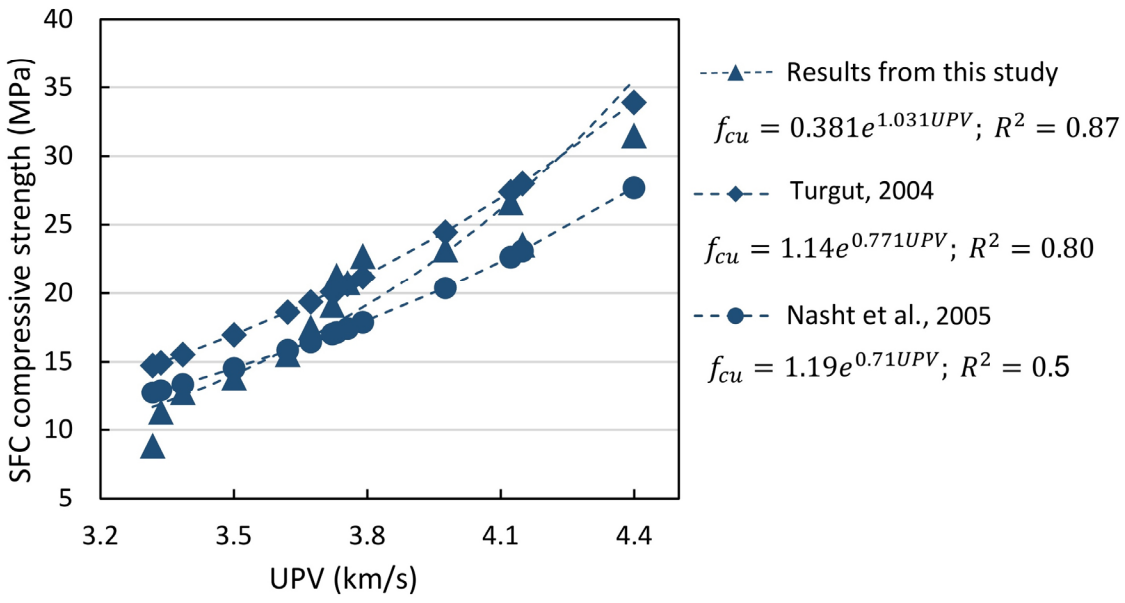

Figure 6.6. Relationships between ultrasonic pulse velocity and compressive strength for both measured and published data (for conventional cement concrete).

Comparable positive relationships between UPV and compressive strength existed for both SFC and conventional concrete, with the strongest relationship $f_{cu} = 0.381e^{1.031UPV}$ in Figure 6.6 associated with SFC specimens assessed as part of this study (R^2 = 0.87).

6.5.2 Compressive strength prediction based on RAP content and geopolymer grout compressive strength

Mathematical models for SFC compressive strength estimation were developed based on RAP content and geopolymer grout compressive strength using the following polynomial regression equation generated from SPSS statistic software:

$$f_{cu} = -0.008RAP^2 + 0.74RAP + 0.35f_{grout} - 0.003RAPf_{grout} - 10.27 \quad (6.2)$$

(R^2 = 0.87)

where f_{cu} is SFC compressive strength (MPa); RAP is RAP content (% by volume) and f_{grout} is the compressive strength of geopolymer grout (MPa).

Meaningful rapid SFC strength predictions were achieved using Equation (6.2), with a relatively high associated R^2 value (0.87). This positive modeling ability is confirmed in Figure 6.7. As shown, both RAP content and geopolymer grout strength had significant impacts on SFC compressive strength, with increasing SFC strength corresponding to decreasing RAP content and increasing grout strength.

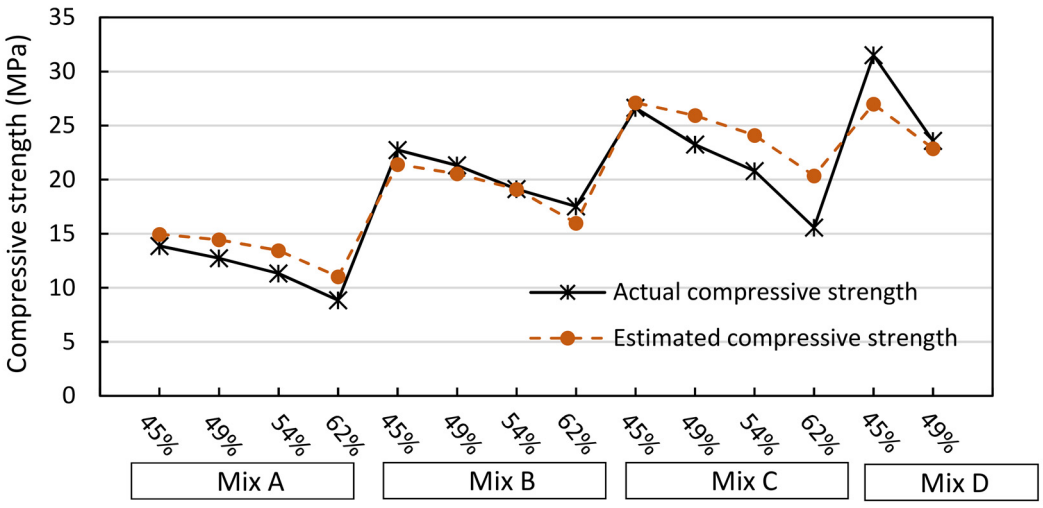

Figure 6.7. Comparison between actual and estimated values of SFC compressive strength obtained from compression experiments and Equation (6.2).

However, it is clear from Figure 6.7 that a slightly decreased prediction accuracy existed for SFC mixtures comprising grout Mix C and D. This trend is possibly explained by the negative influence of low flowability associated with reduced SFC strength of Mix C and D compared to mixes A and B, (as explained in Section 6.4.1).

6.5.3 Compressive strength prediction using machine learning approach

Data preparation for training and validation

A DNN machine learning approach integrated with sensitivity analysis was employed to predict SFC compressive strength after 28-day curing. Sensitivity analysis is commonly used to evaluate how input parameters affect output variation derived by machine learning models (Tenza-Abril et al., 2018). The machine learning models were trained through 42 datasets of input/output values obtained from compression experiments. Each dataset comprised one compressive strength output and six inputs such as RAP content (% by volume), geopolymer grout properties (i.e. flow times, final and initial setting time and 28-day compressive strength) and SFC curing ages. Input and output values, extracted from Table 4.3 (Chapter 4) and Figure 6.3 (Chapter 6), are summarised in Table 6.2. Details of the 42 datasets are shown in Table 6.3.

Table 6.2. Input/output parameters used in the SFC strength prediction training dataset.

Variable	Training parameter	Value
Input	Flow time (s)	9, 33, 85, 609
	Initial setting time (mins)	80, 65, 48, 13
	Final setting time (mins)	140, 105, 90, 30
	Grout compressive strength (MPa)	38, 67, 93, 108
	RAP content (%)	45, 49, 54, 62
	Curing age (days)	28, 7, 3
Output	SFC compressive strength (MPa)	9-32

A data division scheme was applied to reduce possibilities of error and improve the reliability of estimated results. To train the network, 34 datasets were selected randomly, while the other 8 datasets remained untrained as a validation database to confirm the accuracy of the trained network. The proposed DNN-based model was trained and validated in this way using randomly shuffled datasets.

Table 6.3. Details of input and output values for training and validation of machine learning approach.

SFC mixture		Input parameter						Output parameter
		Flow time (s)	Initial setting time (mins)	Finial setting time (mins)	Grout compressive strength (MPa)	RAP content (%)	Curing age (days)	SFC compressive strength (MPa)
SFC-Mix A	1	9	80	140	38	45	28	14
	2	9	80	140	38	49	28	13
	3	9	80	140	38	54	28	11
	4	9	80	140	38	62	28	9
	5	9	80	140	38	45	7	12
	6	9	80	140	38	49	7	11
	7	9	80	140	38	54	7	10
	8	9	80	140	38	62	7	9
	9	9	80	140	38	45	3	11
	10	9	80	140	38	49	3	10
	11	9	80	140	38	54	3	10
	12	9	80	140	38	62	3	8
SFC-Mix B	13	33	65	105	67	45	28	23
	14	33	65	105	67	49	28	21
	15	33	65	105	67	54	28	19
	16	33	65	105	67	62	28	18
	17	33	65	105	67	45	7	18
	18	33	65	105	67	49	7	16
	19	33	65	105	67	54	7	16
	20	33	65	105	67	62	7	13
	21	33	65	105	67	45	3	17
	22	33	65	105	67	49	3	13
	23	33	65	105	67	54	3	13
	24	33	65	105	67	62	3	11

Table 6.3. (Continued).

SFC-Mix C	25	85	48	90	93	45	28	27
	26	85	48	90	93	49	28	23
	27	85	48	90	93	54	28	21
	28	85	48	90	93	62	28	16
	29	85	48	90	93	45	7	24
	30	85	48	90	93	49	7	23
	31	85	48	90	93	54	7	20
	32	85	48	90	93	62	7	14
	33	85	48	90	93	45	3	21
	34	85	48	90	93	49	3	20
	35	85	48	90	93	54	3	19
	36	85	48	90	93	62	3	13
SFC-Mix D	37	609	13	30	108	45	28	32
	38	609	13	30	108	49	28	24
	39	609	13	30	108	45	7	27
	40	609	13	30	108	49	7	20
	41	609	13	30	108	45	3	24
	42	609	13	30	108	49	3	18

Three statistical measures including R^2, RMSE and MAPE were applied to evaluate the accuracy of machine learning approach DNN. These measures provide insights into differences between original and predicted values. Higher R^2 value and/or lower MAPE and RMSE values indicate better prediction performance of machine learning-based models (Dao et al., 2019).

Prediction performance of machine learning approach

Relationships between actual and predicted SFC compressive strength obtained from experiments and machine learning approach respectively are presented in Figure 6.8. As shown, minimal variation existed between actual and predicted values, indicating that the proposed approach had successfully trained itself to predict SFC compressive strength.

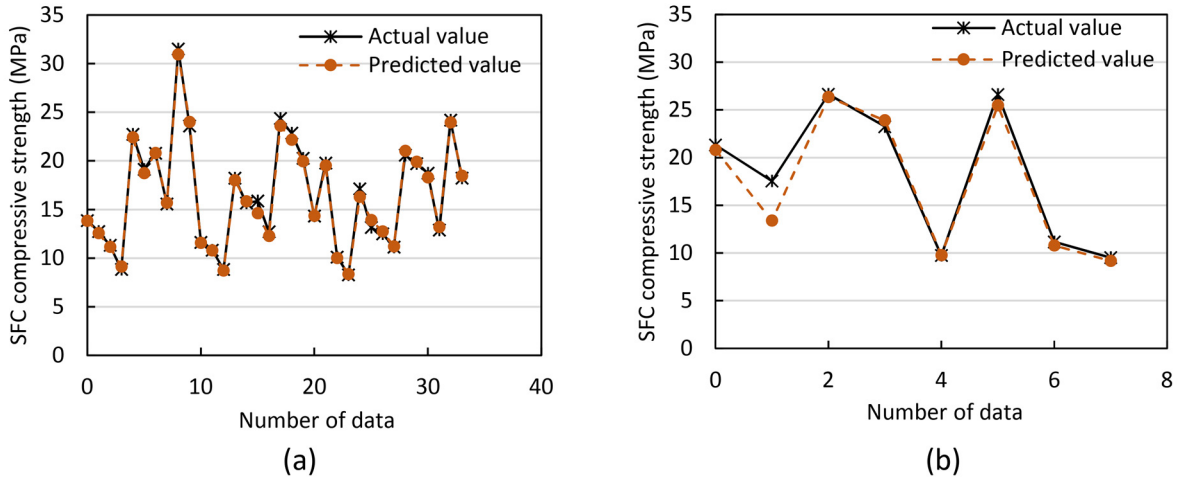

Figure 6.8. Relationship between actual and predicted SFC strength values obtained from experiments and machine learning approaches: (a) DNN training model; (b) DNN validation model.

Figure 6.9 presents the three statistical measures (R^2, RSME and MAPE) used to assess the accuracy of the proposed training and validation models. High strength prediction performance of the proposed approaches is highlighted in this figure, with strong relationships associated with DNN training and validation models (R^2 = 0.994; RMSE = 0.449; MAPE = 1.971 and R^2 = 0.919; RMSE = 1.568; MAPE = 6.438 respectively). With sufficiently high R^2 and low RMSE/MAPE values, this figure supports the validity of the proposed DNN-based model for accurately predicting SFC compressive strength, even though the number of datasets used was relatively low.

Prediction performance for mechanical properties of materials, such as fly-ash based geopolymer concrete, using machine learning approaches including artificial and deep neural networks, has been presented in previous studies (Dao et al., 2019; Huynh et al., 2020b; Ling et al., 2019; Nguyen et al., 2020), albeit with over 72 pairs of input/output values used. In the study by Huynh et al. (2020b), for example, a strength performance

model was presented based on 263 datasets. Associated values of R^2, RMSE and MAPE reported in this study were in the ranges 0.898-0.923, 2.521-3.273 and 9.496-11.54 respectively, so comparable to the work undertake here.

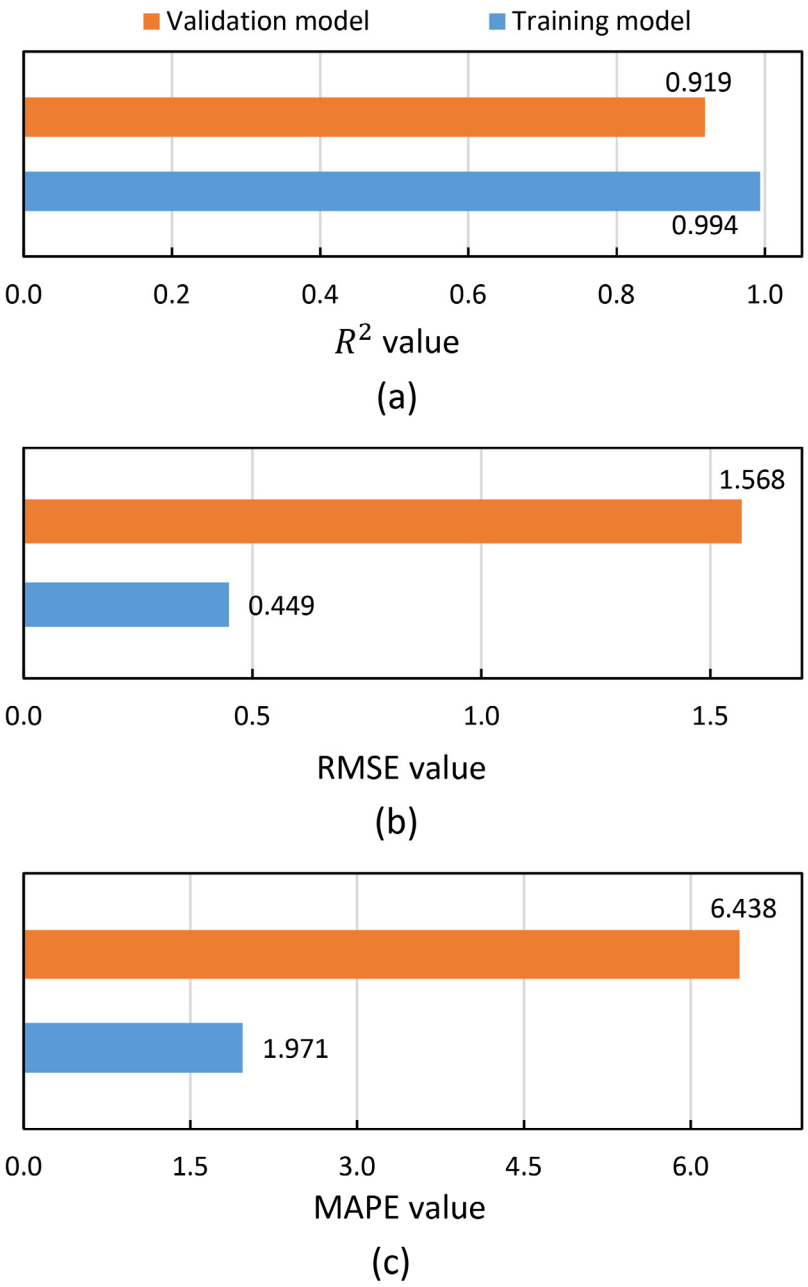

Figure 6.9. Statistical measure values of DNN-based model and change between training and validation values. (a) R^2 value; (b) RMSE value; (c) MAPE value.

Based on the performance predictions presented, work progressed to employ DNN-based modeling for further sensitivity analysis investigation. This involved calculating SFC strength by changing one input variable at a time while maintaining the other five as constants based on their mean values. For example, to assess the importance of RAP content (% by volume), this value was varied from 45-62% while other input parameters such as flow time, initial setting time, final setting time, grout compressive strength and SFC curing age were kept constant at mean values of 123 s, 57 mins, 100 mins, 72 MPa, 52% and 13 days respectively. Data derived from this sensitivity analysis was returned to the training process to estimate compressive strength.

Figure 6.10 shows the results of this sensitivity analysis, from which a pronounced influence (32.1%) of geopolymer grout strength on predicted compressive strength can be seen. This confirms the observations from as previous study by Setyawan (2013) where compressive strength of grouting materials played a significant role in SFC compressive strength.

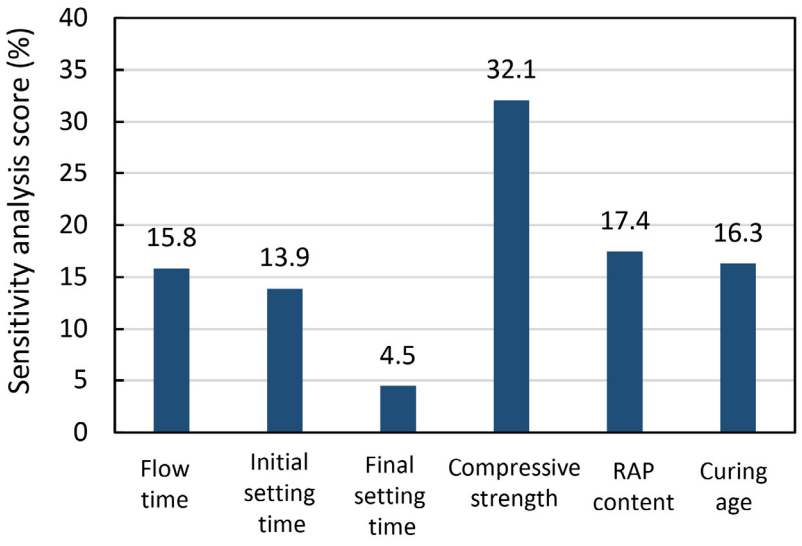

Figure 6.10. Sensitivity analysis scores for the predicted SFC compressive strength.

Additionally, shown in this figure are high sensitivity scores of 17.4%, 16.3% and 15.8% for RAP content, SFC curing age and grout flow time respectively. As such, various factors such as geopolymer grout properties, SFC curing age and RAP content should be thoroughly considered in SFC compressive strength prediction using machine learning approach. In particular based on these findings, it is recommended that geopolymer grout strength is

carefully determined and controlled in SFC manufacturing process owing to its pronounced effect on SFC compressive strength.

6.6 Elastic modulus prediction based on UPV and compressive strength

Elastic stiffness modulus is one of the crucial factors used in pavement thickness design or assessing the current state of existing structures (Highways England, 2006a; Lee et al., 2015; Rao et al., 2016). Table 6.4 presents elastic modulus classifications of typical pavement materials such as concrete, dry lean concrete and bituminous based on the Design and Maintenance Guide 27 (Design and Maintenance Guide, 2011). Elastic modulus values of SFC with hot porous asphalt and cement grouts obtained from previous studies (Afonso et al., 2016; Anderton, 2000; Densit, 2018a) are also shown in this table.

Elastic modulus is often estimated from compressive strength or UPV instead of by direct measurements (Lee et al., 2015). Table 6.5 shows proposed equations to estimate elastic modulus of conventional concrete and geopolymer concrete from compressive strength and UPV in various papers.

In this chapter, elastic modulus was predicted by empirical equations based on both UPV and compressive strength. Models from Yildirim and Sengul (2011), CEB-FIP Model Code 1990 (Comite Euro-International Du Beton, 1993) and Bondar (2009) were used to predict elastic modulus of conventional Portland cement concrete, while equations by (Diaz-Loya et al., 2011; Hardjito and Rangan, 2005; Nath and Sarker, 2017) were used to estimate elastic modulus of geopolymer concrete with or without heat curing. It is noted that compressive strength used for calculating elastic modulus by CEB-FIP model code 1990 (Comite Euro-International Du Beton, 1993) should be less than 50 MPa.

Figure 6.11 shows the relationship between UPV and predicted elastic modulus E_S (GPa) using empirical equations (6.3) – (6.8) from previous studies (Table 6.5). This included using published relationships between elastic modulus and both UPV (Yildirim and Sengul, 2011) and compressive strength (Bondar, 2009; Comite Euro-International Du Beton, 1993; Diaz-Loya et al., 2011; Hardjito and Rangan, 2005; Nath and Sarker, 2017). For given values of UPV, the corresponding compressive strength values were used to calculate elastic modulus by equations from previously referenced studies (Bondar, 2009; Comite Euro-International Du Beton, 1993; Diaz-Loya et al., 2011; Hardjito and Rangan, 2005; Nath and Sarker, 2017). The results were then plotted against values of UPV in the same graph as the values derived from elastic modulus – UPV equation (Yildirim and Sengul, 2011).

Table 6.4. Elastic modulus values for typical pavement materials from the Design and Maintenance Guide 27 (Design and Maintenance Guide, 2011) and traditional SFC with hot mix asphalt of pavements from previous studies.

Material	Classification	Elastic modulus (GPa)	Standards/Studies
Concrete	Poor	<10	Design and Maintenance Guide (2011)
	Average	10-20	
	Good	20-30	
	Excellent	>30	
Dry lean concrete	Poor	<3	
	Average	3-8	
	Good	8-15	
	Excellent	>15	
Bituminous bound	Poor	<1	
	Average	1-4	
	Good	4-7	
	Excellent	>7	
SFC with hot porous asphalt and cement grout		8-14	Afonso et al. (2016)
		13	Anderton (2000)
		8-12	Densit (2018b)
CBGM $C_{8/10}$		15	British In-Situ Concrete Paving Association (2007)

With measured values of UPV and strength from this study used as inputs into related prediction equations, comparable relationships existed for both approaches, with resulting values of elastic modulus E_s ranging from 11-27 GPa, which is higher than traditional SFC with hot porous asphalt and cement grouts obtained from previous studies (Afonso et al., 2016; Anderton, 2000; Densit, 2018a) and falling into 'average' to 'good' categories of concrete pavement in the Design and Maintenance Guide 27 (Design and Maintenance Guide, 2011) (Table 6.4). The equation from CEB-FIB (Comite Euro-International Du Beton, 1993) seems to overestimate the elastic modulus of SFC materials.

Table 6.5. Equations for predicting elastic modulus of PC and geopolymer concrete from previous studies (Bondar, 2009; Comite Euro-International Du Beton, 1993; Diaz-Loya et al., 2011; Hardjito and Rangan, 2005; Nath and Sarker, 2017; Yildirim and Sengul, 2011).

Studies	Applications	Equations
Yildirim and Sengul, (2011)	Conventional Portland cement concrete	$E_s = 6e^{0.076UPV^2}$ (6.3)
Comite Euro-International Du Beton (1993)	Conventional Portland cement concrete	$E_s = 0.018\ (0.1f_{cu})^{1/3}$ (6.4)
Bondar (2009)	Conventional Portland cement concrete	$E_s = 4.7\ (0.8f_{cu})^{0.5}$ (6.5)
Hardjito and Rangan (2005)	Heat cured low-calcium fly ash-based geopolymer concrete	$E_s = 2707\sqrt{f_{cmi}} + 5300$ (6.6)
Diaz-Loya et al. (2011)	Heat cured fly ash-based geopolymer concrete with natural aggregate	$E_s = 0.000037\rho^{1.5}(f_{cu})^{0.5}$ (6.7)
Nath and Sarker (2017)	Fly ash-based based geopolymer concrete with crushed granite cured at ambient temperature	$E_s = 0.00351{f_c}^{0.5}$ (6.8)

where E_s is elastic modulus (GPa); f_{cu} is cube compressive strength (MPa); f_c is cylindrical compressive strength (MPa); f_{cmi} is in-situ compressive strength (90% cylinder strength) (MPa); ρ is density of material (kg/m^3); and μ is Poisson's ratio, which was assumed to be 0.23 for normal concrete (Yildirim and Sengul, 2011).

Figure 6.11 shows that, for elastic modulus prediction, empirical equations reported by Diaz-Loya et al. (2011) and Bondar (2009) using compressive strength f_{cu} fitted best with those using UPV from the study of Yildirim and Sengul (2011). It should be noted that the formulations in studies of Yildirim and Sengul (2011) and Bondar (2009) were applied for E_s prediction of conventional Portland cement concrete, while the equation in the study of Diaz-Loya et al. (2011) was applied for fly ash-based geopolymer concrete using heat curing. Similar to Diaz-Loya et al. (2011), Hardjito and Rangan (2005) used Equation (6.6)

for E_s prediction of low-calcium fly ash-based geopolymer concrete curing at elevated temperature while Nath and Sarker (2017) applied Equation (6.8) for E_s prediction of fly ash-based geopolymer concrete with crushed granite aggregate cured at ambient temperature. The lowest E_s values noted for estimations from studies of Nath and Sarker (2017) and Hardjito and Rangan (2005) was mostly because other equations, except for the one from Diaz-Loya et al. (2011), were obtained from experiments of conventional concrete (Bondar, 2009; Comite Euro-International Du Beton, 1993; Yildirim and Sengul, 2011). These tend to exhibit higher elastic modulus than ambient cured geopolymer concrete of similar grade like the one in the study by Nath and Sarker (2017).

Additionally, as displayed in Figure 6.11, predicted E_s values derived from Equations (6.2, 6.4, 6.6) showed the strongest agreement in the E_s range of 10-20 GPa, corresponding to a UPV range of 3.3-3.8 km/s. This suggests that these equations could provide the best prediction method to assess E_s values of SFC materials in this range.

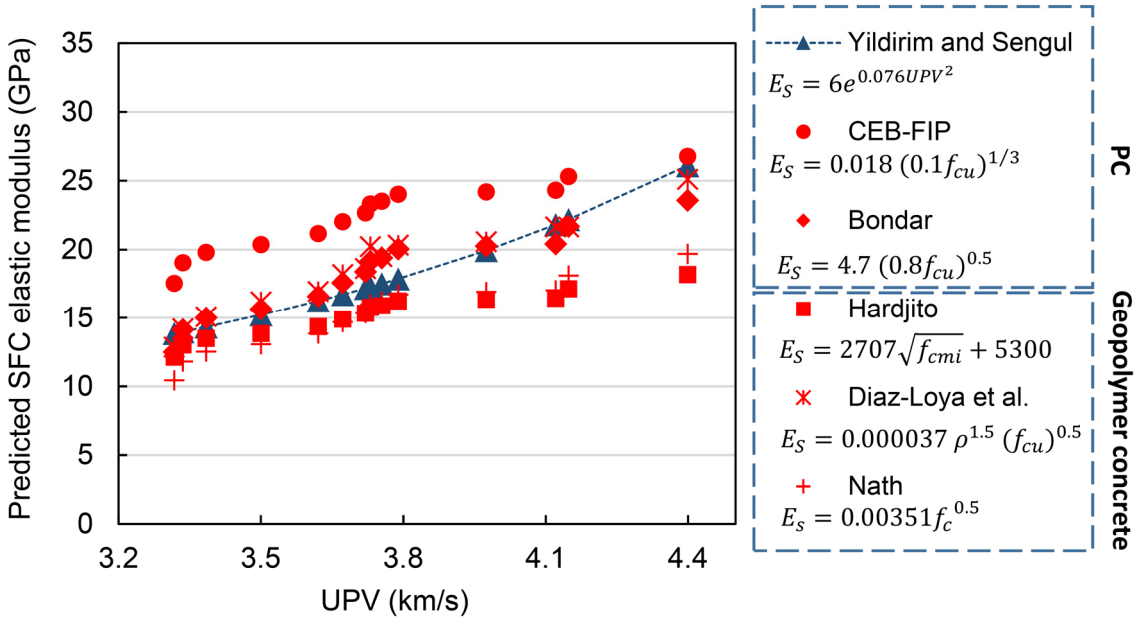

Figure 6.11. Relationship between UPV (km/s) and predicted elastic modulus E_s (GPa) from previous published theoretical equations.

Based on this observation, values obtained from Equations 6.2, 6.4 and 6.6 (Bondar, 2009; Diaz-Loya et al., 2011; Yildirim and Sengul, 2011) were chosen to estimate elastic modulus and determine regression lines for SFC materials from compressive strength f_{cu} and UPV in

Figure 6.12. Proposed equations for elastic modulus prediction of SFC pavement based on the method of least square are as follows:

$$E_s = 4.302 {f_c}^{0.5} \quad (6.9)$$

$$E_s = 1.15\mathrm{UPV}^{2.1} \quad (6.10)$$

Since the coefficient of determination indicates a good fit ($R^2 = 0.94$ for compressive strength vs. elastic modulus and $R^2 = 0.93$ for UPV vs. elastic modulus), equations (6.9) and (6.10) are reliable to estimate elastic modulus of SFC materials from compressive strength and UPV respectively.

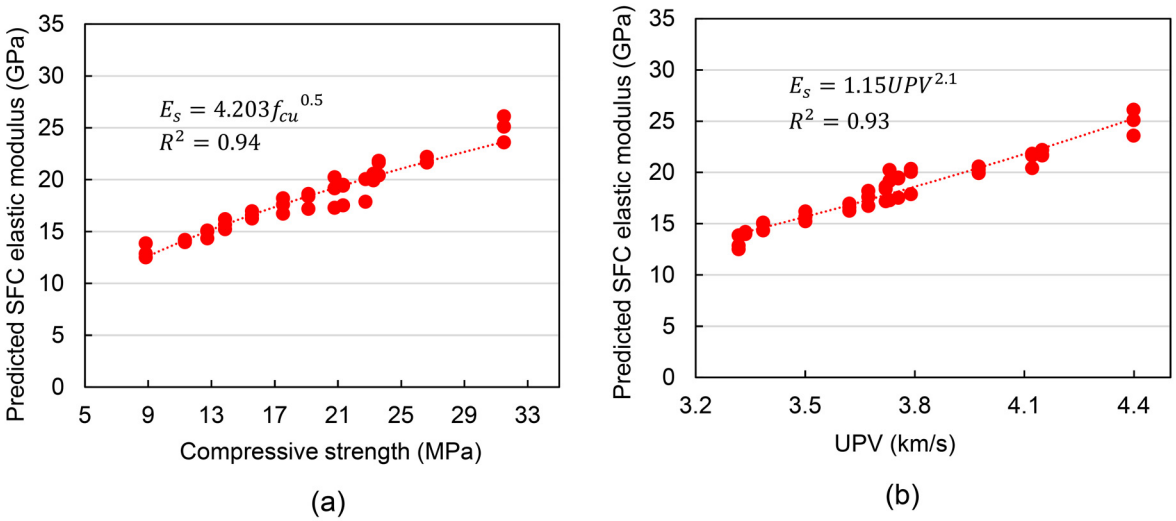

Figure 6.12. Proposed model for predicting elastic modulus of SFC materials incorporating geopolymer grout and RAP based on: a) compressive strength f_{cu} (MPa); b) UPV (km/s).

6.7 Preliminary design for industrial hardstanding application

To investigate the practical implications of the work presented to this point, a preliminary design methodology for industrial hardstandings comprising SFC as a base course is presented in this section. The approach adopted considered SFC as behaving similarly to HBM in accordance with BS 9227:2019 (British Standards, 2019b). Suitable materials included in this standard include cement, slag and fly ash bound granular mixtures in accordance with BS EN 14227:2013-Parts 1-3 respectively (British Standards, 2013e, 2013f, 2013g), with permissible compressive strength classifications in the range $C_{0.4/0.5}$ to $C_{36/48}$ (where the subscript figures define minimum values for cylinder specimens with a

slenderness ratio of two and one, or cubes, respectively). This range encompasses the 28-day strength value range for SFC recorded in this study (9-32 MPa).
In order to illustrate the use of SFC material for use as a base course, an example thickness design was undertaken for an industrial hardstanding in a distribution warehouse specialised for heavy goods vehicles. Assumed design inputs included: maximum wheel load of 10 tonnes; sub-grade conditions (typical sandy layer with 8% CBR) (British In-Situ Concrete Paving Association, 2007).

6.7.1 Thickness design for SFC base course

An example of the design methodology for industrial hardstandings comprising SFC as a base layer is presented in Figure 6.13. The hardstanding surface course was assumed to be an 80 mm thick concrete block paving (CBP) laid on 30 mm sand bedding layer. This surfacing layer, although ignored in the calculation, was assumed to compensate for edge/corner loading conditions that will induce cracks and produce greater stresses than the interior loading condition.

A simplified analytical pavement design approach presented by Williams (1986) was used as a basis of the design methodology, which ignored the contribution of the surfacing and idealised the pavement as a two-layer system comprising HBM (or SFC in this case) on a supporting layer. It should be noted that this design approach was used to determine the pavement layer thickness without considering its service life. The approach recognises that SFC materials will ultimately crack under loading to form discrete slabs (not unlike paving concrete) and considers the stress situation at interior zones away from edges and corners.

For the interior loading condition, the tensile stress (f_t) at the bottom of the SFC base course is given by the expression:

$$f_t = 1.8p\left(\frac{a}{h}\right)^{1.85} log_{10}\left(\frac{E_1}{E_2}\right) \qquad (6.11)$$

where: p is the tyre pressure; a is the radius of tyre contact; h is the layer thickness; E_1 is the layer modulus of elasticity; and E_2 is the foundation modulus of elasticity (approximated from 10 x CBR in MPa).

Equation (6.11) can be simplified by making use of the relationship between maximum wheel load (P) and tyre pressure (p) ($P = p\pi a^2$) and also by simplifying the power function

from 1.85 to 2. As such, the equation may be rearranged to approximate the thickness of HBM layer as:

$$h = \left(0.57\left(\frac{P}{s}\right) log_{10}\left(\frac{E_1}{E_2}\right)\right)^{0.5} \quad (6.12)$$

In the worked example presented in Figure 6.13, the assumed design inputs included: maximum wheel load P (10 tonnes, i.e., 100 kN) and subgrade elastic modulus ($E_2 = 0.08$ GPa). As shown in Figure 6.13 (a), the starting point of the design methodology required selection of a preferred SFC mixture. Selected in this instance was grout Mix B with RAP volume of 62% and 28-day compressive strength of 18 MPa (correlating to strength class $C_{12/16}$ in EN 14227:2013-Part 1 (British Standards, 2013e) since SFC specimen comprising grout Mix B could achieve the highest strength with maximum usage of RAP (62% by volume) compared to other grout types. This enabled subsequent tensile strength, UPV and elastic modulus predictions of 1.7 MPa, 3.7 km/s and 17.9 GPa respectively.

Tensile strength prediction was based on relationships provided in BS EN 1992-1-1:2004 (British Standards, 2014) for conventional Portland cement concrete, while for UPV and elastic modulus, the equations presented previously in Figure 6.6 and Figure 6.12 were used. Using Equation (6.12) above, this led to an SFC base layer thickness design of 280 mm. It is noted that the design thickness of SFC layers was rounded up to the next 10 mm.

Using the same design approach as presented in Figure 6.13, Table 6.6 presents the minimum base thickness required for all of the SFC materials considered in this chapter. The thickness for a typical HDP base layer (i.e., 360 mm CBGM $C_{8/10}$) as recommended by the British In-Situ Concrete Paving Association (2007) is included in this table for comparison. As shown, minimum thickness for SFC base courses ranged from 240-350 mm; values all lower than the conventional CBGM $C_{8/10}$ (360 mm) owing to its lower level of compressive/tensile strength. Illustration of HDP structures comprising either SFC or CBGM $C_{8/10}$ (360 mm) base course layers are shown in Figure 6.14.

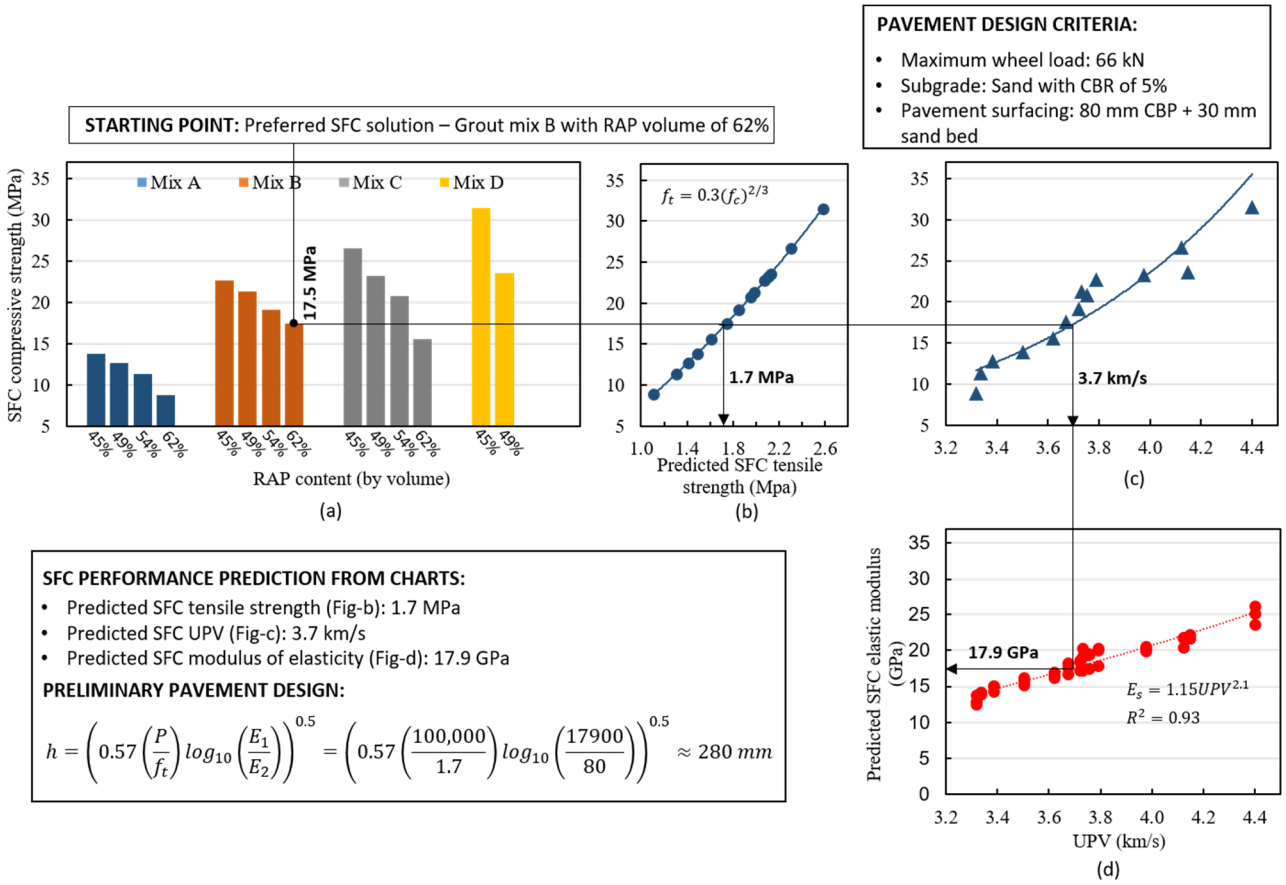

Figure 6.13. Mix design example for SFC utilised as a sub-base layer in a heavy-duty pavement application including: (a) laboratory-based compressive strength data; (b) predicted tensile strength values; (c) laboratory-based UPV data; and (d) predicted elastic modulus values.

Table 6.6. Minimum thicknesses of SFC and CBGM $C_{8/10}$ base courses.

SFC nomenclature	SFC components summary	Equivalent strength class	Minimum thickness (mm)
SFC-Mix A-45	Grout Mix A + 45% RAP	$C_{9/12}$	300
SFC-Mix A-49	Grout Mix A + 49% RAP	$C_{9/12}$	310
SFC-Mix A-54	Grout Mix A + 54% RAP	$C_{8/10}$	320
SFC-Mix A-62	Grout Mix A + 62% RAP	$C_{6/8}$	350
SFC-Mix B-45	Grout Mix B + 45% RAP	$C_{15/20}$	260
SFC-Mix B-49	Grout Mix B + 49% RAP	$C_{15/20}$	260
SFC-Mix B-54	Grout Mix B + 54% RAP	$C_{12/16}$	270
SFC-Mix B-62	Grout Mix B + 62% RAP	$C_{12/16}$	280
SFC-Mix C-45	Grout Mix C + 45% RAP	$C_{18/24}$	250
SFC-Mix C-49	Grout Mix C + 49% RAP	$C_{15/20}$	260
SFC-Mix C-54	Grout Mix C + 54% RAP	$C_{15/20}$	270
SFC-Mix C-62	Grout Mix C + 62% RAP	$C_{9/12}$	290
SFC-Mix D-45	Grout Mix D + 45% RAP	$C_{24/32}$	240
SFC-Mix D-49	Grout Mix D + 49% RAP	$C_{15/20}$	260
CBGM $C_{8/10}$ (British In-Situ Concrete Paving Association, 2007)		$C_{8/10}$	360

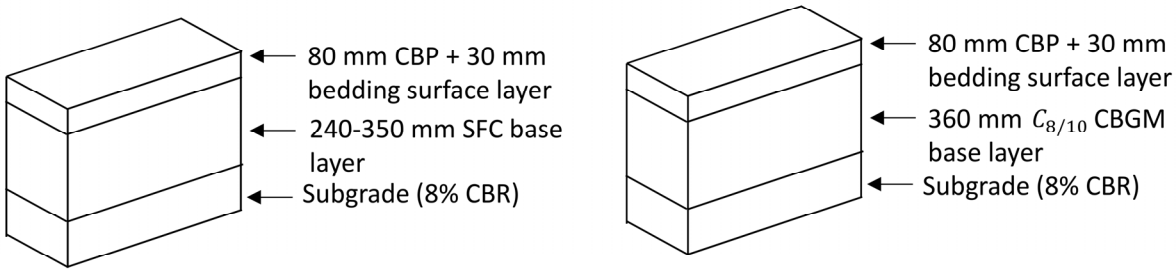

Figure 6.14. Sections of (a) HDP with SFC base layer. (b) Typical HDP with CBGM $C_{8/10}$ base layer.

6.7.2 Material cost analysis for producing HDP

Material cost analysis for producing HDP with the SFC base layer thicknesses presented in Table 6.6 was then performed to assess its economic viability. To simplify the analysis, costs relevant to construction operations and haulage (e.g. labour, fuel, power, water) were not included. The material cost of traditional HDP comprising 80 mm CBP and 30 mm sand bedding layer laid on 360 mm CBGM $C_{8/10}$ base course as shown in Figure 6.14, was considered for comparative purposes.

As the costs of obtaining SFC the constituent materials (including GGBS, FA, MK, SF, ready-to-use alkali activator Geosil® and RAP) for use in this research project were based on retail values, their wholesale prices per tonne were extracted from previous studies (Assi, 2017; Byrne, 2005; Pacheco-Torgal et al., 2005; Vinai and Soutsos, 2019) to provide a more realistic representation of actual costs associated with large-scale projects. Costs per tonne of GGBS, FA, MK, SF, RAP and alkali activator are presented in Table 6.7. The cost of alkali activator containing 45% of solid sodium silicate obtained from the study of Vinai and Soutsos (2019) was used instead of Geosil activator, for which a wholesale price was neither provided in the existing literature nor the supplier. It should be noted that an inflation rate of 1.5 was taken into consideration to obtain current costs of RAP and MK as extracted from studies of Byrne (2005) and Pacheco-Torgal et al. (2005).

Table 6.7. Cost per tonne of SFC constituent materials extracted from previous studies.

SFC constituent materials	Cost (£) per tonne	Reference
GGBS	65	Vinai and Soutsos (2019)
FA	40	Vinai and Soutsos (2019)
MK	40.8	Pacheco-Torgal et al. (2005)
SF	512.8	Assi (2017)
Alkali activator	300	Vinai and Soutsos (2019)
RAP	1.88	Byrne (2005)

Total material costs per volume and area of SFC and traditional CBGM were calculated using the following equations:

$$\text{Total cost/m}^3 \text{ of SFC mixture (£)} = \sum_{i=1}^{n} m_i c_i \quad (6.13)$$

$$\text{Total cost/m}^2 \text{ of SFC base course (£)} = \text{Total cost/m}^3 \text{ of SFC mixture} \times h \quad (6.14)$$

where m_i is mass of constituent material '*i*' per m^3 of mixture (tonne); c_i is cost per tonne of constituent material '*i*' (£), h is the thickness of SFC layer (as presented in Table 6.6) (m).

Table 6.8. Comparative cost per m^3 and m^2 of SFC and CBGM as base course.

Item	Cost/m^3 (£)	Base layer thickness (mm) [+]	Cost/m^2 (£)
Conventional base course			
CBGM $C_{8/10}$ [a]	130	360	47
SFC base course			
SFC-Mix A-45	121	300	36
SFC-Mix A-49	112	310	35
SFC-Mix A-54	102	320	33
SFC-Mix A-62	85	350	30
SFC-Mix B-45	145	260	38
SFC-Mix B-49	135	260	35
SFC-Mix B-54	122	270	33
SFC-Mix B-62	102	280	29
SFC-Mix C-45	154	250	39
SFC-Mix C-49	143	260	37
SFC-Mix C-54	130	270	35
SFC-Mix C-62	109	290	31
SFC-Mix D-45	99	240	24
SFC-Mix D-49	92	260	24
Data published in the literature (for comparative purposes only)			
Metakaolin geopolymer [b]	£122	-	-
Fly ash geopolymer concrete [b]	£75	-	-
Geopolymer concrete [c]	£91	-	-

References:

[a] North Whiteley Consortium, 2018
[b] Pacheco-Torgal et al. (2005)
[c] Assi (2017)

[+] Based on pavement design scenario presented in section 6.7.1.

Table 6.8 shows the total potential cost for producing 1 m^3 of each SFC mixture or 1 m^2 of SFC base layer in HDP which was calculated using the cost formula described above. Costs per m^3 and per tonne of conventional HDP base course (CBGM $C_{8/10}$) and different types of geopolymer materials obtained from previous studies were included in this table for comparative purposes. The cost per m^3 to produce CBGM $C_{8/10}$ was obtained from a report of North Whitely road project in Winchester district (North Whiteley Consortium, 2018).

As shown in Table 6.8, total potential costs of SFC base course per volume and area ranged from £85-£154/m^3 and £24-£39/m^2 respectively, which were dependent on SFC constituent materials. Total costs per unit area (£24-£39/m^2) of SFC base courses with the thicknesses presented in Table 6.6 were less than for CBGM $C_{8/10}$ (£47/m^2). Alkali activator accounted for a majority of the total cost (up to 57%) to produce SFC pavement, highlighting a requirement for the cost of this material to reduce prior to wide-scale commercial realisation of SFC. A wide range of cost of geopolymer materials (£91-£122/m^3) containing similar raw materials such as FA, MK, SF and alkali activator obtained from previous studies due to the large variation in prices of raw material was also presented in this table. This range encompasses the obtained cost range of SFC materials which demonstrated the reliability of cost assessment provided in this study.

6.7.3 Greenhouse gas assessment

Greenhouse gas (GHG) emissions were also analysed for the production of SFC and traditional base courses comprising 360 mm CBGM $C_{8/10}$ in HDP. Emissions related to factors such as transportation, handling, mixing and curing were assumed to be similar for both SFC and CBGM base courses in HDP structures and were thus neglected.

Indicative production processes relating to SFC and traditional CBGM are presented in Figure 6.15. It should be noted that carbon footprint of water production was assumed to be in the mixing stage and was thus ignored in the greenhouse gas assessment. Since GGBS, FA and SF are by-products from electricity, iron and silicon metal production respectively, the collection process of mentioned powders was reported to account for the vast majority of their emission (Higgins, 2006; McLellan et al., 2011). Greenhouse gas emitted from metakaolin production was considered to be from mining, grinding and calcining processes of kaolinite sources at 700°C. For alkali activator, emission of sodium silicate was evaluated instead of the potassium activator used in this study (Geosil) due to a lack of published information. According to a report by the European Chemical Industrial Council (2014), sodium and potassium silicates have similar manufacturing processes where silica sand and

soda ash (or potash in case of potassium silicate) are calcined at approximately 1000°C to create sodium silicate lumps. In order to produce sodium silicate solution, sodium silicate lumps are dissolved in water and impurities are filtered out. Emission generated from RAP production are mainly caused by crushing and fractionation processes (Praticò et al., 2020). Coarse aggregate and sand mainly emit greenhouse gas from washing, grinding and grading processes. Emissions of PC in CBGM $C_{8/10}$ were reported to be generated from calcination process and chemical decomposition by Ma et al. (2016).

Emissions of greenhouse gas were calculated based on the energy usage (kWh) from fuel and electricity according to the following equation (McLellan et al., 2011):

$$GHG = \sum_{i=1}^{n} m_i p_i \qquad (6.15)$$

where GHG is the total greenhouse gas emission per m^3 of mixture (kg CO_2e); m_i is mass of constituent material '*i*' per m^3 of mixture (tonne); p_i is greenhouse gas emission per tonne of constituent material '*i*' (kg CO_2e) which is calculated by the following equation:

$$p = E_F \times ECF_F + E_E \times ECF_E \qquad (6.16)$$

where E_F and E_E are the fuel and electricity energy consumption respectively (kWh); ECF_F and ECF_E are the emission conversion factors of fuel and electricity respectively ($ECF_F = 0.33183$ and $ECF_E = 0.2773$) obtained from the report of the UK Government Conversion Factors for greenhouse gas in 2019 (Climatechange Statistic, 2019). It should be noted that these factors covered the emission of methane (CH_4) and nitrous oxide (N_2O).

Table 6.9 shows the fuel and electricity energy consumption of raw materials of SFC and conventional CBGM $C_{8/10}$ in HDP and their corresponding GHG emissions per tonne of material. Energy usage per tonne of the constituent materials obtained from previous studies was mainly expressed in Megajoule (MJ) which were converted to kWh by multiplying by 0.277 (Ciambrone, 1997). Data on energy consumption from the manufactures of GGBS, FA, MK, SF and alkali activator was obtained from the studies of Higgins, (2006) and McLellan et al. (2011) while the electricity usage for RAP's crushing and grading processes was extracted from the study of Praticò et al. (2020). Fuel and electricity usage for heating and operating the kiln in the production of PC were obtained from the study of Ma et al. (2016).

The amount of CO_2 emitted directly from the chemical decomposition of limestone was reported to be 362.88 kg per tonne of produced PC. Data on energy consumption from coarse aggregate and sand processing were also obtained from the same study (Ma et al., 2016). The mass of raw materials to produce one tonne of CBGM $C_{8/10}$ was extracted from the study of Kore and Vyas (2016).

As shown in Table 6.10, total greenhouse gas emissions of SFC base course were 111.3-166.8 kg CO_2e/m^3 and 35.5-43.3 kg CO_2e/m^2, which was about two times lower than that of traditional CBGM $C_{8/10}$ (215.8 kg CO_2e/m^2 and 77.7 kg CO_2e/m^2). Figure 6.16 shows the emission of each constituent material per m^2 of SFC and conventional CBGM $C_{8/10}$ base courses. PC production contributed most significantly to the emission of traditional CBGM (97.7%) while the production of alkali activator generated the most greenhouse gas in SFC pavement (up to 60.4%).

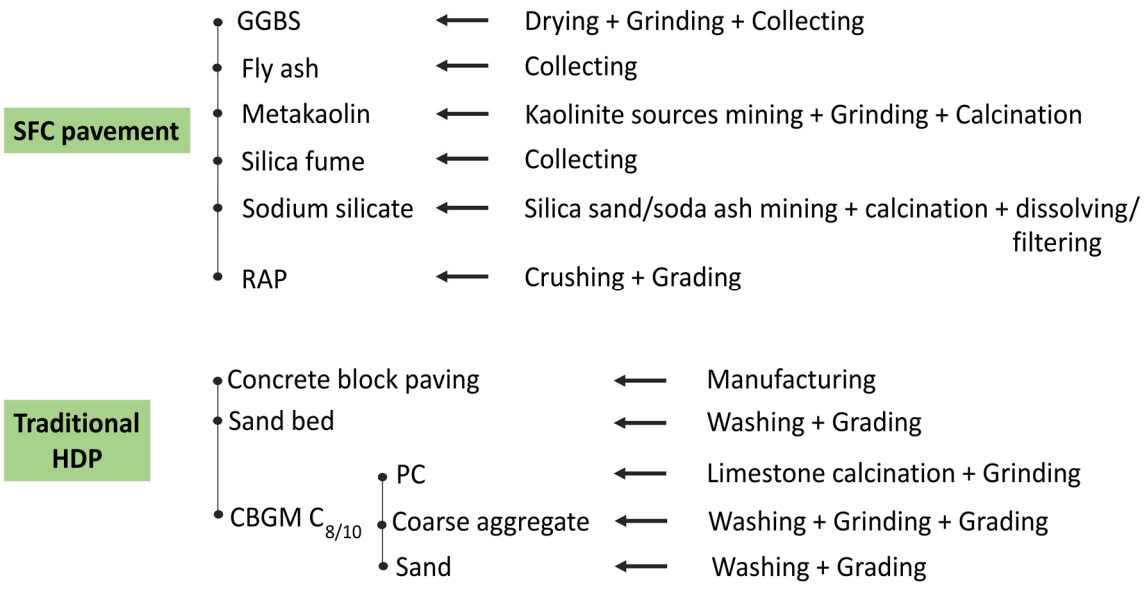

Figure 6.15. Production processes of raw materials of SFC pavement and traditional HDP.

Table 6.9. Fuel and electricity energy consumption of raw materials of SFC and conventional CBGM $C_{8/10}$ base courses in HDP obtained from previous studies.

Constituent materials		Energy usage (MJ/tonne)		Energy usage (kWh/tonne)		GHG emission from fuel (kg CO_2e)	GHG emission from electricity (kg CO_2e)	GHG emission/tonne of constituent material (kg CO_2e)	Reference
		Fuel	Electricity	Fuel	Electricity				
GGBS		0	1300	0.0	361.4	0.0	100.2	100.2	Higgins (2006)
FA		0	100	0.0	27.8	0.0	7.7	7.7	McLellan et al. (2011)
MK		2500	360	695.0	100.1	230.6	27.8	258.4	
SF		0	100	0.0	27.8	0.0	7.7	7.7	
Alkali activator		4800	190	1334.4	52.8	442.8	14.6	457.4	
RAP		0	192.4	0.0	53.5	0.0	14.8	14.8	Praticò et al. (2020)
PC	Calcination	2425.33	1211	674.2	336.7	223.7	93.4	680.0	Ma et al. (2016)
	Chemical decomposition	362.88							
Coarse aggregate		19	-	5.3	9.0	1.8	2.5	4.2	
Sand		0.90	-	0.3	0.0	0.1	0.0	0.1	

Table 6.10. Total greenhouse gas emission of SFC base course and conventional CBGM $C_{8/10}$ base course in HDP.

Items	GHG/m^3 (kg CO_2e)	Base layer thickness (mm) [+]	GHG/m^2 (kg CO_2e)
Conventional HDP base course			
CBGM $C_{8/10}$	215.8	360	77.7
Pavement solutions			
SFC-Mix A-45	144.2	300	43.3
SFC-Mix A-49	136.4	310	42.3
SFC-Mix A-54	126.7	320	40.6
SFC-Mix A-62	111.3	350	38.9
SFC-Mix B-45	166.8	260	43.4
SFC-Mix B-49	157.4	260	40.9
SFC-Mix B-54	145.7	270	39.3
SFC-Mix B-62	126.9	280	35.5
SFC-Mix C-45	166.2	250	41.6
SFC-Mix C-49	156.9	260	40.8
SFC-Mix C-54	145.2	270	39.2
SFC-Mix C-62	126.5	290	36.7
SFC-Mix D-45	157.5	240	37.8
SFC-Mix D-49	148.8	260	38.7

[+] Based on pavement design scenario presented in section 6.6.1.

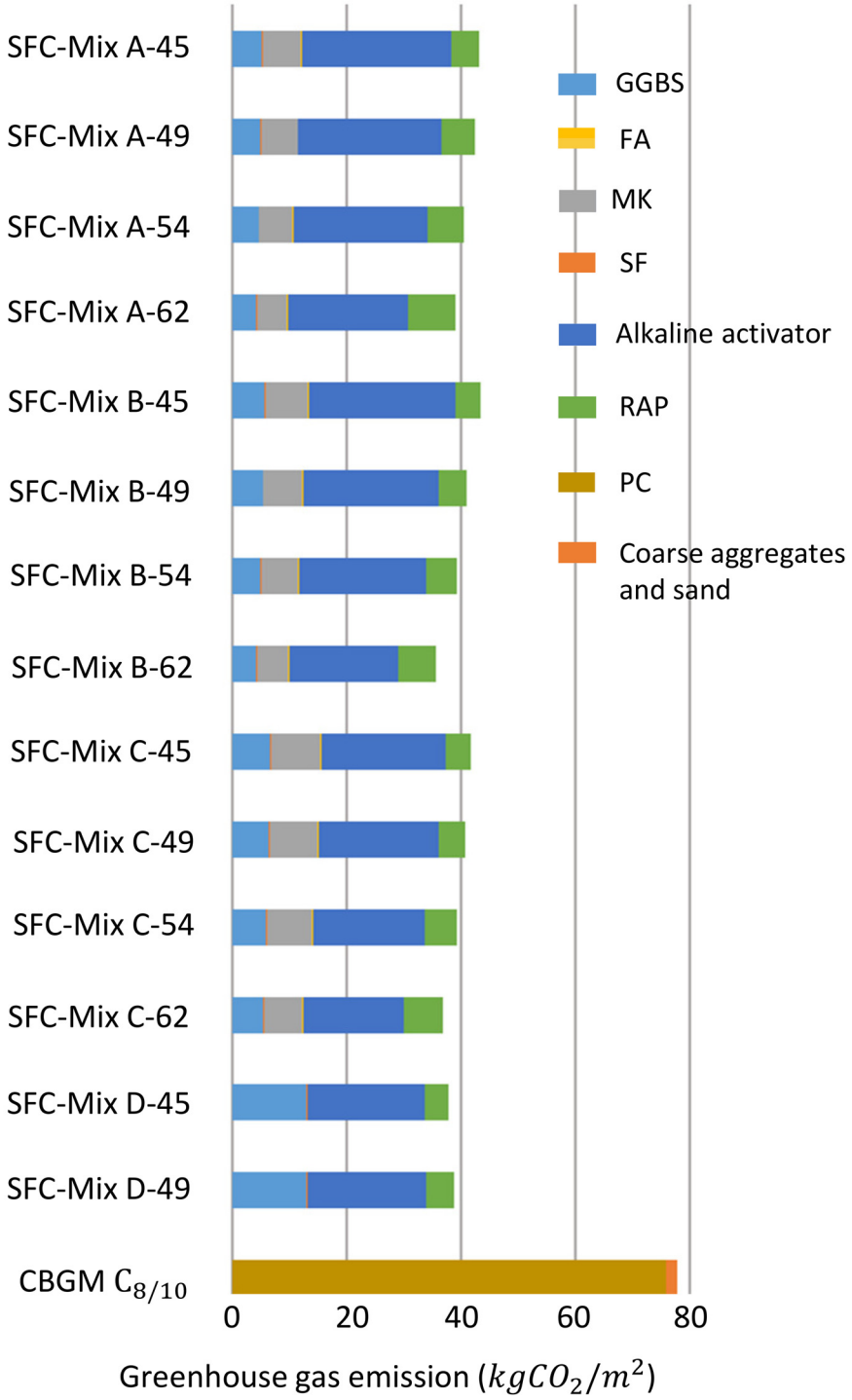

Figure 6.16. Emission (kg CO_2e) of each constituent material per m^2 of SFC base course and 360 mm CBGM $C_{8/10}$ base course in heavy-duty pavement.

6.8 Summary of results

The aim of this chapter was to investigate properties of semi-flexible composite materials incorporating geopolymer grouts and reclaimed asphalt planings to develop predominantly

waste-based pavement materials not requiring heating or mechanical compaction energy. Four mixes of geopolymer grout with contrasting properties were used to impregnate RAP skeletons with solid contents ranging from 45-62% by volume to study the performance of SFC materials. Also, PC concrete control specimens were produced from natural basalt aggregates with solid content of 45% by volume and PC cement grout with w/c of 0.33 for comparison. Based on the results obtained, the following conclusions may be drawn:

- Porosity values ultimately ranged from 20% for SFC specimens comprising grout Mix A ('High' | 'Slow' | 'Low') to 11% for those comprising grout Mix D ('Low' | 'Fast' | 'High') while the porosity of SFC with the same grout type group showed a slight change with a gain in RAP content. This indicates properties of the grout played a more important role in the permeable porosity and density of SFC pavement than the structure of RAP skeleton.
- Similar to permeable porosity, UPV of SFC materials was not greatly affected by the solid content of RAP. The lowest (3.3 km/s) and the highest (4.4 km/s) values of UPV were achieved by SFC with grout mixes A (36 MPa) and D (108 MPa) respectively, which falls into 'Medium-Good' quality category defined for conventional concrete in IS 13311 (Part 1):1992 (Indian Standards, 1996).
- SFC materials showed the ability to gain early strength quickly with 66-84% of their 28-day strength value after three days compared to PC concrete specimens (49%). This advantage offers significant benefits for pavement applications where high early strength leading to early potential exposure to traffic is preferential. Unlike permeable porosity or pulse velocity, both RAP content and parent grout strength had significant influences on compressive strength of SFC materials, with increasing SFC strength corresponding to increasing grout strength and decreasing RAP contents respectively. However, RAP addition seemed to have more negative influences on compressive strength of SFC materials. SFC specimens incorporating high strength geopolymer grout and 45% RAPs could reach compressive strength close to those obtained from the PC concrete control.
- The behaviour of SFC conformed to the mechanical performance levels required by DMRB: Volume 7 - Section 2 (Highways England, 2006a) for base layer made of HBM in accordance with BS 9227:2019 (British Standards, 2019b). As such, this initial investigation has successfully proven the potential suitability of this material.
- Strong correlations between UPV–compressive strength, UPV–elastic modulus and compressive strength–elastic modulus were found for the range of SFCs considered in this study. Given the similarity between this relationship and those established

for ordinary Portland cement-based and heat cured fly ash-based geopolymer materials, published relationships relating UPV and elastic modulus for the latter were adopted to enable preliminary pavement designs incorporating SFC layers.

- Predicted SFC compressive strength values obtained from a DNN machine learning approach were close to those obtained from experiments, providing a meaningful rapid method to predict performance. The accuracy of the DNN model was confirm statistically, with high R^2 (0.919) and low RMSE (1.568) and MAPE (6.438) values obtained. Sensitivity analysis performed for model confirmed that 28-day compressive strength of geopolymer grout was the most dominant factor when predicting SFC compressive strength, with a sensitivity analysis score of 32%. This was followed in order of importance by RAP content (17%), SFC curing age (16%), geopolymer flow time (16%) and geopolymer initial/final setting time (14% and 5% respectively). This analysis indicates the importance of considering a wide range of input parameters in SFC mechanical properties prediction and controlling them carefully during manufacturing processes.
- Examples of SFC used as a base course for HDP in industrial hardstanding were presented. For maximum wheel load of 100 kN, subgrade CBR of 8% and a surface course comprising 80 mm CBP on 30 mm sand bed layer, the resultant SFC thickness requirement for base layer was within the range of 240-350 mm. SFC base course showed promise in replacing traditional methods since their required thicknesses were lower than for CBGM $C_{8/10}$ (360 mm).
- Material cost analysis and greenhouse gas assessments were carried out for all SFC mixtures as well as conventional HDP base course made of CBGM $C_{8/10}$. The production of 1 m^2 of SFC layer costed up to 50% less (£24-£39) and emitted significantly lower greenhouse gas (up to 43.3 kg CO_2e/m^2) compared to conventional CBGM $C_{8/10}$ base course in HDP (£47/m^2 and 77.7 kg CO_2e/m^2). This shows the potential to replace traditional HDP base materials with SFC pavements owing to their economic and environmental benefits.

CHAPTER 7

CHARACTERISATION OF SFC SURFACE COURSE SUBJECTED TO ACCELERATED TRAFFICKING ACTION

7.1 Introduction

The aim of this chapter is to investigate the performance of SFC material incorporating geopolymer grout and RAP as an innovative surface course of pavements. Pavement surface courses must be capable of withstanding and transferring traffic loads to underlying layers, such as the base course, and providing skidding resistance, durability, noise control and drainage. As stated in the guidelines for portable pendulum skid resistance testing (Impact Test Equipment, 2020), the minimum wet SRV suggested for non-critical locations such as motorways and trunk with traffic less than 2000 vehicles per day is 55. Areas that require high friction surfacing comprising calcined bauxite aggregates, such as approaches to pedestrian crossing, junctions and roundabout circulation should possess SRV of over 65 (British Board of Agrement, 2017). The manual for HDP structural design published by Interpave (Knapton, 2008) refers directly to BS EN 13877-2:2013 (British Standards, 2013h) for SRV requirements of 45 in the case of HDP with concrete block paving.

For mean texture depth, the New Roads and Street Works Act 1991 (NRSWA) (Department for Transport, 2010) recommended MTDs of 0.6 and 0.8 mm for concrete and asphalt pavements respectively. McQuaid (McQuaid, 2015) studied traffic-related properties such as skid resistance and mean texture depth of asphalt concrete, stone mastic asphalt and porous asphalt pavements subjected to simulated trafficking using a Ulster University's road test machine. Reported SRVs and MTDs were in the ranges 57-67 and 0.57-0.94 mm respectively after 100,000 wheel-passes, which was equivalent to a period of 8 years of actual traffic. However, for pavement surface courses there are insufficient standards or research regarding eco-efficient materials comprising mostly recycled materials without the need for heating energy and very limited investigation into their traffic-related properties, such as skid resistance and texture depth. Instead, the majority of previous research has focused on engineering properties of SFC surface courses in heavily trafficked areas, such as compressive strength, bending strength, dynamic stability, flexural strength, elastic modulus and moisture susceptibility (Afonso et al., 2016; Cihackova et al., 2015; Hou et al., 2016; Pratelli et al., 2018).

Against this background, a preliminary study of SFC materials incorporating geopolymer grout using industrial by-products as binder and RAP was undertaken to enhance the understanding of its performance as a surfacing material, based on the aforementioned properties. In order to maximise recycling content levels, RAP was additionally fully recycled as the main aggregate type into the pavement surface course. The work reported in this chapter was undertaken to assess the suitability of using combinations of

geopolymer grout and RAP as surfacing layer for SFC pavements. Work was undertaken in two distinct phases. The first was a preliminary investigation into the suitability of different surface course preparation methods. Test specimens were prepared using a single geopolymer grout type and three surface course preparation methods, including the application of a surface dressing layer, exposed aggregate finish with or without brushing. Testing in this instance was for skidding resistance only. The second phase of work investigated the most promising surface finish types in further detail using a range of geopolymer grout types and more comprehensive suite of test methods.

Test specimens were exposed to accelerated traffic using Ulster University's road test machine and periodically assessed for parameters including weight loss, skidding resistance, mean texture depth and surface texture characteristics. To investigate the variation in surface texture due to simulated trafficking, close-range photogrammetry was used to construct and analyse the virtual 3D models of SFC surface texture.

7.2 Phase A: Preliminary assessment of potential surface course methods

In this phase, work was undertaken to initially identify appropriate finishing techniques for SFC pavements based on initial skid resistance values. This property was deemed most suitable for this purpose because it is considered as an important parameter for safe and efficient movement of vehicles and people on pavements (Uz and Gökalp, 2017).

7.2.1 Sample preparation

Test specimens required for skid resistance testing were 305 x 305 x 50 mm in size and in all instances were manufactured in steel moulds. Each specimen comprised a structural pavement layer made using an 8/14 mm open-graded RAP skeleton (45% RAP content by volume) in combination with geopolymer grout Mix B. With "average" performance in terms of physical and mechanical properties (i.e. flowability, setting time and strength), grout Mix B was deemed most suitable as a control for this purpose. In terms of surface finishing types, considered were an applied surface dressing finish, a brushed surface finish to expose aggregate and an exposed-aggregate surface finish without brushing. The methods used for preparing these surface finish types are illustrated in Figure 7.1 and as described in the following sections.

Surface dressing finish

In the case of the SFC pavements studied in this work, 1.18/3.36 mm sized RAP particles were introduced as chippings for the surface dressing method. This approach was chosen instead of using virgin aggregates such as crushed rock, gravel or calcined bauxite as

proposed in the MCHW, Volume 1, Series 900, Clause 922 (MCHW Series 900, 2019). Fresh geopolymer grout, after being poured into the RAP skeletons, also served the role of a binder to hold the smaller RAP chippings in place. This avoided the need for a hot bitumen layer, thereby reducing the virgin bitumen and heating energy demand.

In this instance, specimen preparation followed four steps. Firstly, a 40 mm-thick layer of open-graded RAP skeleton was placed in a 305 x 305 x 50 mm mould (Step 1). Geopolymer grout was then poured slowly onto the RAP skeleton until all RAP surfaces were just completely covered and a 10±1 mm free gap was left to the top of the mould (Step 2). RAP chippings with size 1.18/3.36 mm were then evenly spread over the exposed surface of the fresh geopolymer grout the mould was completely full. The quantity of RAP applied equated to around 11 kg/m^2, which conforms to the 8-11 kg/m^2 level specified for the smallest size chippings (2.8/6.3 mm) stated in Road Note 39 (Bateman, 2016) (Step 3). Finally, the RAP chippings were lightly rolled to ensure that they were embedded into the geopolymer grout surface (Step 4). Specimens were then covered with polyethylene film and allowed to harden at ambient temperature for 28 days.

Exposed aggregate finish (with brushing)

For these specimens, the open-graded RAP skeletons were placed into the full depth (50 mm) of the steel moulds used (Step 1). Next, geopolymer grout was poured into the skeleton until it completely covered the surface of the RAP particles (Step 2). The surface was levelled, left uncovered and allowed to harden at ambient temperature for about one hour (Step 2).

The timing of applying a textured surface by brushing mainly depends on initial setting time of the grout. In this case, the initial setting time of grout mix B was 65 minutes. A stiff-bristled brush was then used to brush specimen surfaces in one direction (transversely to the intended direction of pendulum slider application) to remove excess grout and expose the surface of the RAP particles to a depth of approximately 1 mm (Step 3) according to Clause 1026 in MCHW Series 1000 (2020). Specimen were then covered with polyethylene film and allowed to harden at ambient temperature for 28 days.

Exposed aggregate finish (without brushing)

This method was deemed to offer the simplest construction method and was most robust finish given the fully composite nature of the RAP and geopolymer grout. In this instance, the open-graded RAP skeleton was placed into the full depth (50 mm) of the steel moulds

(Step 1). Geopolymer grout was then poured into the skeleton until only approximately one-third of the surface RAP particles were left exposed (Step 2). After 24 hours covered by polyethylene film at ambient temperature, the specimens were then lightly cleaned with a soft brush to discard any surplus and demoulded. They remained covered by polyethylene film for 28 days until further experiments.

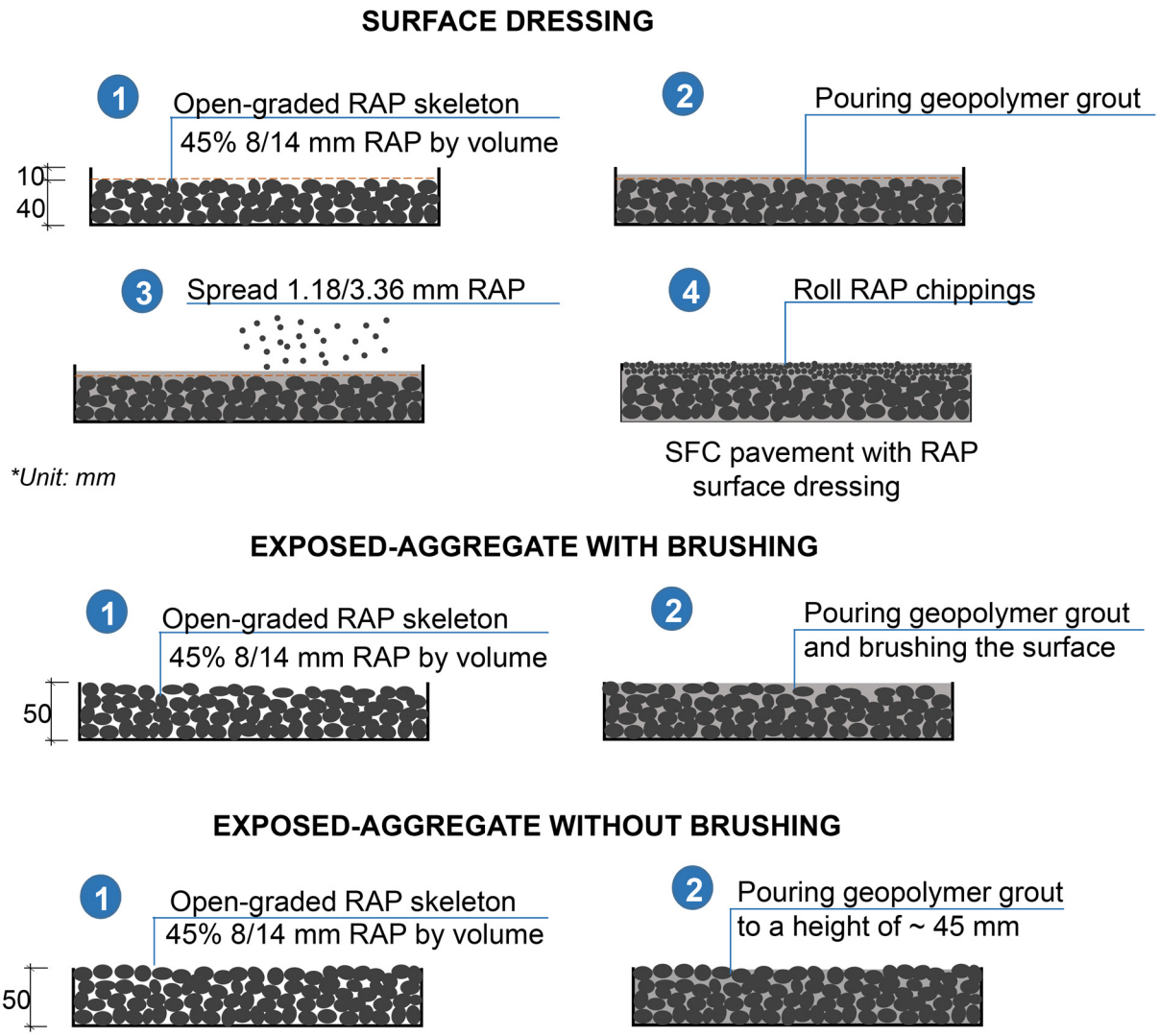

Figure 7.1. SFC pavement preparation with different surface finishing including surface dressing, exposed-aggregate with and without brushing.

7.2.2 Skid resistance investigation

Skid resistance is a friction force existing in the road-tyre interface zone and is considered as a factor to quantify potential traffic safety levels of dry and wet roads (Ahammed and Tighe, 2012; Uz and Gökalp, 2017). High SRV indicates a high-friction surface with lower

risks of accidents caused by wet conditions, while low SRV means the surface tends to have a higher risks of incidences for people or vehicles moving on it (Ahammed and Tighe, 2012; British Standard, 2013). Different minimum SRVs are suggested for various pavement types such as high friction surfacing (type 1, 2 and 3) (see Table 7.1).

Table 7.1. Minimum SRV suggested for surface courses of different pavement types.

References	Pavement type	Minimum suggested wet SRV	
British Board of Agrement, (2017)	High friction surfacing: Type 1	Before traffic wear	≥ 65
		After 100,000 wheel-passes	≥ 70
	High friction surfacing: Type 2	Before traffic wear	≥ 65
		After 100,000 wheel-passes	≥ 65
	High friction surfacing: Type 3	Before traffic wear	≥ 65
		After 100,000 wheel-passes	≥ 65
Impact Test Equipment (2020)	Category A	Roundabouts	65
		Bends with radius < 150 m	
		Approaches to traffic lights	
	Category B	Motorways, trunk and heavily trafficked roads with 2000 vehicles per day	55
	Category C	All other sites	45

As shown in this table, high friction surfacing and traffic sensitive areas such as approaches to traffic lights and major and minor junctions on dual carriageways or roundabout circulation require SRV of at least 65 (British Board of Agrement, 2017; Impact Test Equipment, 2020). According to the guideline for pendulum tester (Impact Test Equipment), motorways, trunk and heavily trafficked roads with 2000 vehicles per days in category B require SRV higher than 55. SRV for other non-critical locations (category C) is suggested to be minimum of 45. Apart from tyre properties and weather conditions, skid resistance is influenced significantly by the microtexture of the aggregates' surface on the top of pavements. Aggregate's coarse macrotexture provides drainage paths on the tyre-road interface to improve wet skid resistance (Highways England, 2006b) (see Figure 7.2).

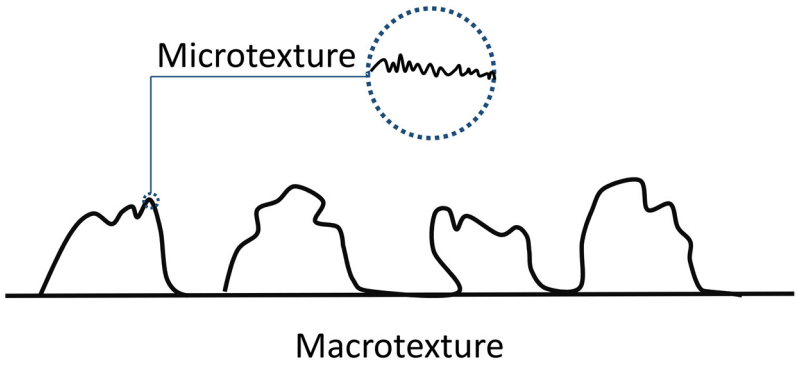

Figure 7.2. Macrotexture and microtexture of a surface (Highways England, 2006b).

7.2.3 Results and discussion

SFC pavement samples incorporating geopolymer grout Mix B and RAP with different surface finishes are shown in Figure 7.3. It can be observed from this figure that the specimens prepared by brushing had some fine surface striations and slightly less exposed RAP particles, but otherwise were more consistent than those prepared without brushing.

Figure 7.3. SFC pavements incorporating geopolymer Mix B and RAPs with different types of surface finishes.

Figure 7.4 shows the initial SRVs in dry and wet conditions. In both conditions, the specimen with the surface dressed finish exhibited the highest values of dry/wet SRV (90/76 respectively). In comparison, dry/wet values for the specimens with the brushed and exposed aggregate finishes were 82/53 and 86/44 respectively. Clearly, respective performance reductions relative to the surface dressed finish were much more pronounced in wet (i.e. reduction factors of 0.7 and 0.58) compared to dry conditions (reduction factors

of 0.91 and 0.95). This may be explained by the fact that the surfaces of the brushed and exposed aggregate specimens were more lightly textured. This led to more water being retained on the pavement surfaces, thereby causing a reduction in wet skid resistance.

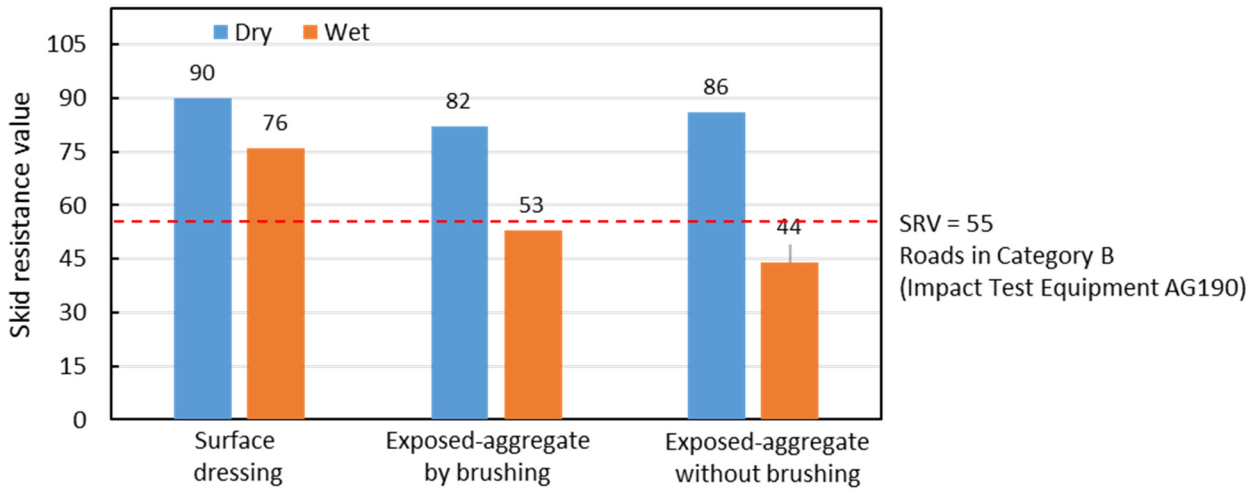

Figure 7.4. Initial skid resistance values of SFC material incorporating grout Mix B and RAP with various types of surface finishes.

Based on these findings, the surface dressing finish was selected for further experimental investigation in Phase B owing to its attainment of the highest dry and wet SRV values. Additionally, its dry/wet SRVs (90/76 respectively) were above the suggested minimum of 55 for road types in Category B (e.g. motorways, trunk and heavily trafficked roads with 2000 vehicles per day) (Table 7.1). Despite attaining the second highest dry SRV value of 86, the exposed aggregate without brushing finish was not selected for further investigation due to its lowest wet SRV of 44.

The brushed surface finishing method was also not progressed for further analysis, mainly given its sensitivity to application variability. For instance, the timing of brushing excess grout to expose aggregates is among the most important issues. An application too soon can result in aggregate loss, while too late can result in undesirable surface texture (Chandler et al., 2003). Given the aim of developing a surfacing solution applicable to multiple application scenarios and grout types, this potential construction variability was not deemed as appropriate.

7.3 Phase B: In-depth assessment of surface course performance

In this phase, work was undertaken to further investigate the appropriateness of pavement surface finishes manufactured using combinations of RAP and geopolymer grout. This involved exposing test samples to accelerated simulated trafficking and periodic testing for weight loss, skid resistance and texture depth/profile.

According to BS EN 13877-2:2013 (British Standards, 2013h), the required compressive strength for concrete pavements used in storage areas, cycleways and footpaths is within the range 8-100 MPa. However, the standard suggests that the minimum strength for concrete wearing courses should exceed 20 MPa. As such, four types of SFC materials with compressive strength in the range 14-32 MPa (SFC-Mix A-45, SFC-Mix B-45, SFC-Mix C-45, SFC-Mix-D-45), as discussed in Chapter 6, were used in this chapter. Although the compressive strength of SFC-Mix A-45 (14 MPa) fell short of the 20 MPa strength requirement for concrete pavements, it was still included in this chapter to widen the investigation of grout strength impact on SFC surface course performance.

7.3.1 Sample preparation

As per Phase A, test specimens were prepared in 305 x 305 x 50 mm steel moulds and applied with a surface dressing described above in section 7.2.1. The combinations prepared for testing are presented in Table 7.2. Considered were four SFC slabs with a surface dressing finish (named: SFC-Mix A, SFC-Mix B, SFC-Mix C and SFC-Mix D). For comparative purposes, a control testing slab (referred to as PC slab) comprising basalt aggregates (45% by volume) grouted with conventional Portland cement grout (PCG control as described in Chapter 6) with surface dressing finish, was also considered. Preparation of the PC slab followed the same procedure as SFC pavements with surface dressing finish.

Table 7.2. Slab combinations and surface textures for Phase B experimental testing.

Specimen name	Aggregate skeleton (% solids by volume)	Grout type (28-day strength)
SFC-Mix A	8/14 mm RAP (45%)	Mix A (36 MPa)
SFC-Mix B		Mix B (67 MPa)
SFC-Mix C		Mix C (93 MPa)
SFC-Mix D		Mix D (108 MPa)
PC slab	8/14 mm basalt aggregates (45%)	PCG Control (84 MPa)

Figure 7.5 provides images of all pavement slabs prior to testing. It is clear from this image that except for SFC-Mix A, the surfaces of most SFC slabs with RAP chippings appeared to be uniform. Shrinkage cracks and excess hardened grout can be seen on the surface of slab SFC-Mix A due to improper surface dressing and curing processes during sample preparation.

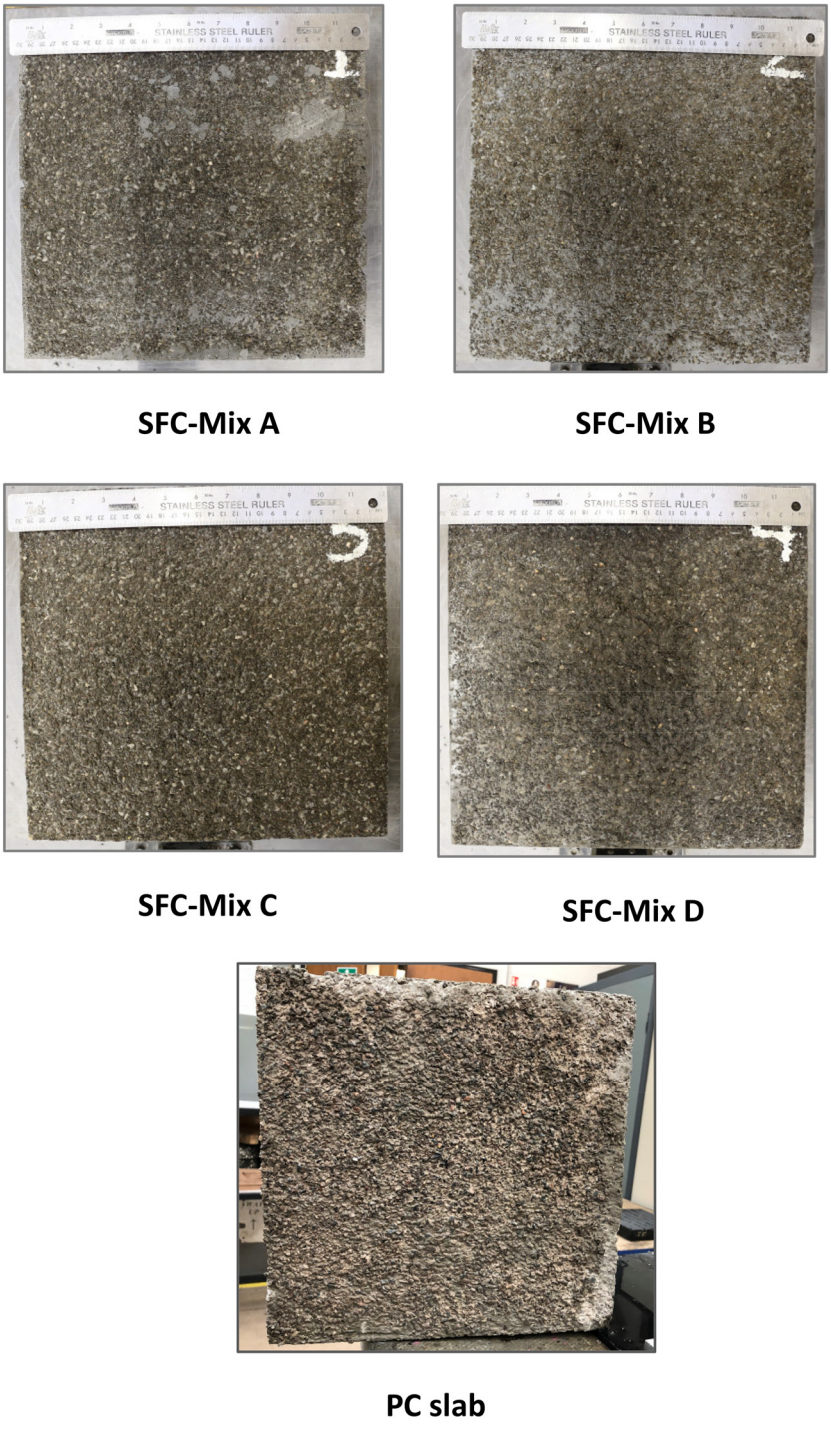

Figure 7.5 SFC and PC testing slabs with surface dressing.

7.3.2 Exposure to simulated accelerated trafficking using RTM

All specimens were exposed to simulated trafficking using the RTM (as described in Chapter 3) prior to assessment for weight loss, skid resistance value and mean texture depth/profile. Under the polishing action of this accelerated trafficking action, the microtexture of aggregate particles is known to gradually change, leading to skid resistance reduction (Roe and Forest, 2005). Tests carried out by RTM are usually undertaken to assess the wear properties of surfacing materials; for example, research by Wilkinson (2017) on the topic of high friction surfacing material or by McQuaid (2015) on the topic of pothole development.

In previous research studies focusing on pavement surfaces for high volume traffic (McQuaid et al., 2015; Nicholls, 1997), up to 100,000 RTM wheel-passes (corresponding to 5-8 years of road traffic) have been considered, with performance equilibrium occurring somewhere between 20,000 and 40,000 wheel-passes. The equilibrium point of approximately 20,000 rotating cycles associated with 80,000 load repetitions was also stated in the study by Wang et al. (2020), in which a circular vehicle simulator with four pneumatic tyres was used to assess MTD and skid resistance of pavements. It should be noted that the load applied by each tyre (4 kN) in the study by Wang et al. (2020) was slightly lower than in this study (5 kN).

Given the exploratory nature of lower grades of pavements in this study, a reduced number of wheel-passes led to the point where serious defects occurred on the surfaces of testing slabs. The RTM was stopped at intervals of 50, 100, 500, 1000, 2000, 3650 and 10,000 wheel-passes to examine changes in SFC specimen characteristics. For the PC slab, the RTM was stopped at intervals of 625, 6350 and 10,000. Given that 100,000 wheel-passes equals to about 8 years of road service life (Nicholls, 1997), the 10,000 wheel-passes investigated in this study were assumed to equate to approximately one year of road traffic.

7.3.3 Weight loss of testing slabs under traffic wear

Influence of simulated trafficking on pavement performance based on weight loss of testing slabs was investigated as part of this study; a phenomenon typically caused by worn-off chippings or segregation of specimens. The surface of each testing slab was cleaned using a soft brush to remove loose particles and weight changes evaluated at each interval of RTM operation using the equation:

$$WL = \frac{M_a - M_b}{M_a} \quad (7.1)$$

where WL is the weight loss at each interval, M_a and M_b are the weight before and after traffic by RTM respectively.

Figure 7.6 shows established relationships between specimen weight loss (% by mass) and the number of wheel passes. After being subjected to simulated trafficking, the weight of SFC slabs reduced to between 1.2-7.5% by mass. As expected, SFC-Mix A showed the highest rates of deterioration, with weight losses of approximately 7.5% after only 650 wheel-passes. Indeed, the edges of these slabs were significantly damaged at this point. As such, testing was not extended beyond 650 passes for this specimen.

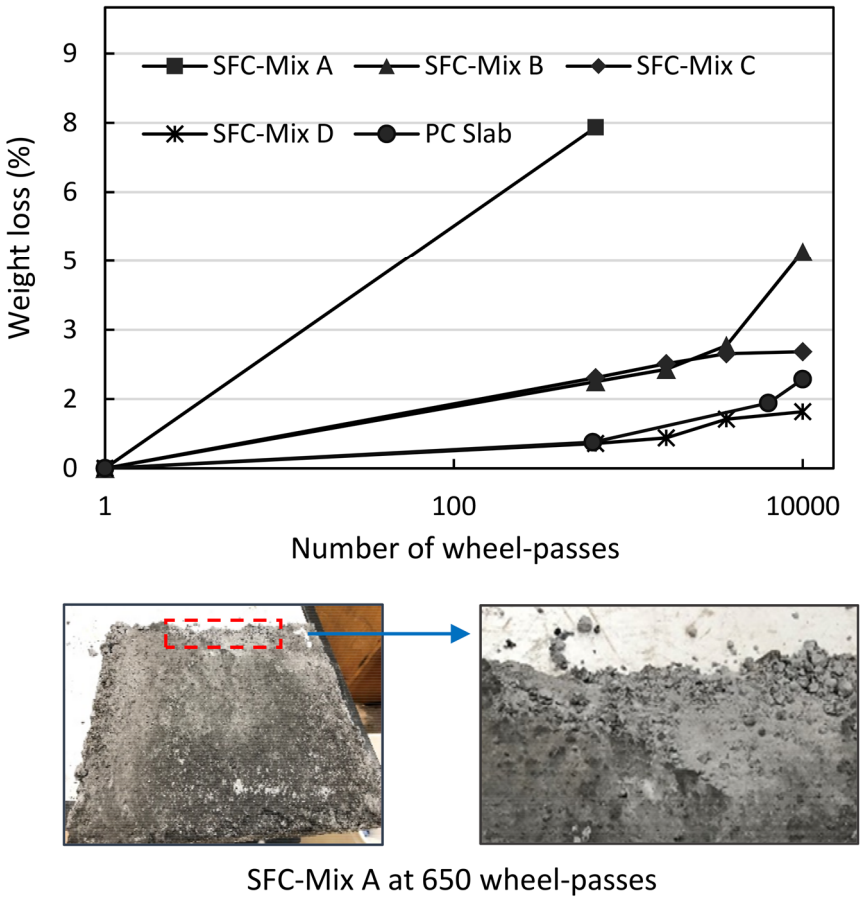

Figure 7.6. Relationship between the weight loss (%) of SFC and PC testing slabs and number of wheel-passes.

Weight loss rates of other SFC slabs, such as SFC-Mix B and SFC-Mix C slabs, were significantly lower. They had approximately 2.5-4.7% weight loss after 10,000 wheel-passes. The PC slab with conventional cement grout and basalt aggregates generally

exhibited a lower weight loss rate of 1.9% compared to the SFC slabs, except for SFC-Mix D. It is noticeable that SFC-Mix D exhibited the lowest weight losses, with values no greater than 1.5% by mass after 10,000 wheel-passes.

7.3.4 Mean texture depth

Mean texture depth is an estimation of surface macrotexture, which is an important factor affecting skid resistance (Highways England, 2006b). MTD values were determined by the sand patch method (known as volumetric patch method) according to BS EN 13036-1:2010 (British Standards, 2010), which is one of the most common tests used to investigate the macrotexture of pavement surfaces (Figure 7.2). An image of the sand patch testing being undertaken on a typical SFC slab (SFC-Mix C) after 650 wheel-passes is shown in Figure 7.7.

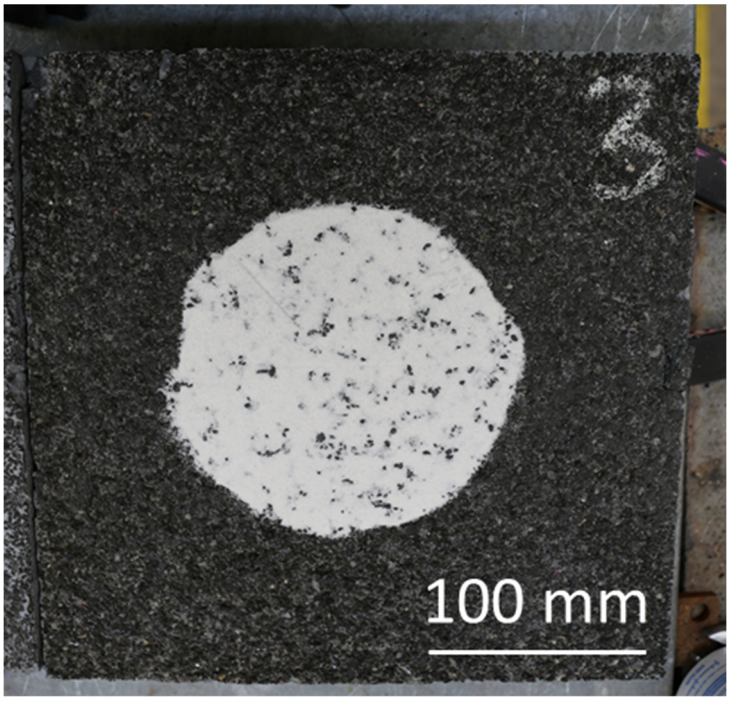

Figure 7.7. Sand patch test of typical SFC slab (SFC-Mix C) after 650 wheel-passes.

Rough surfaces possess high MTD while the surfaces with low MTD are considered to be smoother (Wang and Birken, 2014). Mean texture depth is a measurement for coarse macrotexture, which is one of the main factors affecting wet skid resistance (Highways England, 2006b). Since there is a lack of requirements for MTD of SFC pavements, the MTD values of 0.6 and 0.8 mm recommended in the NRSWA (Department for Transport, 2010) for concrete carriageways and hot rolled asphalt with surface dressing respectively were used as reference values.

Figure 7.8 shows the relationship between mean texture depth of SFC and PC Slab specimens, assessed by sand patch test method and the number of RTM wheel-passes. MTDs of high friction surfacing slab with 1.18/3.36 mm buff calcined bauxite (BCB) subjected to 1-10,000 wheel-passes obtained from the study of Wilkinson (Wilkinson, 2017) and asphalt concrete (AC) pavement subjected to 1-20,000 wheel-passes obtained from the study of McQuaid (2015) were included for comparative purposes. The AC pavement from McQuaid (2015) consisting of 7.2/10 mm sized granite aggregates with polished stone value of 48 and asphalt binders. The authors used the same RTM system for simulated trafficking as presented in this study.

As shown in Figure 7.8, before traffic wear SFC pavements had texture depths ranging from 0.8-1.3 mm, which complied with required minimum MTDs for concrete carriageways and surface dressed HRA (0.6 and 0.8 mm respectively) stated in NRSWA (Department for Transport, 2010). SFC slabs appeared to possess significantly lower initial MTDs than PC slab (1.9 mm) owing to the fact that RAP chippings might have been more deeply embedded into the fresh geopolymer grout during the manufacturing process.

MTDs of SFC slabs remained within the range of 0.9-1.2 mm after 10,000 wheel-passes, which was still in compliance with required values of 0.6-0.8 mm from NRSWA (Department for Transport, 2010). This result suggests promising performance of SFC pavements with RAP chipping dressing finish under simulated accelerated trafficking. It should be noted that the MTDs of PC slab dropped significantly from 1.9 to 1.1 mm after 625 wheel-passes, while SFC texture depth remained almost unchanged. No notable changes in MTD were measured for any of SFC testing slabs as the number of wheel-passes increased, attributable to insignificant RAP chipping loss on SFC surface as shown in Figure 7.6. This possibly demonstrates the existence of good bond strength between RAP chippings and geopolymer grout. In addition, asphalt concrete pavement with lower MTD after traffic wear (approximately 0.5 mm) obtained from the study by (McQuaid, 2015) was deemed to be smoother than MTD of SFC pavements (over 0.9 mm). Given the higher MTDs values, SFC pavements investigated in this study might present better drainage capacity associated with higher wet skid resistance compared to AC pavement (T. Wang et al., 2020).

Compared to high friction surfacing with MTD of 1.4 mm after 10,000 wheel-passes obtained from the study by Wilkinson Wilkinson (2017), MTDs of SFC slabs were significantly lower, indicating SFC pavements were not suitable for being utilised in high friction surfacing system.

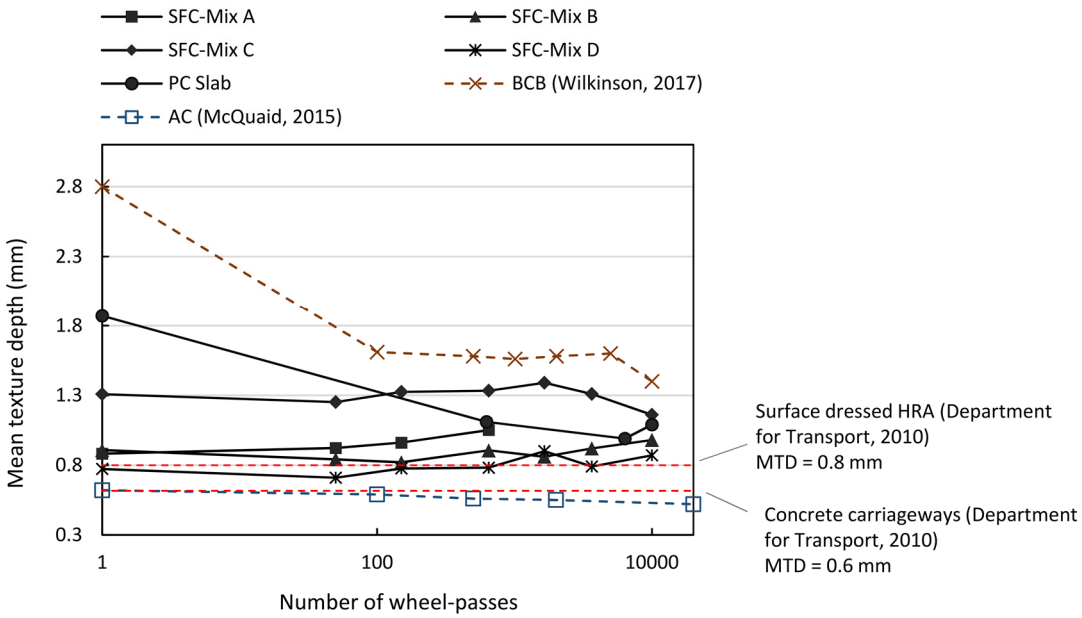

Figure 7.8. Relationship between mean texture depth (mm) by sand patch method and number of wheel-passes for SFC and control specimens.

7.3.5 Skid resistance investigation

Figure 7.9 (a) and (b) show relationships between SRV and the number of wheel-passes for SFC and PC Slab testing specimens in dry and wet conditions respectively, while Figure 7.10 shows the corresponding changes in SRV values of SFC-Mix A and SFC-Mixes B-D between 1-650 and 1-10,000 wheel-passes respectively. Minimum wet SRVs of 55, 45 and 70 required for non-critical locations in Category B and C (e.g. motorways with traffic of less than 2000 vehicles per day) and high friction surfacing system respectively stated in (British Board of Agrement, 2017; Impact Test Equipment, 2020) are also included. SRVs of high friction surfacing slab comprising BCB aggregate subjected to 1-10,000 wheel-passes and asphalt concrete pavement subjected to 1-20,000 wheel-passes extracted from the studies of Wilkinson (2017) and McQuaid (2015) are included for comparative purposes.

As shown in Figure 7.9 (a), at the beginning SFC-Mix A-D slabs with RAP chippings exhibited no notable difference in initial dry SRV (94-100) since the real contact area was mostly between the rubber slider from the pendulum skid resistance tester and RAP chippings. Grout type thus played a minor role in the friction of slider-RAP chipping contact before traffic. These values dropped significantly from 94-100 to 66-80 during the first 150 wheel-passes and started to rise to 92-94 after 10,000 wheel-passes. This corresponds well to the findings from (Wilkinson, 2017), where loose aggregates on slab surface were often worn off during the first 100-150 wheel-passes resulting in decreased friction. After that,

embedded RAP chippings in geopolymer grout were exposed leading to enhanced dry SRV. The PC slab specimen also a showed similar trend where its dry SRV reduced significantly from 95-83 during the first 625 wheel-passes and rose to 97 towards the end of the simulated trafficking test. After 10,000 wheel-passes, there was no noticeable reduction in dry SRVs of SFC slabs (92-94) compared to that before subjected traffic wear (94-100). This implies the low rate of chipping loss on SFC surface after 10,000 wheel-passes, which explained the fact that apart from SFC-Mix A slab, all testing slab behaved similarly towards the end of testing period.

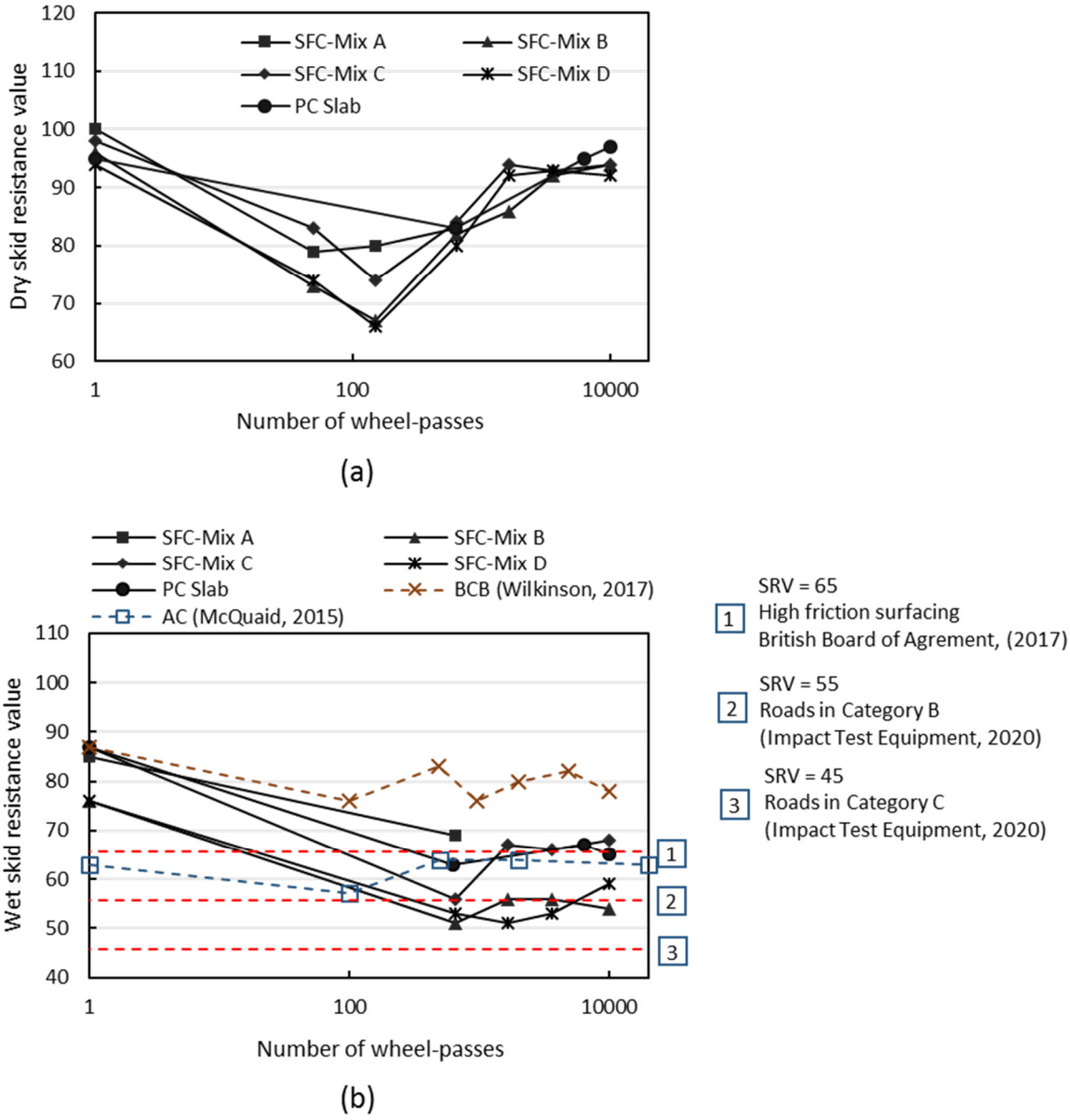

Figure 7.9. Relationship between skid resistance value and number of wheel-passes for SFC and control specimens for: a) dry condition b) wet condition.

As presented in Figure 7.9 (b), SFC specimens yielded significantly lower SRV in wet condition than in dry condition, as would be expected. All the four SFC-Mix A-D specimens started with SRVs ranging 76-85 in wet conditions and their SRVs decreased dramatically after 650 wheel-passes in wet conditions owing to the early chipping loss explained above. Similar trends were noted for the PC Slab specimen with a significant reduction in wet SRV from 87 to 63 after 625 wheel-passes.

All SFC slabs showed higher wet SRV (54-68) than the minimum SRV of 45 suggested for roads in non-critical locations (Category C) stated in Impact Test Equipment, (2020). SFC-Mix C and D showed SRV exceeding the suggested value of 55 for roads in Category B such as motorways (Impact Test Equipment, 2020). Not surprisingly, it revealed the impossibility of utilising SFC with RAP chippings as high friction surface since wet SRVs of SFC slabs were lower than the minimum SRV of 65 required for high friction pavements (British Board of Agrement, 2017). At 10,000 wheel-passes, SFC-Mix C with the highest MTD (1.2 mm) exhibited the highest wet SRV (68), followed by PC Slab with SRV of 65 (MTD = 1.1 mm). SFC-Mix B and D with lower MTD (0.9-1.0 mm) possessed lower wet SRV of (54-59). This highlights the earlier observation that low MTD is associated with reduced frictional property in wet condition (Highways England, 2006b; J. Wang et al., 2020).

As opposed to dry SRV, the frictional property in wet condition among SFC testing specimens varied greatly after 10,000 wheel-passes. For example, specimen SFC-Mix B exhibited wet SRV of 54 while its counterpart comprising grout Mix C showed much higher wet SRV of 68. This is because when the surfaces were wet, SFC-Mix C slab with higher MTD (1.2 mm) allowed water to go through the contact area while SFC-Mix B specimen with lower MTD (1.0 mm) prevented water from penetrating in the surface resulting in decreased pavement friction. This is in good agreement with previous findings reported by (Highways England, 2006b; J. Wang et al., 2020) that the MTD played an important role on the wet skid resistance of road surface.

As shown in Figure 7.9 (b), compared to asphalt concrete pavements with SRV of 63 in McQuaid (2015), SFC-Mix C specimens showed promising skid resistance ability with higher wet SRV of 68. Additionally, significant differences in friction resistance between BCB and RAP chippings were borne out by observations that wet SRVs of 78 of high friction surface containing BCB aggregates extracted from the study by Wilkinson (2017) after traffic wear were much higher than SFC slabs. RAP chippings with the presence of aged bitumen on the surface might prevent exposure of old aggregate to make contact with the rubber slider leading to a reduction in friction. This was referred to as ‘blinded microtexture’ hypothesis

in TRL report PPR060 (Roe and Forest, 2005). Even though the slabs were exposed under short-term trafficking, SFC-Mix B-D pavements could be potentially applied in locations that do not require high skidding resistance in wet condition, such as motorways with traffic less than 2000 vehicles per day (Impact Test Equipment AG190). Additionally, SFC-Mix B-D also showed promising frictional performance to be used as surface layers in heavy-duty pavements since their SRVs exceeded the SRVs of 45 required for heavy-duty surface layers (Knapton, 2008).

As shown in Figure 7.10, the percentages of SRV loss of SFC-Mix A after 650 wheel-passes in dry and wet conditions were 17 and 19% respectively. On the contrary, SRV losses in dry and wet conditions of SFC-Mix B-D after 10,000 wheel-passes were in the ranges 2-4% and 22-29% respectively.

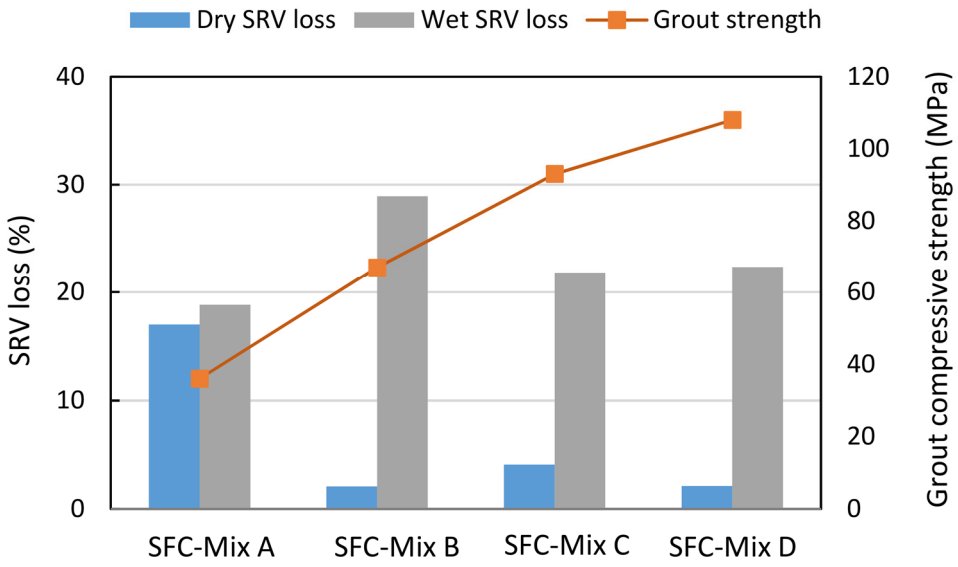

Figure 7.10. Percentage of SRV loss (%) of SFC pavements after 10,000 wheel-passes of simulated trafficking in dry and wet conditions.

Apart from SFC-Mix A, there was no significant reduction in SRV for SFC slabs in dry condition after traffic wear (SRV loss ≤ 4%). Key influences of grout strength on SFC frictional properties can be reviewed in this figure. For example, SFC-Mix A with the lowest grout strength (36 MPa) exhibited the highest dry SRV loss of 17% after 650 wheel-passes, while SFC-Mix D with the highest grout strength (108 MPa) achieved the lowest SRV loss of 2% after 10,000 wheel-passes. This indicates that SFC materials with low strength grout might possess a weak bond between chippings and geopolymer grout leading to RAP chippings being pulled out of the binder after subjected to trafficking. According to

Rizenbergs (1968), these loose chippings develop rolling action on the road-tyre interface of dry pavements leading to friction reduction.

Percentages of SRV loss in wet pavements followed similar trend to SFC in dry condition. For instance, after 10,000 wheel-passes, the SFC-Mix C slab with high strength grout (93 MPa) showed lower SRV loss (22%) compared to SFC-Mix B specimen with average grout strength (67 MPa; SRV loss =29%). This can be explained by the water film on wet surfaces of SFC-Mix B with low texture depth (MTD = 1.0) not being quickly absorbed into its surface, thus creating a slippery condition compared to SFC-Mix C with high MTD (1.2 mm).

7.3.6 Performance ranking of testing specimens

To provide informative insights into overall performance of testing slabs, Table 7.3 presents performance ranking levels ranging from 1-5 of SFC and PC Slab specimens after exposure to simulated accelerated trafficking using RTM.

Overall performance was ranked based on weight loss, texture depth and skid resistance in dry and wet conditions. Rankings 1 and 5 represented the best and worst performing specimens respectively. As shown in Table 7.3, SFC-Mix A exhibited the worst performance in resistance to weight loss due to its highest levels of deterioration. Hence, it was not considered for further performance ranking. A positive correlation existed between grout strength and performance (i.e. weight loss, MTD, dry and wet SRV) with pavements made from higher strength grout exhibiting greater endurance under simulated trafficking. In general, SFC-Mix C specimen outperformed the other SFC specimens and PC Slab with cement grout in most performance factors such as texture depth and skid resistance.

Table 7.3. Performance ranking in terms of weight loss, texture depth and skid resistance values for SFC and PC slab specimens after exposed to traffic wear.

Specimen	Grout strength (MPa)	Performance ranking			
		Resistance to weight loss (%)	Mean texture depth (mm)	Dry skid resistance	Wet skid resistance
SFC-Mix A	36	5	-	-	-
SFC-Mix B	67	4	3	3	4
SFC-Mix C	93	3	1	2	1
SFC-Mix D	108	1	4	4	3
PC Slab	84	2	2	1	2

7.3.7 Analysis of surface texture changes of SFC specimens after simulated traffic wear

Close-range photogrammetry was carried out on SFC-Mix B-D specimens to develop a more comprehensive understanding of effects of simulated accelerated trafficking on SFC surface textures. SFC-Mix A specimen was not considered for this analysis due to its significant damages after a short period of testing time using the RTM.

Figure 7.11 shows the process of surface modelling preparation of a typical SFC slab using Mountainsmap software. The original 2D topography of SFC surfaces was obtained from point cloud XYZ files created from Zephyr software (Figure 7.11 (a)). Form removal using the least square fitting method and surface levelling tools were applied to remove the curvature and flatten SFC surfaces.

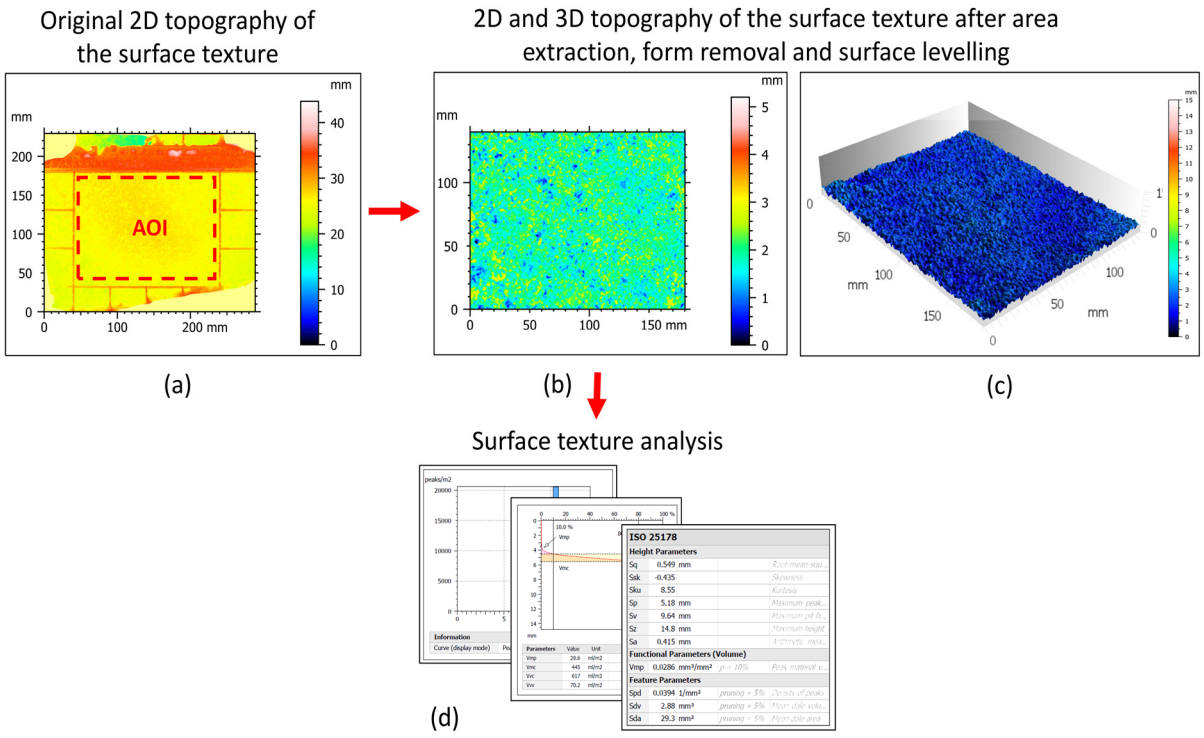

Figure 7.11. Surface modelling preparation and analysis of a typical SFC slab using Mountainsmap software. (a) Original 2D topography; (b,c) 2D and 3D topography after form removal, surface levelling and area extraction processes; (d) Surface texture analysis.

Surface texture analysis was then performed on an area of interest (AOI) of 140 x 180 mm extracted at the central area of SFC slab to investigate the effect of traffic wear on relevant texture parameters (e.g. height, volumetric) (Figure 7.11 (b-d)). This AOI represented the area affected by simulated trafficking where the skid resistance and sand patch tests were performed.

Height parameters (Sa; Ssk and Sku) were used to evaluate the changes in surface texture of testing slabs before and after subjected to traffic wear. Their definitions are presented and listed by names, units and descriptions in Table 7.4 according to Michigan Metrology glossary (Michigan Metrology, 2014).

Table 7.4. Terminologies of surface texture listed by names, units and descriptions from Michigan Metrology glossary (Michigan Metrology, 2014).

Terminology	Unit	Description
Skewness - Ssk	N/A	The symmetry degree of the surface heights about the mean line, Ssk = 0 for evenly distributed surface such as bell curve. Positive value indicates high peaks comprised surface while negative value indicates valley comprised surface.
Kurtosis - Sku	N/A	The presence of extreme peaks and deep valleys around the mean plane, Sku = 3.0 for evenly distributed surface such as bell curve. Sku value greater than 3 indicates high peaks and deep valley structures while Sku value lower than 3 indicates uniform surface.
Average roughness - Sa	mm	Arithmetic mean height of surface texture, which is usually used to indicate the roughness of surface.

Sa, Ssk and Sku were selected for study as they offered a general insight into the surface texture (Bitelli et al., 2012). Figure 7.12 illustrates various typical types of surface textures with different height parameters Sa, Ssk and Sku obtained from ISO 25178-1:2016 (ISO, 2016) and previous studies (Bitelli et al., 2012; Martisius et al., 2018). As shown in this figure, high Sa and Sku or positive Ssk means that the surface contains spikes or deep valleys while low Sa and Sku or negative Ssk show a more uniform and bumpy surface (Michigan Metrology, 2014). Additionally, surfaces with negative Ssk are reported to be a good bearing surface (Kumar and Rao, 2012).

Figure 7.13 (a-b) shows 2D and 3D images of SFC-Mix B-D surface textures before and after 10,000 wheel-passes generated from MountainsMap software. In addition, effects of grout

type on surface texture of SFC pavements after subjected to traffic wear were presented in the peak count histogram presented in Figure 7.14.

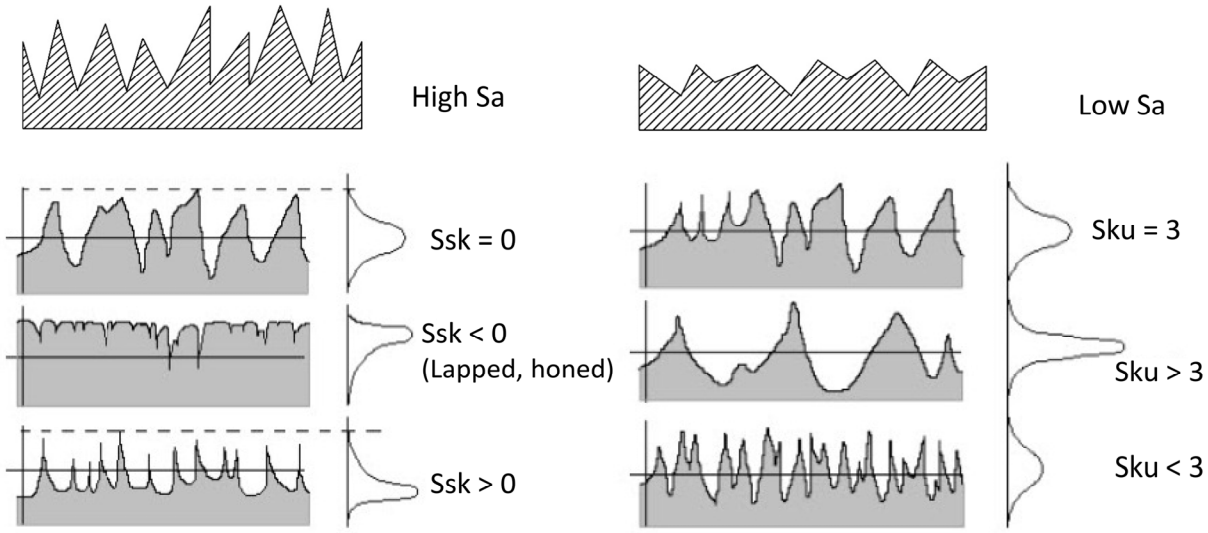

Figure 7.12. Surface texture depictions in terms of various height parameters based on previous studies (Bitelli et al., 2012; ISO, 2016; Martisius et al., 2018).

Visual observation of Figure 7.13 shows the formation of sharp peaks in the initial surface of SFC pavements while smoother surface with rounded peaks were observed in the surfaces of these specimens after being subjected to simulated trafficking of 10,000 wheel-passes. This trend reflects pronounced influences of simulated trafficking conditions on SFC surface textures. For instance, spiky SFC-Mix B surfaces comprising small sized RAP chippings were worn down and smoother after 10,0000 wheel passes as shown in Figure 7.13 (a).

After 10,000 wheel passes, SFC-Mix B specimen with the lowest grout strength among the investigated grout mixes (B-D) exhibited the most lightly textured surface compared to SFC-Mix C and D in Figure 7.13 (c) and (d) respectively. This observation is confirmed by the trend presented in Figure 7.14 (a) where SFC-Mix B specimen possessed the lowest peak count of 2200 peaks/m^2 associated with peak height of approximately 2.5 mm. A similar trend was observed in the cases of SFC-Mix C and D with 2700 and 2600 peaks/m^2 respectively associated with peak height of approximately 3.8 mm (Figure 7.14 (b-c)).

SFC-MIX B (Before traffic wear)

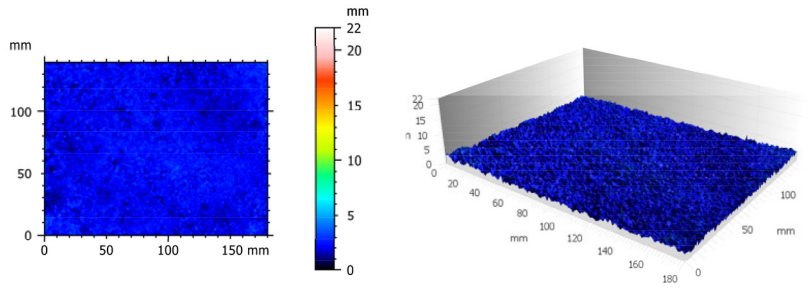

SFC-MIX B (After 10,000 wheel-passes)

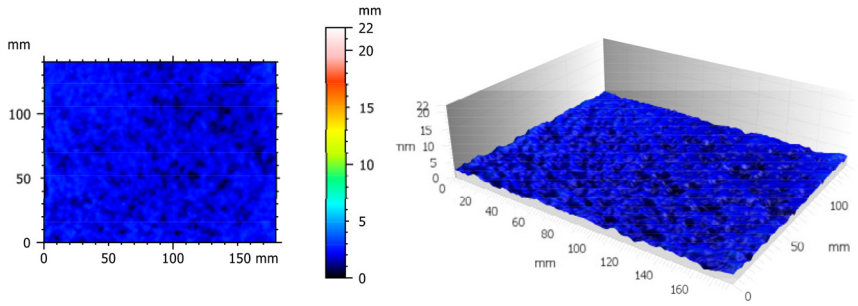

(a)

SFC-MIX C (Before traffic wear)

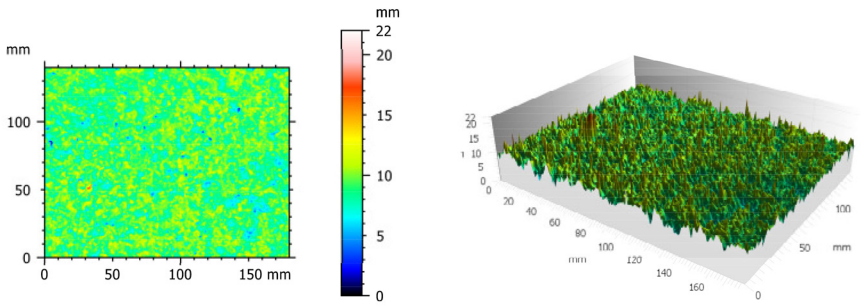

SFC-MIX C (After 10,000 wheel-passes)

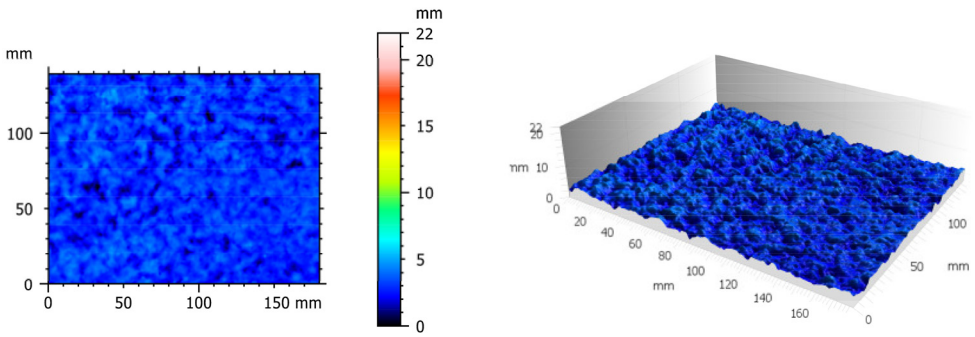

(b)

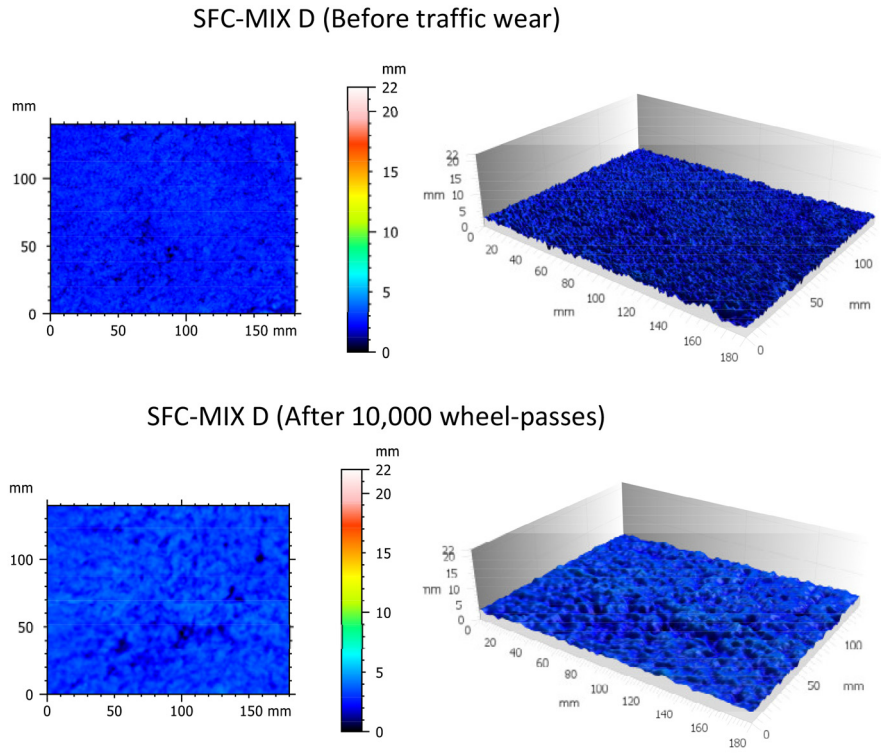

(c)

Figure 7.13. 2D and 3D images of SFC-Mix B-D surfaces before and after traffic wear. (a) SFC-Mix B; (b) SFC-Mix C; (c) SFC-Mix D.

Average roughness Sa

Figure 7.15 shows the relationship between average roughness Sa and the number of wheel-passes of SFC-Mix B-D testing slabs. Sa values of asphalt concrete pavements extracted from the study by McQuaid (2015) are also included for comparative purposes. Roughness values before and after traffic wear of SFC pavements ranged from 0.3-0.9 mm and 0.3-0.5 mm respectively. SFC-Mix C specimens exhibited the highest roughness value (Sa = 0.5 mm) after 10,000 wheel-passes. However, there was notable reduction in Sa of SFC-Mix C specimens during traffic wear (0.9-0.5), which implied major changes in surface texture of SFC-Mix C due to polishing action.

Except for SFC-Mix C, SFC pavements showed similar roughness compared to conventional AC pavement (McQuaid, 2015). However, during traffic wear, average roughness Sa of SFC pavements fluctuated while Sa values of AC pavements remained stable. This trend implied minor changes in AC surface during polishing actions, which are linked to greater endurance under trafficking of AC pavements compared to than SFC pavement.

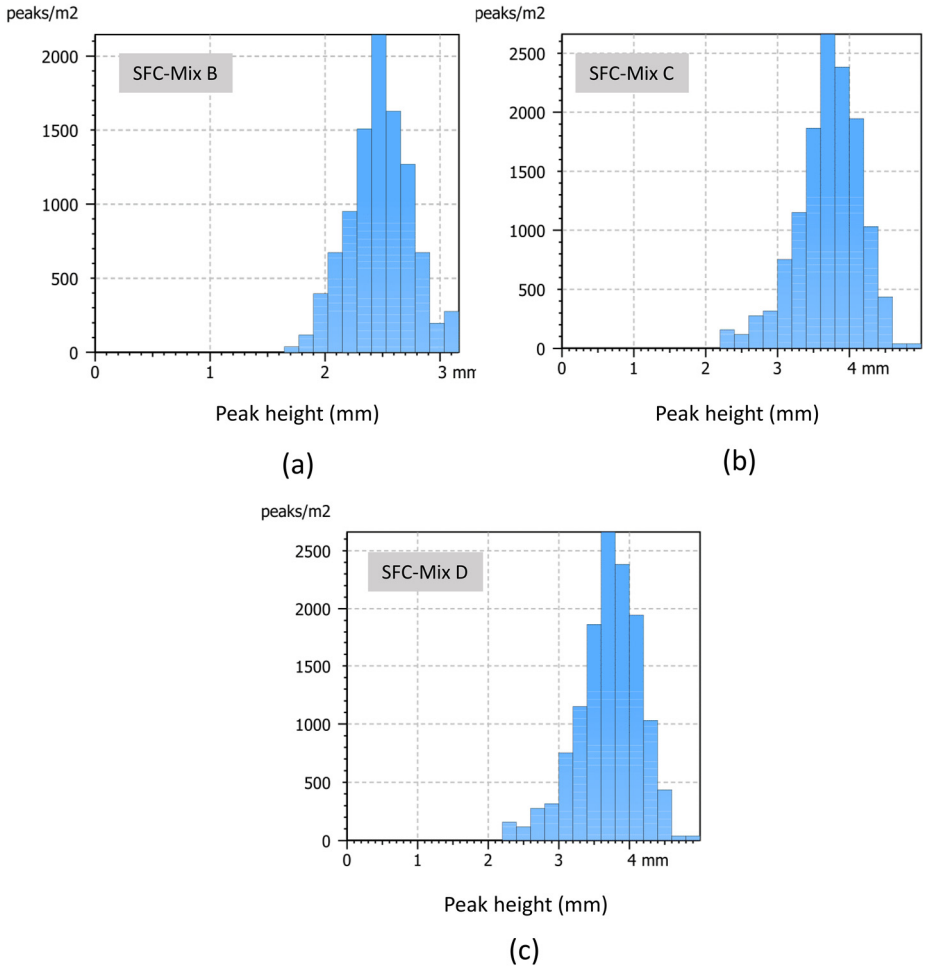

Figure 7.14. Peak count histogram of SFC-Mix B-D specimens after subjected to simulated trafficking of 10,000 wheel-passes.

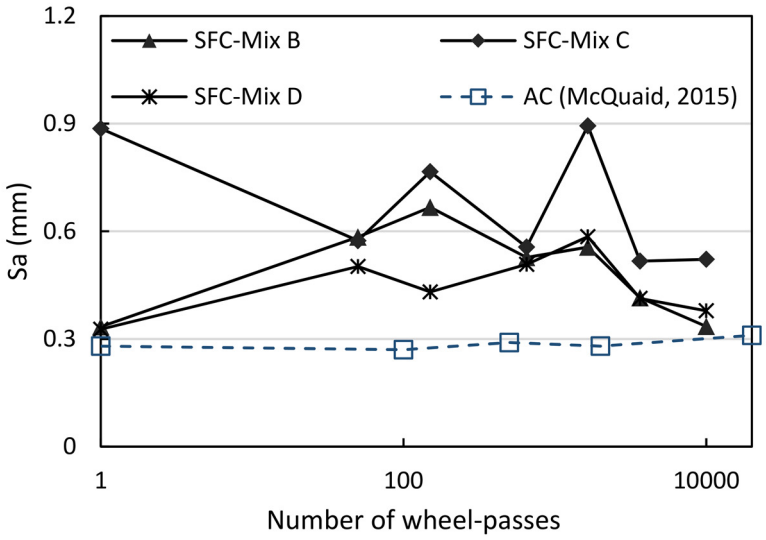

Figure 7.15. Relationship between average roughness Sa and number of wheel-passes of testing slabs.

Skewness Ssk and Kurtosis Sku

Table 7.5 presents skewness Ssk and kurtosis Sku values for SFC-Mix B-D specimens before and after subjected to traffic wear. Ssk and Sku of AC pavements extracted from the study by McQuaid (2015) are included for comparison. As shown in Table 7.5, before traffic wear, all SFC pavements exhibited negative skewness Ssk (-0.01 to -0.6) and kurtosis Sku (3.40-5.63). According to Figure 7.12, this observation indicates that SFC pavements initially possessed consistent surfaces free of extreme peaks (Bitelli et al., 2012).

Table 7.5. Skewness Ssk and Kurtosis Sku values of testing slabs before RTM and after 10,000 wheel-passes.

Specimens	Ssk		Sku	
	Before traffic wear	After 10,000 wheel-passes	Before traffic wear	After 10,000 wheel-passes
SFC-Mix B	-0.01	-0.42	3.40	3.27
SFC-Mix C	-0.15	-0.40	5.63	3.18
SFC-Mix D	-0.60	-0.98	3.88	4.89
AC (McQuaid, 2015)	-0.99	-0.36(*)	4.15	4.05(*)

(*) After 20,000 wheel-passes

After 10,000 wheel-passes, the observed Ssk of SFC-Mix B-D surfaces remained negative (-0.42 to -0.98 and the majority of their Sku values (3.27-4.89) fell close to the normal distribution of 3. As shown in Figure 7.12, this indicates the peaks and valleys were distributed fairly uniform on SFC surfaces due to polishing action by the RTM (Naylor et al., 2016). Negative Ssk (-0.36) and Sku of 4.05 observed in AC pavements (McQuaid, 2015) reflects a similar distribution of peaks and valleys on their surfaces compared to SFC pavements.

Relationships between average roughness Sa and wet/dry SRV of SFC surface courses

Relationships between wet and dry SRV and Sa during traffic wear were investigated to provide a rapid estimation method for SFC skid resistance based on the height parameter Sa. Average Sa and wet SRV relationships were studied in the research by McQuaid (2015), from which low correlation was obtained for asphalt concrete pavements (R^2=0.0682). Therefore, in this study, number of wheel-passes was considered as one of the input parameters along with Sa to estimate SRV of SFC pavements to improve the established relationship. The following polynomial regression equations generated from SPSS statistical

software were proposed to estimate SRV on dry and wet conditions based on the number of wheel-passes and average roughness.

$$Dry\ SRV = 48.4 + 0.009WP - 0.00000048WP^2 + 74.25Sa - 33.9Sa^2 - 0.004WPSa^2 \quad (7.2)$$

(R^2 = 0.919)

$$Wet\ SRV = 29.93 + 0.002WP - 0.00000019WP^2 + 45.3Sa - 15.39Sa^2 + 0.004WPS_a \quad (7.3)$$

(R^2=0.777)

where $Dry\ SRV$ and $Wet\ SRV$ are skid resistance values in dry and wet conditions respectively; WP is the number of wheel-passes; Sa is average roughness.

Sufficiently high R^2 values for both dry and wet SRV (0.919 and 0.777 respectively) estimations confirmed the favourable performance of the two polynomial regression equations. The relationships between experimental and estimated results are additionally presented in Figure 7.16.

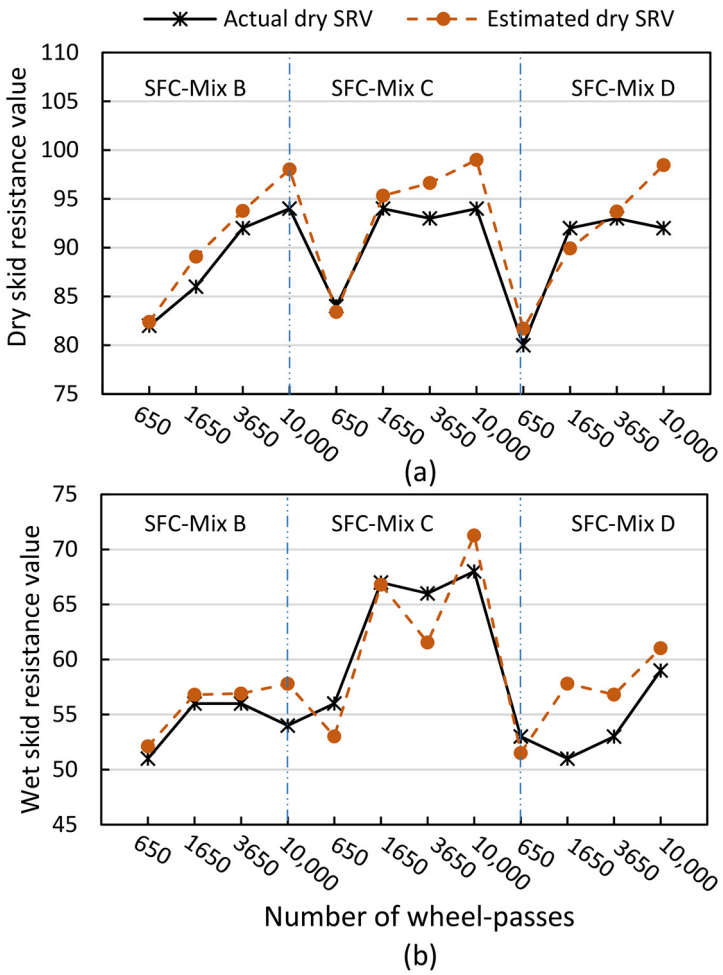

Figure 7.16. Comparison between actual and estimated SRV of SFC specimens obtained from experiments and Equations (7.2) and (7.3).

It should be noted that in this figure SRV values recorded in the range 0-650 wheel-passes were discarded due to their instability. These values were also omitted while generating polynomial equations (7.2) and (7.3) by SPSS software. The established polynomial regression equations can be used as a means for determining SFC skid resistance in dry and wet conditions. This method could reduce the demand of costly equipment, large volume of raw materials and time for specimen preparation.

7.4 Summary of results

Based on the results from laboratory-scale experiments, performance of testing slabs in terms of change in weight, skid resistance and mean texture depth before and after simulated traffic action by the road test machine were discussed. A preliminary trial of SFC pavements with different surface finishes including surface dressing and exposed aggregate with and without brushing was conducted based on skid resistance determined by pendulum test, aiming to improve the surface texture SFC pavements. The results indicated that surface dressing is the most effective surface finish in terms of skid resistance compared to exposed-aggregate surface finish. SFC pavements incorporating various types of geopolymer grouts (Mix A-D) and RAPs with surface dressing finish were examined along with high friction surfacing pavements and conventional AC pavement obtained from the studies by Wilkinson and McQuaid (McQuaid, 2015; Wilkinson, 2017). The use of 3D surface texture analysis technique, known as close-range photogrammetry, utilising 3DF Zephyr software and Digital Surf – MountainsMap was proposed to investigate changes in SFC slab surface textures after being subjected to traffic wear. The findings from this chapter are as follows:

- Percentage of weight loss of SFC pavements after subjected to traffic wear varied from 1.2 to 7.5% by mass. The durability of SFC pavement associated with weight loss was influenced by grout strength, with decreasing weight loss generally related to high strength grout (2.5-4.7% weight loss by mass after 10,000 wheel-passes).
- SFC pavements possessed moderately high MTD ranging from 0.9-1.2 mm after subjected to simulated trafficking, compared to the required minimum MTDs for concrete carriageways and surface dressed HRA (0.6 and 0.8 mm respectively) stated in NRSWA (Department for Transport, 2010). Additionally, SFC pavements with lower MTD than high friction pavements with buff calcined bauxite aggregates (1.4 mm) from (Wilkinson, 2017) were not suitable to be used as alternatives to high friction systems. With higher MTD than conventional asphalt concrete (0.5

mm) (McQuaid, 2015), SFC pavements showed promising performance in drainage capacity associated with sufficient skid resistance in wet condition.

- In general, SFC pavements achieved skid resistance values ranging from 92-94 for dry SRV and 54-68 for wet SRV after subjected to simulated trafficking, which was above the minimum SRV of 45 and 55 required for non-critical locations in Categories B and C with the traffic of less than 2000 vehicles per day respectively stated in (Impact Test Equipment, 2020). However, wet SRVs of SFC pavements were significantly lower than high friction surface with BCB aggregates (SRV = 78). With the exception of SFC-Mix A, traffic wear had a minor effect on dry SRV of SFC pavements with SRV loss ranging from 2- 4%. On the contrary, high SRV loss ranging from 22-29% proved significant influence of simulated trafficking on wet SRVs of SFC pavements.
- Close-range photogrammetry provided valuable information on surface texture change of SFC pavements and thus is a useful tool to investigate their behaviours under simulated traffic action. In general, after traffic wear, SFC pavements possessed higher roughness Sa (0.3-0.9 mm), negative skewness and kurtosis Sku ranging from 3.18-4.89, which showed notable change compared to the initial values before traffic wear. SFC pavements with fluctuated Sa during traffic wear were deemed to be less durable compared to conventional AC pavement with consistent values of Sa.

Overall, despite the fact that the simulated traffic volumes considered using the RTM were not high enough to fully understand the long-term performance of SFC materials as surface courses, it appears that SFC pavements with surface dressing yielded viable pavement material solution for non-critical located roads (i.e. motorways and trunk with traffic of less than 2000 vehicles per day, heavy duty pavement). However, it is inadvisable to utilise SFC materials for high skid resistance areas such as approaches to pedestrian crossing, major and minor junctions on dual carriageway, roundabout circulation areas because the minimum SRV required is 65 (British Board of Agrement, 2017). Also, low strength SFC materials such as SFC-Mix A is not recommended as a surface course for pavements as it showed noticeable segregation after a short time under traffic wear.

CHAPTER 8

DISCUSSION

8.1 Introduction

This chapter presents main outputs extracted from the previous chapters. Findings relating to the six research objectives identified in Chapter 1 and their relevance to the existing literature are also discussed.

8.2 Research objective 1 - Conduct a throughout literature search on relevant subjects including RAP, geopolymer materials and semi-flexible composite pavements.

In Chapter 2, literature relevant to the proposed SFC material and its constituent materials including RAP and geopolymers were critically reviewed. Their practicality in pavement applications was proven by real-world examples. Standards and guidelines for asphalt and concrete pavements were reviewed to help develop a framework of SFC materials specifications.

A review of RAP aggregate found that its typical properties are dependent on the original aggregate and attached aged bitumen layer. In previous research undertaken in countries such as India, Australia and Portugal (Arulrajah et al., 2014; Freire et al., 2013; Mishra, 2015), RAP was commonly blended with crushed rock, limestone or recycled concrete aggregate as main components for base and sub-base layers. Up to 30% RAP by mass can be used as alternative to natural aggregate for pavement base layers, while up to 100% RAP by mass can replace virgin aggregates for sub-base layers. RAP stabilised by Portland cement, slag and fly ash-based geopolymer mixtures showed positive results in compliance with local requirements for base and sub-base courses in Thailand and the US (Hoyos et al., 2011; Puppala et al., 2011). The most common application of RAP is as coarse aggregate for hot mix asphalt surface courses. Up to 60% by mass aggregate replacement by RAP has been used in hot mix asphalt for surface courses in countries including Iraq and Nigeria (Fattah et al., 2017; Ogundipe, 2020). As reported in MCHW, SHW, Volume 1, Series 900, Clause 902 (2019), a lower reclaimed RAP content in pavements is permitted in the UK. A maximum of 15% by mass RAP replacement can be used in surface layers of motorways. The corresponding value for both base and binder courses is 25% by mass. Further tests such as indirect tensile stiffness modulus need to be performed for mixtures containing higher RAP contents. Some contractors (e.g., FM Conway) successfully re-used higher RAP contents (50% by mass replacement) in the surface of a section of the M25, with incorporation of specialised polymer modified binder. Several studies attempted to utilise up to 100% by mass aggregate replacement by RAP in concrete pavements, all resulting in reduced compressive strengths (Hossiney et al., 2008; Huang et al., 2005; Shadmani et al., 2018; Singh et al., 2017). Similar performance reductions were also obtained in cold mix

pavements with over 60% by mass RAP (Afonso et al., 2016; Hugener et al., 2014; Ojum and Thom, 2017).

It was recognised that the properties of geopolymer materials consisting of solid aluminosilicate precursors and alkaline activators were highly dependent on mixture proportions, constituent materials and curing conditions (Güllü et al., 2019; Luukkonen et al., 2018). Geopolymer grouting materials exhibited lower fluidity and rapid strength development than Portland cement grout (Afonso et al., 2016; Güllü et al., 2019). Geopolymers were reported to develop over 80% of their 28-day strength after seven days (Luukkonen et al., 2018). In addition to high compressive strength (70-100 MPa) (Davidovits, 1994), geopolymer materials were found to resist freeze-thaw cycles and adsorb heavy metals including Hg, Si, Al and Cu (Azarsa and Gupta, 2020). Apart from being used as stabilising materials for base and sub-base courses described above, potential applications of geopolymer materials in road applications include artificial aggregates, road repair materials (Silva et al., 2010; Wilkinson, 2017) and surface layers for airport runways and aprons (Glasby et al., 2015). Current use of geopolymer pavements in Toowoomba Wellcamp airport in Australia or cycle and pedestrian pathways in New Zealand (Concrete Institute of Australia, 2011; Glasby et al., 2015) demonstrated its potential in pavement applications. Chapter 2 also provided information on embodied greenhouse gas intensity of geopolymer materials. Results obtained from existing literature have been encouraging where the use of geopolymer cement was claimed to reduce carbon dioxide emissions relative to conventional cement production by 90% (Davidovits, 1994). However, several limitations including the absence of proper standards and guidelines, long-term performance data, inconsistent reactivity of aluminosilicate precursors, upcoming shortages of fly ash and drying shrinkage issues were all noted as potential hindrances to broader application of geopolymer materials.

Conventionally, semi-flexible composite material comprises cementitious grout and open-graded aggregate skeletons with bitumen and air void contents ranging from 3.7-4.6% and 25-35% respectively (Oliveira, 2006). Hydrated lime (Koting et al., 2007) and cationic bituminous emulsion (Pratelli et al., 2018) have also incorporated into hot and cold mixtures of open-graded asphalt respectively. Albeit recommended flow times of 8-10 s (Anderton, 2000), some commercial products such as Densit grout were found to possess lower flowabilities of 10-18 s but with high compressive strengths in the range 92-110 MPa after 28 days. This highlights the need for more transparent and comprehensive research on grouting materials, with wider ranges of workability and compressive strength. SFC

properties were found to significantly depend on the characterisation of its constituent materials such as the open-graded aggregate skeletons and cementitious grouts (Pratelli et al., 2018). Positive performance in terms of compressive strength and stiffness were reported for SFC with hot mix asphalt (Setyawan, 2003), with its stiffness 2.3 times higher than cold mix asphalt SFC (Afonso et al., 2016). However, some commercial products with proprietary mix designs such as Ready to Mix (Pratelli et al., 2018) were claimed to attain better mechanical performances than hot mixture SFC introduced by academic researchers (Afonso et al., 2016; Anderton, 2000). One of the most common applications of SFC materials is surface layers in heavy duty pavements including industrial hardstanding, warehouses, car parks, aircraft apron, etc. Current uses of SFC pavements in London Gateway Container Terminal (the UK), Copenhagen Airport (Denmark) and Rotterdam port (Netherland) (Bonicelli et al., 2019; Densit, 2018a; Road Surface Treatment Association, 2014) were also presented in this chapter.

Since limited standards are available for SFC pavements, general requirements for concrete and asphalt pavements were reviewed to evaluate the feasibility of using SFC in pavement structures. Details of minimum compressive strengths required for sub-base, base and surface courses of new or existing pavements provided in DMRB, volume 7, section 2 (Highways England, 2006a) were reviewed. Also reviewed were MCHW, SHW, Volume 1, series 900 (2019) and 800 (2016); the two main guidelines for constituent materials, specimen preparation and testing of asphalt and concrete pavements respectively. Finally in Chapter 2, a review was undertaken of The British In-Situ Concrete Paving Association (2007) issued guidelines on thickness design, which offers official advice and specification for structures of heavy duty pavements. Included in this document was a method for determining thickness designs of pavement base layers based on the approach introduced by Williams (1986).

8.3 Research objective 2 - Investigate the possible range of fresh and mechanical properties of geopolymer grouts and select suitable grouts for further investigation of SFC materials.

Fresh and mechanical properties of a diverse suite of geopolymer grouts were examined in Chapter 4. The grouts were formulated using various mixture combinations of industrial by-products including FA, GGBS, SF and MK at ambient temperature. Effects of mix design parameters including liquid-to-solid ratio, type of geopolymer powders and mixture proportions on performances of geopolymer grouts were investigated through laboratory testing of Marsh flow cone, Vicat needle penetration and compressive strength. Suitable

grouting materials for further investigation of SFC materials were selected based on contrasting performance classification.

As shown in Figure 8.1, compared to the existing literature, a wide range of performances were observed in terms of flow times, initial setting times, final setting times and 28-day compressive strengths in the case of geopolymer grouts. For SFC with hot mix asphalt compacted and mixed at high temperature (170^{o}C), flow time of resin modified grout containing Portland cement in a study by Anderton (2000) varied from 9-17 s, while the cementitious grout investigated in a study by Afonso et al. (1994) exhibited a wider range of flowability (11-144 s). These flowability ranges were chosen to ensure full grout impregnation and efficient grouting processes for SFC with aggregate skeleton void contents less than 30% by volume (Anderton, 2000). The mix designs of geopolymer grouts with broader flowability (9-841 s) were geared towards selecting suitable grouting materials for cold mixtures of open-graded RAP with various porosity levels. A more significant variance trend of initial and final setting times (13-450 mins and 30-840 mins respectively) was observed in geopolymer grouts compared to cement grouts investigated in previous research in this area. For example, resin modified Portland cement grout for SFC pavements introduced in a study by Anderton (2000) possessed initial/final setting times of 170/285 mins. This setting time trend for geopolymer grout offers more flexibility regarding open SFC grouting times than traditional cement grout. The highest compressive strength in the range 19-108 MPa recorded for geopolymer specimens at the age of 28 days was in line with those obtained from commercial grouting products such as Densit (110 MPa) (Densit, 2018b). This confirmed the possibility of using geopolymer grout as an alternative to commercial cementitious grouting products. By exploiting diverse performance levels of geopolymer grouts, SFC manufacture can be suitable for a broad range of practical uses.

The effects of mix design parameters, including LS ratio and binder content on performance of geopolymer grouts were highlighted in Chapter 4. It was observed that high GGBS content led to low flowability, fast setting and high compressive strength. This confirms previous findings in studies by Zhang et al. (2019) and Saludung et al. (2018) that geopolymer grouts with high GGBS content (up to 100% by mass of binder content) exhibited shortened setting time and increased compressive strength. Saludung et al. (2018) found that the presence of high CaO content GGBS powder (42.4% by mass) accelerated the C-S-H gel forming process. The inclusion of MK was found to reduce flowability and increase setting time and compressive strength of geopolymer grouts. This

trend correlated favourably with previous research (Favier et al., 2014) that defined geopolymers containing MK as mixtures with rheological behaviour. Although high flow times of geopolymer mixes containing MK (over 840 s) were a major challenge for SFC materials, incorporating MK into geopolymers was found to be feasible to replace conventional self-levelling concretes for floor screed applications (Favier et al., 2014). The addition of SF in geopolymer mixtures improved its flowability, setting time and compressive strength. This is consistent with previous findings from the study by Khater (2013) that suggested positive effects of SF on workability and mechanical strength were attributable to small sizes (0.1-0.4 µm) and effective pozzolanic activity of SF particles.

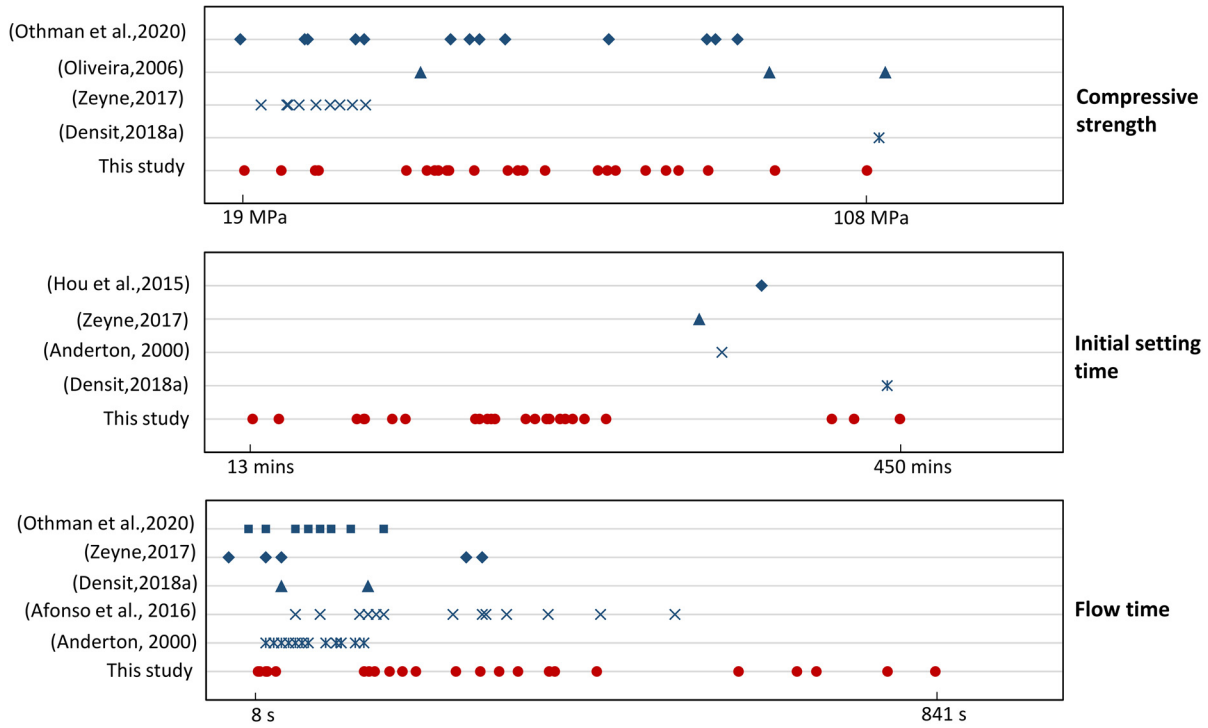

Figure 8.1. Measured values of flow time, initial setting time and compressive strength compared with those from previous studies.

For further investigation of SFC materials in Chapters 5, 6 and 7, geopolymer mixes were selected based on their contrasting performance classifications in terms of their ability to fill the internal void structure of RAP skeletons. Performance was classified in terms of flow time, initial setting time and compressive strength after 28-days curing based on previous studies. It should be noted that each category's minimum and maximum bounds were adjusted to accommodate the ranges of performances (i.e. flowability, setting time and compressive strength) obtained from this study.

8.4 Research objective 3 - Evaluate the potential use of SFC in pavement applications in terms of mechanical properties.

Chapter 6 assessed physical, mechanical and microstructural properties of SFC materials comprising four geopolymer grout mixes with contrasting performances and cold mixture open-graded RAP skeletons with various solids contents (45-62% by volume). Destructive, non-destructive testing and machine learning methods were employed to determine compressive strength and elastic modulus of SFC specimens respectively. SFC compressive strength results were compared with general requirements for HBM base courses (Highways England, 2006a) and concrete pavements (British Standards, 2013h) to evaluate the potential use of SFC materials in base and surface courses respectively. Preliminary examples of the application of SFC materials for the base layer of heavy-duty pavements for industrial hardstandings were also presented.

As presented in Figure 8.2, compressive strength of SFC mixtures ranged from 9-32 MPa and exceeded the minimum strength of 8 MPa required for HBM base layer stated in DMRB, volume 7, section 2 (Highways England, 2006a), indicating it as a viable material solution. Despite possessing the highest compressive strength (108 MPa), grout Mix D was not practically suitable for solid RAP contents of 54% and 62% by volume, owing to its relatively 'slow' flowability (609 s) and 'fast' setting time (13 mins). This resulted in incomplete RAP penetration. Figure 8.2 highlights positive outcomes in terms of compressive strength for SFC mixtures investigated in this study. SFC mixtures with geopolymer grouts outperformed other SFC materials investigated in previous research, including: resin modified pavements (RMP) comprising asphalt concrete and resin modified Portland cement grout (Anderton, 2000) and SFC mixtures comprising hot/cold porous asphalt and cementitious grout (Afonso et al., 2016; Setyawan, 2013). Compared to PC Control specimens comprising basalt aggregates and cement grout, SFC mixtures developed in this study exhibited lower compressive strength. SFC with grout Mix D and 45% by volume RAP was found to behave closer to concrete control specimens than the traditional SFC mixtures in terms of compressive strength.

Additionally, SFC materials showed ability to rapidly gain early strength (66-84% of 28-day strength) after three days compared to Portland cement concrete (49% of 28-day strength). This is encouraging for the applications of SFC pavements in areas where early opening of pavements to traffic is preferential.

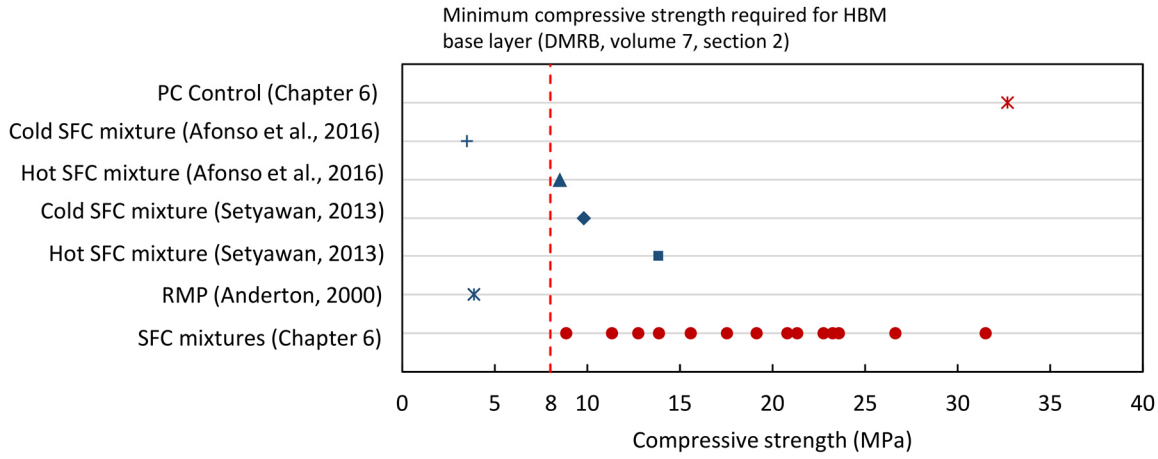

Figure 8.2. Recorded values of compressive strength of SFC mixtures compared to those from existing literature.

In general, SFC performance was influenced by grout properties and RAP content, with improving performances generally associated with decreasing RAP content combined with highly flowable and strong grout. This is consistent with findings from the studies by Setyawan (2013) and Afonso et al. (2016), where infusion of hot mix porous asphalt skeletons with high strength cementitious grout exhibited favourable performance in terms of strength and stiffness. To confirm this finding, sensitivity analysis integrated with a machine learning approach (Deep Neural Network) was carried out to investigate effects of grout properties, RAP content and SFC curing age on SFC compressive strength. This sensitivity analysis was successfully employed in previous studies to investigate the importance of input parameters such as mix proportions and curing conditions on mechanical properties of materials, such as fly ash-based geopolymer concrete (Huynh et al., 2020b; Van Dao et al., 2019) and lightweight aggregate concrete (Tenza-Abril et al., 2018). Compressive strength of geopolymer grout and RAP content were found to be dominant factors in SFC strength prediction, with sensitivity scores of 32% and 17% respectively, followed by SFC curing age (16%). Other grout properties such as flow time, initial/final setting time also played important roles in SFC strength prediction with a total sensitivity score of approximately 35%. Therefore, these mix design parameters need to be considered and controlled carefully during SFC manufacturing process.

Corresponding 28-day compressive strengths of SFC mixtures were found to be 17-39% of the parent grout strength, which was higher than the percentage of 11% reported by Setyawan (2013). This is possibly explained by the fact that SFC mixtures developed in this study had RAP skeletons with higher porosity levels (38-55%) than those in Setyawan's

study (28-32%), leading to higher volumes of grout to be filled in the internal voids and improve the strength. From the investigated SFC mixtures, specimens comprising grout Mix B and 62% RAP were initially chosen as the most viable mixture for use in base layers since it delivered the highest strength (18 MPa) at the maximum usage of recycled aggregates. This conclusion was the first step towards providing a comprehensive evaluation of the sustainability performance of SFC materials, which was further assessed using a cost and greenhouse gas emission analyses in Chapter 6.

The thickness of SFC base courses in heavy duty pavements was calculated based on the compressive strength and elastic modulus obtained from experiments and a UPV-elastic modulus correlation. The pavement structure was assumed to consist of 80 mm thick concrete block paving on a 30 mm sand bed and SFC base layer laid on sandy subgrade CBR 8%. Estimated minimum thicknesses of SFC base layers (240-350 mm) suggested potential savings in material use and cost relative to traditional CBGM $C_{8/10}$ base course. The corresponding thickness of the latter was 360 mm as recommended by the British In-Situ Concrete Paving Association (2007).

In terms of surface course, mechanical properties of SFC materials obtained from this study were compared to the minimum strength required for concrete pavements in BS EN 13877-2:2013 (British Standards, 2013h). All SFC mixtures possessed compressive strengths within the range 8-100 MPa for concrete pavements as required by BS EN 13877-2:2013 (British Standards, 2013h). However, the standard suggested mixtures with compressive strength values of over 20 MPa for use in concrete pavements. As such, SFC mixtures containing either grout Mix A or RAP content over 49% were not recommended for use in surface courses since their compressive strength fell short of the required value.

8.5. Research objective 4 - Identify the benefits of using SFC materials in pavement applications in terms of costs of raw material and greenhouse gas emission.

Based on the thicknesses obtained in Chapter 6, costs of raw materials and greenhouse gas emissions to produce one m^2 of SFC base layer were carried out to evaluate its economic viability and environmental performance. In this work, SFC was considered as an alternative to a traditional 360 mm CBGM $C_{8/10}$ base course in a heavy duty pavement application. Costs, fuel and electrical energy consumption during manufacturing processes used in the analysis were derived from published data in the current literature. The costs associated with construction operations of SFC layers such as labour, fuel, water and power were assumed to be similar as for CBGM layers and, therefore, neglected to simplify analysis.

In general, the cost analysis highlighted significant economic benefits for SFC (£24-39/m^2) compared to traditional CBGM $C_{8/10}$ (£47/m^2) base course. Alkaline activator was found to account for a majority (57%) of total SFC production costs. This finding is consistent with previous research outcomes where activator costs ranged from 41-45% of total production costs of alkaline activated products (Vinai and Soutsos, 2019) or 71-83% for metakaolin and fly ash-based geopolymer concretes (Pacheco-Torgal et al., 2005). This observation indicates that further cost reductions of this material are most likely needed prior to wide-scale commercial realisation of SFC pavements.

The rate of greenhouse gas emission from the production of one m^2 of SFC layer was about two times lower than traditional heavy-duty base course consisting of 360 mm CBGM $C_{8/10}$, indicating impressive environmental advantages. These results were found to correlate well with those in the study of McLellan et al. (2011), where typical greenhouse gas emissions of geopolymer concrete were 44-64% lower than Portland cement concrete. The manufacturing process of alkaline activator (sodium silicate in this case) contributed significantly to emissions associated with SFC pavements, accounting for up to 60% of the total. This confirms observations in previous studies (McLellan et al., 2011; Vinai and Soutsos, 2019), which stated that negative environmental impacts associated with the melting process of sodium carbonate (known as soda ash, Na_2CO_3) and quartz sand (SiO_2) in sodium silicate production hinder the widespread use of geopolymers. Overall, however, the positive economic and environmental aspects of SFC materials highlighted by this work represent an excellent initial step towards a future of sustainable, low-carbon construction materials not requiring heating energy or natural resources.

8.6 Research objective 5 - Investigate the trafficking-related properties of SFC surface courses subjected to simulated traffic wear.

Trafficking-related properties of SFC pavements including skid resistance, mean texture depth, weight loss and surface texture changes were assessed using experimental and close-range photogrammetry methods to enhance the understanding of SFC performance as surfacing materials. Laboratory work was undertaken on SFC slabs comprising four types of geopolymer grout selected from Chapter 4 and 45% by volume RAP solids content. An initial assessment was carried out to identify suitable surface finishing methods for SFC pavements. Testing slabs were prepared using one typical geopolymer grout mix (Mix B) and three surface preparation techniques including surface dressing with RAP chippings and exposed aggregate with/without brushing finishes. Results obtained from skidding

resistance testing showed that surface dressing is the most effective finishing method owing to its highest SRV in dry and wet conditions (90 and 76 respectively).

Following this observation, further testing was performed on SFC pavements comprising four geopolymer grout mixes and 45% by mass RAP solids with a surface dressing finish. These slabs were exposed to simulated trafficking using the road test machine to investigate the suitability of the proposed SFC for surface courses in pavements. Recorded weight loss of SFC pavements caused by worn-off chippings or specimen segregation indicated that all but one mixture containing grout Mix A possessed subsequent durability, with less than 5% loss by mass after subjected to traffic. As anticipated, observation of SFC specimens with grout Mix A (with the lowest strength of 14 MPa) showed significant edge defects and cracks associated with the highest weight loss (7.5%) after a short length of time subjected to simulated trafficking (650 wheel passes). This poor performance confirmed the suggestion in BS EN 13877-2: 2013 (British Standards, 2013h) that low strength concrete with compressive strengths less than 20 MPa should not be used for concrete pavements.

After simulated traffic wear, SFC pavements were found to exhibit mean texture depths (0.9-1.2 mm) in compliance with the minimum MTD of 0.6 and 0.8 mm required for concrete carriageways and surface dressed hot rolled asphalt (Department for Transport, 2010). Not surprisingly, these values were lower than high friction surfacing comprising buff calcined bauxite (Highways England, 2006b; Wilkinson, 2017), indicating the unsuitability of SFC for use as high friction pavements.

In terms of skid resistance, except for SFC-Mix A and B, SFC pavements achieved SRVs exceeding the minimum of 55 required for areas with traffic of less than 2000 vehicles per day (Impact Test Equipment, 2020). SRVs for SFC pavements undoubtedly fell short of the minimum of 65 required for high friction surface established by British Board of Agrement, (2017), confirming the impracticability of using SFC with RAP chippings as a high friction surface. SFC pavements also demonstrated promising friction performance with minor SRV loss (less than 4%) during traffic wear in dry conditions, suggesting its potential use in dry areas such as internal industrial floors. External areas are not recommended for SFC surface courses owing to its poor performance with significant SRV loss in wet conditions (over 20%).

Close-range photogrammetry techniques were found to provide valuable information on surface texture changes of SFC pavements under simulated trafficking loads. Recorded high

roughness (Sa), negative skewness (Ssk) and adequate kurtosis values (Sku) showed noticeable changes in surface texture of SFC after traffic wear. SFC surface courses were found to be less durable under traffic wear compared to asphalt concrete with more consistent values of Sa, Ssk and Sku (McQuaid, 2015). Further investigation is recommended to study long-lasting impacts that trafficking load have on SFC surface courses.

8.7 Research objective 6 - Provide recommendations for possible improvement for further research on SFC materials.

As reported in Chapter 2, the long-term availability of common aluminosilicate precursors such as FA remains a challenge to widespread application of geopolymer materials. In a report by the Department of Energy and Climate Change (2017), a critical shortage of FA is forecasted to be approximately 2 million tonnes in the UK in 2030 due to reduction of power plants. This highlights the needs for research into replacing FA with environmentally compatible materials with long-term availability. Residue fluid catalytic cracking (RFCC) is solid waste from the oil refining industry containing over 90% by mass silica and alumina (Tashima et al., 2012). It was reported to possess high reactive aluminosilicate to be used in cementitious and geopolymer materials. Current research into geopolymer consisting of RFCC for pavement applications is limited. As such, RFCC may provide an applicable alternative to fly ash in geopolymer materials in oil-generating countries where the supply of FA is limited (the UK in this case).

As presented in Chapter 6, commercial sodium silicate activator was responsible for the majority of total raw material costs (57%) and greenhouse gas emissions (60%) due to its manufacturing process involving the incineration of soda ash and SiO_2 at high temperature (approximately 1000^{o}C) (European Chemical Industrial Council, 2014). Negative economic and environmental impacts of sodium silicate activator are among challenges to wide-scale implementation of geopolymer materials. Even though infusion of RAP mixtures with geopolymer grouts in SFC pavements was found to reduce total material costs and greenhouse gas emissions compared to traditional cementitious materials, further work needs to be carried out to develop innovative alternative materials to commercial alkaline activators. Sodium silicate activator made from rice husk ash was considered to replace commercial sodium silicate activator to reduce its cost and embodied carbon in several studies (Foletto et al., 2006; Tong et al., 2018). Rice husk ash is a by-product from the incineration process of rice husk to generate heating energy and electricity for residential and industrial uses in rice-growing countries such as Vietnam, Thailand, Cambodia, China

and India. Rice husk ash with a rich source of amorphous silica (approximately 90% by mass) can be mixed with sodium hydroxide at a temperature of 80°C to produce sodium silicate solution (Tong et al., 2018). In this context, SFC material comprising rice husk ash-based sodium silicate solution and RFCC (as shown in Figure 8.3) is expected to offer economic and environmental benefits compared to SFC materials comprising commercial sodium silicate activator as presented in this thesis.

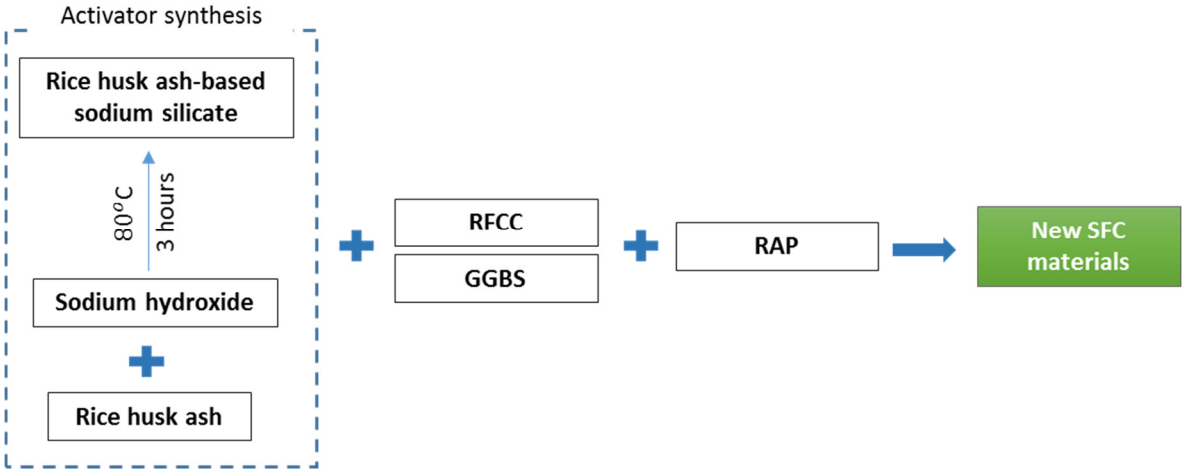

Figure 8.3. Schematic illustration of production process of the new SFC materials comprising rice husk ash based sodium silica and RFCC.

CHAPTER 9

CONCLUSIONS

9.1 Introduction

This chapter aims to respond to the six research questions stated in Chapter 1 based on key findings drawn from the previous chapters. Research contributions, implications and limitations in the field of infrastructure construction are also discussed in later sections.

9.2 Research question 1 - What are the roles of geopolymer grout and RAP in conventional asphalt and concrete pavements?

As stated in the literature review chapter, RAP has been used as a partial or full replacement of natural aggregates in pavement applications such as base and sub-base courses, with stabilisation by cement-based or geopolymer mixtures. Case studies involving a section of the M25 motorway and trunk roads A40 and A1 in the UK showed that up to 50% RAP by mass could be used to blend with natural coarse aggregates in hot mix asphalt surface courses. Efforts to investigate the use of 100% RAP as aggregate in cold asphalt mixture were limited in the existing literature.

To reduce carbon footprints relative to conventional Portland cement-based materials, geopolymer concrete has been used as surfacing materials for airport runways, cycle tracks and footpath, stabilising materials for base course, road repair material and artificial aggregates for surface courses. However, widespread application of geopolymer materials in pavement applications is still hindered by the lack of applicable standards, inconsistent reactivity of precursors, insufficient knowledge of long-term performance and the availability of constituent materials.

Semi-flexible composite pavements comprising RAP and geopolymer grouts have not been comprehensively addressed to date in previously published studies. Instead, cement-based grouts and open-graded asphalt layers are the primary materials currently used for SFC pavements in heavy-duty applications.

9.3 Research question 2 - How do fresh and mechanical properties of geopolymer grout mixes vary regarding the type and composition of their raw materials?

Fresh and mechanical properties of geopolymer grout mixes varied widely depending on the type and composition of their raw materials including GGBS, FA, MK and SF. From 24 geopolymer mixes with different binder combinations and liquid-to-solid ratios (0.27-0.52) produced in this study, the property ranges of fresh and hardened grouts obtained were as follows:

- Flowability: 9-841 s
- Initial/Final setting time: 13-450 mins / 30-840 mins

- 28-day compressive strength: 19-108 MPa

Both binder contents and liquid-to-solid ratio parameters had significant impacts on compressive strength and workability of geopolymer grouts. For mixes with GGBS+FA combinations, high GGBS content (over 80% by mass of binder) resulted in low flowability, quick setting and high compressive strength. Mixes with high FA content (80% by mass of binder) exhibited very slow setting times (800 mins), with several specimens failing to completely harden at ambient temperatures. The inclusion of MK and SF as 20% by mass of binder in GGBS+FA mixes offered improvements in flowability and compressive strengths, as well as prolonged setting times.

9.4 Research question 3 - What is the most suitable application for SFC materials in pavement structures in terms of mechanical properties?

Laboratory assessments of SFC materials with various geopolymer grout types and RAP mixtures with solid contents ranging from 45-62% by volume showed its potential suitability for pavement base courses. This conclusion was drawn from the fact that the SFC material compressive strength range achieved (9-32 MPa) conformed to the general requirement of minimum strength (8 MPa) for base course stated in DMRB, volume 7, section 2 (Highways England, 2006a). Since heavy-duty pavements are considered the most common applications of SFC materials (Densit, 2018b; Plug et al., 2006), examples of SFC serving as a base course of heavy-duty pavements for industrial hardstanding were carried out in this study. Results showed that SFC materials consisting of grout mixes B, C, D and RAP solids content of less than 49% by volume are promising replacements of traditional base course made of CGBM $C_{8/10}$.

In addition to materials for base course, SFC materials showed encouraging compressive strength results that encompassed the strength range of 8-100 MPa for concrete pavements used in general traffic-bearing areas such as storage areas, cycleways and footpaths according to BS EN 13877-2:2013 (British Standards, 2013h). However, this standard also suggested a minimum strength of 20 MPa applied to concrete pavement to satisfy functional reasons. The strength of all SFC mixtures comprising grout Mix A fell short of this suggested minimum. This grout was thus not recommended for pavement surface courses. To produce viable material solutions for surface course, SFC materials consisting of RAP with solid content of less than 49% by volume and grout mixes B, C and D are recommended. Given that the findings were based on mechanical properties of SFC materials only, further research is required to investigate the use of SFC as surface courses in terms of trafficked-related performances.

9.5 Research question 4 - How effective is SFC pavement at improving environmental and economic benefits compared to traditional heavy-duty pavement?

Analyses of raw material costs and greenhouse gas emissions were carried out on the SFC material base courses considered for a heavy-duty pavement application. Costs and emissions related to construction operations such as labour, transportation, power and water were neglected. Total raw material costs and greenhouse gas emission per m^2 of SFC pavement were compared to a traditional base course in heavy-duty paving consisting of 360 mm CBGM $C_{8/10}$ (British In-Situ Concrete Paving Association, 2007).

Results showed that the production of 1 m^2 of the investigated SFC base courses cost up to 49% less and emitted significantly lower (about two times) greenhouse gas emissions compared to traditional CBGM. This highlighted favourable performances of SFC base course in terms of economic and environmental impacts, indicating their viability as an alternative to conventional CBGM in heavy-duty pavements.

9.6 Research question 5 - How do SFC pavements perform when subjected to simulated trafficking?

To select suitable surface finishes, skid resistance of SFC specimens with both surface dressing and exposed-aggregate finishes were initially assessed using pendulum test method. SRV results obtained in dry and wet conditions (90 and 76 respectively) showed that surface dressing was the most effective finish for SFC pavements. Based on this observation, further testing of weight loss, MTD, SRV and surface texture changes were undertaken on SFC specimens comprising four different types of geopolymer grout and 45% RAP solids by volume with surface dressing finish. MTD and SRV of SFC pavements subjected to traffic wear using accelerated road testing were compared to minimum values required for conventional pavements and high friction systems established by codes and standards (British Board of Agrement, 2017; Department for Transport, 2010; Impact Test Equipment, 2020). Results recorded after traffic wear showed that SFC specimen SRV and MTD values exceeded minimum values required for non-critical pavement areas made of concrete and hot rolled asphalt stated in the New Roads and Street Works Act 1991 (Department for Transport, 2010) and roads with traffic less than 2000 vehicles per day as stated in pendulum skid resistance tester guideline (Impact Test Equipment) respectively. However, SFC pavements exhibited lower SRV than the minimum value of 65 required for high friction courses (British Board of Agrement, 2017). These observations indicated that SFC materials could potentially be used in surface courses of non-critical areas with low-volume traffic where high friction property is not required.

9.7 Research question 6 - What are the most effective RAP contents and geopolymer grout types to optimise SFC pavement performance?

In the case of base courses, all SFC mixtures considered were found to be promising alternatives to conventional CBGM in heavy-duty pavements. SFC consisting of grout Mix B exhibited the highest compressive strength at the maximum RAP solids content of 62% by volume, compared to the remaining grouts with the same RAP content. This observation was reinforced by its advantage regarding low production cost (£29/m^2) and greenhouse gas emission (36.7 kg CO_2e) compared to other SFC mixtures.

Among the four geopolymer grout mixes with contrasting properties, all but one considered for SFC materials yielded viable as a surfacing material solution. The use of grout mix A was not practically possible because the corresponding SFC materials exhibited low compressive strength (less than 14 MPa) and serious durability problems related to worn-off chippings and segregation under simulated trafficking. Encouraging results associated with compressive strengths of SFC comprising 45% RAP solids by volume, highlighted its suitability as an alternative to traditional heavy-duty surface course for storage areas, cycleways and footpaths.

9.8 Research contribution

High demand for traditional construction materials such as Portland cement concrete, bitumen and natural aggregates results in significant quantities of carbon dioxide being emitted into the atmosphere through their manufacturing processes. This justifies the need for more sustainable alternatives made from industrial by-products and wastes with minimal embodied carbon in building and infrastructure construction sectors.

With lower carbon footprints and production costs compared to conventional cement-based materials, the semi-flexible composite materials proposed in this research are expected to help bring the construction industry into line with the Climate Change Act, with a carbon emission reduction target of 80% by 2050 (UK Public General Acts, 2008). The uses of RAP and geopolymer binders sourced from industrial by-products (i.e., FA, MK, SF and GGBS) in SFC materials help to offset the relatively high embodied carbon footprint of traditional construction materials. Despite being commonly recycled in infrastructure applications, RAP aggregate often requires high temperature and to be blended with natural aggregates prior to being used in pavement structures (Arulrajah et al., 2014; Fattah et al., 2017; Freire et al., 2013; Lavin, 2003). As such, infusion of 100% RAP aggregate with geopolymer grout at ambient temperature offers a novel type of waste-

based material with a less energy intensive production method that contributes to making the construction industry more sustainable.

By using experimental and computer vision techniques, this research provides fresh insight into the performance of pavements made from SFC materials subjected to different loading types (e.g., compression and simulated accelerated trafficking). The Deep Neural Network machine learning approach was also employed as an effective tool to precisely predict SFC mechanical behaviours based on various input parameters such as geopolymer properties and RAP content. These subjects have been relatively under-studied within the existing literature. For academic researchers, this study is expected to contribute significantly to the establishment of a conceptual framework for implementation of innovative semi-flexible composite materials in the construction sector which has been suffering from the lack of applicable standards and guidelines.

9.9 Research limitations

The proposed SFC materials showed promising performance in terms of physical and mechanical properties as well as economic and environmental benefits and contribute to the delivery of environmentally responsible infrastructure systems. This research, however, suffered from the following limitations:

- Although results obtained showed meaningful rapid performance predictions of SFC elastic modulus based on UPV and compressive strength, mechanical tests such as indirect tensile stiffness modulus are suggested for further research to directly assess SFC elastic modulus and improve the reliability of the proposed methods.
- It is acknowledged that the costs of raw materials and greenhouse gas emission analyses are restricted to SFC production phases. Other factors such as transportation and operations may have effects on the final costs and emissions of SFC.
- Frictional properties obtained from exposing SFC surface course to simulated trafficking of 10,000 wheel-passes remains appropriate for assessing trafficking related properties of SFC as surfacing materials in non-critical areas (traffic less than 2000 vehicles per day). However, exposing SFC surface course to simulated trafficking with higher numbers of wheel-passes is needed to obtain a full understanding of the long-term performance of SFC as surfacing materials.
- All research undertaken in this research was limited to laboratory-scale experiments. As such, field-based demonstration testing is needed to provide a

more comprehensive understanding of the practical behaviour of SFC pavements under real-life trafficking conditions

CHAPTER 10

FUTURE RECOMMENDATIONS

This thesis developed semi-flexible composite materials comprising geopolymer grouts and reclaimed asphalt planing aggregates for sustainable pavement materials. Based on results obtained from experimental and computational methods, the following research directions for further works are recommended:

- An improvement over the current research by developing geopolymer grout comprising rice husk ash-based activator to reduce the cost and environmental impacts of commercial sodium silicate activator. This work can then be applied not only for SFC materials in pavements but also for ground stabilisation and building materials. It is also expected to solve environmental issues associated with rice husk ash disposal in landfills as well as contribute to the market acceptance of agricultural wastes for rice farmers in rice-growing countries such as Vietnam, India, Cambodia and China.
- The use of residue fluid catalytic cracking as an alternative for fly ash is suggested for further work. This work could reduce issues associated with the anticipated shortcoming of fly ash in the coming years as well as oil refining waste disposal in landfills.
- The use of machine learning-assisted numerical analysis is recommended for further research to predict mechanical and traffic-related properties of SFC materials as well as develop their optimised mix designs.
- Long-lasting impact of traffic on SFC surface is suggested for upcoming research using road test machine and close-range photogrammetry method.

REFERENCES

A.M. Mustafa Al Bakri, Kamarudin, H., Bnhussain, M., Nizar, I.K., Mastura, W.I.W., 2013. Mechanism and Chemical Reaction of Fly Ash Geopolymer Cement- A Review. J. Chem. Inf. Model. 53, 1689–1699.

Afonso, M.L., Dinis-Almeida, M., Pereira-De-Oliveira, L.A., Castro-Gomes, J., Zoorob, S.E., 2016. Development of a semi-flexible heavy duty pavement surfacing incorporating recycled and waste aggregates - Preliminary study. Constr. Build. Mater. 102, 155–161.

Ahammed, M.A., Tighe, S.L., 2012. Asphalt pavements surface texture and skid resistance - Exploring the reality. Can. J. Civ. Eng. 39, 1–9.

Al-Majidi, M.H., Lampropoulos, A., Cundy, A., Meikle, S., 2016. Development of geopolymer mortar under ambient temperature for in situ applications. Constr. Build. Mater. 120, 198–211.

Al-Mufti, R., Fried, A., 2018. Non-destructive evaluation of reclaimed asphalt cement concrete. Eur. J. Environ. Civ. Eng. 8189, 0.

Alam, T.B., Abdelrahman, M., Schram, S.A., 2010. Laboratory characterisation of recycled asphalt pavement as a base layer. Int. J. Pavement Eng. 11, 123–131.

Aliabdo, A.A., Abd Elmoaty, A.E.M., Mohamed, M.F., 2018. Permeability indices and corrosion resistance of geopolymer and Portland cement concretes. Mag. Concr. Res. 70, 595–609.

An, J., Nam, B.., Youn, H., 2016. Investigation on the Effect of Recycled Asphalt Shingle (RAS) in Portland Cement Mortar. Sustainability 8, 384.

Anderton, G.L., 2000. Engineering properties of resin modified pavement (RMP) for mechanistic design.

Arulrajah, A., Piratheepan, J., Disfani, M.M., 2014. Reclaimed asphalt pavement and recycled concrete aggregate blends in pavement subbases : laboratory and field evaluation. J. Mater. Civ. Eng. 26, 349–357.

Assi, L.N., 2017. Cost and Fuel Usage Optimization of Activating Solution Based Silica Fume Geopolymer Concrete. University of South Carolina.

ASTM, 1997. Standard Test Method for Density, Absorption, and Voids in Hardened Concrete, ASTM International. ASTM C642-97.

ASTM, 2010. Standard test method for flow of grout for preplaced-aggregate concrete (flow cone method). ASTM Int.

ASTM, 2012. Standard Test Method for Electrical Indication of Concrete's Ability to Resist Chloride Ion Penetration, ASTM International. ASTM C1202-12.

Australian Asphalt Pavement Association, 1997. Open Graded Asphalt: Design Guide.

Azadi, M.R., Taghichian, A., Taheri, A., 2017. Optimization of cement-based grouts using chemical additives. J. Rock Mech. Geotech. Eng. 9, 623–637.

Azarsa, P., Gupta, R., 2020. Freeze-Thaw Performance Characterization and Leachability of Potassium-Based Geopolymer Concrete. J. Compos. Sci. 4, 45.

Bateman, D., 2016. Road Note 39: Design Guide for Road Surface Dressing. Transp. Res. Lab.

Bitelli, G., Simone, A., Girardi, F., Lantieri, C., 2012. Laser Scanning on Road Pavements: A New Approach for Characterizing Surface Texture. Sensors 12, 9110–9128.

Blades, N., Marchant, G., Greening, P., 2006. Impacts of crushed rock quarries on historic villages and cultural landscapes. In: Proceedings of Safeguarded Cultural Heritage - Understanding and Viability for the Enlarged Europe.

Bondar, D., 2009. Alkali activation of Iranian natural Pozzolans for Producing geopolymer cement and concrete. PhD thesis. University of Sheffield.

Bonicelli, A., Preciado, J., Rueda, A., Duarte, A., 2019. Semi-Flexible Material: A Solution for High-Performance Pavement Infrastructures. In: IOP Conference Series: Materials Science and Engineering. IOP Publishing.

Boundy, R., 1979. Development of a Resin/Cement grouted coated Macadam Surfacing Material. University of Nottingham.

British Board of Agrement, 2017. Guidelines document for the assessment and certification of high-friction surfacing for highways.

British Geological Survey, 2019. Mineral Planning Factsheet: Construction aggregates.

British In-Situ Concrete Paving Association, 2007. HBM and Stabilisation: The design and specification of Heavy-duty Paving.

British Standard, 2013. Road and airfield surface characteristics — Test methods Part 4 : Method for measurement of slip / skid resistance of a surface : The pendulum test.

British standards, 1999. Methods of test for mortar for masonry - Part 11: determination of flexural and compressive strength of hardened mortar. Br. Stand.

British Standards, 1990a. Testing aggregates - Part 109: Methods for determination of moisture content.

British Standards, 1990b. Testing aggregates-Part 112: Methods for determination of aggregate impact value (AIV).

British Standards, 1992. Specification for aggregates from natural sources for concrete.

British Standards, 1998. Tests for mechanical and physical properties of aggregates-Part 3: Determination of loose bulk density and voids.

British Standards, 2002. Aggregates for bituminous mixtures and surface treatments for roads, airfields and other trafficked areas.

British Standards, 2004. Testing concrete. Determination of ultrasonic pulse velocity. Br. Stand.

British Standards, 2006. Admixtures for concrete, mortar and grout. Test methods. Part 2: Determination of setting time.

British Standards, 2009. Testing hardened concrete - Part 6: Tensile splitting strength of test specimens.

British Standards, 2010. Road and airfield surface characteristics. Test methods. Measurement of pavement surface macrotexture depth using a volumetric patch technique.

British Standards, 2012a. Tests for geometrical properties of aggregates-Part 1: Determination of particle size distribution — Sieving method.

British Standards, 2012b. BSI Standards Publication Bituminous mixtures — Test methods for hot mix asphalt Part 1 : Soluble binder content.

British Standards, 2012c. Fly ash for concrete Part 1 : Definition , specifications and conformity criteria.

British Standards, 2013a. Concrete — Specification , performance , production and conformity. BS EN 206-2013 A1.

British Standards, 2013b. Tests for mechanical and physical properties of aggregates-Part 6: Determination of particle density and water absorption.

British Standards, 2013c. Bituminous mixtures - Test methods for hot mix asphalt - Part 33: Specimen prepared by roller compactor Mélanges.

British Standards, 2013d. Testing concrete — Part 125 : Methods for mixing and sampling fresh concrete in the laboratory. Br. Stand.

British Standards, 2013e. Hydraulically bound mixtures — Specifications. Part 1: Cement bound granular mixtures.

British Standards, 2013f. Hydraulically bound mixtures — Specifications. Part 2: Slag bound granular mixtures.

British Standards, 2013g. Hydraulically bound mixtures — Specifications. Part 3: Fly ash bound granular mixtures.

British Standards, 2013h. Concrete pavements - Part 2 : Functional requirements for concrete pavements.

British Standards, 2014. Eurocode 2: Design of concrete structures —Part 1-1: General rules and rules for buildings. Br. Stand.

British Standards, 2016. Bituminous mixtures — Material specifications Part 8 : Reclaimed asphalt.

British Standards, 2018a. Bituminous mixtures. Test methods. Stiffness.

British Standards, 2018b. Bituminous mixtures – Test methods – Part 31: Specimen preparation by gyratory compactor.

British Standards, 2019a. Testing hardened concrete - Part 3: Compressive strength of test specimens.

British Standards, 2019b. Hydraulically bound materials for civil engineering purposes – Specification for production and installation in pavements. BS 9227:2019.

Byrne, D.A., 2005. Recycling of Asphalt Pavements Bituminous Mixes. PhD thesis. Napier University.

Cai, X., Huang, W., Wu, K., 2019. Study of the self-healing performance of semi-flexible pavement materials grouted with engineered cementitious composites mortar based on a non-standard test. Materials (Basel). 12.

Carswell, I., Nicholls, J.C., Widyatmoko, I., Harris, J., Taylor, R., 2011. Best Practice Guide for Recycling Into Surface Courses, Transport research laboratory.

Chandler, J.W.E., Phillips, S.M., Roe, P.G., Viner, H.E., 2003. Quieter concrete roads:

construction, texture, skid resistance and noise. Transp. Res. Lab.

Chesner, W., Collins, R., MacKay, M., Emery, J., 2017. User Guidelines for Waste and Byproduct Materials in Pavement Construction.

Ciambrone, D.F., 1997. Environmental life cycle analysis. CRC Press LLC, Florida, USA.

Cihackova, P., Hyzl, P., Stehlik, D., Dasek, O., Šernas, O., Vaitkus, A., 2015. Spetsiaalse tsementmördiga täidetud dreenasfaltbetooni toimivuskarakteristikud. Balt. J. Road Bridg. Eng. 10, 316–324.

Climatechange Statistic, 2019. UK Government GHG Conversion Factors for Company Reporting.

Collins, F., Sanjayan, J.G., 2000. Effect of pore size distribution on drying shrinkage of alkali-activated slag concrete. Cem. Concr. Res. 30, 1401–1406.

Collop, A., Elliott, R., 1999. Assessing the mechanical performance of Densiphalt. In: 3rd European Symposium on the Performance and Durability of Bituminous Materials and Hydraulic Stabilised Composites. Leeds, UK, pp. 343–357.

Comite Euro-International Du Beton, 1993. CEB-FIB Model code 1990: Design code. CEB-FIP MODEL CODE 1990.

Concrete Institute of Australia, 2011. Recommended Practice: Geopolymer concrete.

Copeland, A., 2011. Reclaimed Asphalt Pavement in Asphalt Mixtures: State of the Practice, Federal Highway Administration.

Cristelo, N., Soares, E., Rosa, I., Miranda, T., Oliveira, D. V., Silva, R.A., Chaves, A., 2013. Rheological properties of alkaline activated fly ash used in jet grouting applications. Constr. Build. Mater. 48, 925–933.

Dao, D. Van, Trinh, S.H., Ly, H.B., Pham, B.T., 2019. Prediction of compressive strength of geopolymer concrete using entirely steel slag aggregates: Novel hybrid artificial intelligence approaches. Appl. Sci. 9, 1–16.

Davidovits, J., 1994. Properties of Geopolymer Cements. In: First International Conference on Alkaline Cements and Concretes. Geopolymer Institute, Kiev, Ukraine, pp. 131–149.

Davidovits, J., 2016. State of the Geopolymer R&D 2016. In: Geopolymer Camp. Geopolymer Institute.

Davidovits, J., 2018. Geopolymer concrete: Why did it take so long? In: Geopolymer Camp. Geopolymer Institute, France.

Densit, 2018a. DENSIPHALT - a new generation of joint-free pavements.

Densit, 2018b. Technical data sheet: Densiphalt-Semi flexible and joint free topping where durability and wear resistance are high priorities.

Department for Transport, 2010. New Roads and Street Works Act 1991 : Specification for the reinstatement of openings in highways.

Department of Energy and Climate Change, 2015. UK progress towards GHG emissions reduction targets.

Department of Energy and Climate Change, 2017. Fly ash and blast furnace slag for cement manufacturing. BEIS Res. Pap. no. 19.

Design and Maintenance Guide, 2011. A guide to airfield pavement design and evaluation, 3rd ed, Design and Maintenance Guide 27. Crown.

Diaz-Loya, E.I., Allouche, E.N., Vaidya, S., 2011. Mechanical properties of Fly ash-based geopolymer concrete. ACI Mater. J. 108, 300–306.

Diaz, E.I., Allouche, E.N., Eklund, S., 2010. Factors affecting the suitability of fly ash as source material for geopolymers. Fuel 89, 992–996.

Duran Atiş, C., Bilim, C., Çelik, Ö., Karahan, O., 2009. Influence of activator on the strength and drying shrinkage of alkali-activated slag mortar. Constr. Build. Mater. 23, 548–555.

Dutta, D., Thokchom, S., Ghosh, P., Ghosh, S., 2010. Effect of silica fume additions on porosity of fly ash geopolymers. ARPN J. Eng. Appl. Sci. 5, 74–79.

European aggregates association, 2018. EUPG annual review 2017-2018. Union Eur. des Prod. Granulats.

European Asphalt Pavement Association, 2018. Asphalt in Figures 2018. EAPA.

European Chemical Industrial Council, 2014. Soluble Silicates: Chemical, toxicological, ecological and legal aspects of production, transport, handling and application. Brussels, Belgium.

Farfan, J., Fasihi, M., Breyer, C., 2019. Trends in the global cement industry and opportunities for long-term sustainable CCU potential for Power-to-X. J. Clean. Prod. 217, 821–835.

Fattah, M.Y., Qasim, Z.I., Zuhier, Y.A., 2017. Impact of reclaimed asphalt pavement (RAP) on properties of asphalt mixture for surface layer. Glob. J. Eng. Sci. Res. Manag. 4, 161–170.

Favier, A., Hot, J., Habert, G., Roussel, N., D'Espinose De Lacaillerie, J.B., 2014. Flow properties of MK-based geopolymer pastes. A comparative study with standard Portland cement pastes. Soft Matter 10, 1134–1141.

Fitzpatrick-Schmidt, K., Horsley, C., Tsaknopoulos, D., Zhang, Y., 2015. Geopolymer - The Green Cement. BSc Thesis. Worcester Polytechnic Institute.

Foletto, E.L., Gratieri, E., de Oliveira, L.H., Jahn, S.L., 2006. Conversion of rice hull ash into soluble sodium silicate. Mater. Res. 9, 335–338.

Freire, A.C., Neves, J., Roque, A., Martins, I., Antunes, M., Faria, G., 2013. Use of construction and demolition recycled materials (C & DRM) in road pavements validated on experimental test sections. In: WASTES: Solutions, Treatments and Opportunities. Braga, Portugal.

Garcia-Lodeiro, I., Palomo, A., Fernández-Jiménez, A., 2015. An overview of the chemistry of alkali-activated cement-based binders. In: Handbook of Alkali-Activated Cements, Mortars and Concretes. Woodhead Publishing, pp. 19–47.

Gibson, S., 2011. Reducing the Embodied Carbon Content of Asphalt. University of Strathclyde.

Glasby, T., Day, J., Genrich, R., Aldred, J., 2015. EFC geopolymer concrete aircraft pavements at Brisbane West Wellcamp Airport. In: Concrete 2015 Conference, Melbourne Australia 2015. Wagners, Melbourne, Australia.

Goodfellow, I., Bengio, Y., Courville, A., 2016. Deep Learning, MIT Press, Massachusetts, United States.

Görhan, G., Aslaner, R., Şinik, O., 2016. The effect of curing on the properties of metakaolin and fly ash-based geopolymer paste. Compos. Part B Eng. 97, 329–335.

Güllü, H., Cevik, A., Al-Ezzi, K.M.A., Gülsan, M.E., 2019. On the rheology of using geopolymer for grouting: A comparative study with cement-based grout included fly ash and cold bonded fly ash. Constr. Build. Mater. 196, 594–610.

Gunasekara, C.M., 2016. Influence of Properties of Fly Ash From Different Sources on the Mix Design and Performance of Geopolymer Concrete. RMIT University.

Hadi, M.N.S., Farhan, N.A., Sheikh, M.N., 2017. Design of geopolymer concrete with GGBFS at ambient curing condition using Taguchi method. Constr. Build. Mater. 140, 424–431.

Hardicrete, 2019. Hardicrete Heavy Duty Surfacing.

Hardjito, D., Rangan, B. V, 2005. Development and properties of low-calcium fly ash-based geopolymer concrete. Perth, Australia.

Heneash, U., 2013. Effect of the Repeated Recycling on Hot Mix Asphalt Properties. The University Nottingham.

Hicks, L., 2008. Aggregates supply in England: Issues for planning.

Higgins, D., 2006. Sustainable concrete: How can additions contribute. In: The Institute of Concrete Technology: Annual Technical Symposium. Cementitious Slag Makers Association.

Highways England, 1999. Volume 7: Pavement design and Maintenance - Section 5: Pavement design and construction - Part 2: Bituminous surfacing materials and techniques (HD 37/99).

Highways England, 2006a. Volume 7: Pavement design and Maintenance - Section 2: Pavement design and construction - Part 3: Pavement design (HD 26/06).

Highways England, 2006b. Volume 7: Pavement design and Maintenance - Section 5: Pavement design and construction - Part 1: Surfacing materials for new and maintenance construction (HD 36/06).

Highways England, 2016. Volume 7: Pavement design and maintenance - Section 5: Surfacing and surfacing materials (HD38/16).

Highways England, 2020. CD 236: Surface course materials for construction.

Hobart Equipment, 2009. A200 mixer technical manual (ML-104858).

Horpibulsuk, S., Hoy, M., Witchayaphong, P., Rachan, R., Arulrajah, A., 2017. Recycled asphalt pavement - fly ash geopolymer as a sustainable stabilized pavement material. IOP Conf. Ser. Mater. Sci. Eng. 273.

Hossiney, N., Wang, G., Tia, M., Bergin, M., 2008. Evaluation of concrete containing reclaimed asphalt pavements for use in concrete pavement. In: 2008 TRB Annual Meeting CD-ROM. Transportation Research Record.

Hou, S., Xu, T., Huang, K., 2016. Investigation into engineering properties and strength mechanism of grouted macadam composite materials. Int. J. Pavement Eng. 17, 878–886.

Hoy, M., Horpibulsuk, S., Arulrajah, A., Mohajerani, A., 2018. Strength and microstructural study of recycled asphalt pavement: Slag geopolymer as a pavement base material. J. Mater. Civ. Eng. 30.

Hoyos, L.R., Puppala, A.J., Ordonez, C.A., 2011. Characterization of cement-fiber-treated reclaimed asphalt pavement aggregates: preliminary investigation. J. Mater. Civ. Eng. 23, 977–989.

Huang, B., Shu, X., Burdette, E.G., 2006. Mechanical properties of concrete containing recycled asphalt pavements. Mag. Concr. Res. 58, 313–320.

Huang, B., Shu, X., Li, G., 2005. Laboratory investigation of portland cement concrete containing recycled asphalt pavements. Cem. Concr. Res. 35, 2008–2013.

Hugener, M., Partl, M.N., Morant, M., 2014. Cold asphalt recycling with 100% reclaimed asphalt pavement and vegetable oil-based rejuvenators. Road Mater. Pavement Des. 15, 239–258.

Husain, N.M., Mahmud, H.B., Karim, M.R., Hamid, N.B.A.A., 2010. Effects of aggregate gradations on properties of grouted Macadam composite pavement. In: 2010 2nd International Conference on Chemical, Biological and Environmental Engineering, Proceedings. pp. 128–131.

Huseien, G.F., Mirza, J., Ismail, M., Ghoshal, S.K., Ariffin, M.A.M., 2016. Effect of metakaolin replaced granulated blast furnace slag on fresh and early strength properties of geopolymer mortar. Ain Shams Eng. J. 9, 1557–1566.

Huynh, A.T., Magee, B., Woodward, D., 2020a. A preliminary characterisation of innovative semi-flexible composite pavement comprising geopolymer grout and reclaimed asphalt planings. Materials (Basel). 13.

Huynh, A.T., Nguyen, Q.D., Xuan, Q.L., Magee, B., Chung, T., Tran, K.T., Nguyen, K.T., 2020b. A Machine Learning-Assisted Numerical Predictor for Compressive Strength of Geopolymer Concrete Based on Experimental Data and Sensitivity Analysis. Appl. Sci. 10, 1–16.

Idrissi, A.C. El, Roziere, E., Loukili, A., Darson, S., 2018. Design of geopolymer grouts: the effects of water content and mineral precursor. Eur. J. Environ. Civ. Eng. 22, 628–649.

Impact Test Equipment, n.d. Skid Tester: AG190 - User Guide, http://www.impact-test.co.uk/docs/AG190_HB.pdf, (accessed on 06/11/2020).

Indian Standards, 1996. Non-destructive testing of concrete - Part 1: Ultrasonic pulse velocity. IS 13311.

Ioannidou, D., Meylan, G., Sonnemann, G., Habert, G., 2017. Is gravel becoming scarce? Evaluating the local criticality of construction aggregates. Resour. Conserv. Recycl. 25–33.

Ismail, M., Muhammad, B., Yatim, J.M., Noruzman, A.H., Soon, Y.W., 2011. Behavior of concrete with polymer additive at fresh and hardened states. Procedia Eng. 14, 2230–2237.

ISO, 2016. Geometrical product specifications (GPS) — Surface texture: Areal — Part 1: Indication of surface texture.

JEOL Ltd, 2017. Scanning electron microscope: JSM-IT500 Series.

Jithendra, C., Elavenil, S., 2020. Effects of Silica Fume on Workability and Compressive

Strength Properties of Aluminosilicate Based Flowable Geopolymer Mortar under Ambient Curing. Silicon 12, 1965–1974.

Kalaiyarrasi, A.R.R., Partheeban, P., 2016. Influence of Si/Al ratio on the compressive strength of metakaolin based geopolymers. Int. J. Earth Sci. Eng. 9, 87–91.

Khater, H.M., 2013. Effect of silica fume on the characterization of the geopolymer materials. Int. J. Adv. Struct. Eng. 5, 1–10.

Knapton, J., 2008. Heavy duty pavements: The structural design of heavy duty pavements for ports and other industries. Interpave.

Kogbara, R.B., Masad, E.A., Anupam, K., Scarpas, A., 2018. Griptester measurements and texture-friction relationship. In: Advances in Materials and Pavement Performance Prediction - Proceedings of the International AM3P Conference, 2018. Doha, Qatar, pp. 287–291.

Kore, S.D., Vyas, A.K., 2016. Impact of marble waste as coarse aggregate on properties of lean cement concrete. Case Stud. Constr. Mater. 4, 85–92.

Koting, S., Karim, M.R., Mahmud, H., 2007. The Properties of Bituminous Mixtures for Semi-Flexible Pavement. In: Proceedings of the Eastern Asia Society for Transportation Studies.

Kowalski, K.J., Król, J., Radziszewski, P., Casado, R., Blanco, V., Pérez, D., Viñas, V.M., Brijsse, Y., Frosch, M., Le, D.M., Wayman, M., 2016. Eco-friendly materials for a new concept of asphalt pavement. Transp. Res. Procedia 14, 3582–3591.

Kumar, B.R., Rao, T.S., 2012. AFM studies on surface morphology, topolography and texture of nanostructured zinc aluminum oxide thin films. Dig. J. Nanomater. Biostructures 7, 1881–1889.

Lavin, P.G., 2003. Asphalt pavements: A practical guide to design, production, and maintenance for engineers and architects, Journal of Chemical Information and Modeling. Taylor and Francis Group.

Lee, B.J., Kee, S.H., Oh, T., Kim, Y.Y., 2015. Effect of Cylinder Size on the Modulus of Elasticity and Compressive Strength of Concrete from Static and Dynamic Tests. Adv. Mater. Sci. Eng. 2015.

Li, C., White, D.J., Vennapusa, P., 2015. Moisture-density-strength-energy relationships for gyratory compacted geomaterials. Geotech. Test. J. 38, 461–473.

Li, G., Zhao, Y., Pang, S., Huang, W., 1998. Experimental study of cement-asphalt emulsion composite. Cem. Concr. Res. 28, 635–641.

Li, Q., Wang, Z., Li, Y., Shang, J., 2018. Cold recycling of lime-fly ash stabilized macadam mixtures as pavement bases and subbases. Constr. Build. Mater. 169, 306–314.

Li, Z., Ding, Z., 2003. Property improvement of Portland cement by incorporating with metakaolin and slag. Cem. Concr. Res. 33, 579–584.

Ling, Y., Wang, K., Wang, X., Li, W., 2019. Prediction of engineering properties of fly ash-based geopolymer using artificial neural networks. Neural Comput. Appl. 3.

Lo Presti, D., Khan, R., Abdul Hassan, N., Airey, G., Collop, A., 2014. Laboratory mix design of asphalt mixture containing reclaimed material. Adv. Mater. Sci. Eng. 2014.

Luo, S., Yang, X., Zhong, K., Yin, J., 2018. Open-graded asphalt concrete grouted by latex

modified cement mortar. Road Mater. Pavement Des. 1–17.

Luukkonen, T., Abdollahnejad, Z., Yliniemi, J., Kinnunen, P., Illikainen, M., 2018. One-part alkali-activated materials: A review. Cem. Concr. Res. 103, 21–34.

Ma, C.K., Awang, A.Z., Omar, W., 2018. Structural and material performance of geopolymer concrete: A review. Constr. Build. Mater. 186, 90–102.

Ma, F., Sha, A., Yang, P., Huang, Y., 2016. The greenhouse gas emission from portland cement concrete pavement construction in China. Int. J. Environ. Res. Public Health 13.

Mallick, R.B., Bergendahl, J., 2009. A laboratory study on CO2 emission from asphalt binder and its reduction with the use of warm mix asphalt. Int. J. Sustain. Eng. 2, 275–283.

Manolis, S., 2017. Asphalt Extraction and Recovery Procedures An Introduction. In: OAPC Fall Seminar.

Martisius, N.L., Sidera, I., Grote, M.N., Steele, T.E., McPherron, S.P., Schulz-Kornas, E., 2018. Time wears on : Assessing how bone wears using 3D surface texture analysis. PLoS One 13.

MCHW Series 1000, 2020. Volume 1: Specification for Highway Works Series 1000 Road Pavements - Concrete.

MCHW Series 800, 2016. Volume 1: Specification for Highway Works - Series 800: Road Pavements - Unbound, cement and other hydraulically bound mixture.

MCHW Series 900, 2019. Volume 1: Specification for Highway Works - Series 900: Road Pavements - Bituminous Bound Materials.

McLellan, B.C., Williams, R.P., Lay, J., Van Riessen, A., Corder, G.D., 2011. Costs and carbon emissions for geopolymer pastes in comparison to ordinary portland cement. J. Clean. Prod. 19, 1080–1090.

McQuaid, G., 2015. Development of non-contact 3D measurement of areal pavement texture parameters. Ulster University.

McQuaid, G., Millar, P., Woodward, D., 2015. Use of 3d modeling to assess pothole growth. In: Bituminous Mixtures and Pavements VI - Proceedings of the 6th International Conference on Bituminous Mixtures and Pavements. Taylor and Francis Group, London, pp. 161–166.

Michigan Metrology, 2014. Michigan Metrology Surface Texture Parameters Glossary.

Mineral Products Association, 2011. MPA Cement: Sustainable Development Report 2011.

Mineral Products Association, 2018a. Profile of the UK Mineral Products Industry.

Mineral Products Association, 2018b. Mineral Products Association Sustainable Development Report 2014.

Mishra, B., 2015. A Study on Use of Reclaimed Asphalt Pavement (RAP) Materials in Flexible Pavements. Int. J. Innov. Res. Sci. Eng. Technol. (An ISO Certif. Organ. 4, 12170–12177.

Mohammed, M.H., Pusch, R., Knutsson, S., Hellström, G., 2014. Rheological Properties of Cement-Based Grouts Determined by Different Techniques. Engineering 06, 217–229.

Nasht, I.H., Saeed, H.A., Sadoon, A.A., 2005. Finding an Unified Relationship between Crushing Strength of Concrete and Non-destructive Tests. In: 3rd MENDT - Middle

East Nondestructive Testing Conference & Exhibition. Bahrain, Manama.

Nath, P., Sarker, P.K., 2017. Flexural strength and elastic modulus of ambient-cured blended low-calcium fly ash geopolymer concrete. Constr. Build. Mater. 130, 22–31.

National Statistics, 2018. Monthly Statistics of Building Materials and Components. Dep. Bus. Energy Ind. Strateg.

National Statistics, 2019. 2019 UK greenhouse gas emissions, provisional figures. Dep. Bus. Energy Ind. Strateg.

Naylor, A., Talwalkar, S., Trail, I., Joyce, T., 2016. Evaluating the Surface Topography of Pyrolytic Carbon Finger Prostheses through Measurement of Various Roughness Parameters. J. Funct. Biomater. 7, 9.

Neupane, K., 2018. High-Strength Geopolymer Concrete- Properties, Advantages and Challenges. Adv. Mater. 7, 15.

Nguyen, K.T., Nguyen, Q.D., Le, T.A., Shin, J., Lee, K., 2020. Analyzing the compressive strength of green fly ash based geopolymer concrete using experiment and machine learning approaches. Constr. Build. Mater. 247.

Nicholls, J.C., 1997. Laboratory Tests on High-Fricion Surfaces for Highways, Transport Research Laboratory.

Nicholls, J.C., Carswell, I., Wayman, M., Reid, J.M., 2010. Increasing the environmental sustainability of asphalt.

Nmiri, A., Duc, M., Hamdi, N., Yazoghli-Marzouk, O., Srasra, E., 2019. Replacement of alkali silicate solution with silica fume in metakaolin-based geopolymers. Int. J. Miner. Metall. Mater. 26, 555–564.

North Whiteley Consortium, 2018. North Whiteley Business Case.

Nunn, M., 2004. Development of a more versatile approach to flexible and flexible composite pavement design. Berks, UK.

Nunn, M.E., Brown, A., Weston, D., Nicholls, J., 1997. Design of long-life flexible pavements for heavy traffic. Transp. Res. Lab.

O. Olubomehin, 2016. Development of the National Trunk Roads in Nigeria and the Socio-economic Impact , 1960 – 2013. Lagos Hist. Rev. 15.

Oakes, L., Wilkinson, A., Magee, B., 2019. Preliminary mix design procedure for alkali activated cement mortars based on metakaolin and industrial waste products activated with potasium silicate. In: Proceeding of the 42nd International Conference on Advanced Ceramics and Composites. pp. 209–223.

Ogundipe, O.M., 2020. Investigation into the use of Reclaimed asphalt pavement in asphalt concrete. In: Pasetto, M., Partl, M.N., Tebaldi, G. (Eds.), Proceedings of the 5th International Symposium on Asphalt Pavements & Environment. Springer, Switzerland, pp. 77–87.

Ojum, C., Thom, N., 2017. Effect of binder in recycled asphalt on cold-mix pavements. In: Proceedings of Institution of Civil Engineers: Construction Materials. Institute of Civil Engineers, pp. 205–210.

Okafor, F.O., 2010. Performance of Recycled Asphalt Pavement as Coarse Aggregate in Concrete. Leonardo Electron. J. Pract. Technol. 47–58.

Oliveira, J., 2006. Grouted macadam-Material characterisation for pavement design. University of Nottingham.

Omranian, S.R., Hamzah, M.O., Gungat, L., Teh, S.Y., 2018. Evaluation of asphalt mixture behavior incorporating warm mix additives and reclaimed asphalt pavement. J. Traffic Transp. Eng. 5, 181–196.

Oner, J., Sengoz, B., 2015. Utilization of recycled asphalt concrete with warm mix asphalt and cost-benefit analysis. PLoS One 10.

Pacheco-Torgal, F., Castro-Games, J.P., Jalali, S., 2005. Alkali activated geopolymeric binder using Tungsten mine waste: preliminary investigation. Geopolymer, Green Chem. Sustain. Dev. Solut. 93–98.

Page, E., 2011. Issues of Sustainability and Distributional Equity in Ensuring Mineral Supply : The Case of High Specification Aggregates in England. University of Manchester.

Panzera, T.H., Christoforo, A.L., de Paiva Cota, F., Ribeiro Borges, P.H., Bowen, C.R., 2011. Ultrasonic Pulse Velocity Evaluation of Cementitious Materials. Adv. Compos. Mater. - Anal. Nat. Man-Made Mater.

Plug, C.P., Bondt, A.H. de, Woerd, B.J. van der, Steensma, G., 2006. Imrpoved performance grouted macadams - High performance applications of grouted macadam. In: Ooms Nederland Holding Conference. Avenhorn, Netherlands.

Pradyumna, T.A., Mittal, A., Jain, P.K., 2013. Characterization of Reclaimed Asphalt Pavement (RAP) for Use in Bituminous Road Construction. Procedia - Soc. Behav. Sci. 104, 1149–1157.

Pratelli, C., Betti, G., Giuffrè, T., Marradi, A., 2018. Preliminary in-situ evaluation of an innovative, semi-flexible pavement wearing course mixture using Fast Falling Weight Deflectometer. Materials (Basel). 11.

Praticò, F.G., Giunta, M., Mistretta, M., Gulotta, T.M., 2020. Energy and environmental life cycle assessment of sustainable pavement materials and technologies for urban roads. Sustainability 12.

Provis, J.L., Deventer, J.S. Van, 2014. Alkali-Activated Materials: State-of-the-art Report. RILEM TC 224-AAM.

Puppala, A.J., Hoyos, L.R., Potturi, A.K., 2011. Resilient Moduli Response of Moderately Cement-Treated Reclaimed Asphalt Pavement Aggregates. J. Mater. Civ. Eng. 23, 990–998.

Qingjun, D., Mingyu, Z., Fan, S., Xiaoqiang, Z., 2015. Mechanical behavior and failure mechanism of recycled semi-flexible pavement material. J. Wuhan Univ. Technol. 981–988.

Rao, S.K., Sravana, P., Rao, T.C., 2016. Experimental studies in Ultrasonic Pulse Velocity of roller compacted concrete pavement containing fly ash and M-sand. Int. J. Pavement Res. Technol. 9, 289–301.

Reta, Y., Quezon, E.T., Kumela, T., 2018. Experimental study on the use of reclaimed asphalt pavement as base course materials through blending with crushed stone aggregates. World J. Eng. Res. Technol. 4, 1261–67.

Ricci, R., 2012. Laboratory study of grouted macadams impregnated with mine waste geopolymeric binder. Universita di Bologna.

Rizenbergs, R.L., 1968. Discussion on skid resistance of pavement surface.

Road Surface Treatment Association, 2014. The best kept secret on the roads.

Road Surface Treatments Association, 2017. Code of Practice for Grouted Macadam Surfacing.

Roe, P.G., Forest, R.L., 2005. The early life skid resistance of asphalt surfaces.

Ryu, G.S., Lee, Y.B., Koh, K.T., Chung, Y.S., 2013. The mechanical properties of fly ash-based geopolymer concrete with alkaline activators. Constr. Build. Mater. 47, 409–418.

Safiuddin, M., Hearn, N., 2005. Comparison of ASTM saturation techniques for measuring the permeable porosity of concrete. Cem. Concr. Res. 35, 1008–1013.

Saliani, S.S., Carter, A., Baaj, H., Tavassoti, P., 2019. Characterization of asphalt mixtures produced with coarse and fine recycled asphalt particles. Infrastructures 4.

Saludung, A., Ogawa, Y., Kawai, K., 2018. Microstructure and mechanical properties of FA/GGBS-based geopolymer. In: MATEC Web of Conferences. ICRMCE 2018.

Samantasinghar, S., Singh, S.P., 2019. Fresh and Hardened Properties of Fly Ash– Slag Blended Geopolymer Paste and Mortar. Int. J. Concr. Struct. Mater. 13, 1–12.

Sasui, S., Kim, G., Nam, J., Koyama, T., Sant Chansomsak, 2020. Strength and Microstructure of Class-C Fly Ash and GGBS Blend Geopolymer Activated in NaOH & NaOH + Na2SiO3. Materials (Basel). 13.

Setyawan, A., 2003. Development of Semi-Flexible Heavy-Duty Pavements. University of Leeds.

Setyawan, A., 2013. Asessing the compressive strength properties of semi-flexible pavements. Procedia Eng. 54, 863–874.

Shadmani, A., Tahmouresi, B., Saradar, A., Mohseni, E., 2018. Durability and microstructure properties of SBR-modified concrete containing recycled asphalt pavement. Constr. Build. Mater. 185, 380–390.

Silva, I., Castro-Gomes, J., Albquerque, A., 2010. Geopolymeric Artificial Aggregates as New Materials for Wastewater. In: International Conference on Sustainable Building Affordable to All (SB10). pp. 441–448.

Sims, I., Lay, J., Ferrari, J.I., 1998. Concrete aggregates. In: Peter C. Hewlett (Ed.), Lea's Chemistry of Cement and Concrete. Butterworth-Heinemann, pp. 907–1015.

Singh, M., 2018. Coal bottom ash. In: Waste and Supplementary Cementitious Materials in Concrete: Characterisation, Properties and Applications. Elsevier Ltd., pp. 3–50.

Singh, S., Ransinchung, G.D.R.N., Kumar, P., 2017. Feasibility study of RAP aggregates in cement concrete pavements. Road Mater. Pavement Des. 20, 151–170.

Sivilevičius, H., Bražiunas, J., Prentkovskis, O., 2017. Technologies and principles of hot recycling and investigation of preheated reclaimed asphalt pavement batching process in an asphalt mixing plant. Appl. Sci. 7.

Standards Australia, 1998. Supplementary cementitious materials for use with portland and blended cement Fly ash.

Struers, 2020. About grinding and polishing - Mechanical preparation [WWW Document]. URL https://www.struers.com/en/Knowledge/Grinding-and-polishing#about

Sultan, S.A., Guo, Z., 2016. Evaluating the performance of sustainable perpetual pavements using recycled asphalt pavement in China. Int. J. Transp. Sci. Technol. 5, 200–209.

Sunarjono, S., Hidayati, N., 2019. Physical properties of reclaimed asphalt pavement. IOP Conf. Ser. Mater. Sci. Eng. 674, 1–9.

Taha, R., Al-Harthy, A., Al-Shamsi, K., Al-Zubeidi, M., 2002. Cement Stabilization of Reclaimed Asphalt Pavement Aggregate for Road Bases and Subbases. J. Mater. Civ. Eng. 14, 239–245.

Tahmoorian, F., Samali, B., Tam, V., Yeaman, J., 2017. Evaluation of Mechanical Properties of Recycled Material for Utilization in Asphalt Mixtures. Appl. Sci. 7, 763.

Tashima, M.M., Akasaki, J.L., Castaldelli, V.N., Soriano, L., Monzó, J., Payá, J., Borrachero, M. V., 2012. New geopolymeric binder based on fluid catalytic cracking catalyst residue (FCC). Mater. Lett. 80, 50–52.

Tenza-Abril, A.J., Villacampa, Y., Solak, A.M., Baeza-Brotons, F., 2018. Prediction and sensitivity analysis of compressive strength in segregated lightweight concrete based on artificial neural network using ultrasonic pulse velocity. Constr. Build. Mater. 189, 1173–1183.

Thapa, S., 2015. Design of Cold-In-Place Recycling (CIR) Using Superpave Gyratory Compactor. University of Nevada.

Tong, K.T., Vinai, R., Soutsos, M.N., 2018. Use of Vietnamese rice husk ash for the production of sodium silicate as the activator for alkali-activated binders. J. Clean. Prod. 201, 272–286.

Topçu, I.B., Uygunoglu, T., 2016. Sustainability of using waste rubber in concrete, Sustainability of Construction Materials. Elsevier Ltd.

Tran, B., 2014. Maximising reclaimed asphalt pavement (RAP) content in hot mix asphalt (HMA). Swinburne University of Technology.

Trimurtiningrum, R., Ekaputri, J.J., 2016. Geopolymer grout material. Mater. Sci. Forum 841, 40–47.

Trtnik, G., Turk, G., Kavčič, F., Bosiljkov, V.B., 2008. Possibilities of using the ultrasonic wave transmission method to estimate initial setting time of cement paste. Cem. Concr. Res. 38, 1336–1342.

Turgut, P., 2004. Evaluation of the ultrasonic pulse velocity data coming on field. In: 4th International Conference on NDE in Relation to Structural Integrity for Nuclear and Pressurized Components.

UK Public General Acts, 2008. Climate change act 2008 [WWW Document].

Ulticrete, 2018. Ulticrete: The ultimate heavy duty pavement solution.

United States Environmental Protection Agency, 2005. Benchmarks for storm-water sampling.

Uz, V.E., Gökalp, İ., 2017. The effect of aggregate type, size and polishing levels to skid resistance of chip seals. Mater. Struct. Constr. 50.

Van Dao, D., Ly, H.B., Trinh, S.H., Le, T.T., Pham, B.T., 2019. Artificial intelligence approaches for prediction of compressive strength of geopolymer concrete. Materials (Basel). 12.

Vinai, R., Soutsos, M., 2019. Production of sodium silicate powder from waste glass cullet for alkali activation of alternative binders. Cem. Concr. Res. 116, 45–56.

Wang, J., Xie, J., Wang, C., Zhao, J., Liu, F., Fang, C., 2020. Study on the optimum initial curing condition for fly ash and GGBS based geopolymer recycled aggregate concrete. Constr. Build. Mater. 247, 118540.

Wang, M.L., Birken, R., 2014. Sensing solutions for assessing and monitoring roads. Sens. Technol. Civ. Infrastructures 2, 461–496.

Wang, T., Hu, L., Pan, X., Xu, S., Yun, D., 2020. Effect of the Compactness on the Texture and Friction of Asphalt Concrete Intended for Wearing Course of the Road Pavement. Coatings 10, 192.

Wardhono, A., Gunasekara, C., Law, D.W., Setunge, S., 2017. Comparison of long term performance between alkali activated slag and fly ash geopolymer concretes. Constr. Build. Mater. 143, 272–279.

Wayman, M., Carswell, I., 2010. Enhanced levels of reclaimed asphalt in surfacing materials: A case study evaluating carbon dioxide emissions, Transport research laboratory.

Wilkinson, A., 2017. The use of geopolymer cement for road surface applications. Ulster University.

Williams, R.T., 1986. Cement-treated pavements : materials , design , and construction. Mater. Sci.

Xie, J., Wang, J., Rao, R., Wang, C., Fang, C., 2019. Effects of combined usage of GGBS and fly ash on workability and mechanical properties of alkali activated geopolymer concrete with recycled aggregate. Compos. Part B Eng. 164, 179–190.

Yildirim, H., Sengul, O., 2011. Modulus of elasticity of substandard and normal concretes. Constr. Build. Mater. 25, 1645–1652.

Zhang, H.Y., Kodur, V., Qi, S.L., Cao, L., Wu, B., 2014. Development of metakaolin-fly ash based geopolymers for fire resistance applications. Constr. Build. Mater. 55, 38–45.

Zhang, J., Cai, J., Pei, J., Li, R., Chen, X., 2016. Formulation and performance comparison of grouting materials for semi-flexible pavement. Constr. Build. Mater. 115, 582–592.

Zhang, J., Li, S., Li, Z., Zhang, Q., Li, H., Du, J., Qi, Y., 2019. Properties of fresh and hardened geopolymer-based grouts. Ceramics-Silikaty 63, 164–173.

Zhang, L., Han, X.X., Ge, J., Wang, C.H., 2018. The relationship between compressive strength and flexural strength of pavement geopolymer grouting material. In: IOP Conference Series: Materials Science and Engineering. IOP Publishing.

Zoorob, S.E., Hassan, K.E., Setyawan, A., 2002. Cold mix, cold laid semi-flexible grouted macadams, mix design and properties. In: Performance of Bituminous and Hydraulic Materials in Pavements. Swets & Zeitlinger.